Functionalized Polymer Nanocontainers for Targeted Drug Delivery

Inaugurationaldissertation

zur

Erlangung der Würde einesDoktors der Philosophie

vorgelegt der
Philosophisch-Naturwissenschaftlichen Fakultät
der Universität Basel

von

Samantha Mariela Benito

aus Buenos Aires, Argentina

Basel, 2006

Genehmigt von der Philosophisch-Naturwissenschaftlichen Fakultät
Auf Antrag der Herren:

Prof. Dr. Wolfgang Meier
Dr. Andreas Taubert
Prof. J. P. Maier

Basel, den 28. September 2004

Prof. M Tanner
Dekan

Table of Contents

1. Introduction

1.1. General introduction

In the past decade the interest in nanomaterials based on polymers and amphiphilic self-assembling systems has increased enormously. The main reason for this is the need to find new materials with enhanced performance to replace classic systems facing the demand of industry for increasingly sophisticated systems. A particular interest has been focused on the preparation of carriers, with special emphasis on control of their size and morphology at the nanometer scale.[1]

As a result of the intensive research in this area several approaches have emerged and two main classes of nanocarriers can be distinguished: nanospheres and nanocapsules. Nanospheres, also termed nanoparticles or matrix systems, consist of a polymer matrix, in whose pores other molecules can be encapsulated. They can also serve as molds for engineering more sophisticated materials. Nanocapsules consist of a polymer shell or membrane surrounding a cavity, and can be thought as reservoir systems. These systems are per se encapsulating systems,[2-6] but have been also used as templates.[7]

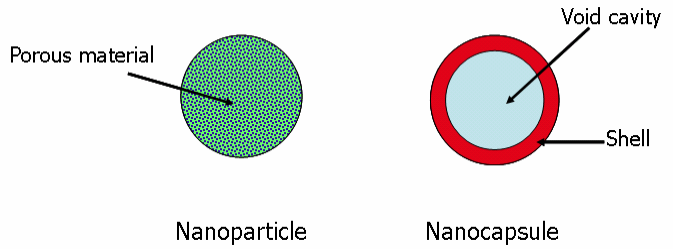

Figure 1.1.1.: Schematic representation of the difference between a porous nanoparticle and a nanocapsule.

Many of these nanostructures have been used in different fields. For instance, nanocapsules can be used as nanoreactors,[8] where they provide a compartmentalized volume in which reactions can take place, thus protecting unstable or labile molecules (enzymes, catalysts, etc.) from hostile environments. Nanoparticles find use in chemistry for chromatography. In the pharmaceutical industry, both systems have been used as controlled-release and targeting devices. In cosmetics, these systems are used as protective shells for the encapsulation of labile substances such as antioxidants. Another area of application is agriculture, where nanocarriers can be used to deliver nutrients to poor soils, and also as delivery systems for fungicides, pesticides, and bactericides. Moreover, in fields such as biochemistry these capsules can serve as matrices to insert membrane proteins and therefore as model systems to study protein association with membranes, or more ambitiously to design artificial ionic pumps and light harvesting systems.[9]

Nanostructured materials have evolved from early and simple systems into more sophisticated complex functional structures and hybrid materials. Using self-assembly, these synthetic systems mimic living organisms. A further challenge is to obtain artificial cells based on this type of self-assembled structures, mimicking the structure and behavior of biological cells. First attempts to obtain artificial cells focused mainly in the incorporation of channel proteins and pores into the artificial membranes.[2, 8, 10-13]

1.2. Cells, membranes, and proteins

Biological cells are complex hierarchical systems, which constitute the basic components in living systems. Their lipidic membranes have a key function providing the required compartmentalization. Cells are highly organized structures and have many functional units known as organelles. Most of these units are isolated from each other by one or more membranes.

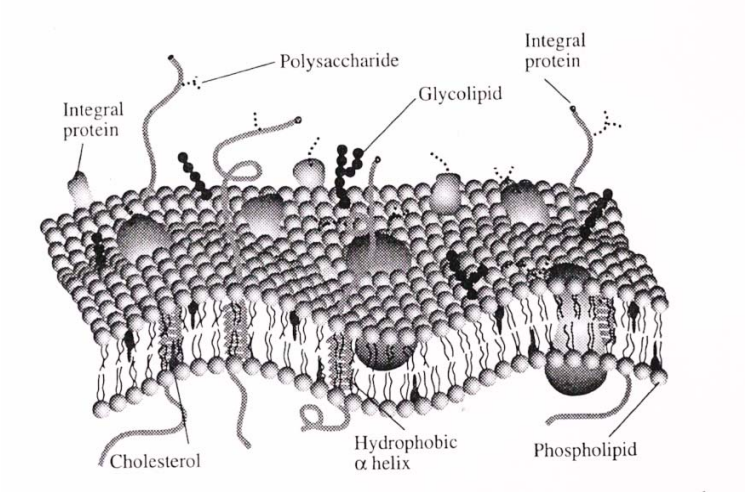

Figure 1.2.1: Graphic representation of a biomembrane, taken from Hamley[14].

Cell membranes not only separate and protect the inner components of a cell from the external environment, but also provide stability and maintain the integrity of the structure itself. Alone, the lipid bilayer forming the cell membrane, with its 3 nm thickness and hydrophobic characteristics, constitutes an ideal barrier for ions and metabolites.[15] In order to provide means of transport and communication with the exterior, nature has developed a wealth of proteins, glycoproteins, and lipoproteins with specific functions, which are able to insert in the biological membrane and allow the selective transport of materials through them.[16] Therefore, in its natural state, biological membranes comprise lipids, proteins, and some carbohydrates, and act as highly selective permeability barriers. Moreover, membrane proteins not only participate in the regulated (passive and active) transport of molecules, but also intervene in selective receptivity, signal transduction and cell recognition, providing anchoring sites for cytoskeletal filaments or components of the extracellular matrix.

Proteins are amongst the most abundant macromolecules in biological systems, counting up to 50% of the total weight in cells. Proteins are key components of biological processes and one of the most versatile found in nature. They can act as enzymes, structural components, or have hormonal activities. Proteins, as any other polymeric materials are composed of repeating units, so-called residues. The repeating units in proteins and oligomers are amino acids, which in the protein are covalently bound through amide bonds, also known as peptide bond. The countless arrangements of 20 amino acids found in nature account for the enormous variety of proteins available.

From the many proteins associated with lipidic membranes; pore forming proteins are amongst the best studies ones. Pore forming proteins, also known as channel proteins are involved in the translocation of ions and metabolites from the external compartment to the cytosol and vice versa.[17] Cells have two special types of membrane-bound proteins to overcome the impermeability of the lipidic membrane, ion pumps and ion channels.[18] Other interesting membrane-bound proteins constitute the receptor family, which serve as recognition sites in the outer surface of the cell membrane and participate in the communication with the external environment.

1.3. Amphiphiles, lipids, and self-assembly

Amphiphilic molecules, that is, molecules with a polar and a non-polar moiety, arrange themselves at interfaces or tend to build aggregates in solution.[15, 19] Amphiphiles are surface-active molecules; at an interface they form monolayers, therefore, lowering the energy of the system, by lowering its surface tension. Examples of common amphiphiles are lipids and detergents.

Lipids constitute a special case of amphiphiles typically consisting of two fatty acid chains linked by ester or acyl bonds to a common backbone, with the most commonly found lipids in nature being glycerol-based lipids.

In aqueous solution, low molecular-weight amphiphilic molecules can, depending on concentration, structure, temperature, and other parameters, build different aggregates such as micelles, vesicles, and lyotropic[1] liquid crystalline phases.[15] The driving force for such aggregation in aqueous media usually is referred to as the hydrophobic effect.

[1] Lyotropic refers to the fact that such phases are formed by amphiphiles as a function of concentration as well as temperature, in the case in which the phases form in function of the temperature only they are called thermotropic phases.[14] I. Hamley, *Introduction to Soft Matter: Polymers, Colloids, Amphiphiles and Liquid Crystals, Vol. 44*, **2000**.

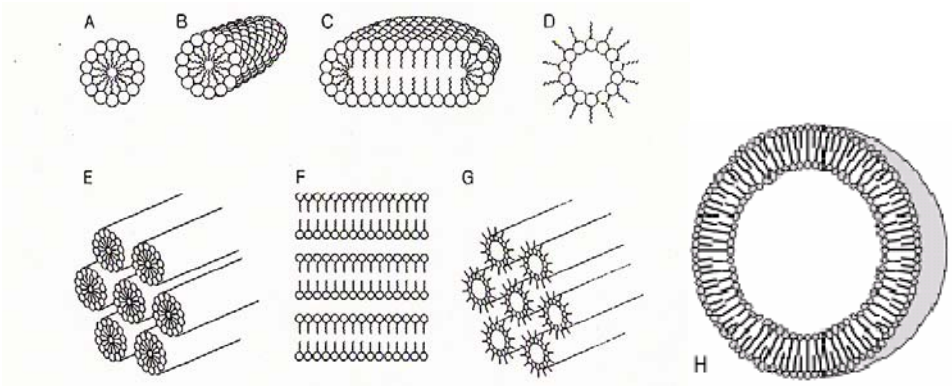

Figure 1.3.1: Schematic representation of some of the different aggregation morphologies found in low molecular amphiphiles: A, spherical micelles; B, rod-like micelles; C, disk-shaped micelles; D, inverted micelles; E, normal cylindrical hexagonal packing; F, lamella; G, inverted cylindrical hexagonal packing; H, double bilayer formation in a spherical vesicle. Taken from Lasic.[15]

The term "hydrophobic effect" was first used by Kauzmann[20] and broadly reviewed by Tanford.[16, 21, 22] According to the IUPAC definition[2] it is "the tendency of hydrocarbons (or lipophilic hydrocarbon-like groups in solutes) to form intermolecular aggregates in aqueous medium, and analogous intramolecular interactions. The name arises from the attribution of the phenomenon to the apparent repulsion between water and hydrocarbons. However, the phenomenon ought to be attributed to the effect of the hydrocarbon-like groups on the water-water interaction". At a crude approximation, the hydrophobic interaction reduces to the preferential interaction of non-polar groups among themselves in a water environment, although the process is much more complex than that. Hydration of non-polar species results in higher ordering of the neighboring water molecules which in turn results in highly unfavorable entropic conditions of the water surrounding the solute. The system, therefore, tends to avoid the unfavorable hydrophobic hydration contribution by forming aggregates, thus reducing the contact of the solute with neighboring water molecules. Nevertheless, the complex thermodynamic factors affecting the hydrophobic effect are still not completely understood and debate among specialists continues. Interesting reviews with the evolution of the concept of the hydrophobic effect throughout time and its thermodynamic implications were recently published.[20, 23]

The hydrophobic effect dictates the self-assembly of lipids into a variety of morphologies. Like lipids amphiphilic polymers also self-assemble in different structures.

[2] 1994,66,1123, IUPAC compendium of chemical terminology, 2nd ed 1997

1.4. Polymers and block-copolymers

Polymers consist of structural or repeating units of low molecular weight covalently connected to each other to give high molecular weight compounds. The small molecules that combine with each other to form these macromolecules are called monomers. Based on their architecture polymers can be classified into linear polymers, branched polymers, and dendrimers.[24] Likewise, branched polymers can be classified according to their structure into comb-like, ramified, or star-like polymers. Dendrimersconstitute actually a special class of branched polymers, in which the ramifications occur in each monomer, giving thus branched branches. [25, 26]

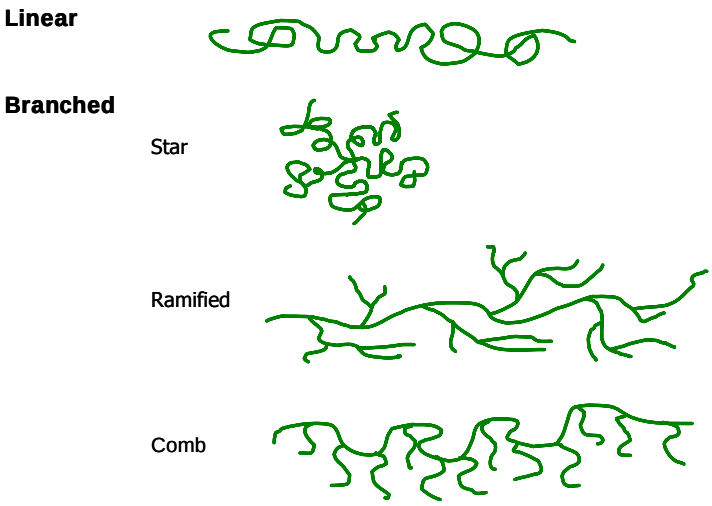

Figure 1.4.1: Representation of the different types of homopolymer architecture.

A polymer that consists of two different repeating units is referred to as a copolymer, whereas polymers containing only one type of repeating unit are named homopolymers.[24] The sequence in which two different repeating units appear gives rise to a further classification within copolymers. A polymer in which the repeating units alternate is called an alternating copolymer, if the repeating units do not have any specific sequencing the copolymer is known as a random or statistical copolymer.[24, 27] If relative long segments of a monomer are present in a block fashion, it is termed a block-copolymer.

Block-copolymers consist of at least two, covalently bound, segments or blocks of different homopolymers.[28] For instance, a triblock-copolymer can have a general form A_n-B_m-C_p, with A, B, C, being different monomer types constituting the different blocks. The subscripts n, m, and p, stand for the degree of polymerization, i.e. the average number of each monomer present in each respective block. Branched structures can also be found among copolymers, graft copolymers being one of the most interesting ones. Graft copolymers can be considered as a special case of

block-copolymers, a comb-like structure in which several blocks of homopolymer B are grafted as branches onto a main chain of homopolymer A, known as the backbone.[28]

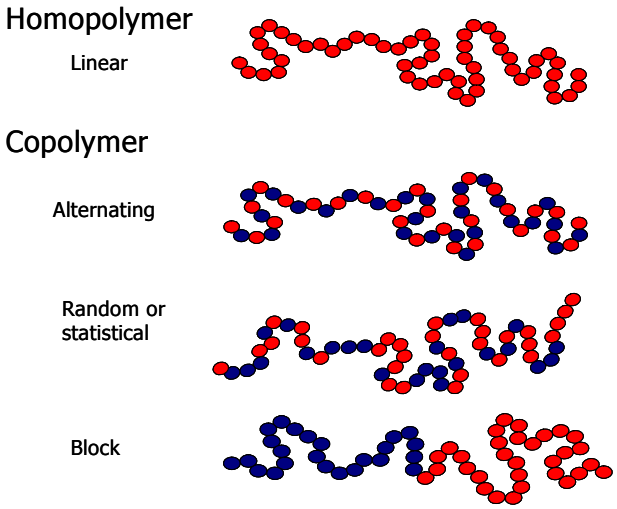

Figure 1.4.2: Representation of linear copolymers, statistical or random, alternate and block-copolymers.

In block-copolymers, by covalently linking two intrinsically different homopolymers, macroscopic phase separation is prevented and limited to the nanometer range. This gives rise to the wide variety of morphologies found for this type of polymers in bulk, including cylindrical, and body-centered cubic micellar structures, depending on the relative volume fractions of the blocks.

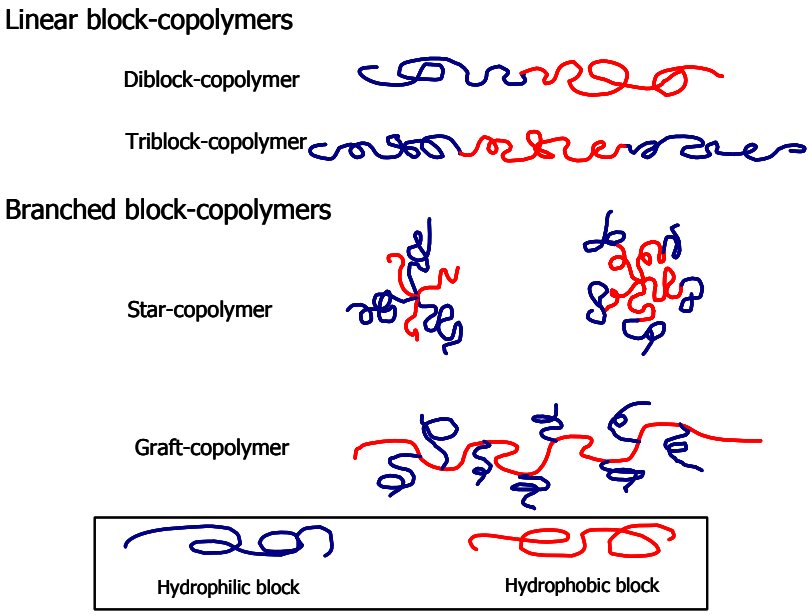

Figure 1.4.3: Representation of different architectures of block-copolymers; linear diblock, triblock, star, and graft copolymer. Adapted from Alexandridis et al.[29]

For amphiphilic block-copolymers the tendency to phase separate manifests itself not only as micro-phase separation in bulk but also as self-assembly in solution. All the parameters that

influence the assembly behavior of low molecular amphiphiles also play a role in the self-aggregation process of amphiphilic block-copolymers and analogous superstructures are observed in solution.

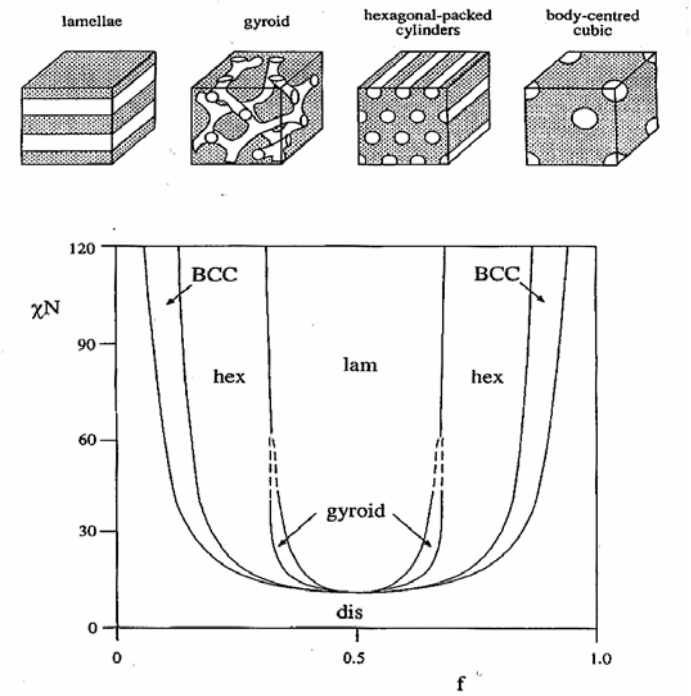

Figure 1.4.4: Schematic representation of the phase diagram and the corresponding self-assembled structures for block-copolymers in bulk, taken from Hamley.[14]

1.5. Aggregation of amphiphilic block-copolymers in aqueous media

Amphiphilic block-copolymers, that is, hydrophobic and hydrophilic blocks covalently linked together, can be considered macromolecular analogues of low molecular weight surfactants, and are usually referred as superamphiphiles.[30, 31] Mainly, the relative length of the blocks determines the assembly behavior in selective solvents.[32-36] It has been found that the formation of different morphologies is a function of total and relative block lengths, temperature, block (chemical) composition, type of solvent, and concentration among other variables.[37, 38]

One special feature of block-copolymer chemistry is that it enables to change the chemical composition, length, and structure of the constituting blocks in order to tune the association characteristics and thus the obtained morphologies. Moreover, by playing with the architecture of the blocks different mesophases can be achieved as depicted in Figure 1.5.1. At low solvent concentrations spherical micelles, rod-like micelles, and vesicles can form, whereas at higher concentration lyotropic liquid crystalline phases are encountered.

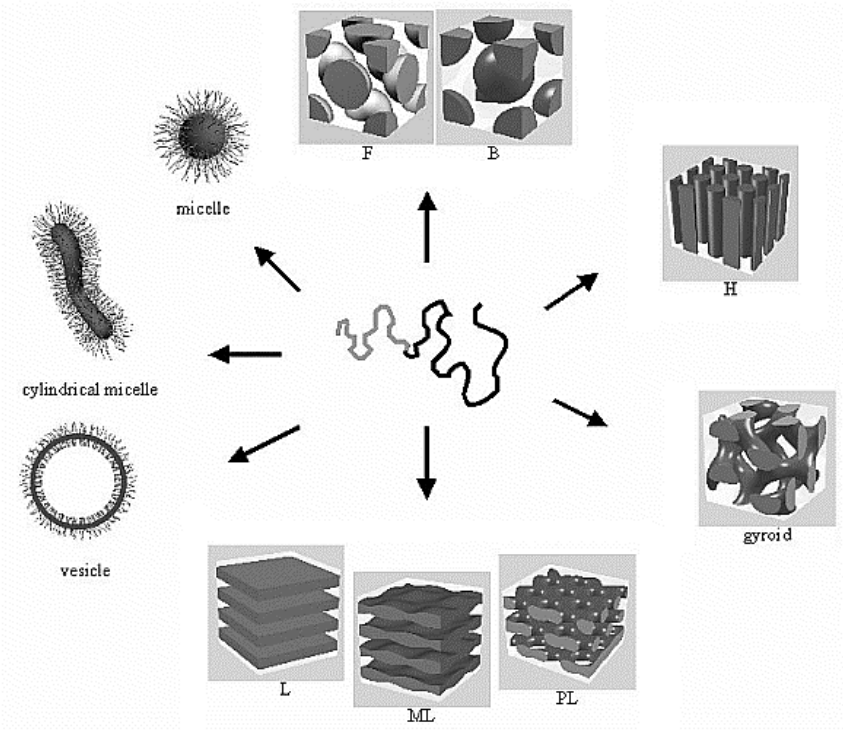

Figure 1.5.1: Schematic representation of morphologies of block-copolymer aggregates found in aqueous media. Taken from http://www.chemie.uni-hamburg.de/pc/sfoerster/forschung.html

Although it is broadly accepted that an aqueous medium is a prerequisite for the self-aggregation of low molecular weight amphiphiles into superstructures, this is not necessarily the case for block-copolymer amphiphiles.[23, 39] Many examples have been presented in which aggregation takes place in other solvents than water.[40, 41] Nevertheless, the aggregates formed in aqueous solutions still pose the main interest since they closely resemble biological systems. Systems based on organic solvent will not be further discussed here.

In the context of nanocarriers, the most interesting superstructures obtained from block-copolymers in solution are micelles and vesicles. The individual block-copolymers constituting these aggregates are termed unimers.[33] By thermodynamic considerations, the unimers are in equilibrium with the aggregates in solution, and the aggregates form above what is known as critical aggregation concentration (cac).[29, 42] Although dictated by thermodynamics, self-assembled structures can and are often kinetically stabilized, that is, shapes, which are not equilibrium ones can be found since they are kinetically trapped.[34, 42]

1.5.1. Micelles

Simple micelles are aggregates with a core-shell structure, occurring in a given concentration range. In aqueous solutions, micellization results from the selective solubilization of the shell-forming block, whereas the core is formed by the hydrophobic non-soluble block. Micelles form above what is known as the critical micelle concentration (cmc) and are dynamic systems. The

slower dynamics of the constituent blocks[43, 44] makes block-copolymer micelles more stable systems compared to lipidic micelles. Intermicellar chain exchange is mainly a function of the type of blocks, i.e. their relative polarity, the overall chain length, and relative block lengths,[45] and can be tailored to be very slow in contrast to lipid micelles, by using blocks with low glass transition temperature (T_g).[43, 46-48] Also in contrast to aggregates formed from low molecular weight surfactants, self-assembled structures based on block-copolymers show higher structural stability, and have a much lower (cac).

Depending on the asymmetry of the constituting diblocks, the micellar structures can be classified as crew-cut micelles[37, 43, 49-51] and star micelles. In crew-cut micelles the relative long blocks form the core where the short ones constitute the corona, whereas star micelles have their cores filled with the short hydrophobic chains, and coronas formed by the long hydrophilic ones (see Figure 1.5.2 b). In the case of triblocks having a hydrophobic middle block normal micelles form, whereas for triblocks with hydrophobic side chains flower-like micelles[3] are observed (see Figure 1.5.2 b). The latter consist of a core of B blocks surrounded by loops of A blocks.[52]

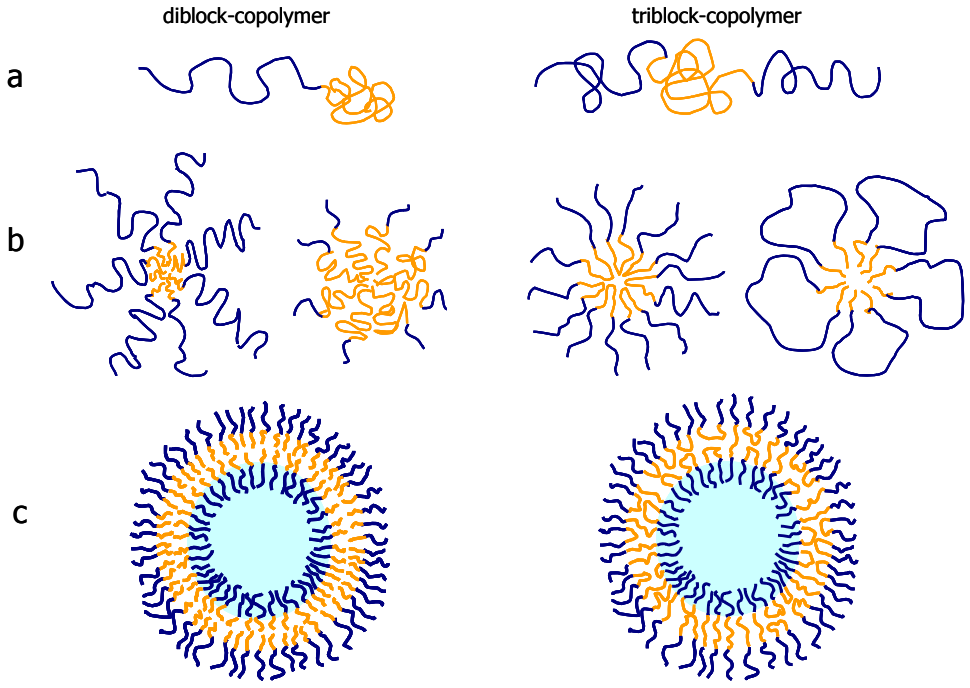

Figure 1.5.2: Schematic representation of: a) unimers in solution, di- and triblock respectively b) star and crew cut micelles for a diblock-copolymer, and normal (ABA) and flower-like (BAB) micelles for a symmetric triblock-copolymer, c) vesicle formation for a diblock and triblock-copolymer respectively.

Diblock-copolymers with long hydrophilic chains tend to form micellar aggregates due to the highly positive curvature of the interface. As the length of the insoluble block increases, the

[3] Flower-like micelles are also known as sunflower micelles or chrysanthemum micelles.

curvature decreases and a transition to rod-like micelles is observed. If the length of the insoluble block increases further then lamellar phases are favored. Depending on the concentration stacked lamella or vesicular structures can be formed.

1.5.2. Vesicles

Vesicular structures are particularly interesting since they are straightforward encapsulation devices, can be used as transport systems, protection devices for labile substances, and nanoreactors, to perform localized chemical reactions at the nanometer level. Vesicles in the case of lipids consist of a closed spherical bilayer.[15, 19] Diblock-copolymer vesicles also form closed hollow-spherical aggregates with bilayer walls,[35] whereas triblock-copolymers self-assemble into vesicles with a more complex association, such as bilayer and stretched or spanning polymers in the membrane[53] (see Figure 1.5.2 c). The formation of vesicles from block-copolymers was broadly reviewed.[31, 34-36]

Polymer vesicles are known for their higher stability and toughness when compared to liposomes.[42]. For liposomes leakage of encapsulated substances is related to the fluidity of the lipid bilayer. In this respect, polymer vesicles are more versatile since their fluidity properties can be tailored by tuning the glass transition temperature of the constituting blocks.

At this point it must be noted that when the constituents are synthetic or natural lipids, the resulting structures are preferentially termed liposomes. The term vesicle, which is more general, includes not only lipidic vesicles but also synthetic surfactants and amphiphilic polymers. As the field broadens new terminology emerges. For instance, vesicular structures obtained from peptidic polymers were termed peptosomes[54-57] whereas the term polymersomes has been used in relationship to vesicles consisting of polymers.[44, 58] In this thesis though, the classical terminology is used, since the new one is not well established yet. Therefore, whenever referring to lipidic vesicles the term liposomes will be preferentially used, reserving the term vesicles for amphiphilic polymers.

1.6. Polymer nanocontainers

Since amphiphilic polymers can form vesicles with a small pool of water inside, they can be regarded as nanocontainers (NCs).[59, 60] The separation from the outer medium is achieved with the polymer membrane. Two important parameters of the membranes are their permeability and their stability. The advantage of synthetic block-copolymers as the building blocks of these nanocontainers is their higher stability over lipids, due to the increased length, conformational freedom, and slower dynamics of the underlying polymers.[36, 43, 44, 46, 61] The thickness of the membrane can be tuned by the nature and length of the hydrophobic chains of the constituting polymers.[36] Addi-

tional stability can be obtained by cross-linking the aggregates, thus, freezing their structures[44, 61] achieving solid-state properties. However, this further reduces the permeability of such capsules.

Nanocontainers comprised solely of block-copolymers show a rather low permeability.[62] For practical purposes, an ideal system would be one that is stable enough to resist handling and diverse technological steps, while at the same time being permeable enough to allow encapsulation and release at will, that is, a switchable or tunable system. This can be achieved, for instance as already demonstrated,[8] by the incorporation of pore proteins in the artificial polymer membrane, such as encountered in cell membranes. Some approaches to regulate the permeability can be triggered by temperature or pH changes.[63, 64] These tunable systems would for example change their conformation depending on one of these parameters.

One can further functionalize these nanocontainers by introducing a plethora of functional groups or molecules in different regions of the vesicular structure. For instance, hydrophobic molecules can be buried within the hydrophobic layer of the membrane. Amphiphilic molecules can be anchored by a long apolar chain inserted into the hydrophobic layer, and therefore present the polar heads on the surface of the vesicle.

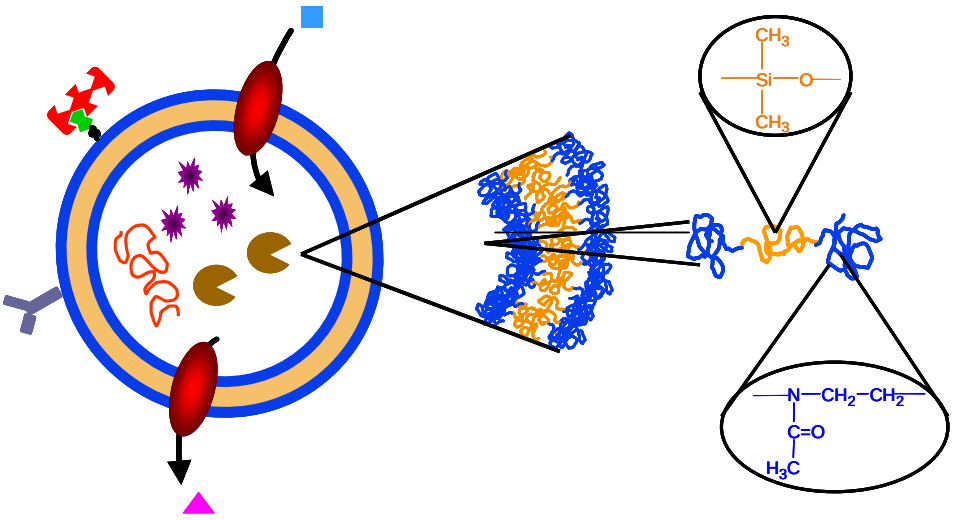

Figure 1.6.1: Constitution of the nanocontainers used in this thesis and the multiple modifications possible.

Furthermore, hydrophilic molecules can be encapsulated in the inner water pool of the vesicle or can be bound to their inner or outer surface. The most stable way to attach a molecule to the surface of vesicles is by covalent bonding. This often requires harsh conditions or organic solvents when high yields are desired, which can disturb or destroy the aggregates. To overcome this, one can functionalize the assembling molecules or unimers prior to aggregation. This approach might be useful only for the attachment of low molecular weight molecules, since steric hindrance might disturb the aggregation process when higher molecular weight molecules are anchored to the assembling polymer.

1.7. General concept of encapsulation

Encapsulation of labile molecules is an important technology field found in many areas of chemistry, pharmaceutics, and biotechnology. Different strategies have been developed and the use for this purpose of microspheres, microcapsules, and liposomes is well established. Nevertheless, it is still a challenge for scientists to design and to fabricate micro- and nanocontainers for various substances with the desired storage, release, and stability properties required for each specific application, therefore this research field is in constant activity. One of the most investigated topics within encapsulation technology is the use of micro- and nanocapsules and particles for drug delivery

1.8. General concept of drug delivery

Basically, the concept behind drug delivery is to provide more constant concentrations in the organism, and to bring the compound with pharmaceutical activity directly to the site of need in order to enhance the effectiveness of action.[65] One way to bring the active substance to the site of action is to modify their bio-distribution by entrapping them in particulate drug carriers such as nanospheres, nanocapsules, or liposomes.[66] The need for encapsulation lies in the instability of many drugs, and in some cases it can improve the bioavailability of the therapeutic compounds. Other reasons for using drug carriers or delivery systems are the poor solubility of some drugs, which may be enhanced by choosing the right carrier. For this usually micellar systems are used since hydrophobic solutes will solubilize in their cores.

By encapsulating drugs in designed carriers, labile drugs are protected from the hostile conditions that they might encounter for instance at the low pH of the stomach. Furthermore, in many cases adsorption can be enhanced and side effects of therapeutic compounds can be minimized. Short circulation times in the blood stream due to rapid clearance through uptake by the reticuloendothelial system (RES) might be increased by choosing carriers that are able to avoid the uptake by the RES.

Within the concept of drug delivery two mechanisms must be taken into account to design such carrier systems, sustained or controlled drug delivery and site directed drug delivery. Controlled drug delivery takes place when a polymer, whether natural or synthetic, is combined with a drug or therapeutic agent in such a way that the active agent is released from the material in a pre-designed fashion. Different profiles for the release of the active substance might be used, for instance, this can be constant over a defined time or cyclic over a time. Additionally, the release can be externally triggered by environmental events.

Site directed or targeted drug delivery occurs when the drug, with the aid of a carrier is delivered to a specific site or organ. Different strategies can be considered, whether the delivery to specific tissues from the circulation is needed or intracellular delivery is required.

1.8.1. Drug delivery based on liposomes

In the past, the interest in liposomes as carriers of molecules was based on their potential to enclose and protect different materials of biological interest and to deliver them, functionally intact and in significant quantities to the interior of many cell types. Nevertheless, in many instances, the use of liposomes proved to be inadequate.[15, 19] The use of liposomes as drug carriers has some limitations, mainly their instability on storage, leading to leaking of the encapsulated material and the easiness of some complement activation leading to recognition by the RES. Two mechanisms are basically used to deliver the substances when using liposomes, a general mechanism of membrane fusion and the more specific receptor mediated endocytosis.

By combining liposomes with hydrophilic polymers, more stable systems could be obtained, usually known as Stealth[4] liposomes.[67, 68] In this systems a covalently attached PEG chain, minimizes the recognition by the RES and therefore helps prolonging the circulation times.[69, 70] It is not intended to review the vast literature on liposome drug delivery and targeting systems, only some exemplifying references are given.[71-73] Walde et al reported an almost exhaustive review on encapsulation with liposomes.[74]

The use of liposomes as carriers for hydrophilic drugs and lipidic micelles for hydrophobic drugs has been one exhaustively explored research area in the field of drug delivery, controlled drug delivery and targeted drug delivery.[75-80]

1.8.2. Polymer based drug delivery systems

Since liposomes present some technical limitations, the need to find new and more stable systems increased and new preparation methods for containers were developed. Several systems have been tested within the last decade or so, mainly consisting of nanospheres (see Figure 1.1.1) a selection of references on this theme is included.[81-84] Porous nanoparticles usually show limited encapsulation capacities; in this respect nanocapsules offer a better approach. Block-copolymer micelles and their use as drug vehicles have been also extensively reviewed.[33, 85-89]

Similar to liposomes, polymeric vesicles could provide a protective environment for labile molecules to deliver them intact to desired targets. Parameters such as size, surface charge, membrane fluidity and stability, presence of coupling groups on the surface, can be used to design the carrier to be adapted to a wide range of experimental conditions. The use of polymeric carriers for drug delivery brings several advantages, on one hand the encapsulated substance is protected

[4] Stealth liposomes consist of lipids conjugated with poly(ethylene glycol) (PEG) forming a protecting brush on the surface of the liposomes, and thus repelling the adhesion of proteins to the liposome's surface.

from degradation, on the other hand processes such as opsonization[5] might be avoided or diminished, additionally, targeted delivery might be introduced by using ligands or antibodies.

1.8.3. Controlled-release systems

Controlled-release is aimed at obtaining enhanced effectiveness of the therapeutic treatment by minimizing both under- and over-dosing, and it is also known as sustained delivery. A frequently desired feature is to achieve a constant level of drug concentration in the blood circulation or at the site of action of the substance, with a minimum of intakes per day and a maximum coverage. Usually drug delivery systems that dissolve, degrade, or are readily eliminated are preferred. Classically three types of processes are involved in the delivery of substances from a carrier system: diffusion, degradation, and swelling followed by diffusion or a combination thereof.

The advantages of sustained delivery systems are mainly the achievement of an optimum concentration, usually for prolonged times, the enhancement of the activity of labile drugs, due to their protection against hostile environments, and the diminishing of side effects due to the reduction of high initial blood concentrations (toxic concentration).

Controlled-release systems can be classified according to the mechanism that controls the release, the most common being diffusion. Diffusion controlled-release takes place when a compound diffuses through the polymer comprising the delivery system (usually a porous nanoparticle). The type of polymer system dictates whether macroscopic diffusion occurs, which usually takes place in polymer matrices containing pores. On the other hand, diffusion can also occur molecularly between the polymer chains. These types of delivery systems are the simplest ones in the sense that the polymer matrix does not undergo any changes in the body, when this happens the system is known as stimuli-responsive.

More sophisticated features can be introduced in the drug delivery systems in order to obtain systems that might deliver the active substance by responding to changes in the environment. These systems are then collectively known as environmentally- or stimuli-responsive systems,[91] and can be designed in such a way that they are incapable of releasing the encapsulated material until it is placed in an appropriate biological environment. For instance, swelling-controlled release systems are initially dry and, when in contact with body fluids will swell. Consequently, in the case of nanospheres, the swelling increases the pore size of the matrix and promotes the diffusion of the active agents into the bulk medium. Hydrogels are mainly used as swelling-release systems.

[5] Opsonization is one of the first steps in the process by which the body recognizes a foreign body (exogenous protein, molecule, or particle). The immune system produces the proper antibodies or complement proteins (opsonins) which bind to the particle to tag it. Via recognition of the opsonins by the phagocytes, the opsonization process promotes phagocytosis, thus, triggering the immune response.[90]I. M. Roitt, *Essential Immunology. 3rd Ed*, **1977**.

Other features of a polymer can be used to externally trigger the swelling, such as changes in pH, temperature, or ionic strength.[42, 92-96] These systems are usually termed intelligent or environmentally sensitive systems.[91] One additional requirement of these triggered systems is that the structural changes are reversible and repeatable upon additional changes in the external environment.

One subset of this type of release systems makes use of the external trigger in order to deliver their contents in a one-shot fashion, in contrast to swelling which is governed by diffusion. These systems can be actually thought to belong also to site specific delivery systems, since they take advantage of the conditions of the milieu to release drugs where an environmental condition is other than at different sites.

Biodegradable polymers are of great interest since these materials are processed within the body under biological conditions giving degraded sub-units that are easily eliminated by the normal pathways of excretion.[83] In most cases, hydrolysis is the degrading reaction which produces smaller and biologically acceptable by-products. Mainly two types of degradation exist: uniform hydrolysis throughout the matrix and surface degradation, or erosion.[82] The last process results in a release rate that is proportional to the surface area of the particle. The most commonly used biodegradable polyesters are poly(lactic acid) (PLA) and poly(glycolic acid) (PGA), and especially their copolymers poly(lactic-co-glycolic acid) (PLG), their degradation is controlled by both drug diffusion and polymer erosion.[97] Contrary to this, polyorthoesters show mainly surface-eroding process.[82]

1.8.4. Site specific or Selective targeting

Site directed targeting to cells or organs is desired to reduce the concomitant negative effects due to the action of the drug in sites other than necessary in the organism. As already mentioned, by encapsulating the drug in a carrier, the distribution process depends on the carriers' characteristics. Moreover, the carrier can be modulated to provide selective targeting to the cell or organ of interest, thus minimizing unwanted systemic side effects. For this purpose, two mechanisms may be used; passive targeting and active targeting.

Passive targeting takes place due to the action of the reticuloendothelial system (RES) in the common response of the organism to destroy foreign materials. Passive targeting is mainly dictated by the physical properties of the carrier and its interaction with plasma proteins. This form of targeting can be used to target diseases that affect the RES, for instance this is used to activate the immune system to destroy tumor cells. Passive targeting usually occurs by phagocytosis of the particle or carrier by the mononuclear phagocytic system, belonging to the RES.

In particular when the disease occurs in cells other than the RES, this kind of uptake must be avoided. In such cases active targeting needs to be used. Active targeted drug delivery occurs when the drug or carrier are directed to specific sites, in particular receptors located on the cell's

membrane or tissue of interest, with the aid of a homing device (antibody, ligand, epitope)[72]. For instance, to provide recognition to specific target cells, antibodies were covalently attached to the surface of liposomes.[98-101]

Active targeting usually involves the attachment of a ligand to the surface of the carrier in order to achieve specific ligand-receptor interaction. Once the targeted interaction takes place, the cell's mechanisms, mainly receptor-mediated endocytosis[6], provides the proper conditions for internalization of the carrier.

1.9. General concept of surface immobilization

Immobilization onto a surface is a prerequisite in order to use nanocontainers in bio-sensing devices. Nanoreactors, that is, nanocontainers functioning as confined reaction vessels with nanoscopic dimensions seem ideal candidates for bio-sensing devices. Immobilized nanocontainers could be used as biosensor chips for the detection, identification, and manipulation of biological entities. The nanocontainers can be loaded with molecules that could, after reacting with the analyte, give a detectable signal (absorbance, fluorescence, etc). Reactions taking place within a confined nanometer space, protected from the surrounding environment, seem ideal candidates for sensor devices. Moreover, immobilized vesicles containing channel and receptor proteins can be used as model systems to study the interactions of these receptors.[102] Usually in a bio-sensing device immobilization takes place onto the surface of a transducer,[103] therefore the need to immobilize the nanocontainers.

Different approaches can be used to achieve immobilization of molecules onto surfaces: physisorption or adsorption, and chemisorption (Figure 1.9.1 a, b, and c). Physisorption through van der Waals or hydrophobic interactions is usually not an advantageous approach since the adsorption obtained is weak and reversible and thus the achieved surface modification is not permanent.[29] One example of this type of immobilization is the Langmuir-Blodgett deposition technique, which in its most basic form uses only hydrophobic or hydrophilic interactions. Physisorption can also be obtained by electrostatic forces and the resulting layers show rather good stability.[104] One well-established approach based on electrostatic interactions is known as the layer-by-layer (LbL) deposition of opposite charged molecules onto surfaces.[104-106]

Covalently attached molecules, that is, chemisorption, on the other hand, render a much more stable system, and usually the modification is irreversible. One example of such an immobilization strategy is found in self-assembled monolayers (SAMs) on gold, via thiol-gold bond forma-

[6] Receptor-mediated endocytosis is a process by which cells internalize molecules or viruses. As its name implies, it depends on the interaction of that molecule with a specific binding protein in the cell membrane called a receptor.

tion.[107, 108] However, the harsh conditions usually needed to promote chemical bonding onto a surface reduce the spectrum of application of chemisorption.

Moreover, in order to promote specific binding between (macro)molecules, one can make use of the readily available and highly specific interactions found in biochemistry (Figure 1.9.1 d). Bio-affinity interactions are widely spread in biologic systems, and include antibody-antigen recognition, ligand-receptor interaction, nucleic acid hybridization or any other biological pair interacting with high affinity.

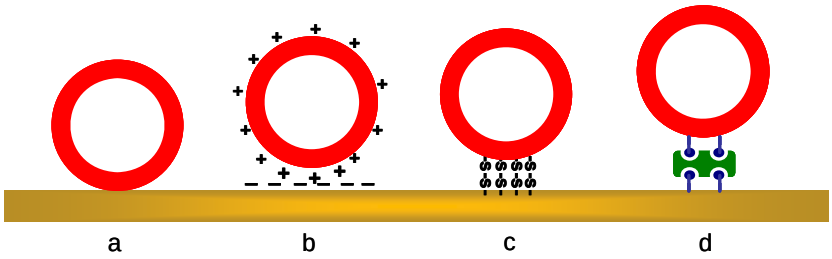

Figure 1.9.1: Different strategies for immobilization onto surfaces; a, physisorption; b, electrostatic interaction; c, covalent bonding (S-Au); d, receptor-ligand interaction (e.g. avidin-biotin).

2. Scope of this thesis

The aim of this thesis is the synthesis and modification of PMOXA-PDMS-PMOXA triblock-copolymers to render vesicular structures able to couple via specific interactions to other macromolecules. The purpose of the functionalization of self-assembling amphiphilic block-copolymers is two-fold: to use them as active targeting delivery systems in the context of active cell targeting and for surface immobilization. Both approaches share a common feature that is the specific interaction of nanocontainers towards receptors, whether these are present on the surface of a cell or a sensor.

The following strategy will be used to introduce specific functionalities to the nanocontainer surface: functional groups will be attached to the water exposed termini of the amphiphilic triblock-copolymers. By doing this, the blocks carrying the desired functionalities as end groups will self-assemble exposing these moieties on their surface. The functionalities on the nanocarrier will function as anchors providing either covalent bonding or highly specific non-covalent bonding, as in the biotin-avidin case. In these self-assembly systems, the average aggregation number will define the average number of functional groups per aggregate, which can be further tailored by mixtures of modified and non-modified polymer. Moreover, by functionalizing the end-groups of nanocontainers, labeled vesicular structures can be obtained for visualization purposes.

The characterization of these functionalized aggregates in regards to their encapsulation behavior and their interaction with specific receptors will be studied in two different systems:

1. Nanocontainers for active targeting of cells can be obtained by attaching ligands to the nanocontainer surface. In order to achieve high specificity, nanocontainers should attach only at particular receptor sites of the targeted cell and not at other sites or areas. Several different ligands can be used, such as antibodies, glycoproteins, and carbohydrates. For the introduction of ligands on the nanocontainer surface we will make use of biotinylated ABA triblock-copolymers, and coupling to the ligands will be achieved via streptavidin bridges. The choice of ligand will be determined by the targeted receptor to render selective targeting nanocontainers with medical use. Their binding and uptake will be studied in vitro with different cell lines. Encapsulation of fluorescent dyes in the polymer cavities will provide a means for visualization of the structures by fluorescent techniques such as microscopy and FCS. Other labeling procedures, such as gold encapsulation, will be studied to be able to inequivocally identify the vesicular structures by TEM and SEM.

2. Surface immobilized vesicles for sensoring purposes can be obtained by surface immobilization via anchoring groups. For this, functionalized nanocontainers can be attached via specific interactions to receptors on a surface. We will investigate the immobilization of biotinylated

nanocontainers onto streptavidin docking sites present on a surface. For this a system consisting of positively charged biotin-derivatized poly(lysine)-g-poly(ethylene glycol) (PLL-g-PEG-b) which interacts electrostatically with negatively charged surfaces of metal oxides[109, 110] will be used to form a surface bound comb PEG with biotin anchoring moeities. This surface will be further treated with streptavidin to render a substrate surface with streptavidin docking sites to which biotinylated nanocontainers will be linked. Adsorption of vesicular structures to the surface will be monitored by quartz crystal microbalance techniques.[111]

Other hydrophobic blocks will be investigated to replace PDMS in PMOXA-PDMS-PMOXA triblock-copolymers. Their synthesis and characterization will be studied with established techniques, whereas their aggregation will be investigated by TEM and DLS.

Functionalization of PMOXA-PDMS-PMOXA nanocontainers by insertion of channel membrane proteins will be used to improve their characteristic low permeability. Insertion of membrane proteins in the polymer membrane will be investigated by Langmuir film techniques. The feasibility of these hybrid protein-functionalized nanocontaines to function as vehicles to entrap small solutes will be investigated.

3. Results and Discussions

3.1. Polymer synthesis, functionalization and characterization

3.1.1. Synthesis of ABA triblock-copolymers

3.1.1.1. Introduction to block-copolymer synthesis

Different approaches can be used to obtain block-copolymers.

1. Living polymerization

The most versatile procedure to introduce additional blocks is the use of living polymerizations. The living character of such polymerizations offers the best-known synthetic route to prepare block-copolymers and at the same time the ability to accurately control the number of repeating units in each block.[27] The strategy is known as a one-pot sequential reaction[7].[24, 113-116] A monomer is initially polymerized until the desired chain length is obtained and then a second monomer is added to the reaction mixture thus continuing the chain growth. By feeding the second monomer into the reaction mixture after the first has completely reacted, the resulting polymer grows linearly in one direction only. This can in principle be repeated as many times as desired. In order to obtain symmetric block-copolymers (e.g. ABA) a bifunctional initiator is recommended.[114, 117]

2. Macroinitiator or telechelic polymerization

A commonly used alternative strategy involves the initiation of the polymerization reaction with active sites bound to pre-existing polymer molecules. The side chains grow from the activated site and the resulting chain length depends on the amount of monomer added to the mixture and the number of active sites present. The main difference between the block- and graft-copolymer approach is the location of the active sites.[27] In the context of block-copolymer formation using this approach, the starting polymer is usually referred to as a telechelic polymer,[118] or macromolecular initiator,[24] and serves as starting point from which the other polymer chains can grow. Several examples of this approach for the synthesis of oxazoline related polymers can be found in the following references.[119-121] For the macroinitiator or telechelic strategy ionic living polymerizations also prove useful to control the polydispersity[8] of the obtained polymer.[27]

---

[7] Also known as one-pot two-stage, one-pot three-stage, or one-pot multistage copolymerizations, giving AB, ABC, ABCD block-copolymers respectively.[112] P. Persigehl, R. Jordan, O. Nuyken, *Macromolecules* **2000**, *33*, 6977.

[8] The term polydispersity describes the distribution in sizes of a given entity. In other words, polydispersity is equivalent to size heterogeneity. For instance polydispersity is used to describe the different lengths of polymer chains, as well as

3. Post-polymerization

A third approach to obtain block-copolymers might involve the post connection of separately prepared homopolymers. In this strategy, known as block-to-block attachment, the different blocks are obtained separately and are connected end-to-end by common chemistry reactions, with or without the aid of a coupling agent.[24] This approach lacks the required characteristics to be used in large scales because separation of the obtained block-copolymer from the homopolymers is a tedious process, almost impossible in the case of amphiphilic block-copolymers.

3.1.1.2. Considerations regarding the polymer selection

Poly(dimethylsiloxane) (PDMS) was chosen as the middle block because of its hydrophobic character, high chain flexibility[9], good oxidative and thermal stability,[24, 123, 124] its very low glass transition temperature (Tg= -123 °C)[125] and its high chemical and biological stability and biocompatibility.[126] PDMS is liquid at room temperature and has a low surface energy (20-23 dynes/cm^2). These unique characteristics can be explained by the fact that the siloxane backbone has a high flexibility, the high bond energy of the siloxane bond, the low intermolecular forces between the methyl groups on silicon, and the partially ionic nature of the siloxane bond. It is used in heart valves, coating of plasma bottles, and due to its high oxygen permeability, for contact lenses.

Poly(2-methyl-2-oxazoline) (PMOXA), also known as poly[(N-acetylimino)ethylene][10], was chosen because of its hydrophilic[113] nature and because of its low toxicity and low protein adhesion.[113, 127, 128] This makes it an ideal candidate for in vivo applications. Poly(methyloxazoline) has a glass transition temperature of 65-70 °C, depending on the molecular weight.[129]

The choice of polymers was made based on considerations regarding the characteristics needed for the production of vesicular structures upon self-assembly of amphiphilic block-copolymers. For this, the middle block should be hydrophobic and display a high flexibility, whereas the side chains should be highly hydrophilic and show also a good degree of flexibility to behave similarly as the well known PEG, imparting stealth features to the surface of the final vesicles. In this respect, poly(2-methyloxazoline) has been recommended by other groups.[130]

for the distribution of sizes of particles or aggregates, such as micelles or vesicles. On the other hand, a monodisperse system contains entities of the same size, hence, it is homogeneous with respect to size.

[9] The poly(dimethylsiloxane) chain is free of steric interferences between its substituents, owing to the length of the Si-O bond (1.65 Å) and the larger angle between Si-O-Si.[122] P. J. Flory, *Principles of Polymer Chemistry*, **1953**.

[10] Poly(2-methyl-2-oxazoline) is also known as poly(N-acetylethylenimine).

Moreover, the mass ratio of hydrophilic to hydrophobic blocks was also kept in the range 20-40 % as found for other vesicle-forming polymers.[31]

3.1.1.3. Results and discussion

Literature indicates two ways for the synthesis from cyclic imine ether monomers: the addition of a second monomer to a living polymerization of the first monomer (one-pot sequential reaction) or the initiation of the cyclic imino ether polymerization by a macromolecular initiator. Here, the latter approach was chosen to prepare ABA type block-copolymers starting from α,ω-telechelic[11] PDMS, (α,ω-bis(3-hydroxypropyl)-poly(dimethylsiloxane)) via cationic ring-opening polymerization (CROP) of 2-methyl-2-oxazolines.

The CROP should provide very a low polydispersity index (PI)[12] for the side chains. A low polydispersity is only assured when all the chains start at the same time. In the case of ionic living polymerizations, the degree of polymerization (DP)[13] of the resulting polymer is found to be very close to the feed ratio of the monomer to initiator.[117]

Fig. 3.1.1.3.1: Chemical structure of the monomer used, 2-methyl-2-oxazoline (left), and of the triflic anhydride.

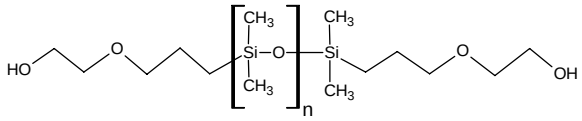

Fig. 3.1.1.3.2: Chemical structure of the telechelic PDMS used as starting material for the synthesis of the ABA triblock-copolymers.

To obtain parallel and simultaneous growth from both end groups of PDMS, its alcohol groups must be converted into more reactive groups first to give a reactive bifunctional macromonomer. For this purpose the starting PDMS is treated with 2.1 equivalents of trifluoromethansulphonic acid anhydride (TfSA) in presence of triethylamine (TEA) at 0 °C under Argon. Triflate groups are ideal candidates for initiation[116] of cyclic imino ether polymerization due to

[11] The term telechelic is used to describe polymers which possess at least two functional (reactive), end groups, that is, α,ω-functionalized polymers[118] O. Nuyken, S. Pask, *Encycl. Polym. Sci. Eng.* **1989**, *16*, 494..

[12] The polydispersity index, PI , which is a measure of the breath of the molecular weight distribution, is defined as $PI = \overline{M}_w / \overline{M}_n$ and therefore is always >1.

[13] The degree of polymerization denotes the number of repeating units per polymer chain, and is described as $DP = M_i / M_o$. The number average degree of polymerization $\overline{DP}$, is given by $\overline{DP} = \overline{X}_n = \overline{M}_n / M_o$, where M_o is the molecular weight of the polymer and $\overline{M}_n$ the number average molecular weight.

the highly living character of the resulting onium/triflate ion pair as the active propagating species.[114, 131]The triflate (TfS) is a very reactive leaving group and strong electrophile, even more than the tosylate,[114, 132] providing a fast leaving group ($CF_3SO_3^-$=TfO^-) upon approach of an attacking methyloxazoline monomer (nucleophile).[133]

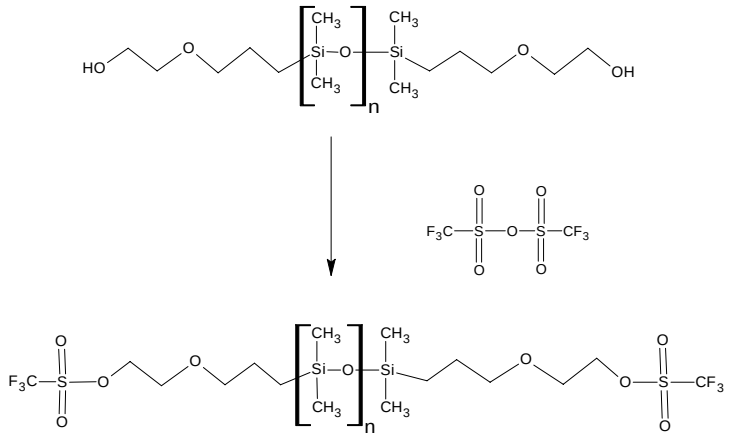

Scheme 3.1.1.3.1: Initial activation step in the synthesis of ABA triblock-copolymers used in this work

A key factor to ensure a proper polymerization and to diminish side reactions is to avoid reaction with water present in the system, which would give a side reaction with the anhydride. In order to minimize this effect, before addition of TfSA, PDMS was dried in hexane under reflux (Soxhlet) over Molecular sieve 4Å.

One disadvantage of the use of triflates is their known oxidizing properties.[134] Since triflic acid is usually used as catalyst for the equilibration reactions of PDMS,[123, 126, 135] it can promote the backbiting of PDMS, by equilibration or redistribution reactions.[123, 124] To avoid this, triethylamine (TEA) was added to form the salt of the acid trifluoromethanesulphonic acid (TfS). The insoluble salt in hexane can be filtered with the aid of a frit glass filter (G4). To obtain a good filtration rate and avoid clogging of the filter, it is necessary to work under cooling conditions. Moreover, for a good separation of the salts from the activated PDMS, the solvent must be first evaporated under vacuum and then the residue re-dissolved with cold hexane (at 0 °C). Only after such procedure was it possible to obtain a good separation of the insoluble salts from the activated PDMS. A complete absence of the salt is a necessary prerequisite for a cationic ring opening polymerization. Any salt present would act as an initiator yielding free poly(methyloxazoline) chains.

Propagation of 2-substituted-2-oxazolines proceeds via nucleophilic attack of the monomer on the C-O bond of the oxazolinium ion.[24] The CROP was performed in dried ethyl acetate and distilled 2-methyl-2-oxazoline. In this step the solvent volume is a key parameter, if the amount of solvent is too low then propagation of PMOXA is hindered due to the high viscos-

ity of the mixture. To end cap the growing methyloxazolinium groups a mixture of potassium hydroxide in methanol was added to the reaction mixture,[117, 136] to yield alcohol end groups.

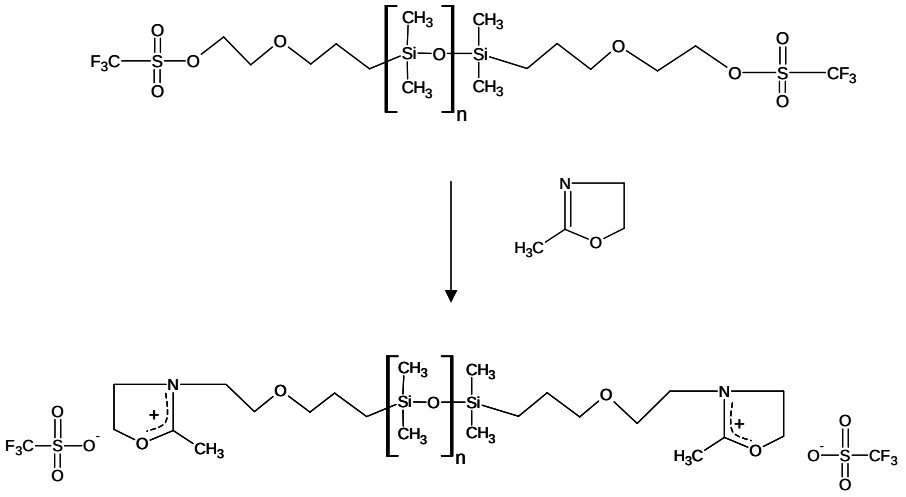

Scheme 3.1.1.3.2: Polymerization step, initially the nucleophilic N atom of the monomer, 2-methyl-2-oxazoline, attacks the carbon adjacent to the triflate groups.

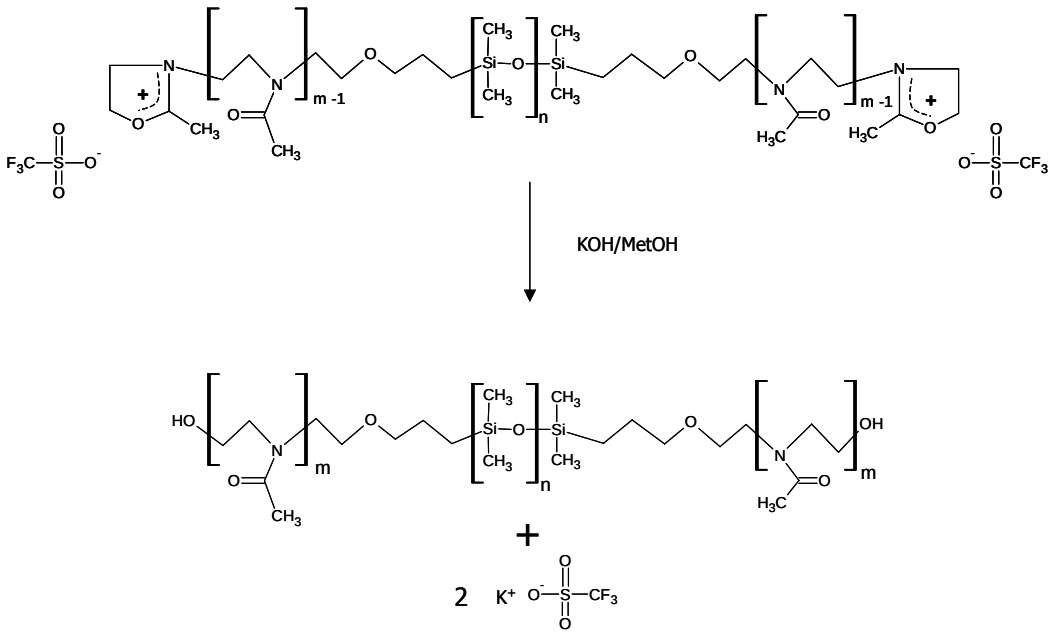

Scheme 3.1.1.3.3: Final step of the polymerization, end capping with OH groups.

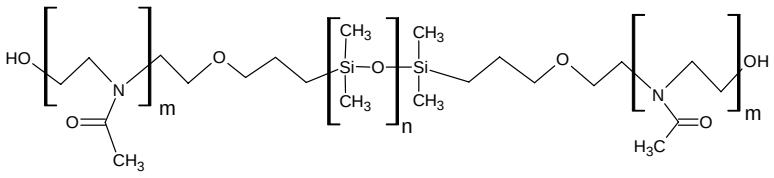

Fig. 3.1.1.3.3: Molecular formula of an alcohol terminated PMOXA-PDMS-PMOXA triblock-copolymer.

Due to the living character of the cationic ring opening polymerization, the degree of polymerization (DP) of the side chains is expected to be close to the monomer/initiator feed ratio[14] ($[M]_0/[I]_0$).[117, 137, 138] From the data of the polymerizations (see Section 3.1.3.1) this value was lower than expected. This can be explained by side reactions, such as the initiation of free methyloxazoline chains from triflates in the reaction mixture. Apparently, these poly(2-methyl-2-oxazoline) free chains were not completely removed by ultrafiltration as expected.

Although living polymerizations can yield narrow molecular weight distributions, here a high polydispersity (PI>1.2) was observed by GPC. This can be attributed to the polydispersity of the starting PDMS block (see Section 3.1.3.1). Usually PDMS is obtained by so-called redistribution type reactions.[123, 124] Gaussian molecular weight distributions are a consequence of the inherent nature of the equilibration reactions of siloxanes. Moreover, this high polydispersity can be worsen if triflic acid is present during the reaction, since it promotes the backbiting of the PDMS chain resulting in broader molecular weight distributions.[123]

3.1.2. End group functionalization of ABA triblock-copolymers

3.1.2.1. Introduction and theoretical considerations

For immobilization purposes we wanted to produce functionalized polymers that are able to interact with other molecules or functional groups on a surface. These functional groups include carboxylic groups, amino groups, thiol groups, and more biology-related ones, such as biotin.

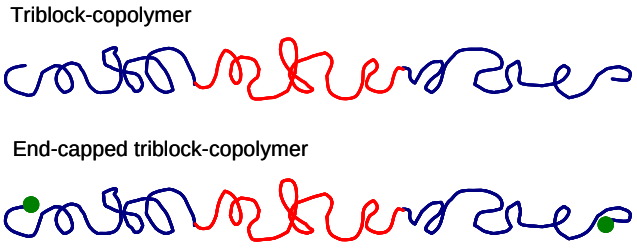

Fig. 3.1.2.1.1: Schematic representation of an end-capped triblock-copolymer.

Polymers can be functionalized although in general this is more difficult than with small molecules because of the occurrence of side or secondary reactions. Conversions and yields found in polymer reactions are usually lower than those of analogous reactions in small model compounds.

Some causes for the difference between the yields encountered in polymer reactions and low molecular weight model compounds are: **1.** Crystalline domains in the polymer that do

[14] Also termed the monomer to initiator initial ratio.

not dissolve completely are not available to the reagent, **2.** Neighboring effects may lead to inhibition of the reaction due to electrostatic or steric effects, or promote the reaction by auto-acceleration, **3.** The environment of the functional group within the polymer molecule might not be the same as in the low molecular weight compound, mainly due to the steric effects from coiling of the polymer backbone or pendant sustituents of the chain.[27]

Here, we wanted to introduce functional groups at the ends of the polymer chain. This results in a somewhat easier reaction procedure, but it must be considered at all times to use reactions that do not disrupt the functionalities already present in the backbone, thus preserving the structure of the polymer. Due to their small size in comparison to the polymer, functionalities at the polymer end should not change the characteristics such as solubility and self-aggregation properties of the polymer. Hence, it is expected that the aggregation characteristics of the base polymer will be retained after such modifications.

To increase the yield of the reactions an excess of the reactant is usually used to shift the reaction to completion. In most cases, even though not all chains are fully functionalized mixtures of modified and unmodified polymer can still be of use. It is not always required that the functionality of the polymer is present at 100% occurrence. It is only important then, to determine the percentage of functionalization.

Two different approaches can be considered for end-group functionalization. The most obvious approach involves the introduction of a functional group during the termination step of the polymerization reaction by end-capping.[28] Cationic ring opening polymerizations require the introduction of a nucleophile to terminate the reaction.[131, 139] For example, the polymerization of 2-methyloxazoline can be terminated with potassium hydroxide in methanol[136, 140, 141], which introduces an alcohol functionality. Other nucleophiles can be used in this termination step to introduce a different functionality.[142, 143] Because the introduction of the functionality takes place as one of the polymerization steps, this approach is usually denominated "direct method",[131] end-capping,[118] or terminator method.[112, 142, 143]

A second approach to introduce an end-group makes use of the broad spectrum of available chemical transformations on an already existing functionality, and it is therefore called, "indirect method"[131] in this thesis. This second approach has the advantage of providing a wide variety of functionalities that may not be accessible by the direct method. One major disadvantage of this approach is the complicated purification.

3.1.2.2. Biotinylated ABA triblock-copolymers

For anchoring vesicles onto surfaces active groups on vesicle surface are necessary. Self-assembled end-capped block-copolymers are the most direct approach to functionalized vesicles. Biotin-streptavidin or similar receptor-ligand coupling provides a platform for anchoring

polymers to other molecules or surfaces (see Section 3.3.1). We have thus used biotinylated ABA triblock-copolymers.

To obtain biotin end groups, the hydroxyl end groups of poly(2methyl-2-oxazoline)-b-poly-(dimethylsiloxane)-b-poly-(2-methyl-2-oxazoline) triblock-copolymer were esterified with biotin,[144] in the presence of dicyclohexylcarbodiimide (DCC) and 4-(dimethylamino)pyridine (DMAP), a known catalyst of the acylation of alcohols.[145]

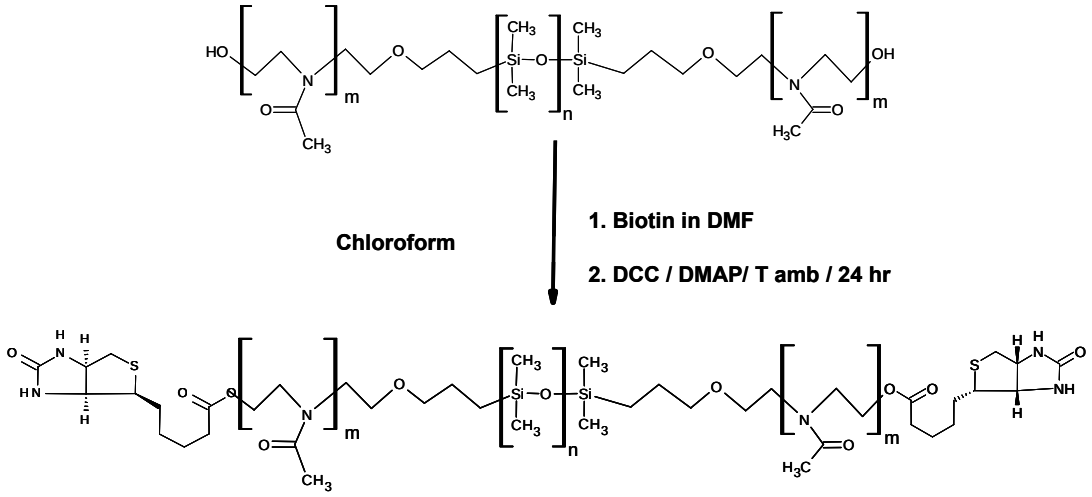

Scheme 3.1.2.2.1: Reaction scheme and conditions for the functionalization of ABA triblock-copolymer with biotin end-groups.

The detailed characterization of the polymer is described in Sections 3.1.3.1 and 3.1.3.2.

3.1.2.3. Fluorescently labeled ABA triblock-copolymers

Fluorimetric techniques are excellent tools for studying dynamics and conformations of polymer chains, and can be used to follow aggregation processes. One option to track or follow vesicles is to covalently attach a fluorescent marker to the constituting unimers.[146] By using the already discussed indirect approach for end-group polymer modification, the existing alcohol groups of the polymer can be coupled to a fluorescent probe.

Selecting criteria for the fluorescent label were reactivity, solubility, and optical properties. Carbonylazide, acyl-nitrile, anhydrides, and n-methyl-isatoic-anhydride are appropriate for reaction in organic solvents.[147] From about ten candidate molecules, 7-diethylaminocoumarin-3-carbonylazide was the most suited for the purpose due to its solubility, emission characteristics, and stability.

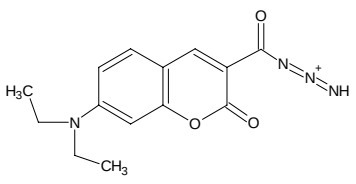

Fig. 3.1.2.3.1: Structure of the coumarin carbonyl azide used

The carbonylazide is thermally converted into the unstable isocyanate via the *Curtius-rearrangement* (see Scheme 3.1.2.3.1). In the presence of hydroxyl groups the isocyanate is converted to a stable urethane. Therefore, it is of key importance to work under water free conditions, otherwise a conversion of the isocyanate into a non-reactive amine would occur.

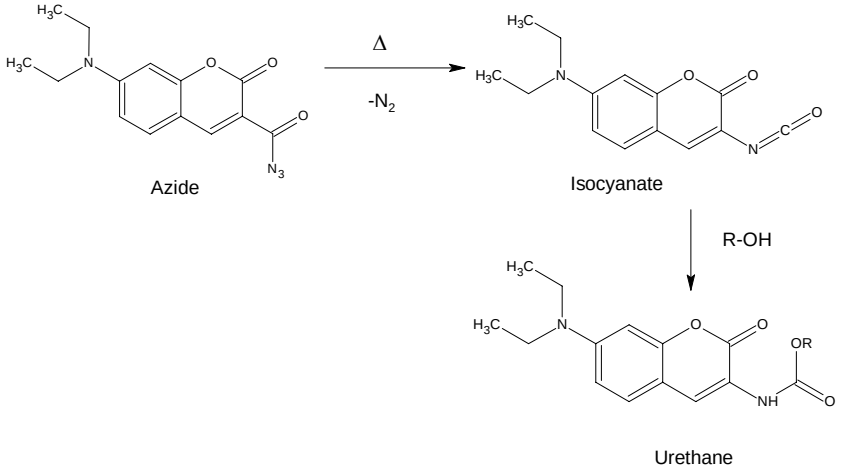

Scheme 3.1.2.3.1: Curtius-rearrangement

With a 20% excess of the coumarin and 22 h of reaction time, a successful modification of the alcohol groups was achieved. The end-capping of the terminal alcohol groups of a PMOXA-PDMS-PMOXA triblock-copolymer with the azide acid group of a fluorescent marker was successful and proceeded with good yields (97%). The degree of functionalization determined by ^{1}H-NMR was only 60%. In order to obtain higher degree of functionalization it would be recommended to increase the excess of the coumarin with respect to the base polymer. The fluorescence properties of the labeled triblock-copolymer are given in Sections 3.1.3.3 and 3.2.2.2.

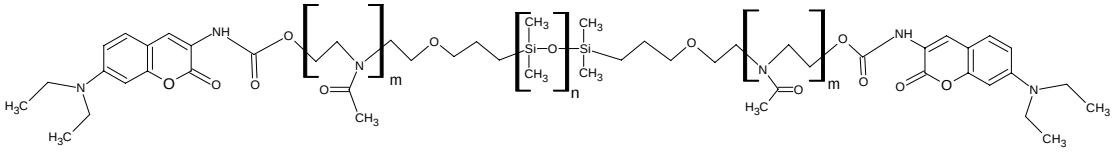

Fig. 3.1.2.3.2: Molecular formula of the coumarin modified polymer.

3.1.3. Characterization techniques and assays

3.1.3.1. Polymer characterization by ^{1}H-NMR, GPC, and IR

NMR can be used to estimate the number average molecular weight of polymers,[24, 123] and sometimes to quantify their end groups when the signals are different from the repeating units. In polymers, as a consequence of slower molecular motions the lines of NMR broaden. This can obscure some peaks in the vicinity of the peaks from the repeating units of the poly-

mer chain. Moreover, owing to the high intensity of the peaks of the repeating units, quantification of peaks of end groups is problematic.

^{1}H-NMR was used for the confirmation of the end-capping of the polymerization reaction. The disappearance of the peaks at 4.4 ppm and 5.0 ppm due to the methylene protons of the terminal oxazolinium group was used to verify termination.[117, 136, 140, 148]

The degree of polymerization of the polymer precursor, PDMS, was calculated from the values of the end group titration reported by the manufacturer and confirmed by the integral ratio of CH_3-Si protons (see signal **a** in Scheme 3.1.3.1.1) to the methylene protons of the side chains (signals **b**, or **f** and **e** in Scheme 3.1.3.1.1).

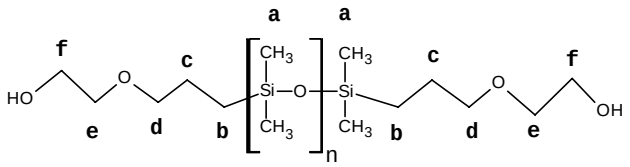

Scheme 3.1.3.1.1: Assignment of the ^{1}H-NMR signals of the pre-polymer PDMS.

NMR signal	ppm	N° of groups	Group	Integral	
a	0	(2xn)+2	O-Si-**CH3**	3 x (2n+2)	6n + 6
b	0.5	2	Si-**CH2**-CH2	2 x 2	4
c	1.5	2	Si-CH2-**CH2**-CH2-O-CH2	2 x 2	4
d	3.7 - 3.8	2	Si-CH2--CH2-**CH2**-O-CH2	2 x 2	4
e	3.7 - 3.8	2	O-**CH2**-CH2-OH	2 x 2	4
f	3.7 - 3.8	2	O-CH2-**CH2**-OH	2 x 2	4

Table 3.1.3.1.1: Peak assignment corresponding to the pre-polymer PDMS.

The pre-polymers were analyzed by GPC and the corresponding values are presented in the following table (Table 3.1.3.1.2).

	GPC			^{1}H-NMR
PDMS Starting block	**Mn (g/mol)**	**Mw (g/mol)**	**PD**	**Mn (g/mol)**
KF6001	2470	3491	1.41	1806
KF6002	2983	5730	1.92	3200
KF6003	5004	8347	1.67	5600
SA-PDMS1	4537	7826	1.72	5600
SA-PDMS1 (2nd peak)	131	218	1.65	
SA-PDMS2	4957	8475	1.7	5600
SA-PDMS2 (2nd peak)	180	231	1.3	

Table 3.1.3.1.2: Results of the GPC examination of the PDMS pre-polymers used as middle blocks. KF is the code of Shin-Etsu Company, SA stands for Sigma-Aldrich.

The second peaks observed (Table 3.1.3.1.2) with the PDMS from Sigma-Aldrich can be attributed to the presence of impurities. Poly(dimethylsiloxanes) are usually synthesized by equilibration or redistribution reactions of cyclic species such as octamethycyclotetrasiloxane (D_4, M_n=296 Da) and hexamethylcyclotrisiloxane (D_3, M_n=222 Da). If not properly removed,

these species contaminate the final product.[123] The KF-series polymers do not show this peak since they were purified by thin-film evaporation.[61] Cyclic siloxanes can be removed by vacuum distillation at 150 °C.[123]

Typical NMR spectra are shown in Fig. 3.1.3.1.1 and Fig. 3.1.3.1.2.

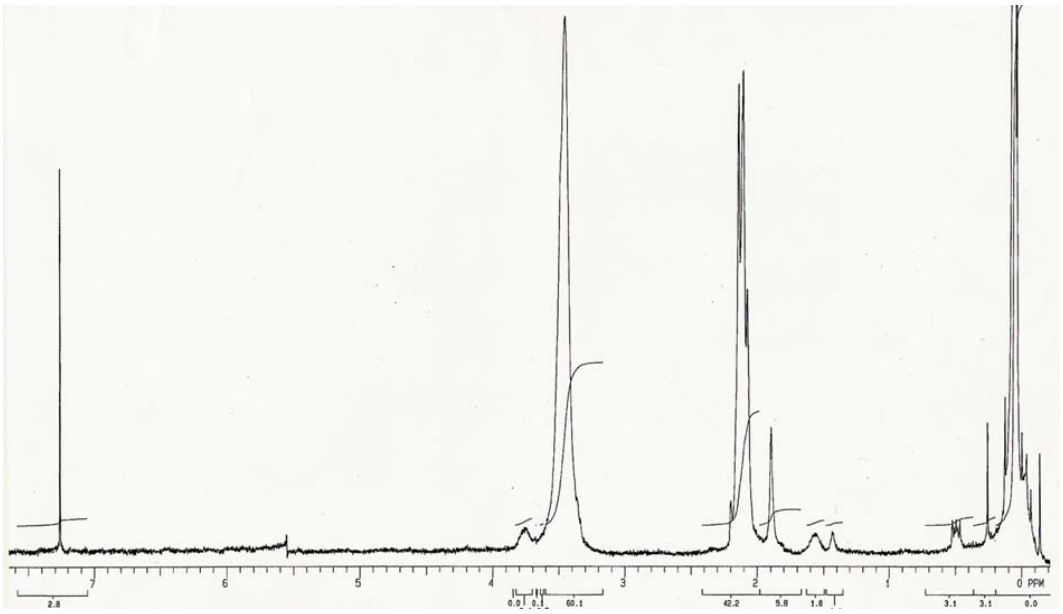

Fig. 3.1.3.1.1: ^{1}H-NMR of JW05 parent (unmodified) ABA triblock-copolymer.

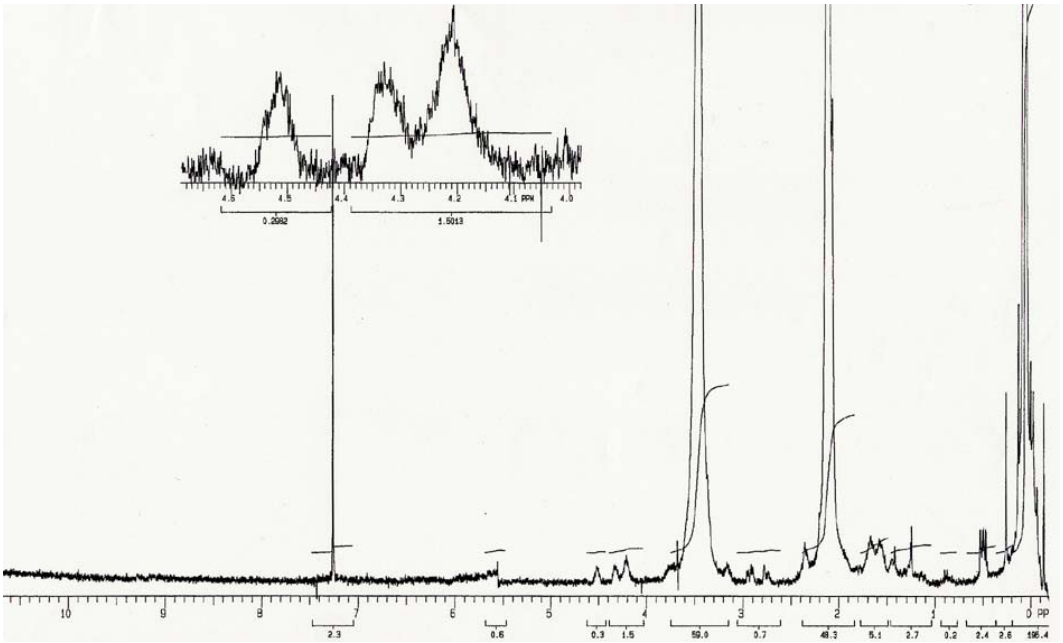

Fig. 3.1.3.1.2: ^{1}H-NMR of biotinylated JW05 polymer (JW05 ModA)

For the biotinylated polymers (JW05ModA and JW05ModB), the presence of the biotin moiety was corroborated via ^{1}H-NMR: 1.5-1.8 (*m*, 12 H, bC**H**$_2$ C**H**$_2$ C**H**$_2$), 2.35 (t, 4H, bO=CO-C**H**$_2$), 2.75 (*d*, 2 H, bSC**H**$_{2a}$CH), 2.91 (*m*, 2 H, bSC**H**$_{2b}$CH), 3.15 (*m*, 2 H, SC**H**(CH)CH$_2$), 4.2 (*m*,

2 H, SCHC**H**NHC=O), 4.32 (*m*, 2 H, SCH_2C**H**NHC=O), 4.5 (*m*, 2 H, N**H**C=O). However, this method for the estimation of the degree of functionalization is not very accurate and significant error is incurred due to imperfect baselines, and mainly due to the large difference in areas.[111, 149] From the ratio of the peak area ascribed to the biotin moiety the degree of functionalization can be estimated to be approximately 50%.[143]

The presence of the coumarin moiety at the ends of the polymer chains was confirmed by the following peaks: 6.5 (m, 1H, C(ar)-**H**), 6.7 (m, 1H, C(ar)-**H**), 7.2 (m, 1H, C(ar)-**H**), 8.2 (m, 1H, C(ar)-**H**). The degree of functionalization with coumarin-labeled triblock-copolymer was estimated to be approximately 60%. It is important to notice that the degree of functionalization was determined by NMR, which is not the optimal method since the signals for the coumarin moiety are quite low compared to those of the polymer itself.

By comparing the integral of the proton signals from the N-acetyl groups of the PMOXA to the signals from the methyl groups bonded to the silicon backbone, the number average molecular weights was determined for the ABA triblock-copolymers. The methylene groups of the PMOXA can be also used for this purpose.[148]

Typical peaks for poly(2-methyl-2-oxazoline) are summarized in Scheme 3.1.3.1.2 and Table 3.1.3.1.3.

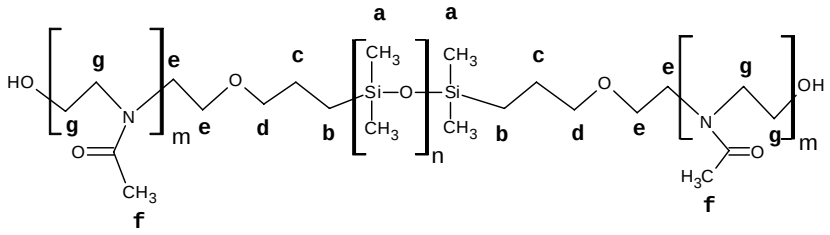

Scheme 3.1.3.1.2: Scheme of the assignment of the ^{1}H-NMR signals for the ABA triblock-copolymer PMOXA-PDMS-PMOXA.

NMR signal	ppm	N° groups per chain	N° of chains	N° of H per group	Group	Integral	
a	0	(2xn)+2	1	3	O-Si-**CH3**	[(2xn)+2] x 1 x 3	6n + 6
b	0.5	1	2	2	Si-**CH2**-CH2	1 x 2 x 2	4
c	1.5	1	2	2	Si-CH2-**CH2**-CH2-O-R	1 x 2 x 2	4
d	3.7 - 3.8	1	2	2	CH2-**CH2**-O-CH2	1 x 2 x 2	4
e	3.3 - 3.5	2	2	2	O-**CH2-CH2**-N-RR'	2 x 2 x 2	8
f	2.0 - 2.2	m	2	3	RR'N-CO-**CH3**	m x 2 x 3	6m
g	3.3 - 3.5	(2 x m)	2	2	N-**CH2-CH2**-N-RR'	(2 x m) x 2 x 2	8m
g'	3.3 - 3.5	2	2	2	HO-**CH2-CH2**-N-RR'	2 x 2 x 2	8

Table 3.1.3.1.3: Predicted proton shifts for the different groups present in the PMOXA-PDMS-PMOXA block-copolymers.

Polymers were characterized by ^{1}H-NMR and as expected from the living character of the polymerization, the degree of polymerization obtained was close to the initial molar ratio of monomer to initiator $[M_0]/[I_0]$.[114] However, in some cases the obtained degree of polymerization for the PMOXA chains was lower than the one expected. This can be explained by the occurrence of side reactions yielding free homopolymer chains.

Polymer	GPC			^{1}H-NMR		
	Mn	Mw	PD	Mn total	Mn PMOXA	Mn PDMS
JW05	5720	9473	1.65	7090	1105	4878
JW05-ModA	5537	9029	1.63	7090	1105	4878
S118	4903	7850	1.60	8490	1445	5600
S119	2767	5215	1.88	9510	1955	5600
S120	4962	8719	1.75	8150	1275	5600
S121	4380	8226	1.87	8490	1445	5600
S122	4264	8316	1.95	8490	1445	5600
S123	4841	9987	2.05	8320	1360	5600
S124	4378	9288	2.12	9510	1955	5600
S125	2867	4796	1.67	8830	1615	5600
S126	1836	2931	1.60	2742	765	1212
S127	2337	4350	1.86	8962	2210	4542
S130	4232	6608	1.56	8830	1615	5600
S131	3738	6607	1.77	8660	1530	5600

Table 3.1.3.1.4: Comparison between GPC and ^{1}H-NMR data. Number average molecular weight (M_n), weight average molecular weight (M_w) and polydispersity (PD) obtained by GPC (solvent: THF, temp. 23°C, polystyrene standard calibration). Number average molecular weight for the total polymer (M_n), and partial number average molecular weights for the constituting blocks obtained by ^{1}H-NMR.

M_n and M_w obtained by GPC tend to be lower than values from ^{1}H-NMR, for both the pre-polymer and the ABA triblock-copolymer. This can be explained by the fact that GPC is a relative technique and this kind of discrepancies are observed when using polymers of different nature for the calibration, e.g. polystyrene.[112, 150, 151] Contrary to this, when calculated based on the known M_n of the hydrophobic block, the M_n of the hydrophilic block obtained by ^{1}H-NMR gives number average molecular weights that are closer to the monomer to initiator ratios. For this reason the overall M_n of the polymer obtained by ^{1}H-NMR has been used throughout this thesis as the nominal molecular weight of the polymer.

The molecular weight distributions observed are rather broad (PD> 1.5). This can be attributed to the large polydispersity of the starting PDMS block (see Table 3.1.3.1.2), because we can expect that the molecular weight distribution of PMOXA is low due the living character of the polymerization. This was confirmed by preparation of homopolymer chains.[114]

The following figures present some typical molecular weight distributions for the ABA triblock-copolymers studied.

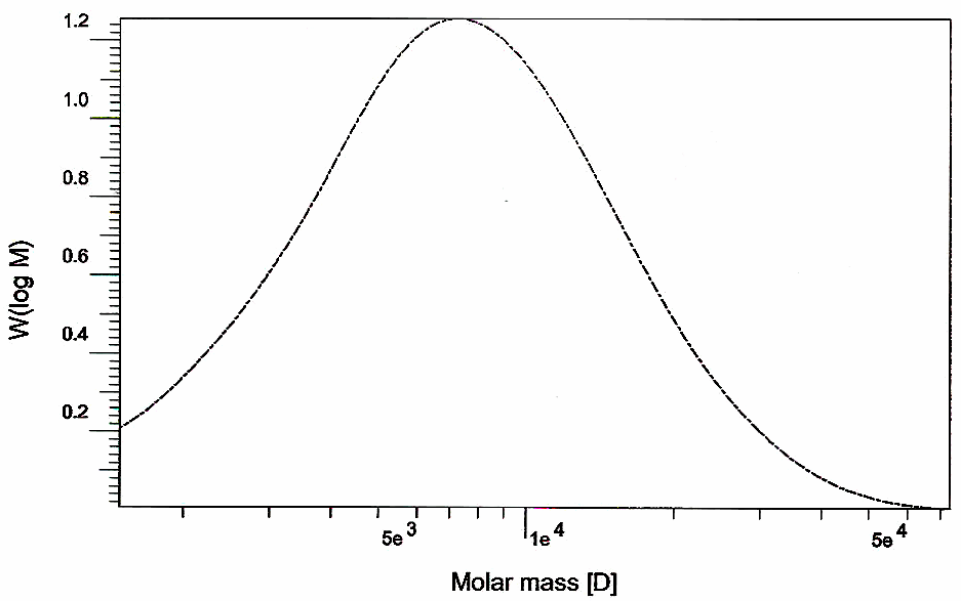

Fig. 3.1.3.1.3: Molecular weight distribution of JW05 obtained by GPC.

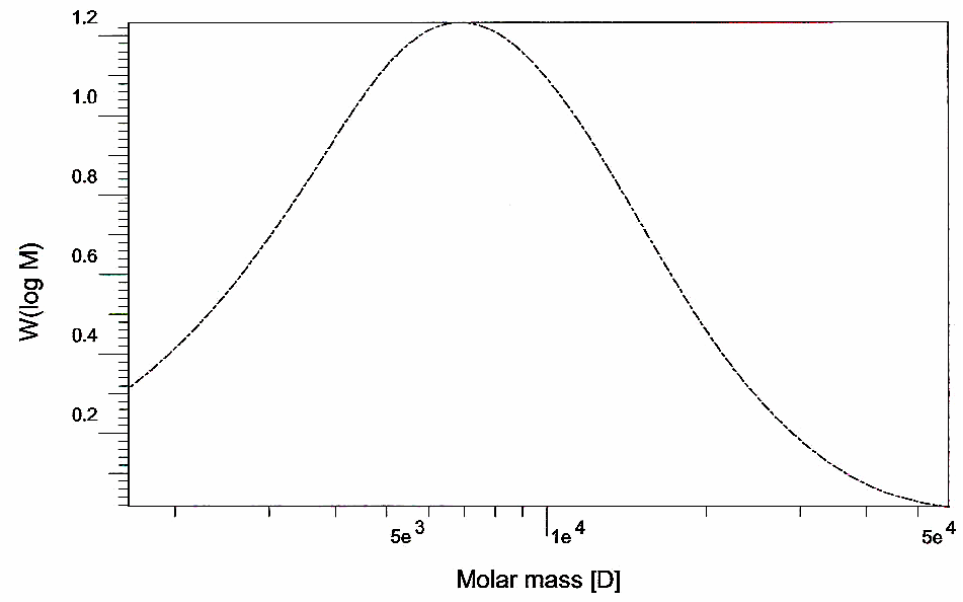

Fig. 3.1.3.1.4: Molecular weight distribution of JW05-ModA (biotinylated polymer) obtained by GPC.

Infrared spectroscopy was used to corroborate the presence of the expected groups in the block-polymers and functionalized polymers. Some typical spectra are shown in Fig. 3.1.3.1.5 and Fig. 3.1.3.1.6.

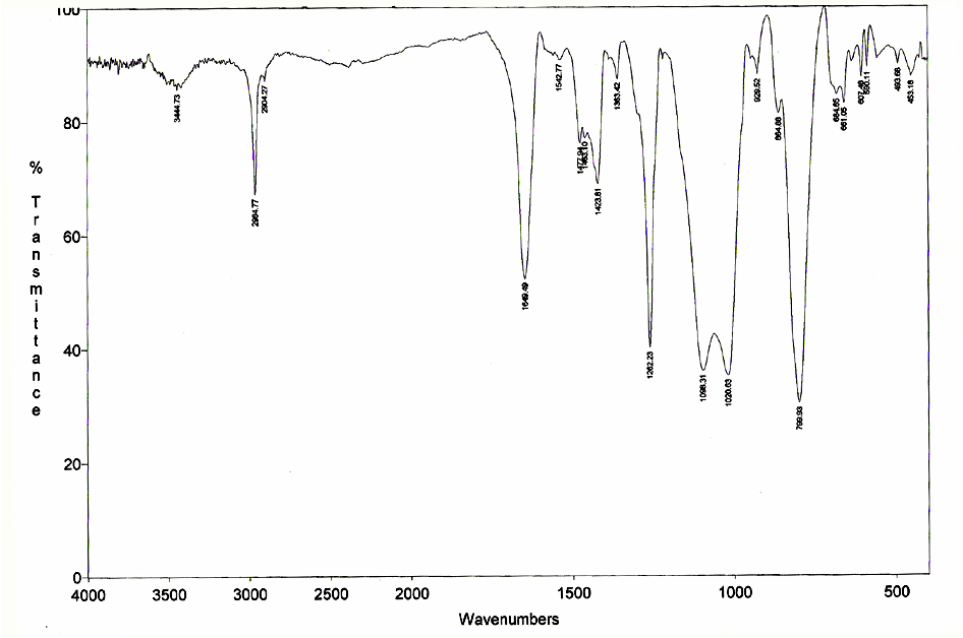

Fig. 3.1.3.1.5: IR spectrum of JW05 parent (unmodified) ABA triblock-copolymer.

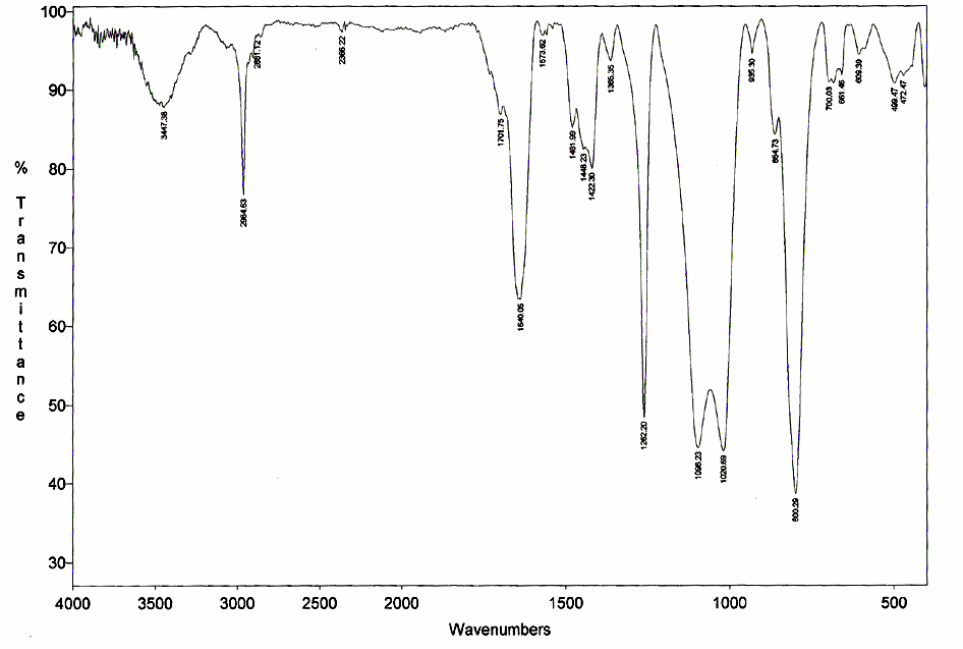

Fig. 3.1.3.1.6: IR spectrum of biotinylated JW05 polymer (JW05 ModA).

The pronounced amide band at 1640-1650 cm^{-1} is characteristic for the presence of a tertiary amide group, which is created upon the ring-opening polymerization of 2-oxazolines.[131, 152] The strong bands at 1480, 1422, and 1363 cm^{-1} are assigned to the CH_3-Si group, whereas the peak at 800 cm^{-1} is due to the $(CH_3)_2$-Si. Peaks at 1097 cm^{-1} and 1020 cm^{-1} correspond to Si-O and Si-O-Si groups, respectively.

3.1.3.2. Characterization and quantification of biotinylated ABA triblock-copolymer

It was of interest, however, to quantify the amount of biotin in the polymer in order to determine the yield of the reaction and for the subsequent coupling with streptavidin. Since ^{1}H-NMR could not yield quantitative results, a method involving a reaction of the amino group of biotin with 4-(dimethylamino)-cinnamaldehyde (DACA)[153] was utilized. This reaction takes place in acid medium forming a red cyanine compound with a λ_{max} of 531 nm that can be detected by UV-Vis spectroscopy.

Only one amino group of the biotin reacts with the DACA,[153] and the reaction proceeds immediately to form the red cyanine, which is stable between 15 and 35 min after formation. Therefore, all samples were measured between 20 to 25 min after addition of the DACA.[153]

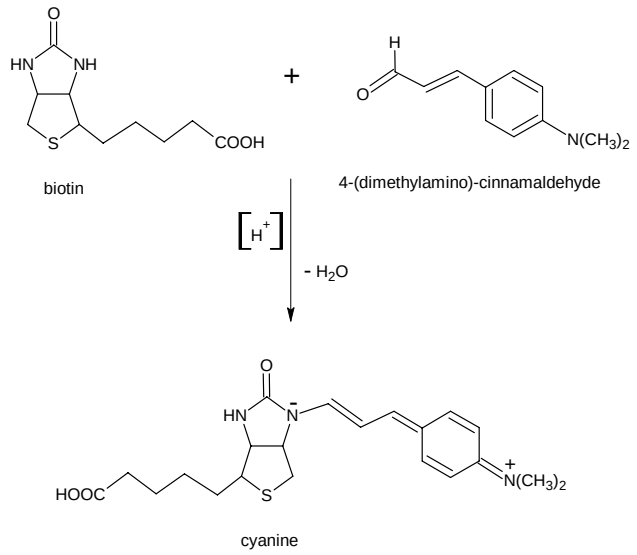

Scheme 3.1.3.2.1: Reaction used for the characterization of biotin. Biotin reacts with 4-(dimethylamino)-cinnamaldehyde (DACA) to give cyanine. Taken from Schiewe et al.[153]

Peak shifts due to the polymer were taken into account by performing the relevant controls in the presence of added polymer. A blank with non-modified polymer (parent polymer) was used as a control. A calibration was performed with biotin and then the biotinylated polymer was analyzed in the same conditions. From the absorption of the biotinylated polymer, the biotin concentration could be established. After addition of DACA, the solution turned yellow when no biotin was present, while the biotin positive control turned red as expected, as well as the polymer containing biotin end-groups. This shows that biotin was detected, even though attached to the polymer and that there were no significant influences from the matrix.

The results of the calibration curve can be seen on Graph 3.1.3.2.1. Two series of biotin concentrations were analyzed as well as two samples corresponding to the modified polymers.

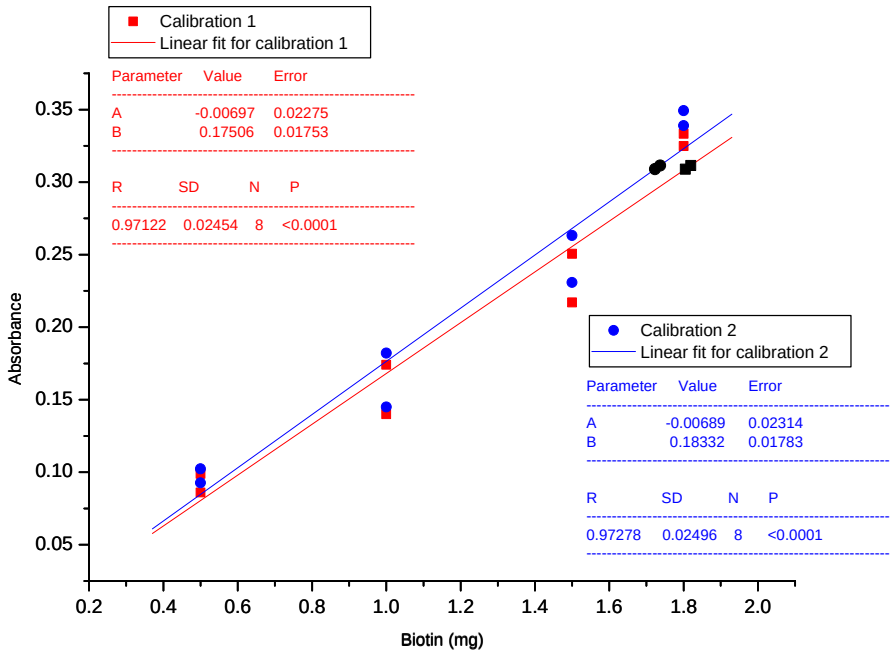

Graph 3.1.3.2.1: Calibration curves for 2 series of biotin samples with the respective linear regression and statistical parameters. The data points in black correspond to the values obtained for the absorbance of polymers ModA and ModB. Both curves have been used to interpolate the amount of biotin present in the polymers.

Polymer	Absorbance	Biotin (mg)-(Calib. 1)	Biotin (mg)-(Calib. 2)	Average Biotin (mg)
Mod A	0.30895	1.8	1.72	1.76
Mod B	0.31153	1.82	1.74	1.78

Table 3.1.3.2.1: Calculation of mass of biotin present in the polymer by the absorbance results obtained from Graph 3.1.3.2.1

Biotin (mg)	Moles biotin	Moles polymer	Molar ratio Biotin/Polymer
1.76	7.20E-06	6.80E-06	1.06
1.78	7.30E-06	6.80E-06	1.07

Table 3.1.3.2.2: Calculus of the molar ratio of biotin to polymer in the samples analyzed.

If each chain of polymer is modified at both ends (at 100% conversion) the molar ratio of biotin to polymer should be two. UV shows that on average only one polymer end is modified with biotin (50% conversion).

However, as the measurements were made in a water/ethanol (50% v/v) mixture, vesicles are present in a small proportion. This was confirmed by DLS measurements (see Section 3.2.2.1). If vesicles form, this implies that only one end of the polymer is available to the reactant. We can thus conclude that the modification with biotin is higher than 50%. However, con-

sidering that the quantification of the amount of vesicles in the solution is rather inaccurate, we cannot attribute a realistic biotin percentage on the modified polymer.

To prove that the biotin detected was not due to a simple mixing of non-attached biotin and polymer, but that it really was tethered to the polymer chains the sample was passed through a column of Sephadex G100. Any non-linked biotin should have been removed by SEC. Analysis of this purified sample gave also a red solution when hydrochloric acid and DACA were added, confirming the covalent attachment of the biotin to the polymer.

3.1.3.3. Fluorescently modified ABA triblock-copolymer

The fluorescence properties of the dye-labeled triblock-copolymer could be qualitatively determined. Since the non-modified polymer also showed an emission band itself, of unknown origin, a control spectrum for the non-functionalized polymer was recorded. The fluorescence of the non-modified polymer is low compared to the labeled one. Coumarin is, therefore, a good marker for the triblock-copolymers.

The optimal excitation wavelength was searched for the coumarin derivative of the ABA triblock-copolymer. Graph 3.1.3.3.1 shows the maximum of the excitation spectrum at 440 nm. Therefore, all subsequent measurements of the emission spectra were done with this excitation wavelength. Graph 3.1.3.3.2 and Graph 3.1.3.3.3 show the fluorescence spectra of the coumarin-modified triblock-copolymer and the parent polymer respectively. The emission spectra were measured in aqueous solutions (96% H_2O, 4% ethanol) at different concentrations.

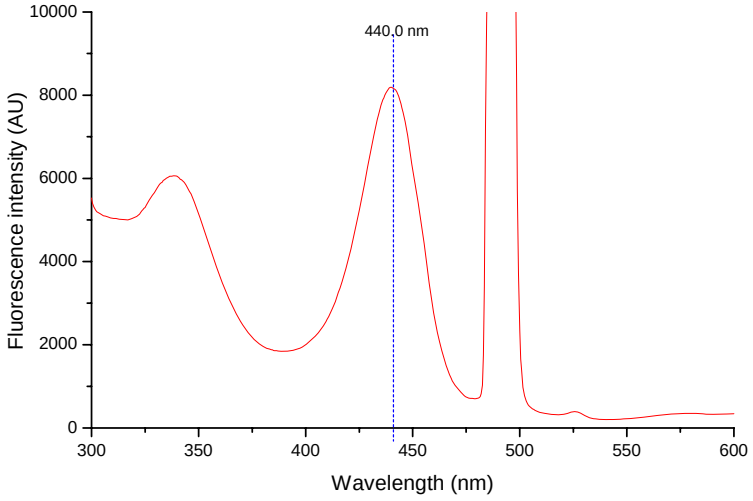

Graph 3.1.3.3.1: Fluorescence spectrum of Cm-PMOXA-PDMS-PMOXA-Cm with variable excitation wavelength (λ_{em} max= 499 nm)

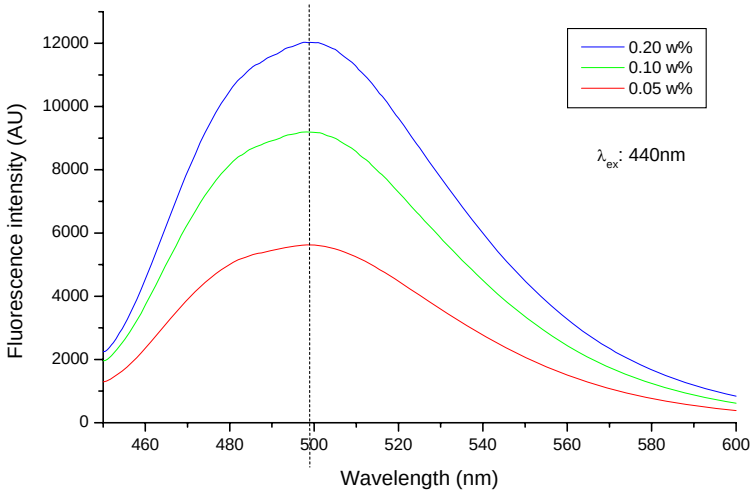

Graph 3.1.3.3.2: Fluorescence spectrum (emission) of Cm-PMOXA-PDMS-PMOXA-Cm with different concentrations.

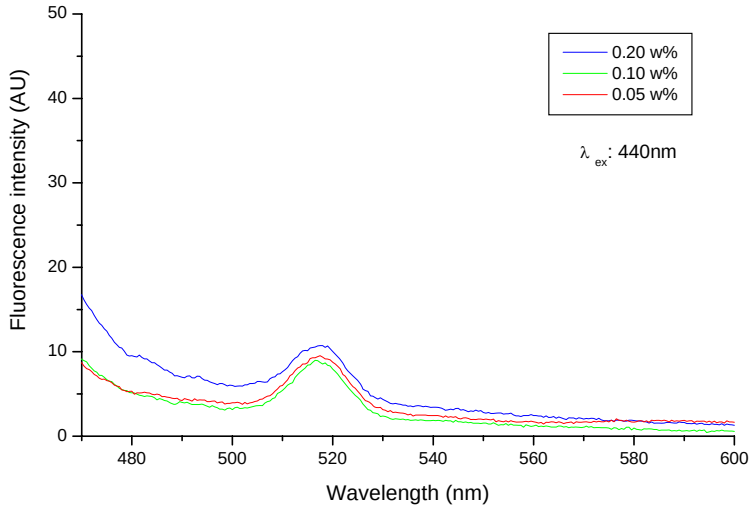

Graph 3.1.3.3.3: Fluorescence spectrum (emission) of PMOXA-PDMS-PMOXA (polymer code S125)

The fluorescent Cm-PMOXA-PDMS-PMOXA-Cm, showed an emission maximum at 499 nm (Graph 3.1.3.3.2), whereas the parent polymer, PMOXA-PDMS-PMOXA, had its maximum emission wavelength at 517 nm (Graph 3.1.3.3.3). This emission does not correspond to Raman scattering, since the maximum position does not depend on the emission wavelength (data not shown). The intensity ratio at the emission maximum between the fluorescently labeled Cm-PMOXA-PDMS-PMOXA-Cm and the non-modified PMOXA-PDMS-PMOXA was approximately 1000:1.

3.1.3.4. Block-copolymer monolayer isotherms

In order to characterize the amphiphilic behavior and the interfacial properties of ABA triblock-copolymers, monolayers of these polymers were prepared and their isotherms were obtained. A typical amphiphilic concentration of 1 mg/ml was used for spreading onto the subphase. Apart from chloroform, various solvents were also studied to get insight into polymer's spreading behavior. However, due to the dissolving characteristics of chloroform for both constituting blocks, and its high volatibility chloroform was the solvent of choice.

A series of compression-expansion cycles were performed to establish the stability of the monolayer films. The measurements were performed at room temperature, but without thermostatization. Hysteresis effects were observed on cycles of compression and expansion of the films, and can be attributed to either dissolution of the polymer in the bulk, internal rearrangement, or difficulty on re-spreading due to slow relaxation times.[154] Hysteresis isotherms are not shown here for simplicity. When possible, the collapse pressure Π_c[15] and the limiting molecular area A_0 for the condensed phase were determined by examination of the obtained isotherms.

Langmuir trough dimensions are usually optimized for small surfactant spreading. Due to the larger size of polymer molecules the available spreading area is too small to obtain the complete isotherm from one spreading aliquot. To overcome this a series of surface pressure versus area isotherms with different amounts of spread aliquots were performed. The complete isotherm curve is then obtained by overlaying of the individual partial isotherms. In the following graphs, the curves presented consist on the overlap of the individual isotherms obtained with different spreading volumes.

Graph 3.1.3.4.1 shows the isotherms of the different polymer studied. All monolayers showed similar results concerning the shape of the isotherms obtained. The pattern of Π-a depends on the chemical structure of the amphiphilic substance and on a number of experimental conditions (temperature, spreading solvent, compression rate, subphase composition, etc.). In general all the isotherms obtained for the different polymers, showed a similar profile. The isotherms presented liquid-expanded (up to 15 mN/m) and condensed (up to 55 mN/m) states. This behavior resembles the one of common low molecular weight amphiphiles, although the starting area per molecule is much higher in the case of polymer amphiphiles.

[15]Collapse pressure can be defined as the highest pressure to which a monolayer can be compressed without detectable expulsion of molecules from the film to form a new phase.

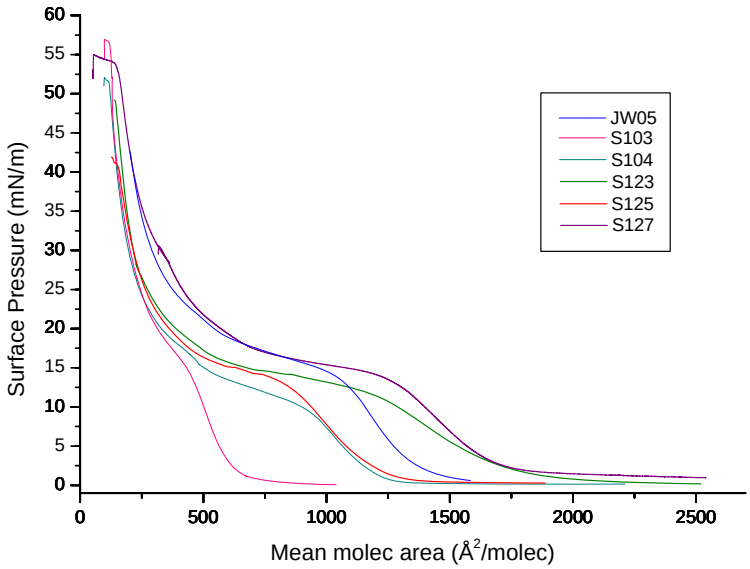

Graph 3.1.3.4.1: Surface pressure versus mean molecular area isotherms for a series of ABA triblock-copolymers for detailed information on the polymer used Table 3.1.3.4.1.

Moreover, all polymer monolayers presented a transition at approximately 15 mN/m. In low molecular amphiphiles this type of plateau region of the surface pressure (Π)-area (A) isotherm in most cases represents a two-phase coexistence region between a fluid-like low-density phase and a condensed phase.[155] Similar transitions have been observed with lipopolymers, and the transition has been attributed to the contribution of the hydrophilic chains, which are supposed to undergo a pancake-mushroom transition.[156, 157] The origin of the pancake-mushroom transition resides on desorption of the polymer chains from the water surface into the subphase. However, the nature of the transition occurring with the ABA triblock-copolymers studied is still not clear, and would require more in depth study. Additionally, to study the transition isotherms at different temperatures should be performed.

As a result of compression of the monolayer film, amphiphilic triblock-copolymers at the air-water interface are expected to undergo conformational changes. In particular for the case of symmetrical amphiphiles with a hydrophobic middle block, the molecules are expected to be in a loose conformation or coiled conformation at low surface pressures. In the gas-like phase the molecules are lying flat adsorbed on the surface in a pancake conformation, whereas in liquid-expanded region mushroom or hemispherical conformations occurs. Upon compression the molecules adopt more packed structures in the condensed states.[154, 158] The conformation expected in the condensed form or solid form, is one in which the middle-block forms an inverted U turn (see Figure 4.7.6) and with the hydrophilic blocks immersed in the subphase in a brush-like conformation.

Collapse pressures were not always observed, this can be explained by the fact that the polymers used show a high degree of flexibility and some water solubility. Collapse is observed when the surface concentration is too high to accommodate the molecules at the available trough area. Partial solubilization at high surface pressure can occur when the amphiphiles show some water solubility.

The limiting molecular area, A_0, obtained by extrapolation of the slope of the isotherm curve in the region of condensed phase, gives an indication of the area per molecule at the most condensed state of the monolayer. Although A_0 can be taken as an indication of the size occupied by a molecule in the condensed state, it is important to notice that as A_0 results from the isotherm it is also influenced by the factors affecting the isotherm. Therefore, A_0 values are only indicative and by no means absolute values. The obtained A_0 for the polymers studied are summarized in Table 3.1.3.4.1, for better comparison the data of the polymers is also displayed. It is worth mentioning that the errors incurred in the determination of A_0 are quite high due to the intrinsic error of the extrapolation procedure.

Polymer $(A)_m$-$(B)_n$-$(A)_m$		A-Block			B-Block			A_0 (Å^2)
Code	Mn (g/mol)	Mn (g/mol)	w %	m	Mn (g/mol)	w %	m	
JW05	7090	1105	31	13	4878	69	62	315
S103	3470	765	44	9	1941	56	22	190
S104	6578	850	26	10	4878	74	62	270
S123	8320	1360	33	16	5600	67	72	304
S125	8830	1615	37	19	5600	63	72	370
S127	8962	2210	49	26	4542	51	59	370

Table 3.1.3.4.1: Number average molecular weight of the polymers studied as Langmuir films and their limiting area A_0 compared to the constituting blocks.

From a quick inspection of the values of A_0 displayed in Table 3.1.3.4.1, the limiting area A_0 seems to be related to the molecular weight of the poly(methyloxazoline) blocks. This relationship was further investigated and Graph 3.1.3.4.2 shows a double logarithm plot of M_n corresponding to the poly(methyloxazoline) chains versus A_0. These logarithmic data can be fitted with a linear regression with a slope of 0.6. This corresponds to the following relationship $A_0 = M_n^x$ with x equal to 0.6, which resembles the scaling law typical of coiled conformations, $\left\langle R_g^2 \right\rangle^{1/2} \propto N^{\nu}$, with ν, the Flory exponent, being 0.6 (for good solvents). This can be interpreted in terms of the conformation of the polymer chains in the most condensed state, which contrary to what expected, they do not form a completely stretched inverted U conformation (see Figure 4.7.6). A similar trend was observed with different ABA triblock-copolymers (see Appendix I), which confirms a behavior independent of the hydrophobic middle block. For a

more universal trend however, polymers with different hydrophilic blocks need to be investigated.

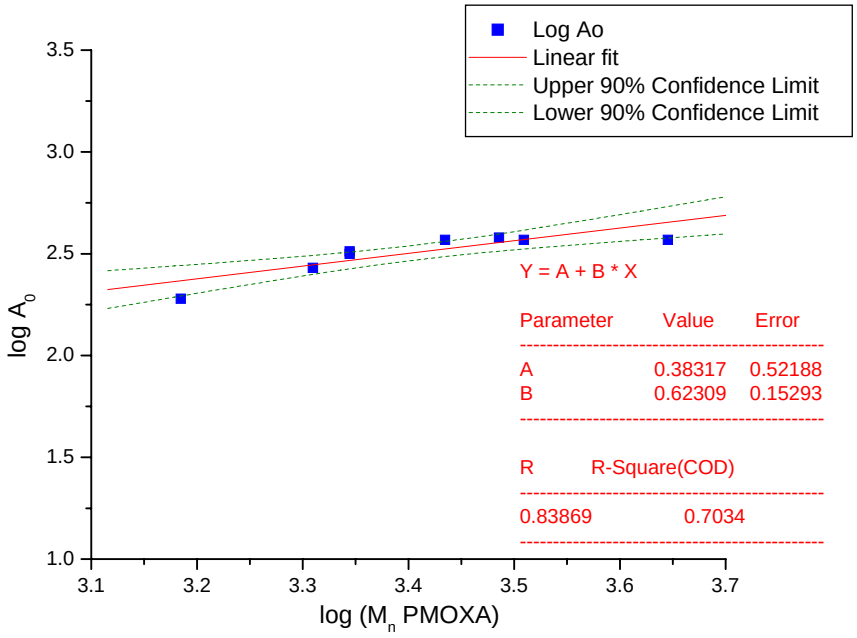

Graph 3.1.3.4.2: Double logarithm plot of M_n of PMOXA blocks versus A_0.

3.1.3.5. Interaction of biotinylated block-copolymer monolayer with streptavidin

One way to investigate the presence of the biotin moiety at the end of the polymer chains is to study its biotin-streptavidin interaction in monolayers. Similar studies performed with biotinylated lipid monolayers showed the formation of a two-dimensional protein domain that was induced by the surface recognition of the biotin docking sites. The interaction of biotinylated lipids spread at the air-water interface with injected streptavidin in the subphase led to the increase of the surface pressure-area isotherms.[159]

In order to investigate the presence of biotin in the modified polymer and to assess its binding characteristics with streptavidin, first monolayers of the biotinylated polymer and the non-modified one were done and their isotherms were recorded (see Graph 3.1.3.5.1).

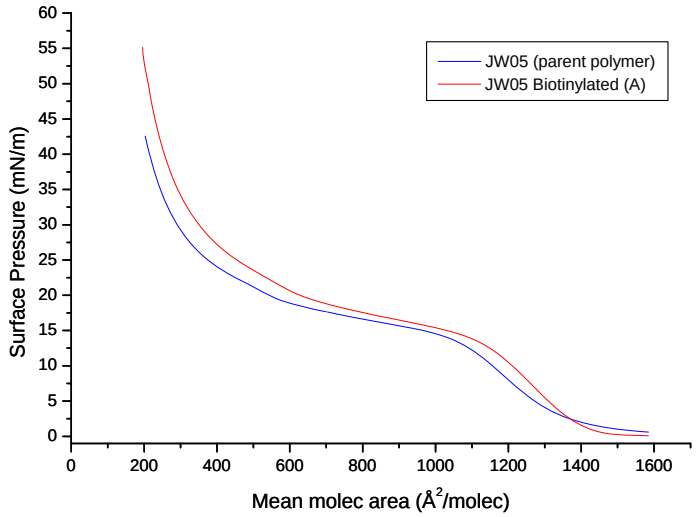

Graph 3.1.3.5.1: Surface pressure area isotherms for the biotinylated and the non-modified polymer respectively.

To investigate surface specific recognition of biotin by streptavidin, streptavidin solutions in PBS buffer were injected under a monolayer of the biotinylated polymer or the parent polymer. After injection of streptavidin in the subphase, a rise in the surface pressure is expected due to the formation of a sublayer of two-dimensional streptavidin crystal.

Graph 3.1.3.5.2 and Graph 3.1.3.5.3 show the same type of interaction for the non-biotinylated polymer and the biotinylated polymer, respectively, after incubation with streptavidin in the subphase. At low surface pressure in the presence of streptavidin, the surface pressure of the system is lower, indicating a certain loss of material in the subphase. This could be readily explained in the case of the biotinylated polymer, where the interaction of biotin and streptavidin could result in a more soluble complex. However, it is not clear why this is also observed with the non-modified polymer.

At surface pressures corresponding to condensed states in the monolayer, both types of polymer incubated with streptavidin, show isotherms with slightly higher surface pressures than the bare polymer isotherms. This can be explained by the unspecific adsorption (or insertion) of streptavidin in the monolayer due to non-specific interactions. Since the change observed is not dramatic, one can expect that the streptavidin might be buried in the bulky polymer chains.

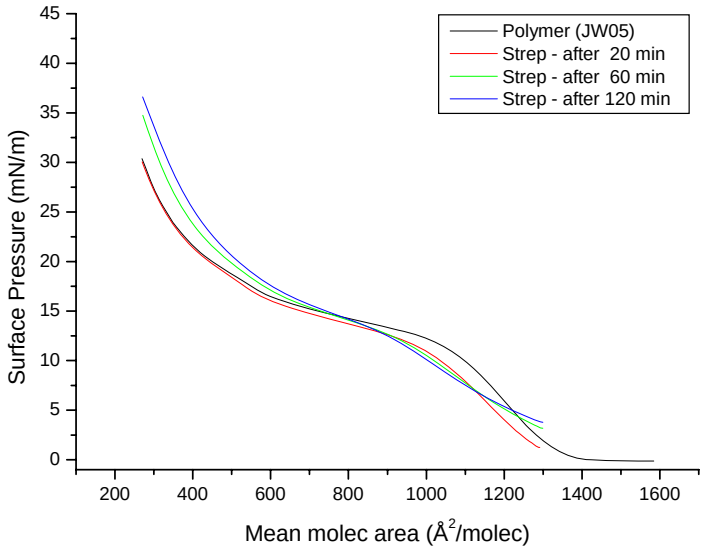

Graph 3.1.3.5.2: Surface pressure versus mean molecular area isotherms for the non-modified ABA triblock-copolymer before and after addition of streptavidin in the subphase at different times after streptavidin addition.

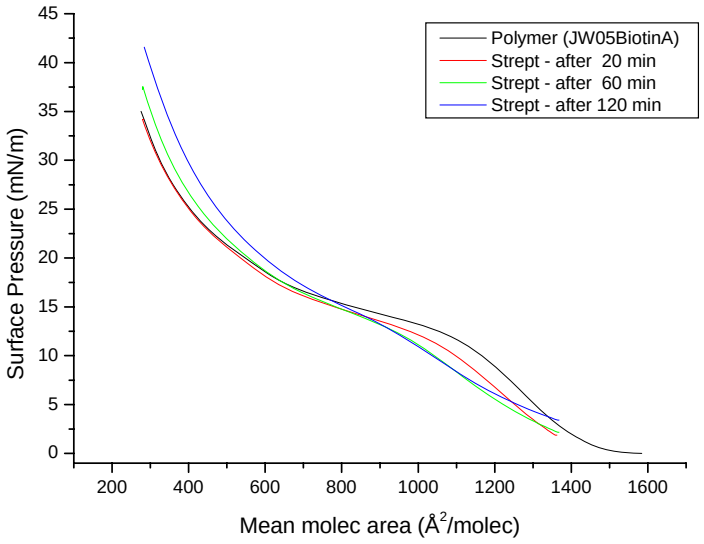

Graph 3.1.3.5.3: Surface pressure versus mean molecular area isotherms for the biotinylated ABA triblock-copolymer before and after addition of streptavidin in the subphase, at different times after streptavidin addition.

There was no significant difference in the behavior of the monolayers of the biotinylated and non-modified polymer after streptavidin injection, which indicated a non-specific interaction. Non-specific interaction would be expected from proteins that also show a relative high surface

activity. Streptavidin has some surface activity as evidenced by control experiments, where Π increase was observed in time for streptavidin adsorbed from the subphase, in absence of a polymer monolayer.

Moreover, one should consider that the high flexibility of the polymers might obscure the effect of the attachment of streptavidin to the monolayer, and prevent the formation of a crystalline two-dimensional array as observed with biotinylated lipid monolayers. In contrast to what observed with lipidic monolayers,[159] which are constituted by rather rigid molecules ordered parallel to the surface, polymer monolayers form much more complicated arrangements at the interface. The conformational flexibility of the polymer chains at the interface might lead to a non-dense packed array of streptavidin, which might not be differentiated from unspecific adsorption. Moreover, the conformation of the polymer chains might impede the freely attachment of streptavidin to the biotin moiety, if the biotin moiety is buried within a polymer coil.

It is worth mentioning also that to avoid unspecific interactions with the polymer monolayer, such as insertion due to the surface activity shown by streptavidin, it might prove efficient to work at higher surface pressures and to monitor the interaction of streptavidin with time at constant surface pressure (see Appendix II Section 6.2.1)

3.1.4. Conclusions and Summary

In this section the synthesis, functionalization, and characterization of amphiphilic triblock-copolymers was presented. Telechelic organofunctionally terminated siloxanes were used to initiate the cationic ring opening polymerization of cyclic monomers to produce ABA block-copolymers.

The molecular weight of the side chains can be controlled by the ratio of the cyclic monomer to the telechelic initiator in the reaction mixture.[126] The functionalization with biotin was achieved by covalently attaching it to the end polymer block via activated ester synthesis. End functionalization of poly(2-methyl-2-oxazoline)b-poly(dimethylsiloxane)-b-poly(2-methyl-2-oxazoline) with coumarin was successful.

All parent polymers and functionalized ones were characterized by different analytical techniques. The behavior of these amphiphilic block-copolymers was also studied by Langmuir films, which showed typical isotherms with a plateaux around 15 mN/m. The limiting areas A_0 were found to be related to the molecular weight of the hydrophilic block, in a relationship that indicated a coiled conformation in the condensed region of the isotherms.

It would be also interesting to study the thermal properties of the obtained ABA triblock-copolymers since it is expected that due to microphase separation, the glass transition temperatures of both blocks can be observed.. This has already been studied in similar block-copolymers containing poly(dimethylsiloxane) and poly(ethyloxazoline).[124, 136]

3.2. Vesicle preparation and characterization

3.2.1. Introduction

The association of block-copolymers in aqueous solutions depends both on the total length of the polymer and the relative ratio between the blocks.[31] The hydrophilic-hydrophobic ratio controls the geometry of the morphology obtained and a minimum total length is required to observe aggregation. By decreasing the length of the hydrophilic blocks at constant hydrophobic block-length, a transition from spherical micelles to worm-like micelles and finally to vesicular structures is observed,[31, 34, 35, 44, 47, 48, 50] that is there is a tendency to form aggregates with less curvature.

Due to the usually low solubility and slow dynamics of the constituting unimers, i.e. the single block copolymers, the conformation and size of the aggregates obtained depend on the preparation conditions. These non-equilibrium vesicles are kinetically trapped structures. Equilibrium processes governed by thermodynamics play much less a role on the formation of vesicle structures.[42] Thermodynamic stability is related to the integrity of the aggregate, in other words, the disassembly into the constituting unimers and is given by the cac. Due to the slow dynamics of polymer chains, a vesicle can exist under its cac if it is kinetically stable. Kinetically stable systems are usually obtained with blocks having low T_g.[88]

By tailoring the preparation method, vesicle size, distribution, and morphology can be manipulated. The preparation method determines the mono or polydispersity of vesicle size. Basically, depending on the solubility of the constituting blocks, two methods exist for preparation of block copolymer aggregates.[89]

A common strategy to prepare vesicles from amphiphilic block-copolymers involves the solubilization of the block-copolymer in a suitable organic solvent of medium polarity (non-selective solvent), i.e. able to solubilize both blocks. Bringing the polymer solution into aqueous media promotes the self-assembly into superstructures. The organic solvent is generally removed by either evaporation or dialysis.[37, 41, 51] Usually this method is the method of choice to obtain vesicles from block-copolymers with low water solubility and high T_g.

A co-solvent for both blocks is required when glassy hydrophobic blocks (e.g. polystyrene) are used,[160] since hydrophobic domains need to be broken in order to disperse the solid polymer in water. On the contrary, for blocks with low T_g, this is not a restriction and the polymers can self-assemble without the need of co-solvents. Nevertheless, during the dispersion in aqueous media, the dynamics of the process is obviously slow due to the intrinsic slow dynamics of polymers chains.

The polydispersity of the vesicles can be narrowed with an extrusion step.[42, 61] Extrusion is broadly used for liposome preparation,[74] a reduction in size and lamellarity is achieved by passing a polydisperse suspension repeatedly through filters of defined pore size.

Polymer vesicles were also obtained by directly dispersing the polymer in aqueous solutions, under organic solvent free conditions.[13, 30, 31, 44, 53] This preparation method, usually called the direct dispersion or dissolution method, involves only the addition of the copolymer to water or another aqueous medium.[88]

Vesicles are versatile systems for the encapsulation of both hydrophilic and hydrophobic substances.[42] Usually the encapsulation takes place during vesicle formation, and therefore it depends on the method used. The encapsulation yield can be described by the entrapment efficiency (EE). The EE is defined as the amount of material encapsulated in the vesicles related to the total amount of substance present during the vesicle formation and encapsulation procedure.[74] Post encapsulation can be also achieved and this topic is treated in Appendix II.

3.2.2. Results and discussion

The formation of small, unilamellar vesicles from triblock-copolymers could be achieved according to an already described procedure,[61] which will be termed here the standard or ethanol-injection-extrusion method. The polymer was initially dissolved in ethanol to yield a clear homogeneous solution, from which the preparation technique takes its first name.[161] This solution was then added dropwise under stirring to the preferred buffer, leading to triblock-copolymer vesicles of a rather broad size distribution. By applying several extrusion cycles the vesicle size can be controlled, from where the second part of the methodology's name arises.

When encapsulating or incorporating proteins into the membrane of the vesicles, the presence of organic solvents might promote denaturation and should be avoided. Therefore, softer methods need to be used. Following a procedure reported for the preparation of vesicles from PEO-PPO-PEO,[53] vesicles of ABA triblock-copolymers were obtained by direct dispersion in aqueous media followed by extrusion to form vesicular structures.

Similar to liposomes detergents can be used to introduce membrane proteins into the walls of the vesicles obtained by direct dispersion.[74, 162] Incorporation of proteins in lipid bilayers was found to be favored by detergent disruption.[163] This approach has been adapted for polymer vesicles, giving then a "softer" method for insertion of membrane proteins. In this method the use of organic solvents is avoided. The method is simple; polymer vesicles prepared by direct dispersion method are destabilized with detergents to promote insertion of membrane proteins. Reconstitution of membrane proteins takes place in the presence of the detergent. Finally, in a last step the detergent is removed with the aid of Biobeads (BioRad). These specifically absorb detergents and therefore facilitate the formation of the proteo-vesicles.[163, 164]

3.2.2.1. Vesicle characterization by DLS, SEC, and TEM

A complete light scattering study (SLS and DLS) on vesicles obtained by the standard or injection method has been reported.[61] However, the polymer used here was functionalized and from a different batch. Therefore, a DLS study was performed for the biotinylated polymer.

The standard method yielded rather monodisperse vesicles from polymer JW05 by with a R_H of 98 nm (cumulant analysis and Williams-Watts). Analysis of the biotin modified polymer (JW05ModA) render a R_H of 124 nm by cumulant analysis.

The direct dispersion vesicles from polymer JW05 show a high polydispersity. Analysis of the data indicated the presence of two populations, with R_H 105 and 340 nm respectively (cumulant analysis). Cumulant analysis allows the characterization of polydisperse samples but is not optimized for multiple populations. Therefore, the uncertainty of these values is high. Williams-Watts analysis could not be used since it is only suited for two rather monodisperse and separated populations. No other method of analysis can be used since the two distributions seem to be rather close and broad, therefore they overlap, difficulting thus the interpretation.

The new soft proteo-vesicle preparation method (direct dispersion/detergent and Biobeads) was characterized by DLS performed after each step of the vesicle preparation. Additionally, TEM was used to corroborate these data. The diffusion coefficients were calculated by cumulant analysis and extrapolation to 0° angle. Since no concentration dependence was performed only apparent diffusion coefficients and therefore apparent hydrodynamic radii were obtained. For better visualization, the results of cumulant analysis are complemented by size distributions obtained by CONTIN analysis corresponding to observations at 90°.

Figure Fig. 3.2.2.1.1 shows a bimodal population of vesicles and large aggregates, as discussed above. Similar behavior was reported in other systems.[88] TEM showed the presence of large tubular morphologies and smaller spherical aggregates. This indicates the coexistence of different morphologies, a phenomenon already observed with other amphiphilic block-polymers. [34, 35, 165] An averaged R_{Happ} of 294 nm was obtained by cumulant analysis (PDI: 0.4).

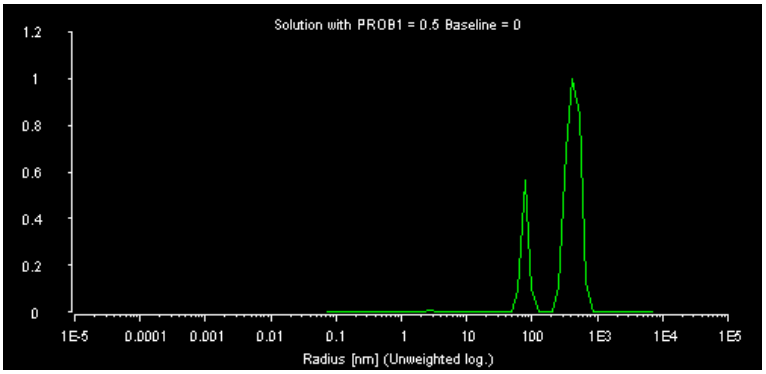

Fig. 3.2.2.1.1: Size distribution obtained by CONTIN analysis after the 1st preparation step. The corresponding apparent R_H obtained by cumulant analysis was 294 nm.

Upon addition of detergent to the system, the larger aggregates are disturbed and formation of smaller aggregates is favored as seen in Fig. 3.2.2.1.2. The bimodal size distribution can be attributed to the presence of a vesicle population and one of detergent micelles. Moreover, this lower size population can be due to a vesicle to micelle transformation induced by the addition of micelle forming surfactants such as octylglucoside and Triton X-100 as observed with lipid vesicles.[166] Cumulant analysis rendered an averaged R_{Happ} of 82 nm with a PDI of 0.4.

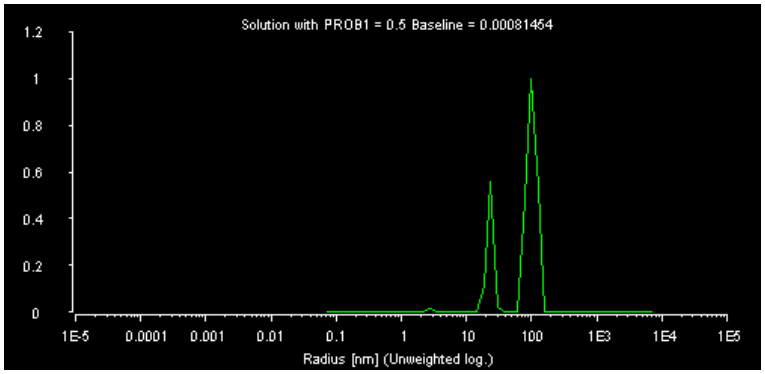

Fig. 3.2.2.1.2: Size distribution obtained by CONTIN analysis after the 2nd preparation step. The corresponding apparent R_H obtained by cumulant analysis was 82 nm.

Removal of detergent with Biobeads yields a monomodal broad size distribution as seen in Fig. 3.2.2.1.3, with a R_{Happ} of 116 nm and PDI of 0.4 obtained by cumulant fitting. As a consequence of the slow removal of detergent, formation of smaller aggregates in comparison to the initial aggregates (see Fig. 3.2.2.1.1), seems to be favored,.

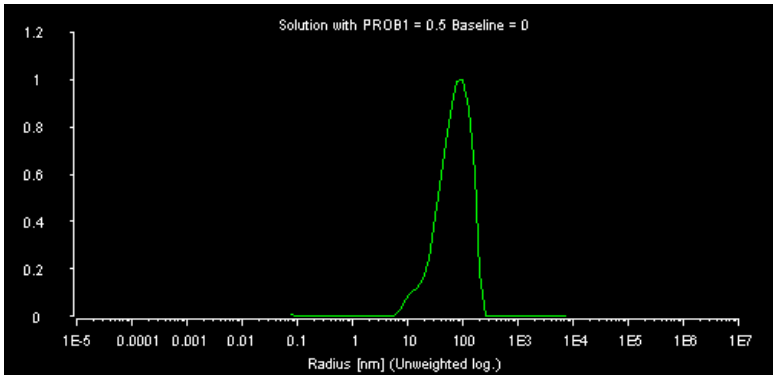

Fig. 3.2.2.1.3: Size distribution obtained by CONTIN analysis after the 3rd preparation step. The corresponding apparent R_H obtained by cumulant analysis was 116 nm.

In Fig. 3.2.2.1.4 the effect of chromatographic separation can be seen. This step seems to slightly improve the dispersity (PDI 0.25) of the aggregates without significantly changing their size (R_{Happ} 112 nm).

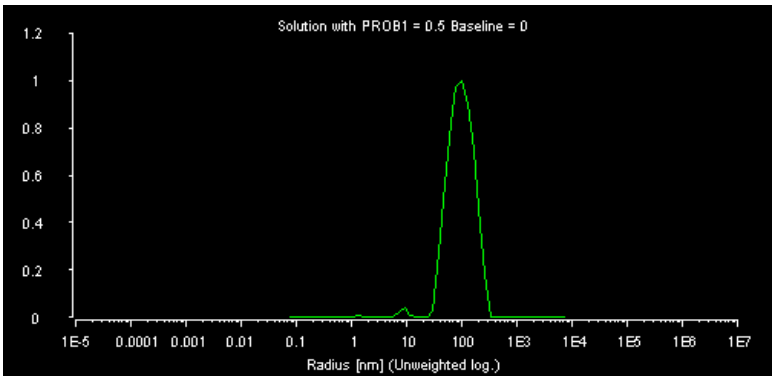

Fig. 3.2.2.1.4: Size distribution obtained by CONTIN analysis after the 4th preparation step. The corresponding apparent R_H obtained by cumulant analysis was 112 nm.

Usually, the EE is rather low with these preparation methods. As a consequence, there is always non-encapsulated material that must be removed from the system. Removal and recycling of non-encapsulated substances can be carried out either by size exclusion chromatography, centrifugation, or dialysis.[42] Size exclusion chromatography not only allows the separation of non-loaded low molecular weight molecules from the polymer aggregates,[167] but also provides a means for studying the polydispersity of the vesicles. The best performing gel was Sepharose 4B.

Two eluting peaks were observed for polymer vesicles separated with a Sepharose 4B column (Graph 3.2.2.1.1). This revealed a two-size population of vesicles prepared by the standard method, which was not detected by DLS due to their similar sizes. The fractions of the different peaks were collected and studied by TEM and DLS.

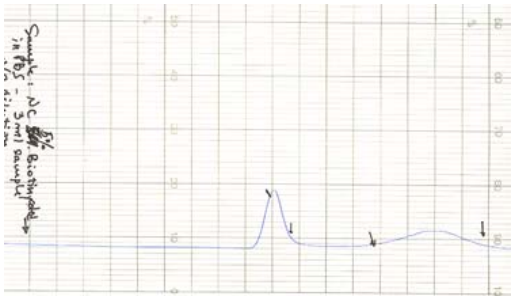

Graph 3.2.2.1.1: Chromatographic separation (Sepharose 4B) showing two populations of vesicles.

TEM of samples of vesicles before SEC (data not shown) showed a high concentration of aggregates, with vesicles and tubes superimposed which difficulted the analysis.

Picture 3.2.2.1.1 shows TEM pictures of vesicles corresponding to the first chromatography peak in which tubes (R_{TEM}=20 nm) and spherical aggregates (R_{TEM}=20 to 120 nm) can be seen. DLS analysis of the first peak rendered a R_H of 80 nm by cumulant analysis, and of 88 nm by Williams-Watts. The radius obtained by DLS is an average property, and the value obtained falls between the ones observed by TEM.

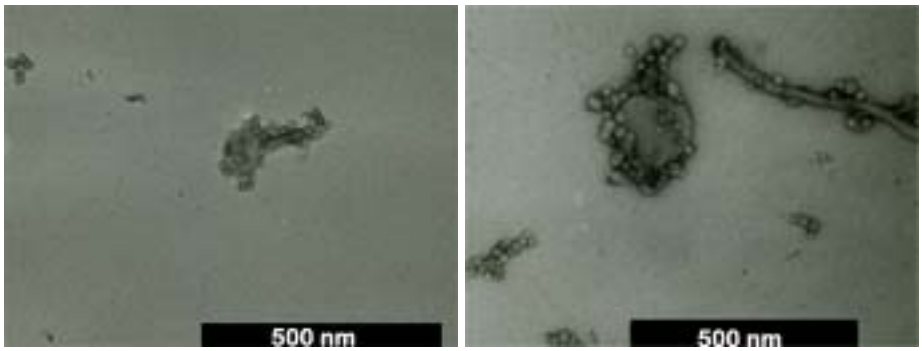

Picture 3.2.2.1.1: TEM of first chromatography peak (Sepharose 4B), vesicles prepared by standard ethanol method.

Picture 3.2.2.1.2 displays TEM pictures corresponding to the second chromatography peak. In this case, a concentrated sample of small monodisperse vesicles (R_{TEM}=12 nm) can be observed. DLS observations yielded a R_{Happ} of 19 nm by cumulant analysis, and of 27 nm by William-Watts fitting. The sizes observed by DLS correspond qualitatively to the ones obtained by TEM although by a factor of two smaller for TEM.

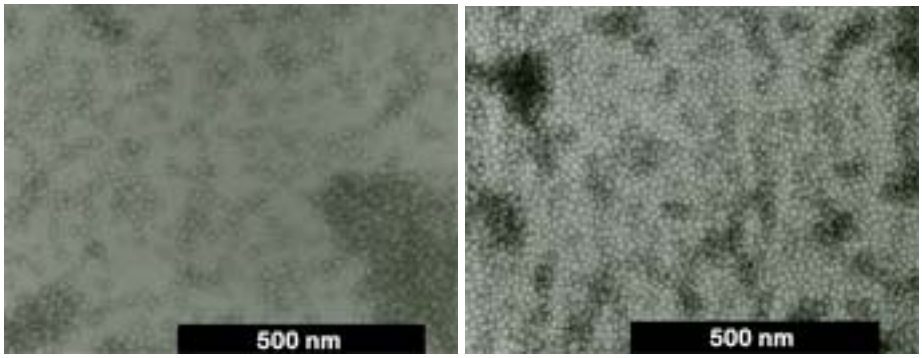

Picture 3.2.2.1.2: TEM of second chromatography peak (Sepharose 4B), vesicles prepared by standard ethanol method.

These results can be interpreted as follows: The hydrophilic to hydrophobic ratio dictates whether micelles, rod-like structures or vesicles form,[31] and the typical 20-40 w% hydrophilic weight fractions for liposome forming lipids applies as well for polymer vesicles. Cylindrical structures and micelles form upon increasing this ratio (40-50%).[58] The polymer investigated here has a hydrophilic weight ratio of 31%, therefore, vesicles should predominantly form. However, the polydispersity of the polymer chains might influence the resulting structures: In similar vesicular systems polydisperse chains segregate within a vesicle wall with short chains towards the inner layer and long ones oriented to the external layer.[166, 168, 169] Fig. 3.2.2.1.5 shows a schematic representation of the situation expected for an ABA triblock-copolymer.

The presence of a high percentage of short chains or chains of high hydrophilic content might promote the formation of smaller vesicles, eventually rod-shaped and spherical micelles. Therefore, the presence of two populations can be attributed to the polydispersity of the consti-

tuting unimers. Moreover, impurities due to hydrophobic homopolymer would also promote the formation of micellar structures, as has been already observed for polystyrene.[50]

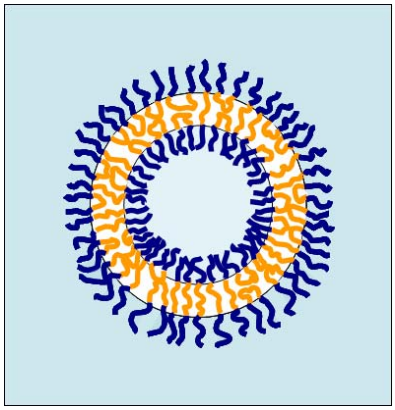

Fig. 3.2.2.1.5: Representation of the membrane constitution of a vesicle formed from ABA triblock-copolymers. Adapted from Schillen et al.[53].

3.2.2.2. Fluorescent Giant Unilamellar Vesicles

Giant unilamellar vesicles (GUVs) are large vesicles with sizes in the range of 5 to 200 μm.[170-172] By being directly observable with light microscopes, such systems are interesting in the academic field, helping to characterize the smaller counterparts. Fluorescent GUVs can be best characterized with confocal laser scanning microscopy.

GUVs consisting of a mixture of 1 w% Cm-PMOXA-PDMS-PMOXA-Cm and 99 w% PMOXA-PDMS-PMOXA were prepared by electroformation,[173] a process in which a thin film of polymer on adjacent electrodes was phoresed by alternating current into aqueous solution.[44] Giant vesicles with diameters of the order of 1 μm were obtained, as observed with phase transmission microscopy. However, the continuous movement of the vesicles on the surface made the observations somewhat difficult. To immobilize the vesicles, they were treated with Mowiol 4-88 solution. Unfortunately no vesicles could be observed in any of the 8 samples examined. This could be explained by a disturbance of the self-assembled structure in presence of Mowiol. The stability of such GUVs is still not well investigated, however, it seems that at room temperature they are not so stable and survive only a few days.

3.2.2.3. Trapped volume of vesicles

In order to estimate the encapsulation capacity of the vesicles, the approach of Oku et al. was followed.[174] They describe a method for measuring the trapped volume in liposomes without the need of removal of the non-encapsulated dye, using calcein as a fluorescence probe. Calcein belongs to the compound family of fluorescein, and as fluorescein it shows a high quantum yield. For quenching experiments calcein is better since it forms a chelate quenching complex with divalent metal cations, whereas fluorescein does not.[175, 176]

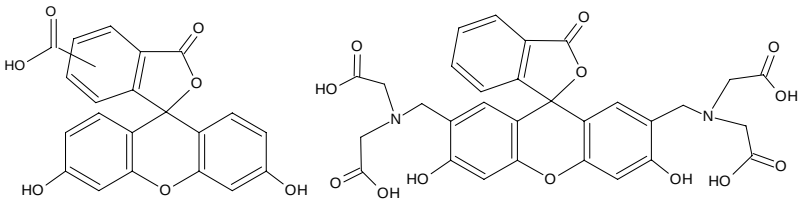

Fig. 3.2.2.3.1: Structure of 5(6)-Carboxyfluorescein (**a**) and of calcein (2,7-Bis[N,N-bis(carboxymethyl)aminomethylene] fluorescein) (**b**)

Graph 3.2.2.3.1 shows experiments using the recommended Triton X-100 as destabilizing detergent. Disruption did not occur for polymeric vesicles. This little or absent influence in the disruption of the polymeric vesicles can be attributed to their more stable membranes.[44] Therefore, as an alternative, octyl-polyoxyethylene (o-POE) was chosen as detergent.

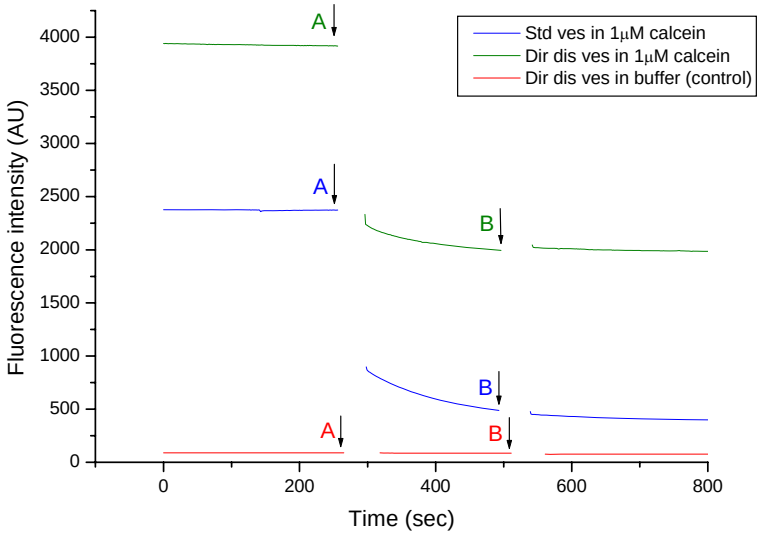

Graph 3.2.2.3.1: Curves showing the influence of Triton X-100 on the disruption of polymer vesicles in calcein 1 μM (without removal of non-encapsulated calcein). The arrows indicate the addition of Co^{2+} (A) and Triton X-100 (B). A control, consisting of empty vesicles is also shown. The polymer used was S131.

Repeating the experiments without removal of free calcein, but with o-POE as disturbing agent resulted again in little vesicle disruption evidenced by no decrease of fluorescence after detergent addition (Graph 3.2.2.3.2, arrow B). If the detergent destroys the vesicular structures the dye should be released and quenched by the cobalt ions present in solution, which should result in a decrease of fluorescence intensity. However, a slight increase in fluorescence upon addition of o-POE (Graph 3.2.2.3.2, arrow B) was observed. Although contrary to what expected, this behavior can be explained by the fact that if the encapsulated material was self-

quenched within the vesicles, an increase in fluorescence would occur upon release of the dye to the bulk medium due to concomitant dilution.

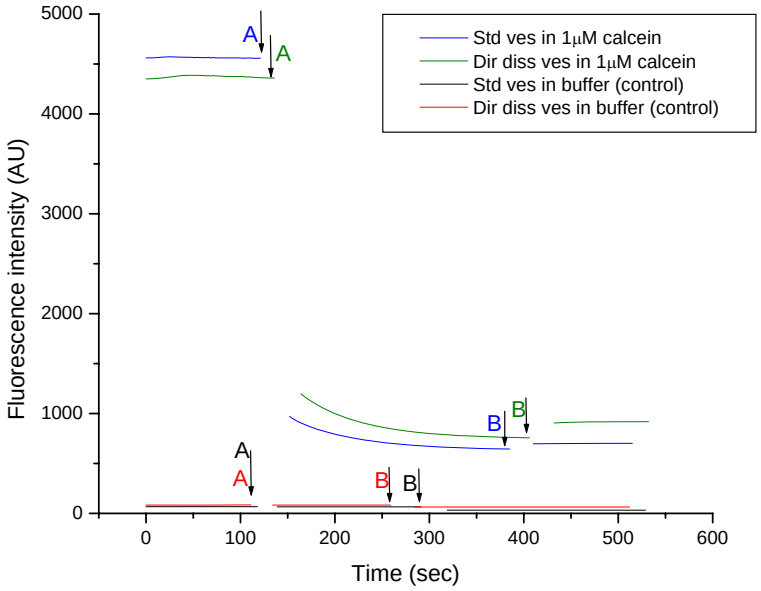

Graph 3.2.2.3.2: Fluorescence of vesicles prepared with different preparation methods in calcein (1 μM) without removal of free calcein. The arrows indicate the addition of Co^{2+} (A) and o-POE (B). Controls consisting of empty vesicles are also shown.

Since the experiments without removal of non-encapsulated calcein were no conclusive and did not allow the quantification of the encapsulated material, new experiments were performed in which non-encapsulated calcein was removed by SEC (see Section 4.10). Again little or no influence was observed when adding detergent to the system (data not shown).

Further trials inverting the addition of detergent and quencher were performed, which should shed some light on the influence of the detergent on the disruption of the vesicles.

The results of the experiments with inverse addition of quencher and detergent are shown in Graph 3.2.2.3.3. Addition of o-POE (arrow A) resulted in increase of the fluorescence intensity as expected when an encapsulated dye under self-quenching concentrations is released to the bulk medium. However, upon addition of an excess of cobalt ions a residual fluorescence was still observed. Since total quenching was never observed, it is possible that some dye was incorporated in the membrane and thus, it was not available for quenching.

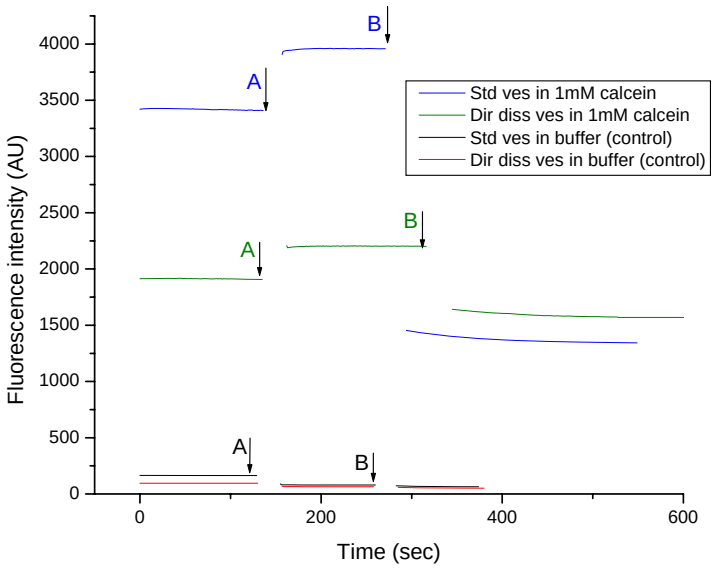

Graph 3.2.2.3.3: Inverse addition of quencher and detergent to vesicles prepared by different methods. The arrows indicate the addition of o-POE (A) and Co^{2+} (B). Controls consist of empty vesicles.

Liposome membranes can be made leaky with detergents. The disruptive effect of classical surfactants on their membranes results in the release of the entrapped dyes.[177]. The higher stability of polymer vesicles, due to their hyperthick membranes, [31] is mostly an advantage. However, this higher stability reduces the possibility of lysing the membranes by established protocols used with lipidic counterparts.[42] It can be concluded that detergents cannot completely destroy the vesicles. This prevented a quantification of the encapsulated substances and therefore the trapped volume in polymer vesicles could not be determined.

3.2.2.4. FCS studies of vesicles

Vesicles containing encapsulated sulforhodamine were analyzed by fluorescence correlation spectroscopy (FCS). The influence of different preparation methods and concentration of loaded fluorescent probes was investigated. For calibration of the pinhole and count per molecule, solutions of free sulforhodamine were also analyzed.

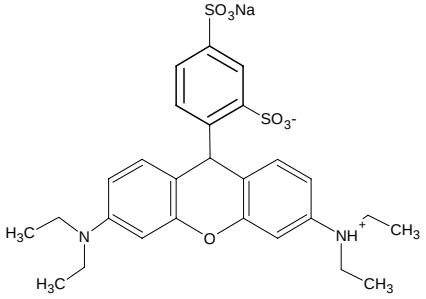

Fig. 3.2.2.4.1: Molecular structure of sulforhodamine B.

From the diffusion coefficients obtained, vesicle sizes could be estimated by the inverse proportionality of the diffusion coefficient to the hydrodynamic radius, as given by the Stokes-Einstein relationship (see page 114). This gives an indication of the order of magnitude of the size of the aggregates. A typical diffusion time (τ) of 30 μs was observed for the free diffusing sulforhodamine B.

Vesicles prepared by two preparation methods and purified by SEC to remove non-encapsulated dye were examined by FCS and TEM. The FCS results are summarized in Table 3.2.2.4.1. Vesicles prepared by the direct dispersion method showed the presence of large aggregates and rod-like structures with diffusion times of 30 ms.

For vesicles prepared by the standard ethanol method two peaks were obtained after chromatography purification. Analysis of the first peak showed rather low concentration of aggregates, which could not be studied by FCS. The second chromatographic peak showed a more homogeneous population of small aggregates in high concentration with diffusion times of 660 μs. This corroborates the results observed before (see Section 3.2.2.1). It is worth mentioning that in all samples a small percentage (1.8-11%) of free diffusing dye was also observed.

sample name	CPM (KHz)	CR (KHz)	diff. time 1 (μs)	diff. time 2 (μs)	particles 1 (%)	particles 2 (%)	N° of particles	correlation
DD-21	362.182	126.162	30	20178	9.3	90.7	0.343	3.912
DD-22	765.05	631.447	30	29780	11.7	88.3	0.803	2.245
DD-23	1640.829	1865.227	30	47488	6.8	93.2	1.119	1.893
DD-24	1470.904	2035.152	30	31238	8.6	91.4	1.357	1.737
EM 2p-25	14.074	295.523	30	558	2.8	97.2	20.675	1.048
EM 2p-26	6.335	662.227	30	707	11	89	101.672	1.01
EM 2p-27	27.764	405.446	30	636	2.5	97.5	14.478	1.069
EM 2p-28	14.206	586.459	30	680	5.8	94.2	40.312	1.025
EM 2p-29	38.191	319.948	30	628	1.8	98.2	8.376	1.119
EM 2p-30	9.544	434.463	30	743	6	94	43.667	1.023

Table 3.2.2.4.1: Results of FCS studies of sulforhodamine encapsulation by two vesicle preparation methods: direct dispersion (in blue) and standard ethanol method (2nd peak) (in green). Results obtained for each sample are averages of 5 autocorrelation functions obtained during 30 s at λ_{ex} 543 nm. CPM stands for counts per molecule, whereas CR for count rate.

In order to establish a relationship between the initial concentrations of fluorophore and the encapsulation efficiency of the fluorescent marker, a series of concentrations of sulforhodamine were encapsulated in vesicles prepared by two different preparation methods and investigated with FCS.

The results of the count rate, that is, the intensity per aggregate, showed for the direct dispersion method a linear relationship between the initial concentration of fluorescent dye and the encapsulated one between 30 μM and 30 mM of sulforhodamine. It is worth mentioning that the occurrence of autoquenching seemed to be low, which can be attributed to the fact

that vesicles formed via the direct dispersion method are quite large. For the case of the standard ethanol method, the trend observed is similar (results not shown).

Previously the encapsulation of enzymes was only indirectly proved, i.e., by means of their enzymatic reactions in a nanoreactor[8, 59]. It was of interest though, to prove the encapsulation of proteins by a direct method and whenever possible estimate the amount of protein encapsulated.

FCS is an ideal technique for the quantification of fluorescent-labeled probes in small volumes. To assay the encapsulation of proteins, vesicles were prepared by two different methods in the presence of a solution containing Alexa-488-Avidin (0.15 mg/ml) in PBS buffer and were chromatographically purified to remove non-encapsulated protein. The results of the fitting of the autocorrelation functions are presented in Table 3.2.2.4.2. Free dye, Alexa-488 showed a diffusion time of 25 μs with the set up used. Additional control experiments with empty vesicles in PBS (not shown) and free Alexa-488-Avidin (0.015 mg/ml) in solution were also performed (see Table 3.2.2.4.2 in red). Free Alexa-488-Avidin showed a small component of free dye (19%) when analyzed with a two-component fit.

The counts per molecule (CPM) observed for vesicles with encapsulated protein were always higher than for empty vesicles (75, 11, and 16 KHz for empty vesicles prepared by direct dissolution, standard method (1st peak), and standard method (2nd peak) respectively). Moreover, when comparing the CPM of vesicular structures with free Alexa-488-Avidin the ratios observed are 6 and 12 for vesicles prepared by direct dissolution and standard method (1st peak) respectively. Therefore, encapsulation of fluorescently labeled proteins can be concluded from the analysis of the FCS data.

sample name	CPM (KHz)	CR (KHz)	diff. time 1 (μs)	diff. time 2 (μs)	particles 1 (%)	particles 2 (%)	N° of particles	correlation
DD a	145.581	28.825	25	2490	13	84	0.198	6.059
DD b	165.847	21.7	25	3355	9	91	0.125	8.982
EM 1st peak a	197.901	62.384	25	2228	2.9	88.7	0.32	4.121
EM 1st peak b	462.63	47.075	25	4299	4.1	95.9	0.101	10.931
EM 1st peak c	256.782	17.742	25	4241	2.9	97.1	0.069	15.587
EM 2nd peak a	19.819	192.756	25	513	17.7	82.3	10.181	1.098
EM 2nd peak b	20.119	19.337	25	414	7.7	92.3	1.018	1.982
EM 2nd peak c	13.25	102.017	25	384	8	83	8.033	1.124
Alexa-Avidin	25.763	345.683	124	-	100	-	14.787	1.068
Alexa-Avidin	25.763	345.683	25	144	18.9	81.1	13.847	1.072

Table 3.2.2.4.2: Results of FCS studies of Alexa-488-Avidin encapsulation with two vesicle preparation methods: direct dispersion (in blue) and standard ethanol method (in green). ControlsResults obtained for each sample are averages of 5 autocorrelation functions obtained during 30 s at λ_{ex} 488 nm. CPM and CR stands for counts per molecule and count rate respectively.

The results obtained are not surprising when considering that a diffusion time of 3.5 ms (EM 1st peak) corresponds approximately to a vesicle size of 110 nm, whereas for free avidin

the obtained diffusion time of 145 μs corresponds to its known size (4.5 nm). The sizes obtained from the diffusion times correspond to 95 nm for the direct dissolution, and 15 nm for the 2nd peak from the standard method. Additionally, the morphology of the vesicles was investigated by TEM in the samples analyzed by FCS. TEM corroborated the findings of FCS, in relation to the relative sizes of the structures found.

3.2.2.5. Density determination and Sedimentation velocity studies

One way to verify protein insertion in the membrane of lipidic vesicles is by analytical ultracentrifugation. Insertion of membrane proteins leads to changes in the density of the vesicular structures, and thus to a different sedimentation speed.[178] Therefore, ultracentrifugation is a technique to prove the insertion of channel proteins in vesicle membranes.

Moreover, it turned important to determine the density of the nanocontainers. Knowledge about the density of the polymer vesicles could help determine the use of centrifugation as a separation technique from other species.

The density of polymeric vesicles prepared according to the standard method (solvent injection and extrusion), proteo-vesicles with OmpF in their membranes, and vesicles with a soluble protein encapsulated (peroxidase) were investigated by analytical ultracentrifugation. Graph 3.2.2.5.1 displays the results presented as a plot of ηs^0 versus ρ.

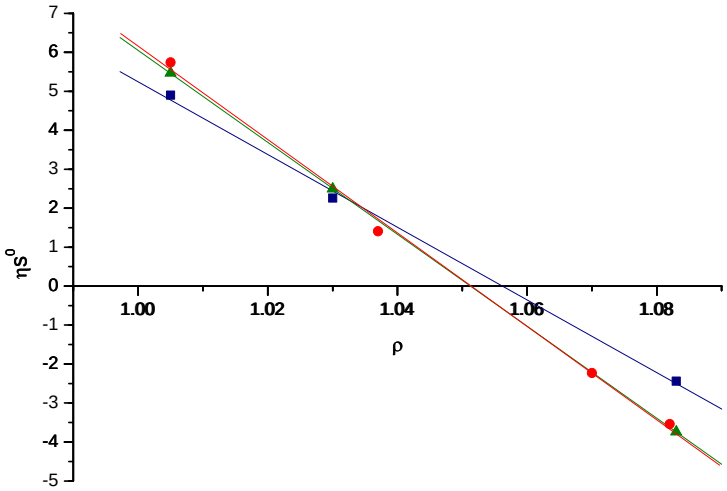

Graph 3.2.2.5.1: Viscosity corrected sedimentation coefficient versus density of the solvent and corresponding linear regressions for three samples: blue squares polymer vesicles (JW05) in PBS, green triangles polymer vesicles containing OmpF (1st chromatography peak) and red circles polymer vesicles containing OmpF (2nd chromatography peak).

The polymeric vesicles have a density of 1.0562 g/ml. Knowledge of the vesicle density allows the use of centrifugation as a separation technique. Based on density differences, for

instance, vesicles can be separated from more complex media (see Appendix II) or from non-incorporated proteins in their membranes.

The density of the proteo-vesicles was determined as 1.0514 g/ml. Incorporation of proteins in the polymer membrane would render vesicles with higher density than plain vesicles. From the difference in the density values a quantification of the inserted proteins could be possible. However, this was not the case. The discrepancy between the expected and obtained value could be attributed to the low concentration of the sample, due to its previous chromatographic purification to remove any non-incorporated protein channel. OmpF has been already used in similar studies with lipid vesicles and in higher concentrations.[178] The density of the vesicles containing encapsulated peroxidase could not be determined due to the low concentration of the sample and problems with its absorbance.

3.2.3. Conclusions and Summary

From the data obtained of SEC, DLS and TEM, the coexistence of different morphologies can be concluded. The coexistence of vesicular structures and spherical or cylindrical micelles has been already observed in other systems.[42-44] This can be attributed to the high polydispersity[16] of the constituting unimers. For instance, unimers containing higher hydrophobic character may tend to form lamellar structures, while those with higher hydrophilic character would form micelles.

The two different preparation methods yield aggregates of different sizes, which can find applications in different fields. For instance small vesicles with a narrow size distribution can be used for applications that involve size limitations, such as drug delivery, while the larger ones can be of interest in applications that need an increase in the capacity of encapsulation.

Fluorescently labeled giant vesicles were prepared and analyzed with phase contrast microscopy and confocal fluorescence microscopy. However, one problem arose in the visualization of such entities. The giant vesicles could not be fixated in the object slide, and since they were in constant movement this impeded their proper visualization and photography.

The encapsulation efficiency of the vesicles could not be assessed by standard fluorescent techniques due to the high stability of the vesicles to detergent disruption. FCS measurements confirmed the encapsulation of low molecular dyes and labeled proteins in the interior of the vesicles. The density of the vesicles and proteo-vesicles was obtained by ultracentrifugation studies.

[16] In block-copolymers polydispersity is determined by both molecular weight distribution and a composition distribution.

3.3. Biotinylated Nanocontainers for selective targeting of cells

3.3.1. Introduction to Biotin-Avidin technology

Avidin binds ($K_d=10^{-14}$ M) to biotin almost irreversibly.[179] This affinity binding is quite strong (~35 kT per bond) [180, 181] and has been thoroughly studied since its discovery, and it is the basis of what it is known today as the biotin-avidin technology. The advantage of such an interaction is that it does not require harsh conditions to occur; it is highly stable, and can be used in a variety of conditions.

Both avidin and streptavidin are homotetramers, which means they are comprised of four identical monomer units, each carrying a binding pocket for biotin.[182] Moreover, these proteins have a two-fold symmetry with two pairs of biotin-binding sites on opposite sides of the protein, allowing thus its straightforward application as anchoring molecule.[111] Additionally, biotin is a small molecule that can be easily attached covalently to molecules, surfaces, macromolecules, etc.

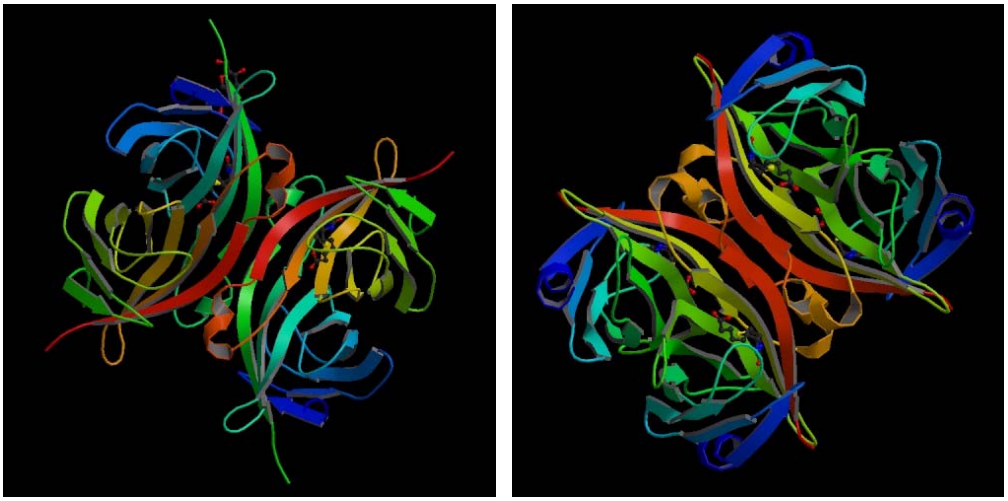

Pic. 3.3.1: Ribbon structures of avidin (left) and streptavidin. Protein codes 1AVD and 1STP respectively from Protein Data Bank http://www.rcsb.org/pdb/. Avidin (left): 3D-structure of the tetragonal crystal form of egg-white avidin in its functional complex with biotin at 2.7 Å resolution. Streptavidin (right): structural representation streptavidin complex with biotin.

3.3.2. Criteria for material selection and targeting strategy

To design polymer-based nanocontainers (NCs) with medically useful functionality, amphiphilic polymers were modified with biotin as described in Section 3.1.2.2. In our approach we have made use of the biotin-avidin technology to provide a flexible platform for the surface modification of NCs.

By attaching ligands, NCs with surface associated targeting information can be obtained. The ligands can act as homing devices by binding to surface epitopes or receptors on target

cells. NCs bearing streptavidin moieties in their periphery can be coupled to ligands by streptavidin-biotin interactions. By using a mixture of functionalized and non-functionalized block copolymers, vesicles with optimal ligand spacing could be obtained to efficiently couple to cell surfaces. The approach used here has the following advantage: In symmetrically end-functionalized block-copolymers a substantial portion of the functional groups face the inner aqueous compartment. However, by coupling streptavidin and the ligand after vesicle preparation, the three-component conjugate is exclusively positioned on the outer leaflet of the polymer membrane. The strategy used for ligand functionalization of the NCs is illustrated in Figure 3.3.1.

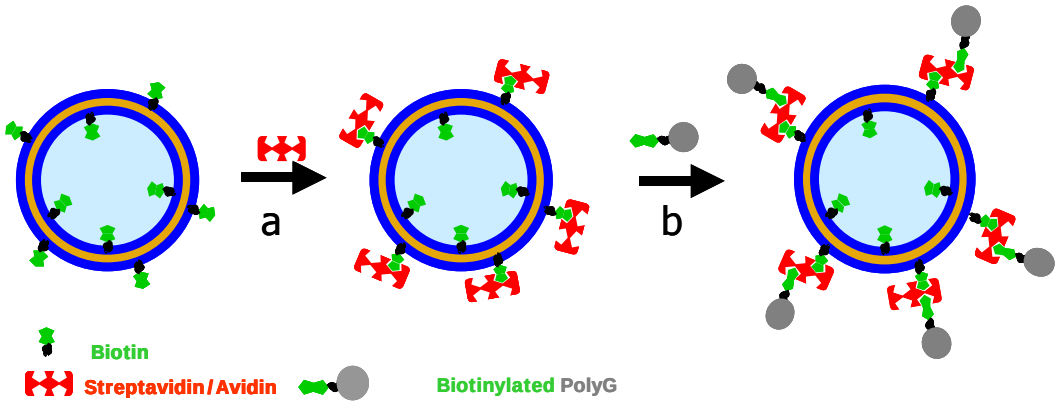

Figure 3.3.1: Strategy of the functionalization of NCs with the ligand polyG, in a first step biotinylated NCs are incubated with streptavidin (a), after removal of non-attached streptavidin, the NCs are subsequently incubated with polyG (b) to yield fully functionalized NCs.

We chose macrophages as model cell's culture systems, since they are believed to be involved and play a key role in atherosclerosis acute cardiac syndromes.[183] Macrophages are one of the most important components of the complex immune defense system. Normally, macrophages are essentially down regulated with respect to expression of surface receptors and function. Macrophages may become activated, resulting in considerable increase in size and phagocytic function. There are several stages for the activation and upon further activation, the surface components of the macrophages change considerably, in particular the content and type of receptors.[90, 184] The THP1 lineage, human leukemia, was chosen since it mimics human macrophages in vitro[185] and because of their high intrinsic expression of scavenger receptor A1 (SRA-1) upon differentiation. The COS-7 cell line was chosen since it can be genetically modified to express the SRA-1 coupled to the fluorescent marker enhanced green fluorescent protein (EGFP) for microscopical visualization. COS-7 cells do not express scavenger receptors in their native state and therefore, are particularly suited as its own negative control.

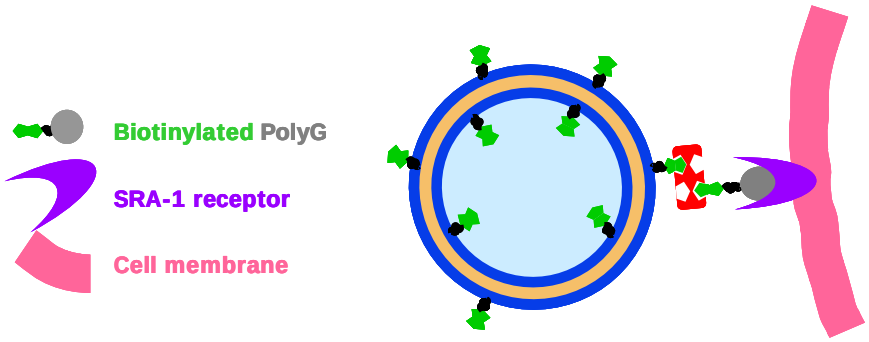

Figure 3.3.2: Targeting strategy towards receptors found on the cell's surface.

Activated macrophages express a scavenger receptor (scavenger receptor class A or SRA, types I and II).[186, 187] This receptor is involved in the uptake of lipoproteins by endocytotic pathways, and participates in the formation of lipid-foam cells, which is the first step in the formation of atherosclerosis.[187] The normal ligand for this receptor is the oxidized low-density lipoprotein (OxLDL). Investigations showed that other polyanionic macromolecules such as polyguanylic acid (polyG), a polynucleotide, serve as well as ligands for the scavenger receptor A.[187] From the many known affinity ligands for SRA1, we have chosen polyG[188] (23 mer) for the design of our specific-ligand targeting system, since polyguanylic acid quadruplexes are known to interact very specifically with SRA-1 receptors.[189]

By means of our enriching collaboration with the group of Dr. Med. P. Hunziker, our interest focused mainly in atherosclerosis and myocardial infarct, which directed the choice of cell lines and ligand used. But it must be highlighted that the findings might be regarded as universal, although for the studies we had to restrict to one type of cell line and one receptor. Moreover, the use of the biotin-streptavidin coupling reaction enables us to remain flexible on our system and to easily change the ligand. A covalent bonding of the ligand to the constituting polymer chains of the nanocontainer is not excluded, but several drawbacks might be pointed out. Bulky ligands might influence the aggregation behavior of the amphiphilic building blocks, whereas a new reaction must be carried out for each desired ligand, with its consecutive purification steps, which in the case of amphiphilic block-copolymer pose many inconvenients. On the contrary, a simple system based on the biotin-streptavidin high affinity, let us remain flexible in the choice of ligand, and the attachment of the ligand requires only a short incubation time under physiological conditions, with a rather simple purification step.

3.3.3. Results and discussion

3.3.3.1. Chromatographic separation

Chromatographic separations were needed to remove non-attached streptavidin. Graph 3.3.3.1.1 shows some typical chromatrograms: **a**) a control sample containing non-biotinylated

NCs incubated with avidin, **b**) biotinylated NCs incubated with avidin, and c) sample containing only avidin. Chromatogram **c**), confirms that the last peak, i.e. the peak on the right hand side of each chromatograph, is due to free avidin. One important feature observed in Graph 3.3.3.1.1 is the height of the first peak (left peak in **a** and **b**), which is higher for the biotinylated NCs bound to avidin. Initially, this was attributed to the higher amount of mass corresponding to coelution of streptavidin coupled to NCs. However, this increase was higher than expected. If due to the amount of streptavidin co eluted with NCs, the increase in area of the first peak in b should correspond to the difference between the areas of the second peak in chromatographs a and b. It is obvious that the increase is higher and a more complete study of the UV-vis characteristics of the complex between streptavidin and biotinylated polymer vesicles was carried out (see Section 3.3.3.2).

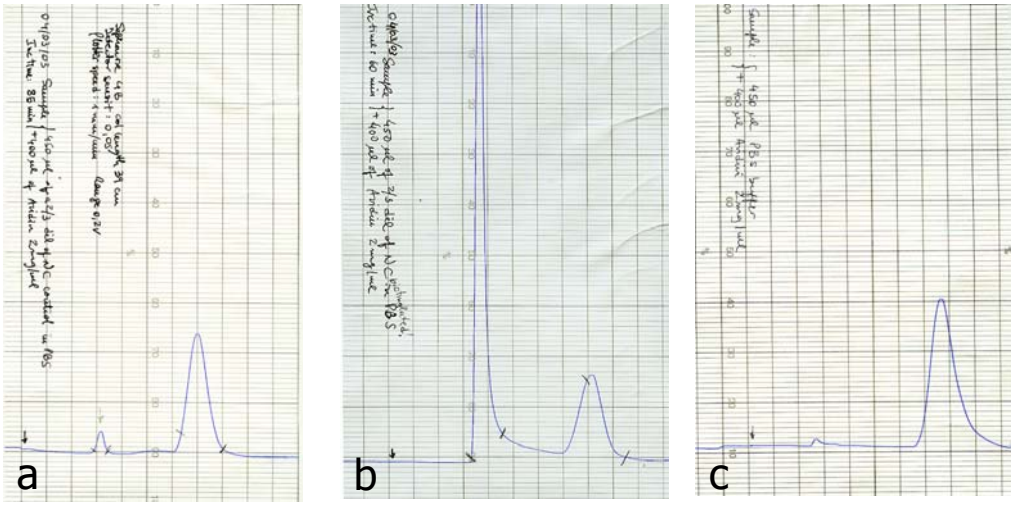

Graph 3.3.3.1.1: Chromatographs for the separation of non-bound avidin with Sepharose 4B, a) control sample containing only NC (non-biotinylated) incubated with avidin, b) biotinylated NC incubated with avidin, c) avidin.

3.3.3.2. UV-vis characterization of biotin-streptavidin conjugation

Since in the chromatograms of samples containing biotinylated NCs incubated with streptavidin the peak corresponding to the polymer vesicles was always significantly higher than that without streptavidin, it was obvious that at 280 nm also a difference in the absorbance was occurring. The binding of biotin to streptavidin can be observed via the shift in absorbance of the tryptophan group of the streptavidin.[159, 182] This can be used to determine the attachment of streptavidin to the biotin moieties on the NC surface. For this purpose a series of spectroscopic studies of the interaction of the biotinylated polymer and avidin were performed. A series of samples were studied, with modified or unmodified polymer. Also controls consisting just of biotin and avidin, and mixtures thereof were performed.

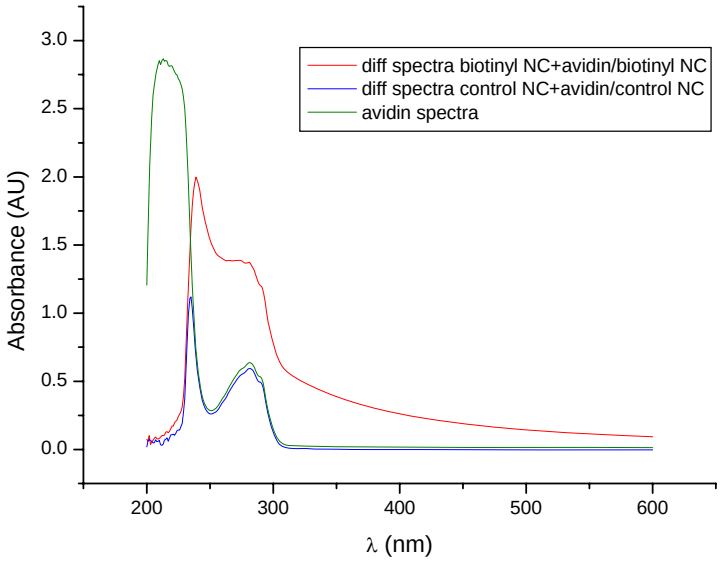

Graph 3.3.3.2.1: Comparison of the difference spectra of biotinylated NC incubated with avidin minus biotinylated NCs (red), difference spectra of control NCs incubated with avidin minus control NCs (blue), and the spectra of avidin (buffer as blank).

As seen in Graph 3.3.3.2.1 and contrary to expected,[159, 182] no shift in the maximum of the spectra was observed for avidin bound to biotin or to biotinylated NCs. This could be due to low resolution of the spectra. Nevertheless, quite an increase in the absorption was detected in the case of biotinylated polymer bound to avidin (red curve), indicating that binding indeed took place. This increase is higher than the sum of the spectra of polymer vesicles and avidin and corroborated the observations from SEC. In particular, this increase can be attributed to the specific interaction of biotin and avidin since no such increase was found for mixtures of non-biotinylated polymer vesicles incubated with avidin. In the latter case only the contribution of free avidin was detectable in the spectra.

In order to verify the attachment of streptavidin to the nanocontainers, samples were analyzed prior and after chromatographic separation. In order to account for dilution factors taking place during chromatographic separation, the controls consisting of NCs incubated with streptavidin non-chromatographized were diluted to one-third. Graph 3.3.3.2.2 shows the spectra of only NCs (curve blue), and the NCs incubated with streptavidin prior (green curve) and after chromatography. A clear peak with maximum at 276 nm is observable in the case of samples containing streptavidin. Even after chromatographic separation, the contribution of absorbance at 280 nm is due to both polymer absorbance and the absorbance due to streptavidin, which confirms the binding of streptavidin to the biotin on the surface of the NCs.

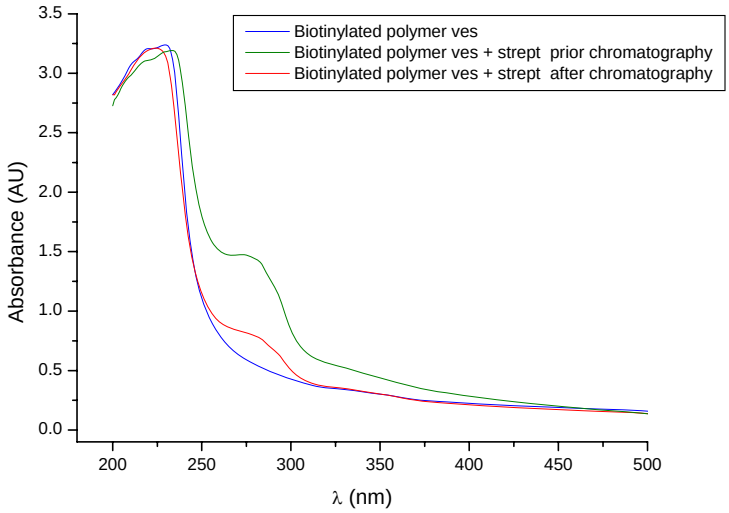

Graph 3.3.3.2.2: UV-vis spectra of polymer vesicles (1/3 dilution, blue), polymer vesicles incubated with streptavidin prior to chromatography separation (biotin/strept. ratio= 6.3, 1/3 dilution, green), and polymer vesicles incubated with streptavidin after chromatography purification (biotin/strept. ratio= 6.3).

Graph 3.3.3.2.2 also shows that not all the streptavidin added to the system attaches to the NC surface. This is evident by comparing the green and the red curves of Graph 3.3.3.2.2, which correspond to the NCs prior and after chromatography respectively. By subtracting the curve of the NCs (blue curve) from the samples containing NCs and streptavidin (green or red curve, respectively), the amount of streptavidin can be quantified. If one takes the corrected curve of the NCs and streptavidin prior to separation as the total streptavidin added to the system (100%), that is both streptavidin bound and free, then, the corrected curve of the incubated vesicles after chromatography represents the amount of streptavidin bound to the nanocontainers. This calculation resulted in 26% of streptavidin bound to the nanocontainers when the initial ratio of biotin to streptavidin was 6.4. This low attachment can be explained by the presence of the polymer chains in the surroundings of the biotin moieties, which could create a polymer cloud decreasing the ability of biotin to interact with streptavidin. As a consequence, less biotin moieties would be available for coupling.

The coupling procedure used to control the surface density of the ligand was achieved by mixing functionalized and non-functionalized polymer. Conjugation of biotinylated vesicles to streptavidin can result in vesicle aggregation, a phenomenon already observed with liposomes.[190, 191] Due to its multiple binding sites in opposite sides of the molecule, streptavidin can form tri-dimensional networks if a streptavidin molecule is sandwiched between two or more NCs.[192] This intervesicle cross-linking via streptavidin bridges must be avoided. This can be achieved by using an excess of streptavidin. Streptavidin although was soluble in aqueous solutions, has indeed a limited solubility, which prevented in certain cases the use of excess

avidin. Various ratios of streptavidin to biotin were investigated in order to optimize the system, the optimal system found consisted on a 450 μl aliquot of NCs containing 10% biotinylated of the total polymer with a polymer concentration of 3.3 mg/ml incubated with 450 μl of avidin (2 mg/ml). This renders a biotin to avidin ratio of 1.57.

3.3.3.3. TEM and SEM studies on biotinylated nanocontainers

After having optimized the system for the ratio of biotin to streptavidin and corroborated that attachment indeed took place. It resulted interesting to analyze the ligand labeled NCs, i.e. already functionalized with polyG, as they bound to the cell surface or once they were internalized within the cells. For this two types of experiments were performed, namely at 37ºC and at 4ºC. At low temperature, cellular transport processes like endocytosis are inhibited,[193] whereas binding to receptors can still take place. At 37°C both processes occur and receptor binding is usually followed by internalization or uptake.

Picture 3.3.3.3.1 shows ligand labeled NCs on the surface of an SRA-1 expressing COS-7 cell before uptake; that is, in experiments in which receptor-expressing cells were incubated with functionalized NCs for 2 h at 4°C. The spherical structures observed are typical of vesicles, and have the expected sizes. No NCs were detected by SEM in control experiments when using cells that did not express the receptor. Moreover, no NCs were observed when using NCs devoid of biotin or ligand (data not shown).

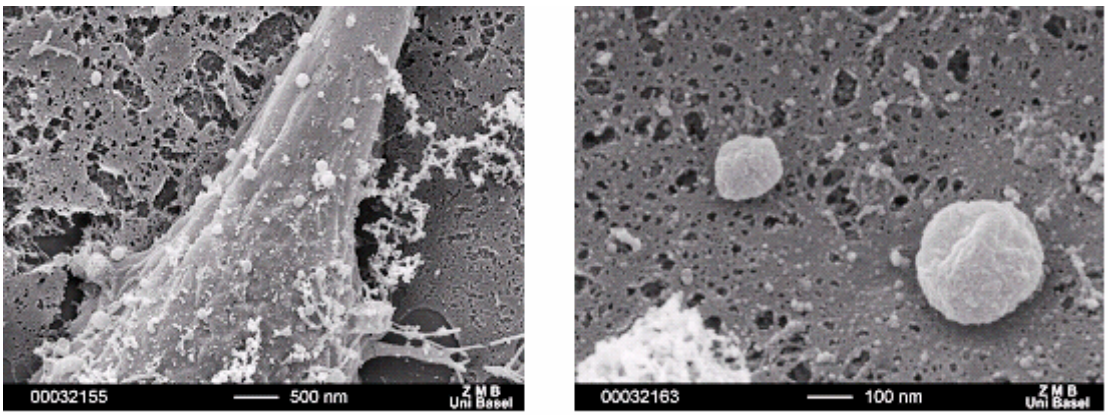

Picture 3.3.3.3.1: SEM images of biotinylated NC on the surface of a COS-7 cell.

When incubated at 37 ºC, the NCs were taken up by the cells. This was confirmed since no NCs were observed by SEM on the surface of receptor expressing cells incubated with ligand labeled NCs at 37 °C. The uptake can be attributed to a SRA-1 receptor mediated endocytosis, since this type of active transport processes is related to this receptor class.[194]

Picture 3.3.3.3.2 shows the TEM studies of sections of cells that showed vesicular structures accumulated in organelles (most probably the Golgi apparatus).

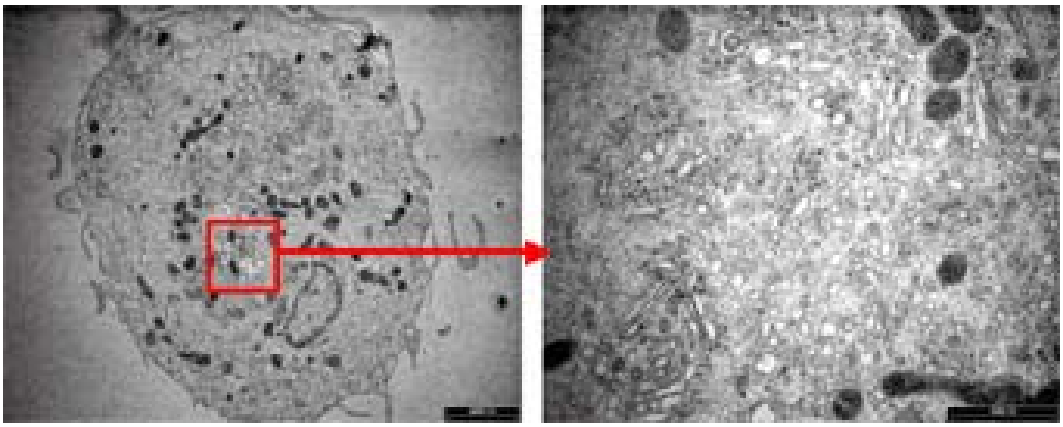

Picture 3.3.3.3.2: TEM of biotinylated NC after internalization in cells.

For a clear identification by TEM and SEM it was necessary to label the nanocontainers to discriminate them from other structures found in cells. This could be achieved by biotinylated gold or gold-labeled streptavidin. For this biotinylated NCs were incubated with Au-labeled streptavidin and the non-attached streptavidin was removed chromatographically. In Picture 3.3.3.3.3 it can be observed that not many NCs were labeled with Au-streptavidin (left) which can be explained by a low ratio of Au-labeled protein as seen with a control of only Au-streptavidin (Picture 3.3.3.3.3 right).

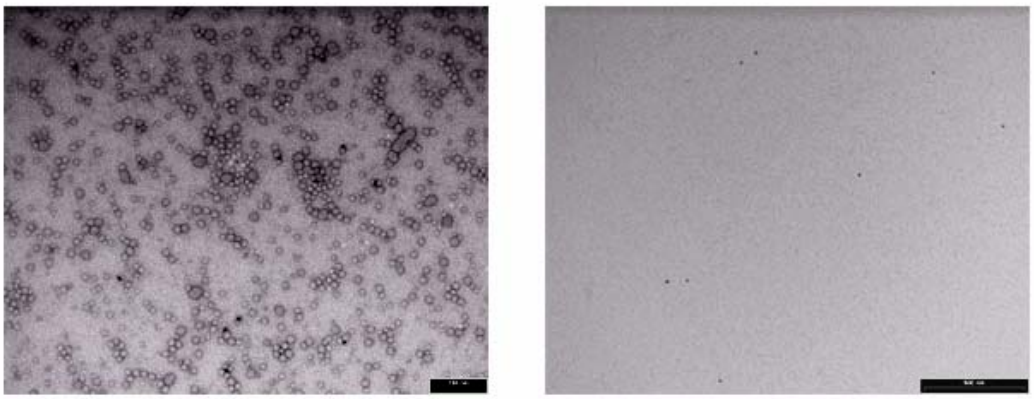

Picture 3.3.3.3.3: TEM pictures showing biotinylated NC incubated with gold-labeled streptavidin (inc time 16 h), scale bar=200 nm (left) and gold-labeled streptavidin, scale bar=500 nm (right)

This low degree of gold labeling of the streptavidin did not allow its use as a marker. The needs to track NCs into the cells and determine the location of their accumulation lead to the idea of the encapsulation of gold nanoparticles within the nanocontainers (see Section 3.4).

3.3.3.4. Binding and Uptake analyzed by Fluorescence Microscopy

The receptor-specific binding and uptake of NCs in transgenic cell lines was followed by fluorescence microscopy. Visualization of NCs was achieved by encapsulation of sulforhodamine

as described in Sections 3.2.2.3 and 3.2.2.4. The purification step to remove the non-attached streptavidin allowed also removing the non-encapsulated fluorescent probes.

Fig. 3.3.3.4.1 shows a confocal microscopy of transfected COS-7 cells, co-expressing SRA-1 receptors and EGFP (left, in green), incubated at 37°C in the presence of targeting, i.e. polyG functionalized NCs loaded with sulforhodamine (right, in red). Fig. 3.3.3.4.1 shows good co-localization (middle) of both fluorescent probes indicating receptor-ligand binding. Controls performed with COS-7 cells that did not express the receptor SRA-1 or NCs that had no polyG, showed poor or no co localization. Moreover, NC and receptor associated fluorescence showed always co-localization in intracellular vesicles whenever polyG NCs and receptor were present.

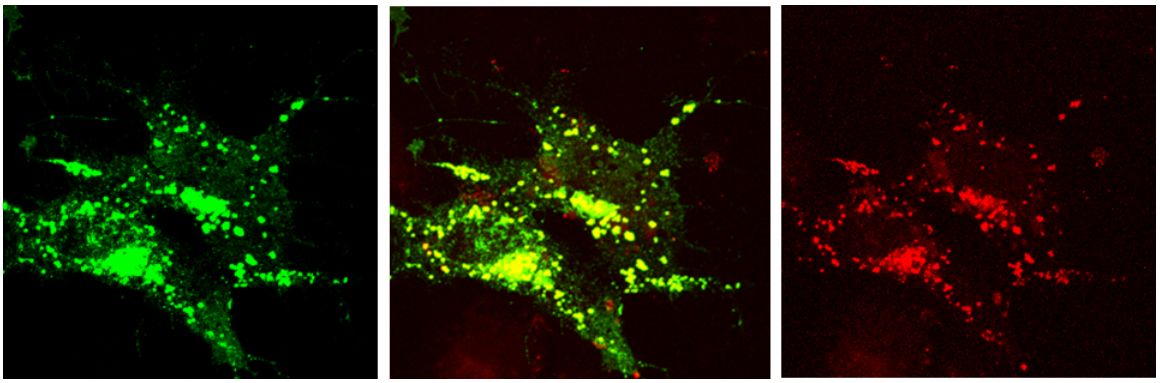

Fig. 3.3.3.4.1: COS-7 cells incubated with NCs at 37°C showing binding and uptake. Left: green channel representing the receptor location due to co expression with EGFP. Right: Sulforhodamine loaded NCs visualized in the red channel. Middle: merge indicating co localization of both receptor and NCs.

Fig. 3.3.3.4.2 shows phase contrast and fluorescence microscopy pictures of differentiated THP-1 macrophages (middle, in green) after binding and uptake of polyG-functionalized sulforhodamine containing NCs (right, in red).

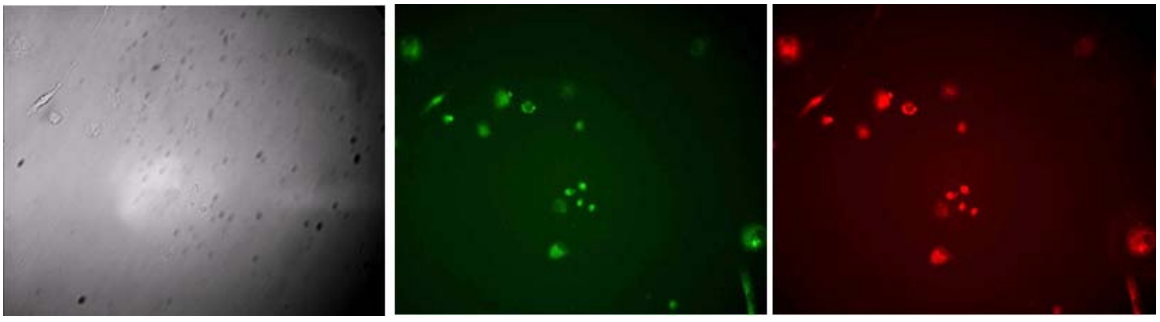

Fig. 3.3.3.4.2: THP-1 cells as visualized with phase contrast microscopy (left), and fluorescence microscopy (middle and right). Cells were permeated and stained, and can be seen in the green channel (middle), whereas NC were loaded with sulforhodamine and detected in the red channel (right).

Fig. 3.3.3.4.3 shows the confocal fluorescence pictures of THP-1 cells incubated NCs with and without ligand. As it can be seen in the middle column, the merge of the channels corresponding to the cells (left, in blue) and the NCs (right, in red) only show co localization when polyG functionalized NCs were present. Corroborating thus the receptor specificity also in this cell line. The kinetics of the uptake were also followed (experiments not shown) by time-lapse fluorescence microscopy. Rapid uptake was observed within the first 30 minutes, whereas after 3 h a saturation condition was achieved.

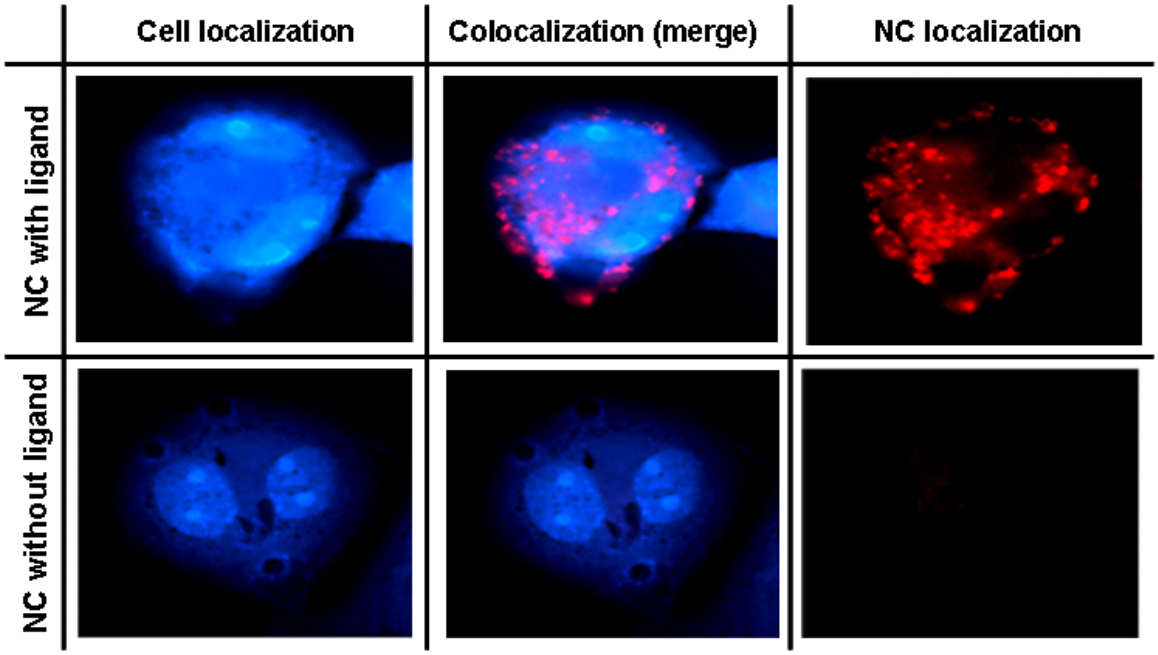

Fig. 3.3.3.4.3: Fluorescence confocal microscopy showing THP-1 activated macrophages incubated with NCs with polyG (upper layer) and without polyG (under layer). Cell localization is depicted in the left column for both NCs with (upper) and without (lower) ligand. NCs localization is shown in the right column. In the central panel the merge is shown, in which co localization of cell surface and NC is evident.

Fig. 3.3.3.4.4 displays the quantitative determinations of the uptake of fluorescently labeled NCs by COS-7 cells expressing SRA1/EGFP fusion receptors[195] as well as control cells lacking the receptor. Quantification was performed by measuring the emission intensity for each cell in different spectral bands, corresponding to the receptor-associated green fluorescence or the red NC fluorescence, respectively. Significant uptake was only observed in cells expressing targeting receptors and NCs containing ligands. This supports a high receptor specificity for transfected COS-7 cells expressing SRA-1, as expected. Interestingly, absence of unspecific binding and uptake is confirmed by the lack of uptake observed with all the controls performed.

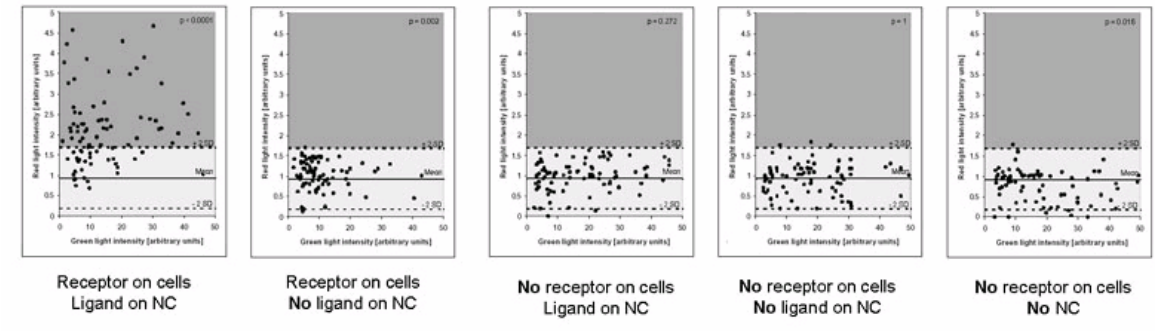

Fig. 3.3.3.4.4: Determination by quantitative bispectral fluorescence microscopy of specific and unspecific NCs uptake by COS-7 cells with and without SRA-1 receptors. For each individual cell the intensity of the emitted light was measured for two different spectral bands. The ordinate corresponds to the red channel, due to NC uptake. The abscissa corresponds to the green fluorescence as given by the co expression of EGFP and SRA-1. The mean (solid line) and standard deviation (broken line) correspond to the negative control consisting of cells devoid of receptor incubated with NC without polyG (d). Significant uptake is taken for values higher than the standard deviation of the negative control and is depicted in gray.

Similar quantification experiments were performed with THP-1 derived macrophages. This cell line always expresses SRA-1 therefore no cell controls can be performed. However, controls consisting of ligand free NCs showed no significant uptake as depicted in Fig. 3.3.3.4.5, whereas THP-1 cells treated with polyG functionalized NCs showed a striking vesicular uptake.

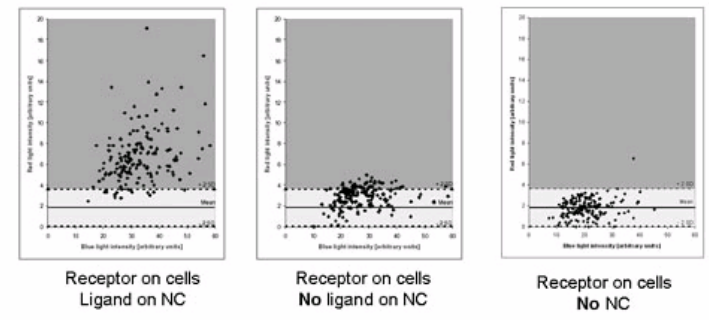

Fig. 3.3.3.4.5: Determination by quantitative bispectral fluorescence microscopy of specific NCs uptake by THP-1 activated macrophages expressing SRA-1. For plot details see Fig. 3.3.3.4.4. Significant uptake, i.e. higher than the standard deviation is depicted in gray.

All experiments performed on cells treated with NCs further confirmed the binding of the complex polyG-biotin-streptavidin-biotin-NC which takes place on cell surfaces followed by internalization by what is believed to be the endocytotic pathway. Interestingly, activated macrophages, known for their avid particle uptake, showed no significant uptake of NCs in the absence of ligand. This low unspecific binding observed supports the "stealth" properties of the NC surface, due to the presence of low protein binding polymer brush.

To investigate the selectivity of the NC towards the targeted cells in favor to other cells, an in vivo situation was simulated by the use of a mixed cell culture system. For this purpose, activated macrophages (THP-1) were cultured alone or in mixed cultures with smooth muscle

cells or endothelial cells. Fig. 3.3.3.4.6 shows the results obtained for mixed cultures of macrophages and vascular smooth muscle cells (VSMCs) and each cell incubated separately.

Upon incubation of different cell types separately and mixed cell cultures with polyG functionalized NCs loaded with sulforhodamine the fluorescence images shown in Fig. 3.3.3.4.6 were obtained. The left column shows images of THP-1 cells as incubated with polyG functionalized NCs. A notable co localization is evident from the overall distribution of blue fluorescence, due to THP-1 autofluorescence, and red fluorescence, due to encapsulated sulforhodamine. The central column shows the images obtained with VSMCs incubated with NCs, from the absence of fluorescence in the red channel corresponding to the presence of NCs it can be concluded that no uptake of NC took place with this cell line. Mixed cultures of THP-1 and VSMCs only showed co localization of THP-1 cells (in blue) and NCs as depicted in the left column of Fig. 3.3.3.4.6. Similar results were obtained for mixed cell cultures of human macrophages with human endothelial cells (not shown). Neither vascular cells nor endothelial cells showed NC uptake. NCs bound only to SRA-1 expressing macrophages.

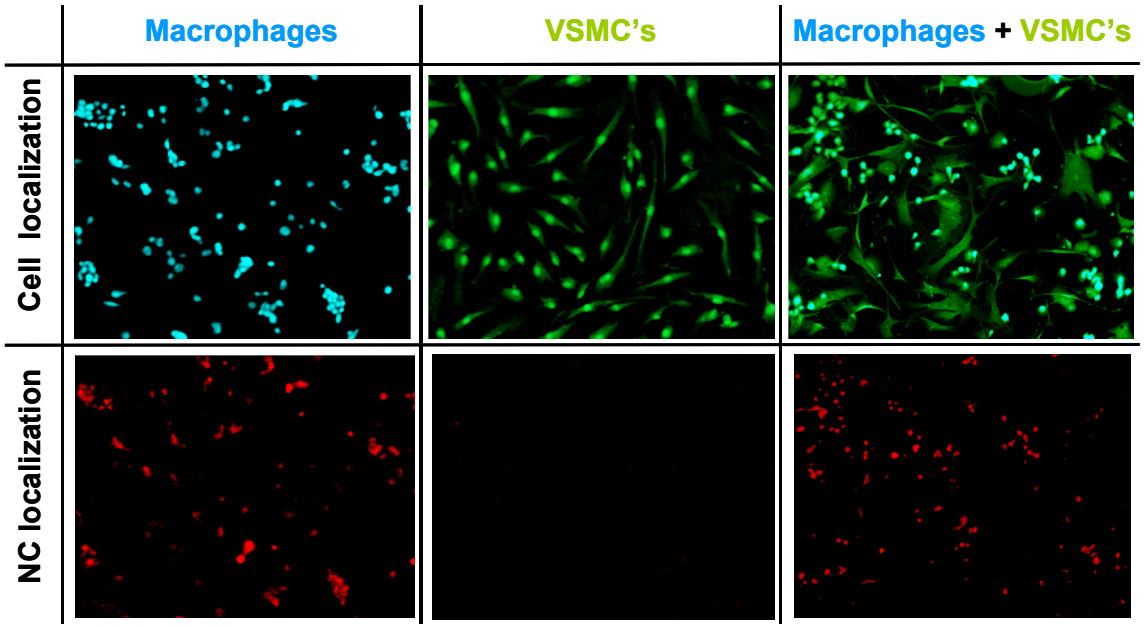

Fig. 3.3.3.4.6: Fluorescence microscopy of different cell lines and mixtures thereof, showing the selectivity of targeting of polyG functionalized NCs. Macrophages (THP-1) (upper left) incubated with sulforhodamine encapsulated NCs (lower left); vascular smooth muscle cells (VSMCs) (upper middle) incubated with sulforhodamine encapsulated NCs (lower middle); cell culture mixture of THP-1 and VSMCs (upper right) incubated with NCs. NCs were loaded with sulforhodamine and detected in the red channel, whereas THP-1 showed blue autofluorescence in the blue channel, VSCMs were dyed.

The selectivity of the targeting of polyG functionalized NCs towards cells expressing SRA-1 was thus confirmed since no detectable uptake of these NCs was observed with cells which do not express this type of receptor (vascular smooth muscle cells and endothelial cells).

3.3.3.5. Cytotoxicity studies

Within the studies performed on the targeting nanocontainers, preliminary cytotoxicity tests were carried out. The results are presented in Graph 3.3.3.5.1, which shows that the mortality of cells incubated with NCs was in the range of the untreated cells. A positive control of camptothecin showed high-expected cell mortality.

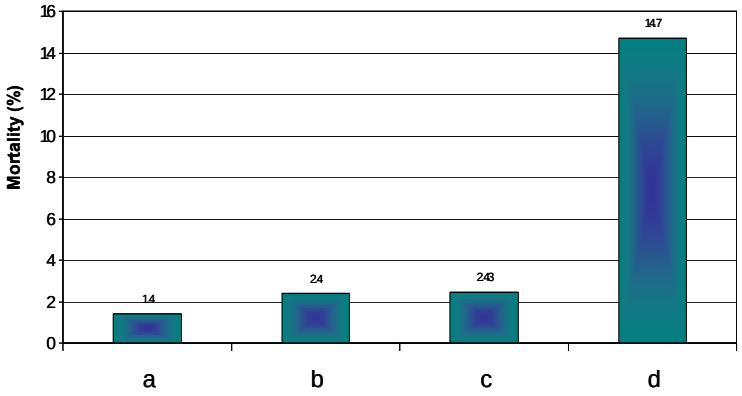

Graph 3.3.3.5.1: Results from apoptosis assays, a) untreated cells; b); cells treated with NCs control (neg. control); c) cells treated cells treated with NCs containing streptavidin and polyG; d) cells treated with camptothecin (tox. pos. control).

Viability percent can be calculated as $Viability(\%) = (N_t / N_c) \times 100$, where N_t and N_c are the number of surviving cells in the treated groups with NCs, and in the untreated group respectively. The viability obtained for ligand labeled NC was 98.98%, which indicates low toxicity.

The results of a [3H]adenine release assay with non-functionalized and polyG functionalized NCs indicated no evidence of toxicity. For the negative control, i.e., untreated differentiated THP-1 cells, the total cell bound adenine release at 4 h was 11.1% (±2.9%) and 35.5% (±4.8%) at 24 h. A positive control consisting of differentiated THP-1 cells treated with 10% ethanol gave an adenine release of 51.6% (±3.6%) at 4 h and 59.9% (±3.3%) at 24 h. Differentiated THP-1 cells treated with non-functionalized and functionalized NCs yielded an adenine release of 15.4% (±2.6%) and 15.1% (±2.6%) at 4 h and of 35.6% (±2.0%) and 36.7% (±1.4%) at 24 h respectively. The toxicity observed for NCs was not significantly different from that of untreated cells (negative control). These results confirm the previous findings and demonstrate the biocompatibility of the chemical building blocks. Thus, it can be concluded that PMOXA-PDMS-PMOXA polymer NCs do not exhibit cell toxicity. However, systemic toxicity should be evaluated as well as distribution and accumulation in different organs.

Although sterilization processes have not been investigated up to now, it is important to notice that the preparation method for the nanocontainers, by filtration through pores of diameters less than 0.45 nm provides a means for sterilization by itself.[184]

3.3.4. Conclusions and Summary

Receptor specific, fully synthetic polymer NCs for targeting of cells were studied. By using ligands as homing devices, it is possible to target a cell line specifically as demonstrated with polyG functionalized NCs. Biotinylated NCs allow for a large degree of freedom in functionalization making polymer NCs a flexible platform for targeting delivery systems.

NCs binding and uptake took place only with receptor containing cells. The uptake by the targeted cells is believed to occur by an active endocytotic process. Contrary to this, no binding and uptake of functionalized NCs was detected in cells which do not express the targeting receptor SRA-1, whether cells that naturally do not express it or transgenic modify ones.

Interestingly, activated macrophages, cells well known for their intrinsic high uptake activity, did not show binding and uptake of ligand-deprived NCs, which supports the stealth characteristics of the NCs making them ideal for specific targeting. Selectivity towards the targeted cell line was investigated in cell culture mixtures, where binding and uptake was observed only for the target cell line. Furthermore, no cell cytotoxicity was observed in preliminary tests.

Sterilization of the NCs should be further investigated. Most promising methods for this are gamma irradiation, and electron beam irradiation.

3.4. Gold encapsulation

3.4.1. Introduction

In order to follow the pathway of the nanocontainers into the cells, it was decided to pursue a gold nanoparticle encapsulation. Gold nanoparticles are interesting since they have a high contrast in TEM, making them ideal markers of structures. The loading of liposomes with colloidal gold proved to be useful for overcoming the problem of resolving the intracellular liposomes from other native vesicular structures found in cells.[196]

In the case of liposomes it is well established, that following receptor-mediated endocytocis the intracellular fate of liposomes and their encapsulated molecules is to encounter a low pH compartment.[196] In the case of polymeric vesicles accessing the cell via an active targeting pathway as in our case, it needed to be clarified what kind of intracellular structures the vesicles would encounter. Therefore, encapsulation of gold particles was intended as a method of tracing the fate of the nanocontainers in vitro.

Encapsulation of gold nanoparticles would also provide a further proof of the hollowness of the structures used. In particular by a combination of hydrophobic and hydrophilic gold nanoparticles it might be possible to show if there was a small percentage of micellar structures coexisting with the vesicular structures, as found in other block-copolymer systems.[44] It could also serve as a tool for proving the hollowness of tubular or rod-like structures obtained with other vesicle preparation methods.

3.4.2. Results and discussions

3.4.2.1. Encapsulation of pre-formed gold nanoparticles

Different approaches were used to encapsulate pre-formed gold nanoparticles in the inner volume of the nanocontainers. Established protocols were used to prepare the gold nanoparticles.

For this purpose, hydrophilic and hydrophobic gold nanoparticles were prepared, and subsequently encapsulated in polymer nanocontainers. Hydrophobic thiol-capped gold-particles of different sizes could be obtained.[197, 198]

A method developed by Gittins et al. was used to prepare hydrophilic coated gold nanoparticles.[199] The procedure is based on the preparation of gold nanoparticles in an organic solvent, similar to hydrophobic particles, but with a last step involving the exchange of thiol ligands, and the subsequent transfer of the modified particles to an aqueous solution (so-called post-synthesis modification),

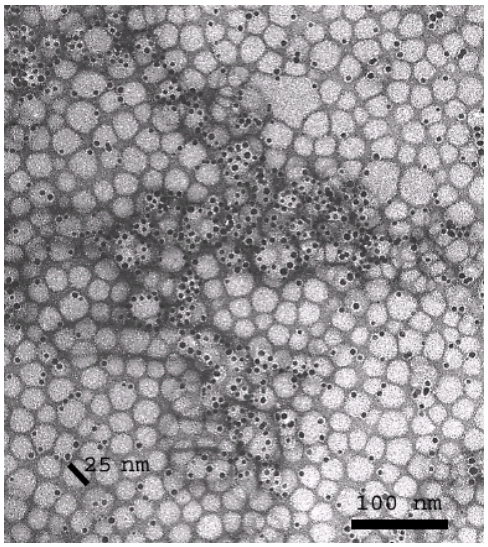

Picture 3.4.2.1.1: TEM picture of a vesicle sample prepared by the standard injection/extrusion ethanol method with hydrophilic gold particles previous to chromatographic separation.

TEM pictures showed no encapsulation of gold nanoparticles with any of the encapsulation approaches using pre-formed gold nanoparticles (hydrophobic and hydrophilic gold). In the case of hydrophobic gold particles this would be expected when having a system with only vesicular structures. However, for the hydrophilic gold particles encapsulation was expected and either did not occur, or did not occur to a significant degree. This can be due to steric hindrance effects occurring during the preparation of the polymer vesicles. Another plausible explanation could be that destruction of the encapsulated entities could have taken place during the chromatographic separations used to remove the non-encapsulated gold.

There are only a few publications dealing with the direct encapsulation of gold nanoparticles in liposomes, which might indicate that the procedure itself is not favored, that is, the encapsulation of a particle in a vesicle is not very likely. This can be also interpreted under statistical considerations, and whenever reported, the encapsulation of gold nanoparticles in liposomes was also very low. Moreover, several groups reported that the density of the gold might influence the low encapsulation observed as well with pre-formed gold nanoparticles in liposomes.[200, 201] Other groups reported that colloidal gold as it is, that is, without any stabilization, can not be encapsulated in liposomes, since for high loading efficiency high concentrations are needed, at which gold sols precipitate.[200]

As this approach was not successful, other ways of introducing gold into the void volume of the nanocontainers had to be tried, for example by the direct formation of the particles within the vesicles.

3.4.2.2. In situ gold encapsulation

In situ gold encapsulation can be obtained, by encapsulating a gold salt in the nanocontainers and subsequent formation of the particles in the inner cavity of the nanocontainers. This not only turns out as a means of obtaining encapsulated gold but might also prove to be a new method for the templating of gold nanoparticles. For this purpose, three different methods of in situ gold particle preparation were tested.

In a first method (AUM in situ 1) polymer vesicles were loaded with gold particles by direct generation of the colloid within the pre-formed vesicles.[196, 200] This method involved the preparation of gold nanoparticles at pH 6 with subsequent heating, which should promote the reduction of the salt.

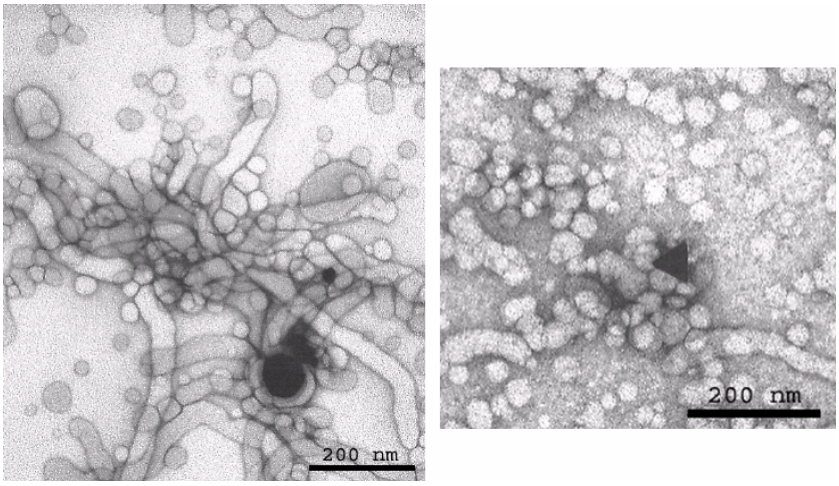

Picture 3.4.2.2.1: TEM pictures of the vesicles obtained by the standard ethanol method (polymer JW05) and the AuM in situ 1.

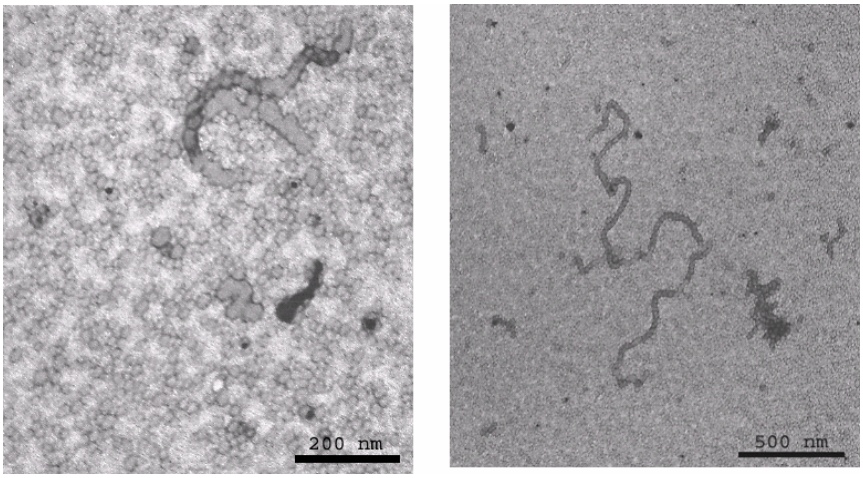

Picture 3.4.2.2.2: TEM pictures of the vesicles obtained by the standard ethanol method (polymer S131) and the AuM in situ method 1.

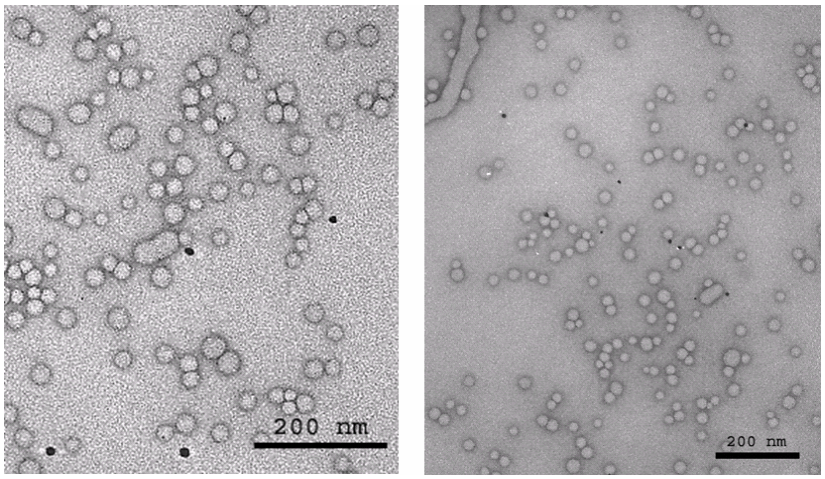

Picture 3.4.2.2.3: TEM pictures of the vesicles obtained by the direct dispersion method (polymer JW05) and the AuM in situ method 1.

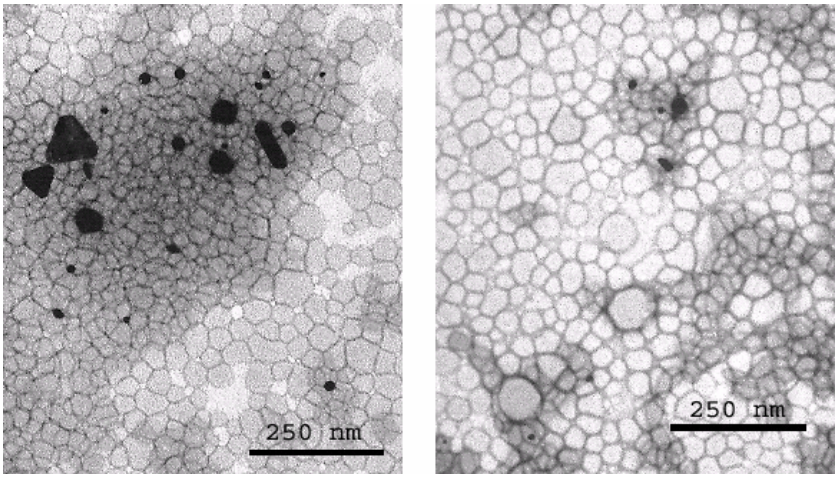

Picture 3.4.2.2.4: TEM pictures of the vesicles obtained by the direct dispersion method (polymer S131) and the AuM in situ method 1.

As it can be seen in Picture 3.4.2.2.1 to Picture 3.4.2.2.4, no gold encapsulation took place for any of the two polymers used or any of the vesicle preparation methods when the Au in situ method 1 was used. This was surprising since a similar method was also reported for in situ encapsulation of gold nanoparticles in liposomes.[202]

In the second method (AUM in situ 2) the chloroauric salt was encapsulated at initial pH 3 to inhibit the formation of gold particles during vesicle preparation. The pH was then changed to pH 6 and the sample was incubated 30 min, this pH change induced the reduction to metallic gold.[203] This approach is a slight modification of the preparation used before (AUM in situ 1).[200]

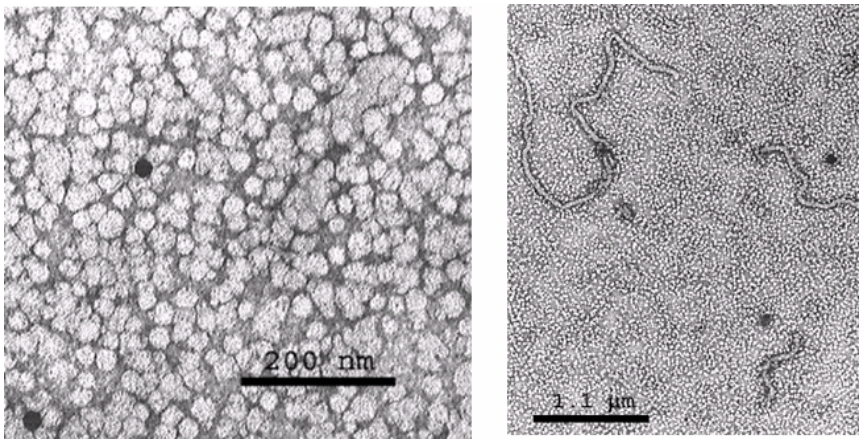

Picture 3.4.2.2.5: TEM pictures of the vesicles obtained by the standard ethanol method (polymer JW05) and AuM in situ2.

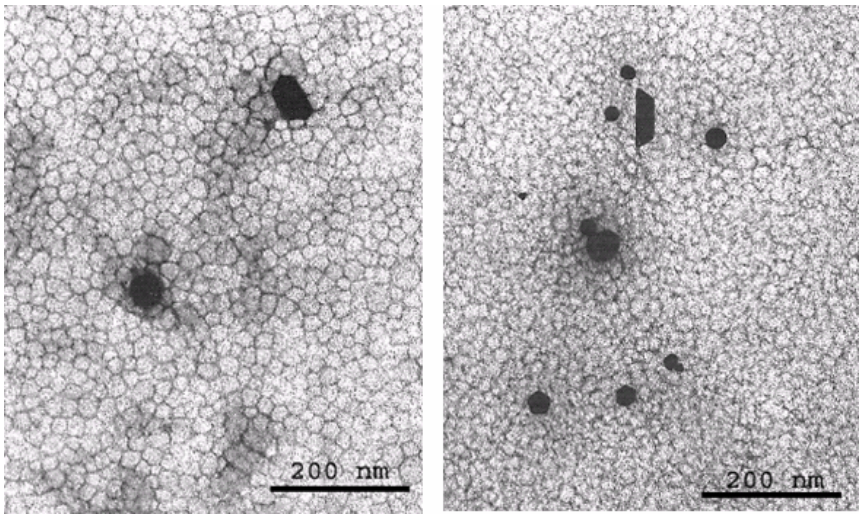

Picture 3.4.2.2.6: TEM pictures of the vesicles obtained by the standard ethanol method (polymer S131) and the AuM in situ 2.

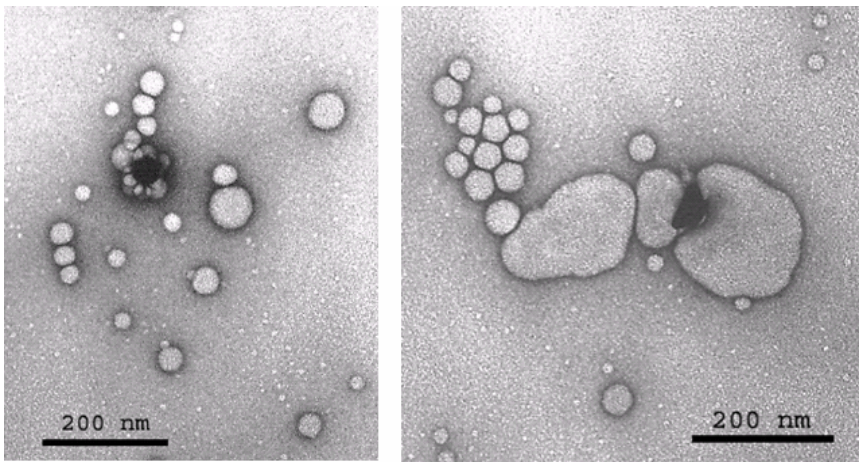

Picture 3.4.2.2.7: TEM pictures of the vesicles obtained by the direct dispersion method (polymer JW05) the AuM in situ 2.

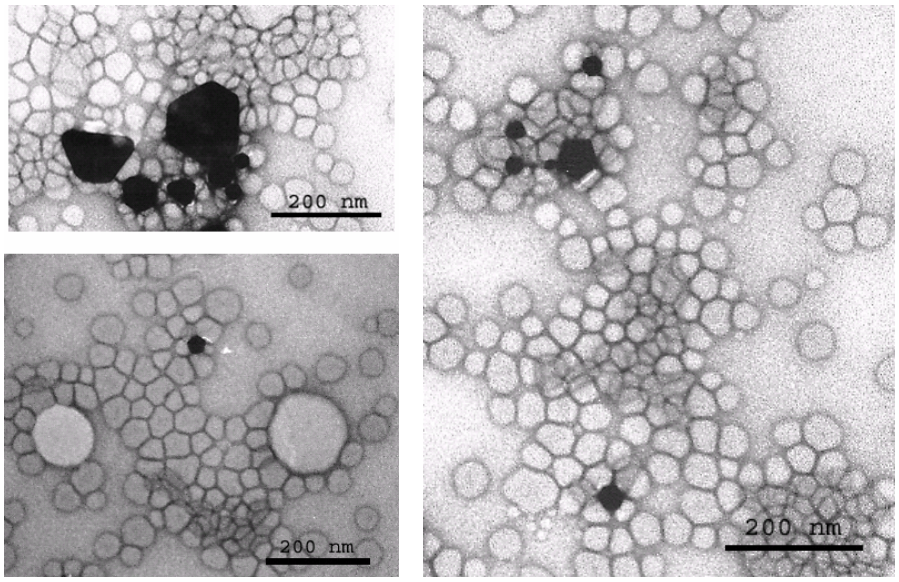

Picture 3.4.2.2.8: TEM pictures of the vesicles obtained by the direct dispersion method (polymer S131) and the AuM in situ 2.

Again with this second method, no encapsulation of gold was achieved as it can be seen in Picture 3.4.2.2.5 to Picture 3.4.2.2.8.

In general, no significant gold encapsulation inside the vesicles was found with any of the methods attempted. Either the formation of triangular or hexagonal plates of gold, that is, gold crystals growing preferentially in the 111 plane[204] nanoparticles were obtained. Gold particles appeared mostly at the interface between two or more vesicles, but rarely in their interior. Therefore, it cannot be concluded that the in situ encapsulation of gold was successful.

A modification of the first in situ gold formation approach was attempted. It involved the addition of the reducing agent (citrate) in a second step, that is, after formation of the vesicles. It is worth mentioning that in this case the vesicle preparation was diluted by a factor of 2 in comparison with the methods previously described. In addition, taking into account that the chromatographic separations further dilute the samples, it is not surprising that the TEM pictures obtained in this case showed particularly diluted systems. Nevertheless, no gold encapsulation was observed either, which is expected when considering the relative impermeable membrane of the polymeric vesicles. A large anion such as citrate it is not likely to permeate the vesicular membrane. Also worth mentioning is the fact that the vesicles prepared in $HAuCl_4$ (12.72 mM) and the gold salt solution itself were stable for more than one week. Regarding the stability of the samples after addition of citrate, it was observed that the gold aged in these samples, which is clearly a consequence of the non-encapsulation of the gold. If the gold particles would have been encapsulated in the vesicles, then no aggregation should have occurred and the gold suspensions would have been stable on storage.

A third method comprising the photoreduction of gold salts by means of UV irradiation was also attempted. The protocol described by Sato et al.[205] involved the use of a $NaAuCl_4$ solution for the preparation of the vesicles was used. It comprised a subsequent UV irradiation step to promote the Au reduction, with resulting particles with sizes ranging from 5 to 7 nm. In this case a solution of 0.4 mM $NaAuCl_4$ was encapsulated in vesicles prepared with two different methods, standard and direct dispersion methods and two different polymers. Contrary to what expected the vesicle samples reacted prior to UV irradiation, on stirring overnight, and these samples were not further analyzed by TEM.

In a similar photoreduction approach,[204] the formation of spherical nanoparticles was reported in the presence very low concentrations of polymer and gold salts. When lower concentrations of $NaAuCl_4$ and polymers were used, again no significant gold encapsulation was observed. This was intriguing since other groups have reported the in situ formation of gold particles by photoreduction in liposomal systems.[204, 206, 207]

In general, in situ encapsulation of gold in liposomes seems to be also not very successful, since only a few papers dealt with such an approach. It is clear that in the case of the vesicles formed by the standard, or so-called ethanol method, the ethanol might be a factor playing a role in the reduction of gold chloride, since it is known that ethanol induces the reduction of metals in solution.[208] What was unexpected was that the polymer itself seemed to also promote the gold chloride reduction, as found in the samples prepared by direct dispersion. One can suppose that the alcohol end groups of the polymer might participate in the reduction of the gold salts in a similar way as low molecular weight alcohols do. Another plausible explanation could be the presence of impurities in the polymer, which might promote the reduction of the chloroauric acid.

3.4.3. Conclusions

Neither encapsulation of pre-formed and in situ formation of gold nanoparticles was achievable with the procedures attempted. Effects such as steric hindrance, or density mismatch of the gold particles can be attributed to the non-encapsulation found with pre-formed particles. On the other hand, for the in situ formation of gold nanoparticles, usually a premature reduction of gold took place, which might be due to the ethanol present in the samples made by the standard injection/extrusion method, or impurities in the polymer in the case of the direct dispersion method.

Since the encapsulation of gold nanoparticles turned out to be unsuccessful, it was not possible to trace the fate of polymer vesicles in cells in in-vitro experiments. The proof needed to verify if these structures correspond to the nanocontainers was attempted by the gold encapsulation, which failed.

3.5. Vesicle immobilization onto surfaces

3.5.1. Introduction

Biosensors are a continuously growing field of investigation. One important characteristic common to most biosensors is the immobilization onto a surface. For instance, liposomes have been immobilized on surfaces to produce sensors. [209] This technology can also be applied to polymer vesicles. It is thus interesting to investigate the potentiality of polymeric vesicles as immobilized sensors. The interest on the immobilization of polymeric vesicles on surfaces resides on the possibility to improve sensor systems. Special features of polymer vesicles include their higher stablility over lipidic counterparts, and versatility on the choice of constituting blocks, functionalization, etc. Moreover, their ability to incorporate functional transmembrane proteins, encapsulated guest molecules, and to function as stimuli-responsive structures make surface-immobilized vesicles attractive candidates for applications in nanoscale sensing devices. Amongst other things, the use of polymeric vesicles proves advantageous since they possess higher stability, and a lower cac, therefore, they can stand the washing steps usually required for biosensors. Moreover, the nanoreactors concept[8, 59, 210] brought to a surface might function by itself as a bio-sensor device.

Not only in the field of biosensors there is a need for coupling molecules to solid supports that render the material biologically functional, but also in biomaterials, chromatography, and many areas of biotechnology. Ideally, immobilization of a biomolecule to a surface should take few steps, be applicable to an array of surfaces (polymers metals and ceramics), and provide stable and functional molecular films.

Immobilization is usually achieved by either physisorption or chemisorption techniques. Physisorption usually results in surfaces that suffer from denaturation, leaching and inconsistency in the activity of the adsorbed layer. Chemisorption of biomolecules does not suffer from the aforementioned disadvantages and provides a durable linkage between the molecule and the surface.[211] However, chemisorption needs in some cases the use of rather harsh conditions, which are not always desirable when manipulating labile substances such as proteins. In this respect very specific anchoring approaches can be found in bioaffinity coupling, such as epitope-antibody, ligand-receptor, and nucleic acid pairs.

The immobilization of nanocontainers onto surfaces can be achieved by different approaches. One is by the attachment of thiol-functionalized nanocontainers onto gold surfaces via S-Au bonding.[212] Another strategy would be to combine the strategy used by Prof. Dr. Marcus Textor's group with our polymer based nanocontainer. The protocol for surface modification that has been developed in the group of Dr. M. Textor,[109, 110] allows the preparation of surfaces with different specificity for binding.[111] The approach is based on the use of two different ad-

sorption characteristics towards the bulk of the solution, on one side a non-fouling or protein repellent PEG surface, and on the other side a bio-affinity binding moiety given by biotinylated PEG chains. The adsorption of the PEG chains to the surface is achieved through grafting to a poly(lysine) backbone. This allows the electrostatic adsorption of the positively charged poly(lysine) onto negatively charged metal oxide surfaces.[109, 110]

In order to provide specific adsorption of nanocontainers to sites on the surface, biotinylated nanocontainers were chosen.[212] This type of bio-affinity interactions should render more stable and specific attachment than simple physisorption, and attachment under milder conditions when compared to chemisorption. The general use of biotin-streptavidin technology was already discussed in Section 3.3.1.

Moreover, immobilization onto surfaces can be combined with different patterning approaches[209, 213-217] rendering more complex sensor chip architectures.

3.5.2. Results and discussions

3.5.2.1. Quartz crystal microbalance with dissipation experiments

The strategy used to immobilize nanocontainers onto a surface was carried using the approach developed in Dr. M. Textor's group and in close collaboration with them. Their approach, displayed in Scheme 3.5.2.1.1 a, consists on adsorption of a graft copolymer composed of a poly(lysine) backbone and poly(ethylene glycol) graft chains (PLL-g-PEG).[109, 110] These graft copolymers can be immobilized onto surfaces by electrostatic adsorption of the positively charged backbone onto negatively charged metal oxide surfaces.[104-106] Since poly(ethylene glycol) is protein repellent, it is highly suited for bio-sensing devices.[109] Furthermore, these graft copolymers were functionalized with biotin to render a platform for biotin-streptavidin technology.[111]

The graft copolymer used to promote adsorption onto the substrate was PLL(20)-g[3.5]-PEG(5)/PEGbiotin(3.4)30%. In this case PLL(*x*)-g[*y*]-PEG(*z*)/PEG(*w*)*v*% means that the graft copolymer has a PLL backbone of *x* kDa, a grafting ratio (lysine monomer to PEG pendant chain) of *y*, and a PEG pendant chain of *z* kDa. The biotinylation degree is given by the percentage *v*, whereas *w* describes the molecular weight of the biotin bearing PEG chain. In short, the factor 3.5 means that 2 out of 7 lysine residues are attached to PEG chains, while 30% indicates that 3 out of 10 PEG chains are biotinylated. These proportions have been found to give the best coverage to avoid unspecific binding of plasma proteins, while favoring the specific anchoring of streptavidin reducing steric hindrance effects.[111]

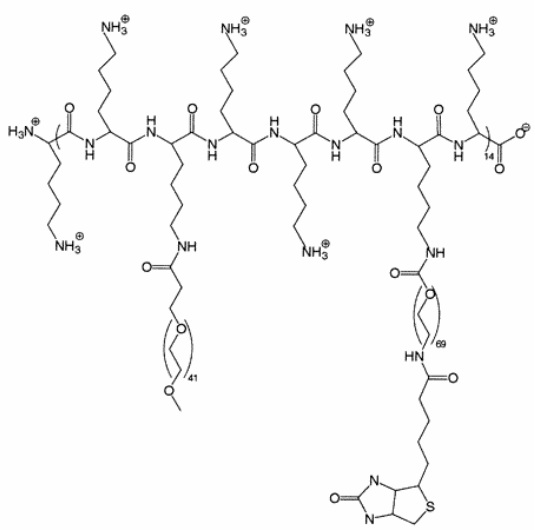

Fig. 3.5.2.1.1: Molecular structure of the PLL-g-PEG-biotin used in this section. Taken from[111].

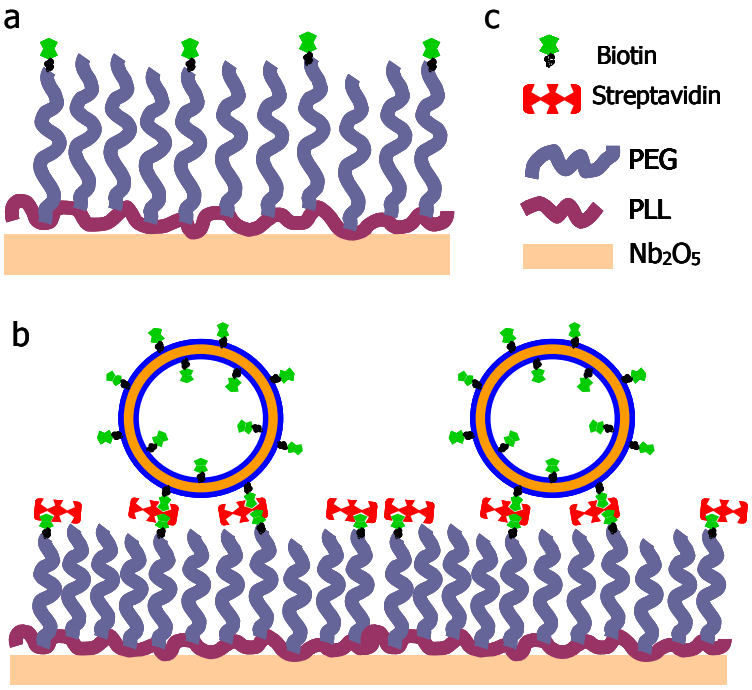

Scheme 3.5.2.1.1: Immobilization approach using PLL-g-PEG biotin and biotinylated NC, a) the graft copolymer PLL-g-PEG containing pending biotin moieties is adsorbed in a first step onto a negatively charged metal oxide surface, b) after the introduction of a streptavidin layer, biotinylated NC labeled with biotin can be anchored to the resulting streptavidin layer, c) abbreviations and description of the codes used in this scheme.

In order to immobilize the polymer vesicles onto a surface, first a layer of PLL-g-PEG biotinylated graft copolymers (PLL-g-PEG-biotin) was adsorbed onto a niobium oxide surface

(see Scheme 3.5.2.1.1, a). After rinsing with buffer[17], the surface was subsequently exposed to a solution of streptavidin, which coupled to the biotin present on the graft copolymer. Subsequently, the layer was rinsed with buffer, and exposed either to biotinylated nanocontainers or control nanocontainers without biotin (see Scheme 3.5.2.1.1, b).

The adsorption steps were followed by their corresponding frequency shifts and dissipation changes. When necessary, other overtones are also displayed. In all cases the adsorption of PLL-g-PEG was accompanied by a frequency shift of about 44 Hz (arrow 2 in Graph 3.5.2.1.1 and Graph 3.5.2.1.2) as expected from previous experiments[18]. The adsorption of the streptavidin to the biotin present on the graft copolymer gave an expected frequency shift (arrow 4 in Graph 3.5.2.1.1 and Graph 3.5.2.1.2) of 22 Hz.[212] By knowing the frequency shift, the thickness of the streptavidin layer can be calculated via the Sauerbrey relation (see Section 4.19.1). This corresponds to a two-dimensional array of streptavidin with a layer thickness of approximately 4.7 nm, which coincides well with the crystallographic[218] dimensions of streptavidin of 4.5x4.5x5.5 nm^3, and a hight of 4.65 nm found with AFM.[219]

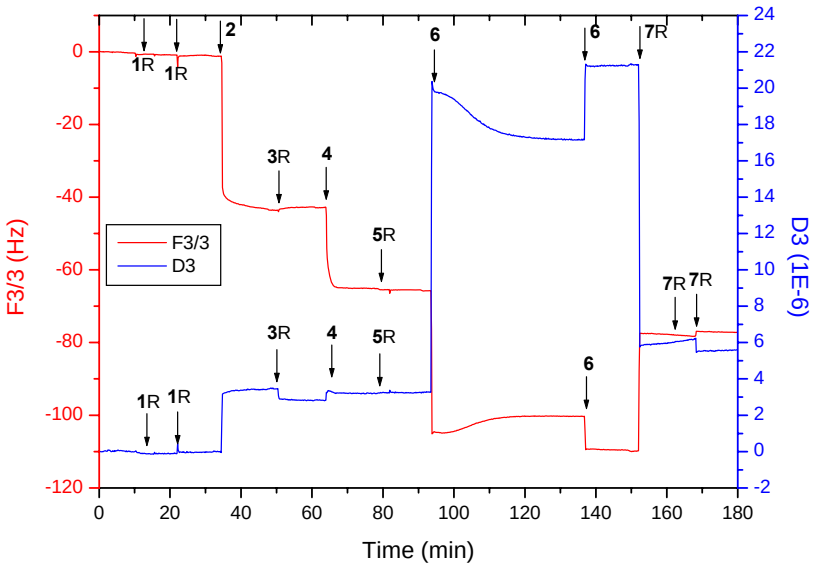

Graph 3.5.2.1.1: Frequency shift and dissipation for the immobilization of biotinylated NCs onto a streptavidin functionalized surface. Steps of the procedure are depicted with arrows as; 1: rinse with PBS, 2: addition of PLL-g-PEG 30% biotinylated in PBS (0.5 mg/ml), 3: rinse with PBS, 4: addition of streptavidin in PBS (0.02 mg/ml), 5: rinse with PBS, 6: addition of vesicle's solution biotinylated NC (50% biotin), 7: rinse with PBS.

[17] Rinsing steps are required for the elimination of loosely physisorbed species.

[18] Fernanda Rossetti (ETH, Zürich), personal communication.

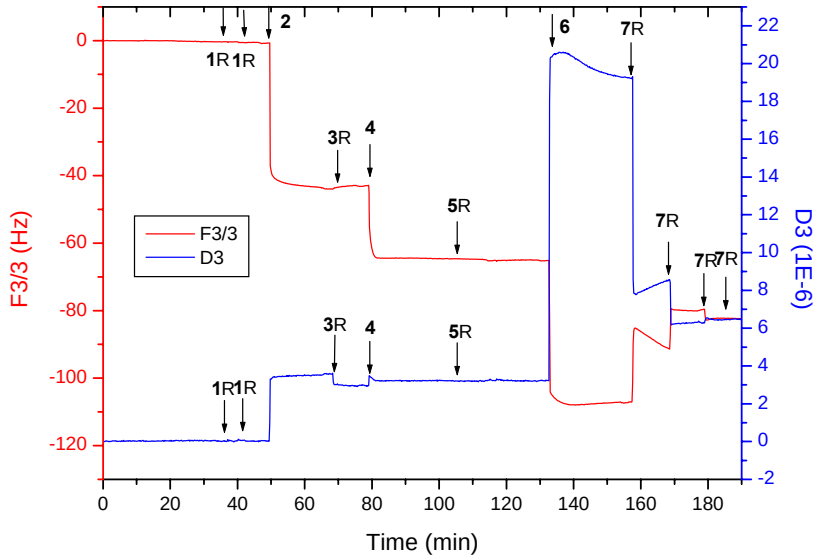

Graph 3.5.2.1.2: Frequency shift and dissipation for the immobilization of control NCs onto a streptavidin-functionalized surface. Steps of the procedure are depicted with arrows as; 1: rinse with PBS, 2: addition of PLL-g-PEG 30% biotinylated in PBS (0.5 mg/ml), 3: rinse with PBS, 4: addition of streptavidin in PBS (0.02 mg/ml), 5: rinse with PBS, 6: addition of vesicle's solution NC control (0% biotin), 7: rinse with PBS.

With biotinylated nanocontainers a very slow decrease of the frequency was observed. This can be attributed to the slow dynamics of vesicle diffusion. Contrary to what expected, for the control experiments without biotin, the same results were obtained and no desorption of the vesicles was achieved after several rinsing steps. The initial frequency shift can be attributed to diffusion and unspecific adsorption to the protein layer, which would be the same in the case of vesicles with and without biotin. However, after the rinsing step, the unspecific adsorbed vesicles should have been removed. To analyze if the observed behaviour is due to unspecific adsorption, experiments with other proteins should be performed.

Moreover, it is plausible, that the amount of streptavidin attached to the first layer of graft copolymer might influence the ability of the nanocontainers to approach the streptavidin surface. Another possible explanation for the same behavior encountered with biotinylated and non-biotinylated nanocontainers could be due to steric hindrance. The biotin moieties might not be able to approach the streptavidin surface, resulting thus in a similar effect observed with biotinylated and non-biotinylated vesicles.

The changes in dissipation after rinsing the adsorbed vesicles could be due to changes in the viscosity of the buffer in contact with the sensor, as previously observed[19]. If there is a

[19] Q-news Volume 3, Issue 1, March 2003. www.q-sense.com

large difference in the viscosity of the bulk buffer in comparison with the vesicle suspension, a decrease in the frequency shift and the dissipation can be explained by the fact that the replacement of the vesicle solution with buffer solution changes the viscosity of the layer coupled with the sensor. Nevertheless, if after the rinse with buffer the frequency does not return to the initial value prior to vesicle exposure (or baseline), then an adsorption has taken place.

To minimize the effect of the difference of the viscosity of the nanocontainer suspension and the rinsing buffer, the vesicle suspension was diluted to one third of its original concentration and the measurements were repeated in the same manner as already described.

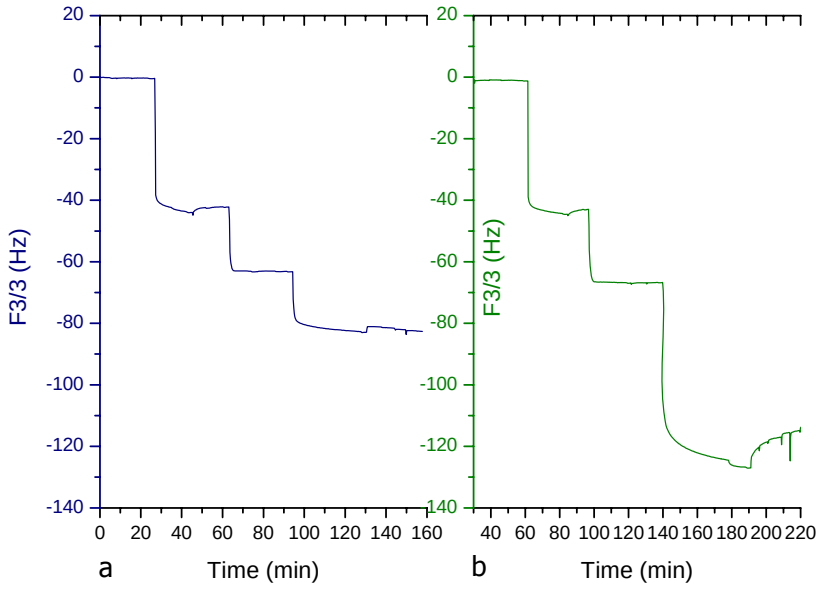

Graph 3.5.2.1.3: a) frequency shift and dissipation for immobilization of biotinylated NCs (dilution 1/3) onto a streptavidin functionalized surface (in blue), b) frequency shift and dissipation for immobilization of control NCs (dilution 1/3) onto a streptavidin functionalized surface (in green).

Graph 3.5.2.1.3 shows that the effect of washing with buffer was less noticeable and correlated well with the previous interpretation due to viscosity differences. Nevertheless, for both biotinylated nanocontainers and non-biotinylated nanocontainers adsorption was observed again which indicates non-specific adsorption. Contrary to what it was expected, non-biotinylated control vesicles, showed even higher frequency shifts.

The binding capacity of the nanocontainers should depend also on the coverture of the biotin motif on its surface. Various ratios were used to modify the surface concentration of biotin on the nanocontainers to find the most suitable ratio, that is able to promote interaction but that at the same time reduces the intrinsic steric hindrance of the bulky biotin-(strept)avidin system. However, this led to no significant changes observable. Nevertheless, other conditions

should be investigated, for instance, lowering the coverage of streptavidin layer, which might also reduce the steric hindrance.

In order to determine the steric hindrance contribution to the adsorption, the stratified approach was slightly modified. Biotinylated PLL-g-PEG was initially adsorbed onto the niobium oxide surface (see Scheme 3.5.2.1.2 a). In a second step, (biotinylated) nanocontainers previously incubated with streptavidin and subsequently purified by size-exclusion chromatography were introduced in the QCM-D measuring chamber (see Scheme 3.5.2.1.2 b).

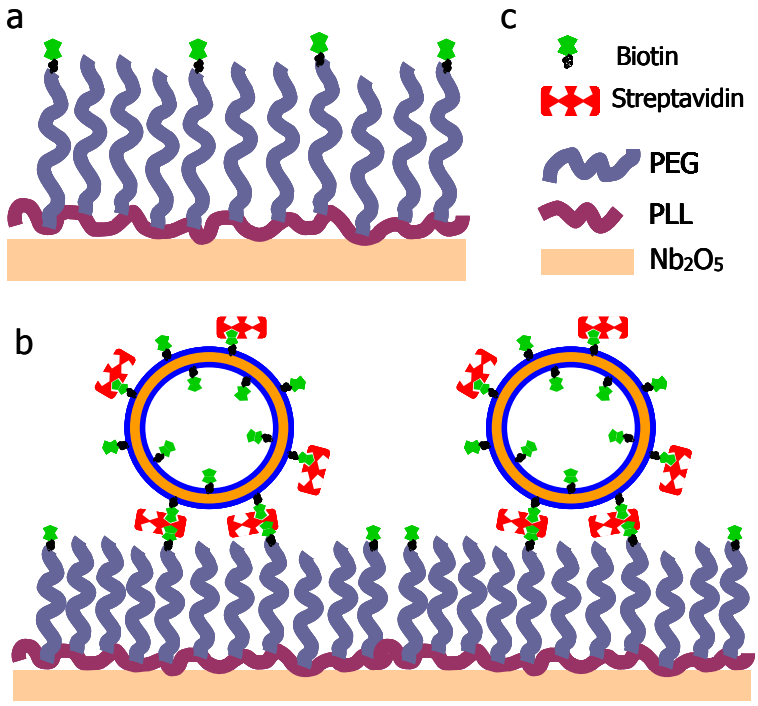

Scheme 3.5.2.1.2: Second immobilization approach, a) the graft copolymer PLL-g-PEG-biotin is adsorbed in a first step onto a metal oxide surface, b) biotinylated NC labeled with streptavidin could be anchored to the biotin moieties present at the graft polymer surface, c) abbreviations and description of the codes used in this scheme.

Graph 3.5.2.1.4 shows that the expected frequency shift due to preferential adsorption of biotinylated vesicles was not observed. Moreover, no quantitative difference between the adsorption of biotinylated or non-biotinylated nanocontainers could be obtained. The observed curves only rendered one evident qualitative difference between the two systems: the adsorption profile. With biotinylated vesicles the frequency shift tends to be slower, whereas with control vesicles, the frequency shift was abrupt. A slower frequency shift might indicate either slower dynamics or a process requiring a certain equilibration time, as might be the case with the biotinylated nanocontainers.

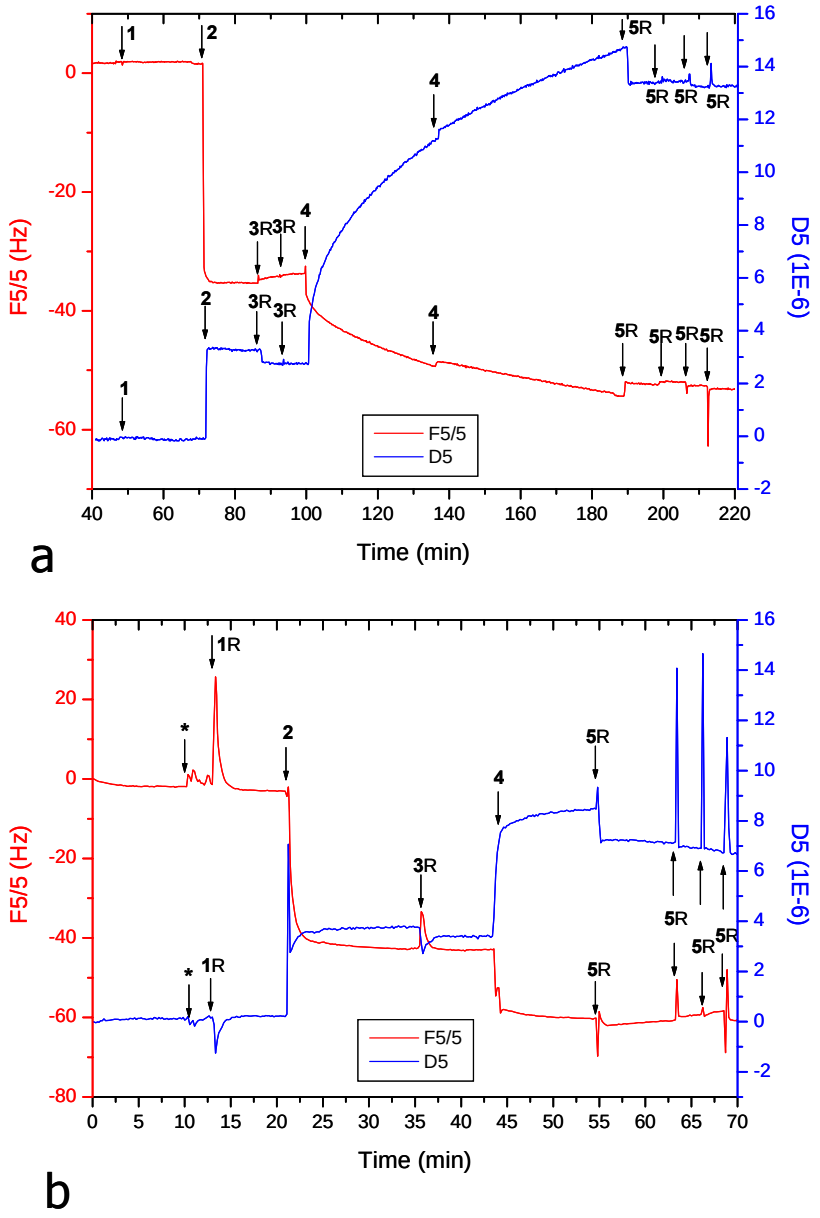

Graph 3.5.2.1.4: Adsorption profile of biotinylated NCs, according to the second second approach, a) NCs containing 10% biotin, b) NC control (0% biotin). Steps are represented as; 1: rinse with PBS, 2: addition of PLL-g-PEG 30% biotinylated in PBS (0.5 mg/ml), 3: rinse with PBS, 4: addition of complex of NC (x% biotin)/streptavidin (chromatography purified), 5: rinse with PBS.

It should be emphasized that after addition of each analyte, the chamber was rinsed with buffer, which in some cases produced spikes (see Graph 3.5.2.1.4, b). This is due to the change of the solution in contact with the sensor crystal, and is also very temperature sensitive. If the chamber was not properly thermostated those spikes were quite intense.

Since the previous results indicate unspecific adsorption between the polymer vesicles and the streptavidin coated surface, several controls became necessary. The adsorption of the

polymer vesicles on protein layers and the interaction between the polymer vesicles and the graft copolymer was thus assessed. This last contribution to the unspecific adsorption can be discarded on the basis of theory of polymer segregation or immiscibility.[46, 220] However, an interaction due to unspecific adsorption on proteins contradicts the reported low protein adsorption of poly(2-methyl-2-oxazoline) polymers.[113, 127] Nevertheless, it proved interesting to assess the protein adherence in the particular case of the vesicles used.

To determine the unspecific adsorption of nanocontainers onto protein-rich surfaces, a layer of bovine serum albumin (BSA) was deposited onto a gold electrode. After rinsing with buffer, the BSA layer was let in contact with a suspension of nanocontainers. The frequency shift observed after addition of the polymer vesicles indicated that some unspecific adsorption took place. Although, it cannot be ruled out that the polymeric vesicles displace some BSA due to a higher preference for the gold surface than the protein.

3.5.3. Conclusions

In conclusion, the desired specific immobilization on surfaces was not achieved. The reasons for this behavior are not yet clear. One plausible explanation is the unspecific adsorption on the protein layer. Another factor that could contribute to the low adsorption observed in the case of biotinylated vesicles might be due to steric hindrance.

Complimentary techniques to study surface deposition are optical waveguide lightmode spectroscopy (OWLS),[109-111] and ellipsometry. The main difference on the results obtainable by optical techniques and QCM-D is that the latter technique also reports the amount of water adsorbed with the system.[212, 221-223] So in the case of vesicles, QCM-D takes into account the encapsulated water in their void interior. Moreover, QCM-D can provide additional information on the structure of the immobilized substance and the kinetics of the process. [212]

The adsorption of thiolated nanocontainers on gold surfaces might be an alternative approach for the immobilization of nanocontainers onto surfaces.

4. Materials and Methods

4.1. Materials

Polymers, monomers, reactants for synthesis

Poly-(dimethylsiloxane) (α,ω-bis(3-hydroxypropyl)poly(dimethylsiloxane)) (PDMS) (CAS#: 156327-07-0) (nominal M_w=5600 g/mol) was purchased from Aldrich, Shin Etsu Silicone (KF 6001, M_n=1806 g/mol, n=21; KF 6002, M_n=3200 g/mol, n=40; KF 6003, M_n=5600 g/mol, n=72), Wacker (purified PDMS, a gift from Ciba-Vision) (M_n=1942 g/mol, n=22; M_n=4878 g/mol, n=62) and Wacker (IM 11, M_n=1212 g/mol, n=14; IM 15, M_n=4542 g/mol, n=59). The M_n was calculated from end group titration values. 2-methyl-2-oxazoline (CAS#: 1120-64-5), triethylamine (TEA) (CAS#: 121-44-8), trifluoromethanesulfonic acid anhydride (TfSA) (CAS#: 358-23-6), D-(+)biotin (cis-(+)-tetrahydro-2-oxothieno [3,4]imidazoline-4-valeric acid) (CAS#: 58-85-5), N-N'-dicyclohexylcarbodiimide (DCC) (CAS#: 538-75-0), 4-(dimethylamino)pyridine (DMAP) (CAS#: 1122-58-3), 7-(diethylamino)coumarin-3-carbonylazide (CAS#: 157673-16-0), and solvents were purchased from Fluka. All reagents and solvents were of at least analytical grade, and when not otherwise stated, were used as purchased. For aqueous solutions, buffers, and ultrafiltration either bi-distilled or Milli-Q type water was utilized.

Buffers

Phosphate buffer saline (PBS) (137 mM NaCl, 2.6 mM KCl, 6.4 mM Na_2HPO_4, 1.4 mM KH_2PO_4, pH 7.4), Hepes (4-(2-hydroxyethyl)-1-piperazineethanesulfonic acid), Mops (3-N-morpholinopropanesulfonic acid), and Tris/HCl (10 mM) were prepared according to the standard procedures for buffers.

Fluorescent dyes

Calcein (2,7-Bis[N,N-bis(carboxymethyl)aminomethylene]fluorescein) (CAS #: 1461-15-0) and carboxyfluorescein (5(6)-Carboxyfluorescein) (CAS #: 72088-94-9) were purchased from Fluka. Alexa-488-avidin and sulforhodamine B (3,6-bis(diethylamino)-9-(2,4-disulfophenyl)-hydroxide, inner salt, sodium salt) were from Molecular Probes.

Detergents

Triton X-100 and octyl-polyoxyethylene (o-POE) were purchased from Sigma and Alexis Company (Läufelfingen, Switzerland), respectively.

Proteins

Avidin, streptavidin, and bovine serum albumin (BSA) were from Fluka. OmpF porin was expressed from BL21 (DE3) competent cells containing the plasmid pGompF and purified by Dr. A. Graff. The stock solution of the protein contained 1% octyl-POE, 20 mM Tris/HCl, 100 mM NaCl pH 8 (1.6 mg/ml).

Other materials

4-(dimethylamino)-cinnamaldehyde (DACA) of analytical grade was from Merck. Extrusion filters (Millex Durapore-PVDF, pores 0.45 μm, 0.22 μm), ultracentrifugation devices (Centricon Amicon YM cut-off 30000 Da) and membranes for ultrafiltration (Amicon Ultrafiltration membrane, regenerated cellulose, cut-offs 1000, 3000, 5000, and 10000) were all from Millipore (Switzerland). Biobeads SM2 were from BioRad and were cleaned two times with methanol and then washed several times with water prior to use[224]. Sephadex G100, Sepharose 4B and Sephacryl S 300-HR chromatographic gels were purchased from Sigma-Aldrich. Mowiol 4-88 was obtained from Plüss-Stauffer (Oftringen). Streptavidin 10 nm colloidal gold labeled was purchased from Sigma-Aldrich. 1-dodecanothiol 98% (lauryl mercaptan), hydrogen tetrachloroaurate (III) trihydrate (chloroauric acid) 99%, sodium tetrachloroaurate (III) dihydrate, 99% sodium borohydride 99%, toluene (certif. ACS), hexane (certif. ACS), ethanol 95%, isopropanol 98%, K_2CO_3 anhydrous, citric acid monohydrate pro analysis, disodium hydrogen citrate sesquihydrate, trisodium citrate dihydrate, NaCl, were purchased from Sigma-Aldrich, tetraoctyl ammonium bromide 98% (TOAB) and 11-mercaptoandecanoic acid (MUA) were from Fluka. Sodium dodecyl sulfate (SDS) was purchased from Fluka and the detergent for the cell was Cleaner from Cobas Integra, Roche. Poly(L-lysine)-g-poly(ethylene glycol)/poly(ethylene glycol) biotin (batch code FD-02-2) (PLL-g-PEG-b) with a grafting ratio of 3.85 and a biotin percentage of 27.6 (nominal 30%) was a kind gift from Prof. Dr. M. Textor, ETH Zürich. The poly(L-lysine) chain was 20 kDa and the poly(ethylene glycol) side chains 2 kDa. Phorbol ester was from Calbiochem. EDTA was from Sigma. Raw polyguanylic acid (23mer oligonucleotides) with its 5' biotinylated end obtained from Amplimmun AG was treated with phenol as described[225]. It was then dialyzed from bi-distilled water and lyophilized. Before use it was dissolved in KCl 0.4 M, 0.04 M TrisHCl (pH 8.0) containing 1 mM EDTA. The solution was dialyzed versus hundred volumes of 1.0 M salt followed by dialysis against water and lyophilization. THP1 human leukemia acute monocyte line and COS-7 cells were both purchased from ATCC (Manasas, VA).

4.2. Synthesis of ABA triblock-copolymers

Example of polymerization: Polymerization of S125

A total of 20 g of PDMS (3.57 mM, M_n=5600 g/mol) were dissolved in 150 ml of freshly distilled hexane and refluxed in a Soxhlet apparatus during 24 h. After cooling to room temperature, 1.14 ml (8.21 mM) of freshly distilled TEA was added with stirring directly to the reaction mixture through one of the lateral mouths under Argon flow. Subsequently the system was cooled to 0 °C. A mixture of 10 ml hexane (fresh distilled) and 1.24 ml TfSA (7.50m mM) was added dropwise with a dropping funnel during 30 min under a N_2 atmosphere and the reaction was stirred for one hour at 0 °C. The hexane and the non-reacted TEA were removed by high

vacuum. The remaining viscous material was dissolved in 100 ml fresh hexane. The insoluble salt was filtered through a glass frit (G4) under Argon. After filtration the solvent was removed by high vacuum to yield 16.12 g of yellow oil. This activated pre-polymer was directly used without any extra purification for the polymerization reaction of 2-methyl-2-oxazoline.

For the polymerization, 16.12 g (2.75 mM) of activated PDMS were dissolved in 200 ml freshly distilled ethyl acetate. Subsequently, 12 ml (140.99 mM) freshly distilled 2-methyl-2-oxazoline was added to the reaction vessel. The reaction was kept at 40 °C with constant stirring for 64 h. Once brought to room temperature, the reaction was stopped by introducing 5.4 ml of 0.5 M KOH in methanol and stirred further for 6 h. The solvent was removed by rotary evaporation, and the remaining solid was dissolved in ethanol. The raw product was purified by ultrafiltration from a water:ethanol mixture in an ultrafiltration cell device (Millipore Ultrafiltration Stirred Cell 76 mm, 300 ml) with a 3000 Da cut off membrane (regenerated cellulose). An off-white powder was obtained by lyophilization of the aqueous suspension of the polymer.

The following yields were obtained: activation step 16.12 g (77%), polymerization 24.1 g (99%), total yield 24.1 g (76%). The degree of polymerization was estimated to be 19 for the side chains by NMR ($M_{n(PMOXA)}$=1615 g/mol), accounting for a total molecular weight of 8834 g/mol (PMOXA 37 w%).

4.3. End-group functionalization of ABA triblock-copolymers

Biotinylation of ABA triblock-copolymers

A slight modification of a reported biotinylation procedure was followed.[144] A total of 2 g of ABA triblock-copolymer (PMOXA-PDMS-PMOXA, code JW05, M_n=7090 g/mol) was dried on a Soxhlet apparatus with chloroform (70 ml of freshly distilled chloroform, over phosphorous pentoxide) overnight. A total of 610 mg of biotin were suspended in 20 ml DMF (dried over molecular sieve 4 Å). 800 mg of DCC (dicyclohexylcarbodiimide) previously left overnight to dry on a vacuum line to dry were suspended in 10 ml of DMF. After cooling the ABA in $CHCl_3$ to room temperature under argon the biotin and the DCC were added with a syringe under argon flow. One spatulum tip (6 mg) of 4-(dimethylamino)pyridine (DMAP) was added. The reaction was left stirring at room temperature for 48 h. Initially the reaction mixture seems like solids in suspension, whereas towards the end the reaction mixture has the appearance of a semitransparent solution like a concentrated polymer solution.

The solvents were evaporated on a vacuum line. To purify the product, 100 ml cold acetone was added to the raw product and centrifuged for 30 min. The supernatant was removed from the centrifuge tubes and the solid residue was again treated with cold acetone to extract remaining polymer, and centrifuged 30 min. Both supernatant aliquots were collected and evaporated in a rotary evaporator. The remnant solid was dissolved in 300 ml of a wa-

ter:ethanol (1/2 V/V) mixture and subsequently cleaned by ultrafiltration (Millipore ultrafiltration cell, membrane cut-off 5000 Da).

Coumarin functionalized ABA triblock-copolymer

A total of 0.94 g (1.06 mM) of polymer (PMOXA-PDMS-PMOXA, code S125, M_n=8834 g/mol) was dissolved in 50 ml of freshly distilled chloroform and dried under reflux in a Soxhlet apparatus for 15 h at 60 °C. The system was cooled to room temperature under a stream of Argon and 75 mg (2.61 mM) of 7-(diethylamino)coumarin-3-carbonylazide previously dissolved in 3 ml chloroform were added. The reaction mixture was stirred at 60 °C for 22 h. After cooling to room temperature, the solvent was removed by rotary evaporation yielding 5.8 g of yellow-reddish raw product. The raw product was dissolved in a water:ethanol 2:1 mixture and the solution was centrifuged to remove insoluble impurities. The supernatant was purified by ultrafiltration (water:ethanol 2:1, 5000 Da cut-off membrane of regenerated cellulose, 3 bar) until the filtrating waters contained no more fluorescent dye (determined by fluorescence spectroscopy). Finally, the product was lyophilized to render a bright yellow powder. The yield obtained was 960 mg (97% related to the PDMS constituting block) with a calculated theoretical molecular weight of 9350 g/mol (considering derivatization of both end groups). The degree of functionalization obtained by NMR was ca. 60%.

4.4. Spectroscopy techniques - ^{1}H-NMR and IR

^{1}H-NMR spectra were recorded with a Bruker 300 or 400 MHz using $CDCl_3$. Spectra were analyzed with MestRec23 software. IR spectra were recorded from KBr pellets with an ATI Mattson, Genesis Series FTIR spectrometer.

4.5. Gel Permeation Chromatography

4.5.1. Theoretical description

Gel permeation chromatography (GPC),[20] is a polymer characterization technique for determining the number average molecular weight $\overline{M}_n$, the weight average molecular weight $\overline{M}_w$, and the polydispersity PD. These quantities are defined as follows.[226]

[20] Gel permeation chromatography is synonymous of size exclusion chromatography, and the same principles apply in both cases. However, historically, the term gel permeation chromatography was used for non-aqueous systems which evolved into analytic HPLC instruments, whereas the term size exclusion chromatography has been used in relationship to protein purification in aqueous systems, and remained more a preparative technique.

$$\overline{M}_n = \frac{\sum n_i M_i}{\sum n_i} = \frac{\sum w_i}{\sum w_i / M_i} \qquad \overline{M}_w = \frac{\sum n_i M_i^2}{\sum n_i M_i} = \frac{\sum w_i M_i}{\sum w_i} \qquad PD = PI = \frac{\overline{M}_w}{\overline{M}_n}$$

The fractionation is based on the hydrodynamic volume of the polymer in solution. Therefore, temperature and solvent play an important role in the determination of the molecular weight since both factors determine the size of the coil of the polymer chains in solution. A linear polymer chain in good solvents adopts a coil conformation, with a hydrodynamic volume (V_h), which is proportional to the molecular weight.

GPC is a relative technique based on calibrations; polymer standards are used for this purpose. To avoid this one can also use a universal calibration, based either on PS or PEO of narrow molecular weight distribution. Using Einstein's relationship for intrinsic viscosity [η][122]

$$[\eta]M = 0.025 N_A V_h$$

The universal calibration is:[122]

$$[\eta] = \Phi \langle \bar{r}_g^2 \rangle^{3/2} / M$$

Plotting $\log[\eta]$ vesus $\log M$ all polymer fall into a linear regression, this semi-empirical relationship known as the Mark-Houwink-Skurada equation has the form:[226]

$[\eta] = KM^a$, K and a are constants depending of polymer, solvent, and temperature.

Determining $[\eta]$ with an online viscosimeter, allows for the use of the Mark-Houwink-Skurada equation to obtain the molecular weight of the sample. Another possibility is if K and a b are known for the standard polymer (2) and the analyzed polymer (1), then, the molecular weight of the latter can be obtained from:

$$\log M_1 = \left(\frac{1}{a_1 + 1}\right) \log\left(\frac{K_1}{K_2}\right) + \left(\frac{a_2 + 1}{a_1 + 1}\right) \log M_2$$

4.5.2. Experimental part

GPC measurements were performed with a PLgel Mixed-C (5 μm particle size) column (300x7.5 mm) and THF as eluent in an Agilent modular system (Agilent 1100 Series Module GPC) with two detectors were used, a UV fixed wavelength (λ=254 nm) and a refractive index (RI). Poly(styrene) standards of narrow molecular weights (Polystyrene Easical vials, Agilent technologies) were used for calibration. Injection volumes were 50 μl and polymer concentrations 1 mg/ml. Flow rates were 1ml/min and measurements were performed in thermostized columns at 23°C. Chromatograms, molecular weight distributions, and molecular weight averages were analyzed with the software ChemStation for GPC.

4.6. Quantification of biotinylation of ABA triblock-copolymer

For the quantification of biotin in the modified polymers an assay with 4-(dimethylamino)-cinnamaldehyde (DACA)[153] was performed. This reaction takes place in acid medium forming a red cyanine compound with a λ_{max} of 531 nm that can be followed by UV-Vis spectroscopy. For a detail description of the reactions taking place see Section 3.1.3.2.

A blank with just polymer without modification (parent polymer) was used as a control. The biotinylated polymer was analyzed in the same conditions as the other samples, obtaining in this case through the use of the calibration curve a value for the amount of biotin attached to the polymer. For the calibration curve with biotin, the following concentrations of biotin were used 0.5, 1, 1.5, and 1.8 mg/ml in a mixture of 1/2 (V/V) ethanol/H_2O (final volume 4 ml). As a blank for the biotin samples a solution of 2 ml ethanol plus 2 ml water was used. In the case of the modified polymer a blank consisting of a solution of 50 mg of parent polymer (sample BC1) in 4 ml ethanol/H_2O mixture (1/2 V/V). Two replicas of the modified polymers were analyzed (sample BC2); each consisted of 50 mg of the biotinylated polymer in 4 ml ethanol/H_2O mixture (1/2 V/V). A positive control (BC3) consisted of a mixture of 48.3 mg of parent polymer and 1.7 mg biotin in 4 ml ethanol/H_2O mixture (1/2 V/V). Scans of each sample against the respective blank were performed. Subsequently, to each cuvette 0.1 ml of concentrated HCl was added, followed by 1ml (1g/l) DACA solution. After 20 min the spectra ($\Delta\lambda$=450-605 nm, λ_{max}=531 nm) was monitored. After addition of DACA solution BC1 turned yellow while solution of samples BC2 and BC3, turned red as expected.

To prove that the biotin detected was bound to the polymer the sample was purified by SEC (Sephadex G100). The purified polymer was lyophilized to retrieve the powder. The following samples were analyzed: BC4 (25 mg of polymer JW05ModA, purified by SEC and lyophilized), BC5 (25 mg of polymer JW05), each dissolved in 3 ml H_2O/ethanol (1/3 V/V). To each sample 0.1 ml of concentrated HCl was added, followed by 1 ml of DACA solution (1 g/l), and after 20 min, the absorption scan (400-700 nm) was registered. A red color was produced in the case of BC4, while a yellow solution was obtained in the case of BC5 after addition of DACA.

4.7. Langmuir film experiments

4.7.1. Theoretical description

Surface pressure measurements are used to characterize surface-active agents. Water-insoluble amphiphilic substances form monomolecular insoluble films at the air-water interface. Such films, referred to as Langmuir monolayers, form after a small volume of amphiphile solution in a volatile and preferably water-immiscible solvent is spread dropwise on a liquid surface. Solvent evaporation leads to a uniform layer, where the hydrophobic moiety is immersed in

water and the hydrophobic part floats on the surface.[155] Gibbs monolayers are obtained when soluble amphiphiles are injected on a subphase. Their adsorption equilibrium can be monitored by the changes in surface pressure with time.[227, 228] Langmuir films refer to a floating monolayer and must be distinguished from Langmuir-Blodgett films, which are thin films obtained by sequential deposition of monolayer films onto a substrate.

An important factor in the formation and stability of monolayers at the air-water interface is the ratio of hydrophilic and hydrophobic moieties in the molecule. If the hydrophilic part is too large or too polar, then the substance dissolves in the subphase, on the other hand if the hydrophobic segment is too large, then the molecules build multilayers or do not spread.

Equilibrium may be reached very slowly, therefore, some monolayers might be in a metastable state instead of a true thermodynamic equilibrium. If a surfactant is forming a monolayer, then it favors expansion of the interface and therefore reduces the surface tension.

The interfacial free energy of the system can be measured as the surface tension γ. Surface tension can be defined as the work required to expand the surface isothermically by unit area. Thermodynamically, at equilibrium the surface tension is described by the partial derivative of the free energy functions with respect to the area,[229]

$$\gamma = \left(\frac{\partial F}{\partial A}\right)_{T,V,n_i} = \left(\frac{\partial G}{\partial A}\right)_{T,P,n_i}$$

The change obtained in surface tension on spreading a monolayer is known as the surface pressure. Normally, in Langmuir film experiments the surface pressure Π is measured, which can be interpreted as a two-dimensional analogue of pressure, and is given by:[229]

$$\Pi = \gamma_0 - \gamma$$

γ_0 and γ are the surface tension in absence and presence of the monolayer.

The equipment consists of a planar Teflon trough that can be of different geometries. This trough contains the subphase, and can have built-in movable barriers to modify the total area of the surface. The barriers are made of Delrin a hydrophilic material.[230]

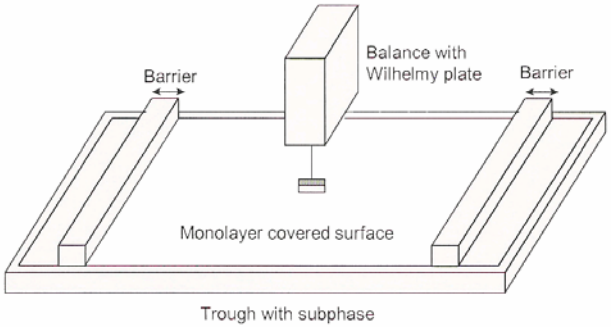

Figure 4.7.1: Illustration of a Langmuir rectangular trough with a Wilhemy plate electrobalance and symmetrically movable barrier system.[230]

The differences in surface tension are measured by means of a Wilhemy-plate, a sensitive electrobalance that measures the force on a plate partially immersed on the subphase. The net force acting on the plate can be described by:

$$F = \rho_p g l_p w_p t_p + 2\gamma\left(t_p + w_p\right)\left(\cos\theta\right) - \rho_l g t_l w_l h_l$$

The total force is the sum of the gravity force, the surface tension both acting downwards, and the buoyancy due to the displaced water acting upwards. In this equation ρ_p, l_p, w_p, t_p are the density, length, width, and thickness of the plate respectively, ρ_l is the density of the subphase liquid, h_l is the depth of immersion of the plate in the liquid, g is the gravitational constant, γ is the surface tension of the liquid, and θ the contact angle between the liquid and the plate.[229] This can be better visualized on Figure 4.7.2:

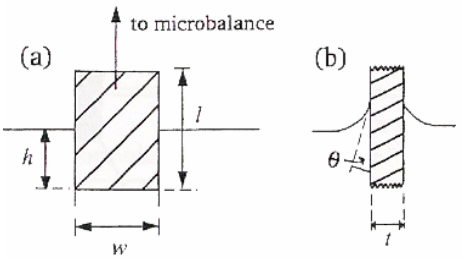

Figure 4.7.2: Wilhemy plate, (a) front view, (b) side view.[229]

Different materials can constitute the plate, the most common being filter paper. If the plate is completely wetted, then $\cos\theta = 0$, and if the thickness of the plate is much smaller than its width, that is, if $w_p >> t_p$, then:

$$\Pi = -\Delta\gamma = -\Delta F / 2w_p$$

The surface pressure is usually measured against the area of the trough (A) or the area per molecule (a). This last is obtained by dividing the film area A by the total number of molecules forming the film.

$$a = \frac{AM}{CN_A V} = \frac{A}{cN_A V}$$

Where M is the molecular weight of the monolayer-forming material, C the concentration of the spreading solution in mass per unit volume, c the molar concentration, and V the spread volume.

For Langmuir films, plots of the surface pressure (Π) as a function of the area per molecule (a) are known as Π-a isotherms. As its name suggests, isotherms must be performed at constant temperature, since the properties of a monolayer are highly temperature dependent. Other factors affecting the formation of a monolayer and the shape of the resulting isotherms

are the nature of the amphiphile, the type of subphase (ions presents, pH), compression rate, and spreading solvent, among others. A typical isotherm of a small amphiphile has the general form depicted in Figure 4.7.3.

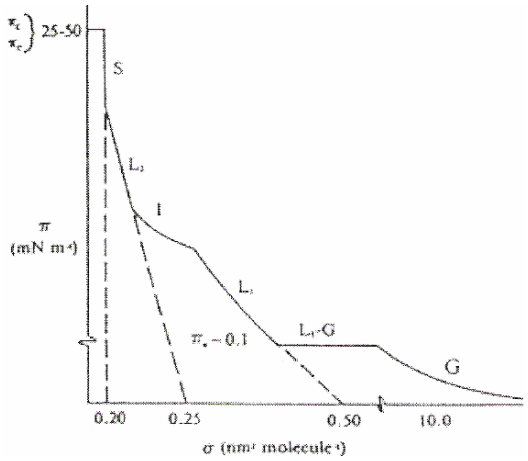

Figure 4.7.3: Typical isotherm of a lipid, showing the different phase transitions and the collapse pressure π_c. Taken from Gaines.[231]

Figure 4.7.4: Corresponding diagrams for the situation encountered in the different phases of a Langmuir film. Taken from Roberts.[232]

In most cases the isotherms can be divided in different regions, or so-called phases, that relate to the state of the molecules in a two-dimensional ordering. At low pressures, the molecules are far from each other as in a gas, therefore, this is termed the "gas phase". Upon compression the molecules come closer giving what is termed a liquid-expanded phase. At higher surface pressures, condensed phases are observed that relate to either liquid or solid phases and are termed after them. In these condensed phases the molecules are densely packed, and therefore loose most of their freedom. Figure 4.7.4 shows a scheme of the different states found in a two-dimensional ordering at the air-water interface.

In the "solid" phase region, small area changes increase drastically the surface pressure, reaching the collapse pressure Π_c, when no more molecules can be accommodated in a two-dimensional ordering. On the onset of Π_c molecules are ejected from the monolayer into the subphase (hydrophilic compounds) or the superphase (hydrophobic molecules) giving poorly defined multilayers.

A useful parameter for the characterization of substances with the Langmuir technique is the limiting area, A_0, which is obtained by extrapolation of the slope found in the "solid" region of the isotherm to zero pressure. The physical interpretation of this parameter is the hypo-

thetic area occupied per molecule in the condensed state under the supposition that the monolayer is vertically ordered and densely packed.

Polymer films

In contrast to small molecules, films of a polymer on a subphase can be obtained even when no amphiphilicity is present on the molecule. Also isotherms of polymers do not show a sharp transition or phase transformations. According to Crisp,[233, 234] two types of polymer films can be obtained: condensed films and expanded films. The first one is characterized by high viscosity and rigidity, with a steep pressure versus area curve, whereas the later show a gradual increase of the surface pressure and a collapse pressure.[235] A schematic representation of different polymer films is shown in Figure 4.7.5.

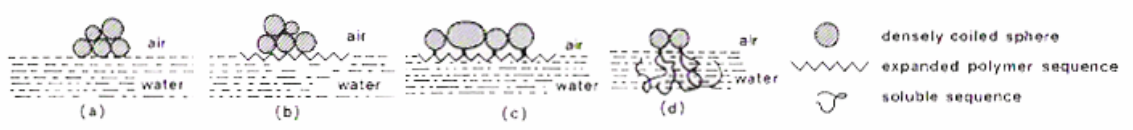

Figure 4.7.5: Possible polymer orientations at a air-water interface for different polymer types.[236]

According to different authors, the term monolayer is used in different contexts. It can refer not only to the monomolecular film but also to a monolayer whose constructing unit is a coiled sphere or a soluble chain of polymer.[236] By analogy to low molecular weight compounds, a monomolecular film can be thought as the monomer base of the polymer taken as a unit.

Amphiphilic block-copolymers are a particular case in the study of Langmuir films. Figure 4.7.6 shows possible conformation of ABA type block-copolymer monolayers obtained upon compression, a) at low compression, in the gas region of the isotherm the molecules are spread and floating on the monolayer in a pancake conformation, b) in the liquid expanded phase, the conformation adopted is a mushroom conformation for the hydrophilic blocks, c) as the compression increases, in the liquid condensed phase, the polymer adopts a brush conformation in the subphase, d) condensed phase, the stretching of the polymers is maximum.

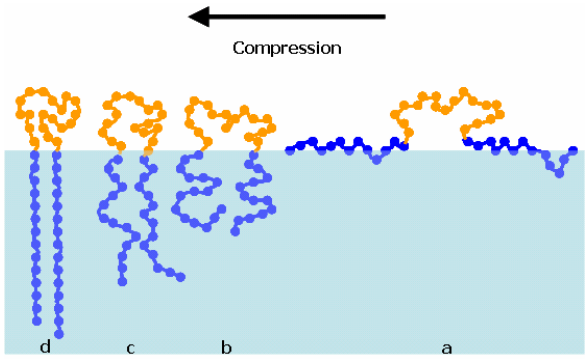

Figure 4.7.6: Effects of the compression on the possible conformation of ABA type block-copolymer monolayers, a) low compression or gas region, b) liquid expanded phase, c) liquid condensed phase, d) condensed phase.

Protein insertion in Langmuir monolayers

The Langmuir technique provides a useful way to study protein interactions with lipid monolayers. Mainly, the incorporation of membrane proteins in lipid layers is studied. The procedure is quite simple in principle; the lipid monolayer is spread and compressed to a certain desired surface pressure, usually in the region of condensed phase, to obtain a floating film. Subsequently, a protein is injected in the subphase beneath the monolayer and the changes in surface pressure are recorded. If the protein inserts in the membrane the forces exerted in the lateral direction are increased, therefore the surface pressure increases.

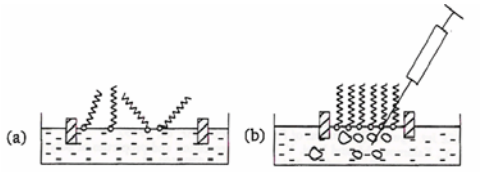

Figure 4.7.7: (a) Formation of a lipid monolayer. (b) Protein injection in the subphase on a rectangular trough.[229]

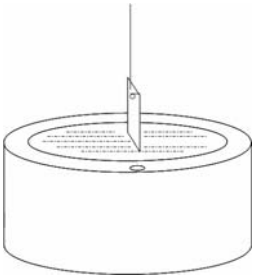

Figure 4.7.8: Schematic representation of a cylindrical trough, for the study of protein insertion in monolayers. The orifice is for injection of the protein without disturbing the floating film. Adapted from Han et al.[237]

Soluble proteins such as streptavidin[21] can also be investigated with Langmuir films. Typically, a monolayer of a biotinylated lipid in contact with streptavidin in the subphase will "irreversibly" bind to the streptavidin and form two-dimensional crystalline domains. The general process is described in Figure 4.7.9 a).

In Figure 4.7.9 b), different cases of protein interaction with monolayers are depicted. It is important to notice that if a protein adsorbs instead of inserting in a monolayer, this would not induce a change in the surface pressure of the film.

[21] Streptavidin-biotin interaction is described in Section 3.3.1.

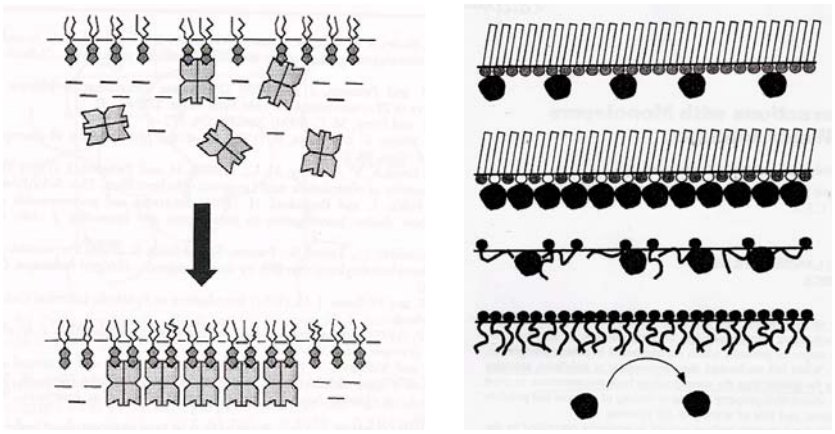

Figure 4.7.9: a) Streptavidin binding to a biotinylated lipid monolayer, results in crystalline domains.[229] b) Adsorption of proteins on monolayers of amphiphiles. Large circles represent soluble proteins. From top to bottom: lipid monolayer, mixed lipid monolayer, PS-PEO at low surface pressure (liquid expanded state), PS-PEO at high surface pressure (condensed state) when it shows protein repellency. Taken from Britt et al.[238]

4.7.2. Experimental part

The Langmuir Film Balance equipped with a Wilhelmy balance was provided by KVS Ltd. The Mini-trough consisted of one solid piece of PTFE with 2 symmetric Delrin barriers and had a volume of 220 ml and a surface of 24225 mm^2 (26 x 75 mm^2). Before each measurement, the trough was thoroughly cleaned with a tissue soaked in chloroform, the same procedure was followed with ethanol, and then the trough was left drying a few minutes. Subsequently, the through was filled with filtered (Millex Durapore-PVDF, Millipore 0.45 μm filters) bidistilled water or buffer. A few compressions with only water were run in order to check the absence of impurities in the subphase.

Pure polymer monolayer isotherms

Stock solutions of the polymers were prepared by dissolving the polymers in chloroform in order to obtain a final concentration of polymer of 1 mg/ml. The aliquot of the polymer solution in chloroform was dropped with a Hamilton syringe on the surface of the subphase, 15 min were allowed for evaporation of the solvent and spreading of the monolayer. The isotherms were recorded at room temperature and with a barrier speed of 15 mm/min.

In order to obtain the complete monolayer isotherm, a series of different volumes of spread polymer had to be used. The overlapped curves are presented in the results and discussion section (see Section 3.1.3.4), which consist on the superposition of the individual isotherms obtained with different spreading volumes.

Interaction of biotinylated polymer Langmuir films with streptavidin

For these experiments a non-modified (JW05, Mw=7090 g/mol, 1.2 mg/ml in $CHCl_3$) and a biotinylated ABA triblock-copolymer (JW05 ModA, Mw=7090 g/mol, 1.2 mg/ml in $CHCl_3$)

were used. The subphase consisted of filtered PBS (0.45 μm pore Millex Durapore-PVDF). A solution of streptavidin (16 U/mg) of 0.2 mg/ml in PBS, filtered with a 0.22 μm pore Millex Durapore-PVDF was used for injections under the subphase.

Typically a 15 μl or 20 μl of polymer solution in $CHCl_3$ was added over the subphase with a Hamilton microsyringe, placing the droplets as to obtain even coverage. After allowing 15 min for $CHCl_3$ evaporation and stabilization of the monolayer, compression and expansion cycles were carried out to obtain the isotherm for each polymer.

A 15 μl polymer aliquot (M_n 7090 g/mol, 1.2 mg/ml concentration), corresponds to 2.5 10^{-9} moles. If each chain has two biotin moieties, then $5x10^{-9}$ moles of biotin are present. This corresponds to a theoretical 1.5 μg of biotin (calculated as free biotin). A minimum of 0.1 mg of streptavidin (16 U/mg) was needed to bind to the theoretical amount of biotin present, which was added as a 500 μl aliquot of a 0.2 mg/ml stock solution of streptavidin.

These 500 μl were injected as 5 portions of 100 μl into the subphase in 5 different positions of the trough. After waiting for 20 min for diffusion and stabilization of the subphase, isotherms were recorded in a two-cycle run. A series of 2 cycles (compression and expansion) were performed at different time intervals after streptavidin injection on the subphase.

4.8. Methods of vesicle preparation

4.8.1. Standard (solvent-injection-extrusion) or Ethanol method

This methodology was already described[61] and in this thesis it was slightly modified. A total of 50 mg of polymer (pure polymer or mixed in order to obtain the desired final percentage of functionalized polymer) was dissolved in 250 μl of ethanol (99%). When necessary, the mixture was slightly heated to promote dissolution of the polymer. After cooling, the ethanolic solution was slowly added to 5 ml of aqueous solution (bi-distilled water, buffer, or a solution containing a molecule to encapsulate in the interior of the vesicles). A minimum of 4 h of stirring was allowed; in certain cases overnight stirring was performed. Subsequently, the vesicles were extruded through 0.45 μm and 0.22 μm filters (Millex Durapore-PVDF, Millipore) between 6 and 10 times. This procedure ensures formation of unilamellar vesicles with diameters dictated by the pore size of the extrusion filters and a with more monodisperse size distribution[61].

4.8.2. Direct dispersion method

50 mg of triblock-copolymer powder were directly dispersed in 5 ml buffer solution. The dispersion was stirred overnight, and extruded through filters (Millex Durapore-PVDF, Millipore 0.45 μm and 0.22 μm, 6 to 10 times each) to narrow the polydispersity of the vesicles and to remove large aggregates.

4.8.3. Electroformation (GUV)

Prior to use the gold electrodes and the Teflon housing were cleaned and dried in a desiccator for 30 min. Aliquots of 50 μl of polymer solution in $CHCl_3$ (1 w%) were deposited with a Hamilton syringe on the electrodes and the $CHCl_3$ was evaporated with a gentle stream of N_2. The electrodes were placed for 30 min in a desiccator to dry. Finally, the electrodes were introduced in the Teflon housing and the well was filled with 4.5 ml bi-distilled water. During one hour the system was placed under an AC current of 5 V and 10 Hz and finally 15 min in an AC current of 5 V and 5 Hz. The electrodes were removed and the vesicles pipetted out of the well.

4.9. Methods of proteo-vesicle preparation

4.9.1. Standard (solvent-injection-extrusion) or Ethanol method

A total of 50 mg of polymer was dissolved in 250 μl of ethanol (99%), and to this mixture an aliquot of the protein stock solution was added. The resulting mixture was then dropped slowly into 5 ml of solution (buffer or buffer containing molecules for encapsulation). After stirring for 1 h the suspension was filtered as described above.

4.9.2. Direct dispersion/Detergent and Biobeads method

Vesicles were prepared according to the direct dispersion method (see Section 4.8.2) Then a 12.5 μl aliquot of Triton X-100 10% was added to the system to achieve a 0.5% final concentration of Triton, followed by two sonication cycles of 2-10 min each. Afterwards, the membrane protein stock solution was added and the samples were left stirring 3-6 h at 4 °C. Then, 100 mg of Biobeads[163] were added to remove the detergent from the system. After an incubation of 5 h in the presence of Biobeads the beads were left to decantate and the supernatant containing the vesicles was removed.

Prior to use, the Biobeads were cleaned two times with methanol and washed several times with water to remove impurities[224]. The required amount of Biobeads depends on the choice of detergent[164] and its amount. To enhance the efficiency of detergent adsorption, the total amount of Biobeads necessary was added in three aliquots, in 1 h steps, and then the sample was stirred for 6-8 h at 4 °C. The supernatant containing the proteo-liposomes was centrifuged (Heraeus, 5000 rpm during 20 min.) to remove any remaining Biobeads fragments.

4.10. Size Exclusion Chromatography

Size exclusion chromatography (SEC)[22] can be used to separate molecules, or aggregates due to their size. Some important parameters commonly used in size exclusion chromatography are:

Column cross sectional area $= A = \pi r^2$

Column bed volume $= V_c = A \cdot L$

Linear velocity $= \mu = Q/A$

With L and r the column length and radius and Q the volumetric flow rate (ml/h).

The total volume of the column V_t is the sum of the volume of the eluent outside the pores V_0, the volume of liquid inside the pores of the matrix V_i and the volume of the matrix gel V_m.[239]

$$V_t = V_0 + V_i + V_m = r^2 h\pi$$

V_0 is known as the dead volume or void volume and represents the elution volume of an excluded substance, that is, for an excluded substance $V_0 = V_e$, with V_e the elution volume of a particular molecule.

The coefficient of partition (K_{av})[23] between intra and extra granular phases, it is defined for a substance and a type of gel of given porosity as:[239]

$$K_{av} = \frac{(V_e - V_0)}{(V_t - V_0)}$$

Molecules that are smaller than the lower limit of exclusion (included substances), elute together as one peak and determine the lower limit of a gel. The upper limit of a gel is dictated by the size of the molecules that are unable to enter the pores of the gel. The gel does not separate molecules (excluded substance) with sizes bigger than the upper limit of exclusion, or smaller than the lower limit of exclusion, that is, there is no separation out of the range of fractionation. If a molecule elutes with time or volume greater than the lower limit of exclusion of a gel then there is interaction occurring with the gel and $K > 1$.

---

[22] Gel permeation chromatography is synonymous of size exclusion chromatography, and the same principles apply in both cases. However, historically, the term gel permeation chromatography was used for non-aqueous systems which evolved into analytic HPLC instruments, whereas the term size exclusion chromatography has been used in relationship to protein purification in aqueous systems, and remained more a preparative technique.

[23] K_{av} is also defined as the equilibrium constant for distribution between the gel pores and the fluid phase.

The range of fractionation or separation for a given gel and column parameters can be described graphically as depicted in Figure 4.10.1.

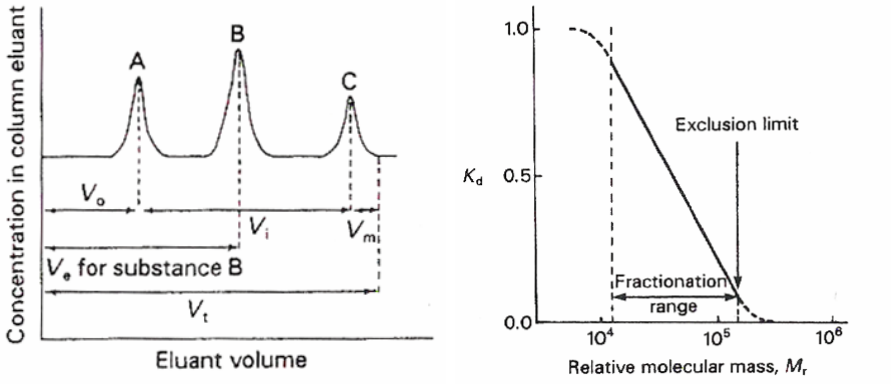

Figure 4.10.1: Left: separation parameters in SEC, Right: schematic representation of the fractionation range of SEC. Taken from Braithwaite et al.[239]

4.10.1. Preparative Chromatography

For the removal of non-encapsulated substances, non-inserted membrane proteins, and non-attached (strept)avidin, preparative SEC separations were performed. Columns from Bio-Rad (Econo-columns) and a detector (Pharmacia Biotech Optical unit UV-1, Pharmacia LKB Control Unit UV-1) with fixed wavelength (280 nm) were used. Typical column size was 1 cm internal diameter, and lengths from 10 to 40 cm according to the gel and samples involved. Gels and buffers were always degassed prior to use. For most separations either Sephadex G-100 or Sepharose 4B gels were used. Typical loading (injection) volumes were 1 to 1.5 ml and the buffer eluted through the column by gravitational force, with normal flows of 0.5 ml/min.

4.11. UV-Vis measurements

The UV-Vis measurements were performed with a Safas Monaco UV mc2 spectrophotometer SP2000. To verify the attachment of (strept)/avidin to the surface of biotinylated nanocontainers the UV-vis spectra of the following samples were acquired:

Sample description	Amount	Avidin (2 mg/ml)	Buffer (PBS)	Ratio (biotin/avidin)
Biotin (1 mg/ml)	450 µl	250 µl	300 µl	2.5
Biotinylated NC (10 mg/ml)	200 µl	250 µl	650 µl	3.8
Control NC (10 mg/ml)	200 µl	250 µl	650 µl	-
Biotinylated NC (10 mg/ml)	200 µl	0 µl	900 µl	-
Control NC (10 mg/ml)	200 µl	0 µl	900 µl	-
Biotin (1 mg/ml)	450 µl	0 µl	550 µl	-
Control Avidin	0 µl	250 µl	850 µl	-

Table 4.11.1: Sample description for the assessment of avidin interaction with biotinylated NCs.

The following samples were analyzed in order to differenciate between attachment prior and posterior to the chromatography purification.

Sample description	Amount	Avidin (1 mg/ml)	Ratio (biotin/avidin)
NC 10% Biotinylated (6.6 mg/ml)	750 µl	750 µl	6.4
NC control (0% biotin) (6.6 mg/ml)	750 µl	750 µl	-
NC 10% Biotinylated (6.6 mg/ml)	750 µl	750 µl	31.4
NC control (0% biotin) (6.6 mg/ml)	750 µl	750 µl	-

Table 4.11.2: Sample description for the assessment of avidin interaction with biotinylated NCs.

All spectra were performed with buffer as blank, additionally the difference spectra were acquired when necessary against the polymer vesicles, biotinylated or non-biotinylated respectively, or (strept)avidin. All measurements were done at room temperature (20-25 °C).

4.12. Fluorescence measurements

4.12.1. Theoretical description

The detected fluorescence intensity is proportional to the concentration of the fluorescent probe. This relationship is expressed in the form:[240, 241]

$$I_{obs} = \Phi I_0 (1 - 10^{\varepsilon c \ell})$$

Where I_{obs} is the detected fluorescence intensity, I_0 the original intensity, and Φ the quantum yield. The exponentials are respectively, ε the molar extinction coefficient, c the fluorophore concentration, and ℓ the length of the optical path through the sample.

One important interference which can occur in fluorescence spectroscopy is due to the fact that the total intensity measured by the detector is given not only by the fluorescence emitted by the sample but also due to scattered light. For this reason in samples containing vesicular structures, well known for their scattering properties, a control without fluorophore was always performed in order to account for undesired scattered light signals.

One common investigation in the context of fluorescence experiments is the quenching of the fluorophores. Two quenching processes might take place. The first is known as static quenching. In this process, the quenching agent (Q) forms a stable complex with the fluorophore in the ground state, which is intrinsically non-fluorescent while the remaining uncomplexed fluorophores emit with the regular quantum yield. One typical indication of static quenching are non-linear Stern-Volmer[24] plots. The second quenching process that can take

[24] Stern-Volmer plots are plots of the F_0/F versus concentration of quencher, with F_0 being the fluorescence of the fluorophore in absence of quencher and F in the presence of quencher.

place, and usually is more common, is called dynamic quenching or collisional quenching. Quenching occurs when the quencher collisions with the fluorophore while the fluorophore is in the excited state, which reduces the lifetime of the excited state. The most examined consequence of this type of quenching is the reduction in fluorescence yield however; one can also study the decrease in lifetime.[240, 241]

4.12.2. Experimental part

Steady state fluorescent measurements, that is, emission and excitation spectra as well as time dependence measurements, were performed in a Jasco FP 773 instrument. For most experiments the slits for emission and excitation were adjusted to 10 nm (when otherwise they were adjusted to 5 nm). The experiments were performed at room temperature (20-25 °C).

Fluorescently dye-labeled ABA triblock-copolymers

The following dispersions of polymers were prepared and their fluorescence spectra analyzed. A 96 w% H_2O, 4 w% ethanol solution was prepared in accordance with the standard method of preparation of vesicle structures containing 0.2 w% PMOXA-PDMS-PMOXA, 0.2 w% Cm-PMOXA-PDMS-PMOXA-Cm[25]. Aliquots of 2 ml of these dispersions were placed in quartz cuvettes and the measurement of the spectra was performed. Subsequently measurements were performed on 1:1 dilution of the previous described samples with bi-distilled H_2O.

The reported excitation and emission wavelengths of the coumarin are respectively, λ_{ex}=390 nm; λ_{em}=478 nm in methanol, according to the provider. The optimal excitation wavelength for the coumarin modified ABA triblock-copolymer, Cm-PMOXA-PDMS-PMOXA-Cm was found to be 440 nm. Therefore, this excitation wavelength was used for the emission spectra measurements, whereas the scanned emission range was 460-600 nm.

Trapped volume in vesicles

For these assays the following polymers were tested: S131 (M_n=8660 Da, n=72, m=18) and JW05 (M_n=7090 Da, n=62 m=13). Vesicles were prepared according to standard and direct dispersion methods (see Section 4.8). As a fluorescence probe calcein (Mr=622.5 g/mol, λ_{ex}=470 nm, λ_{em}=515 nm) was used. To avoid interference with the quencher, samples were prepared in Mops (3-N-morpholinopropanesulfonic acid) buffer since not only it has the right pH range but also it is well known for its non-complexing behavior with metals.[242, 243]

Two types of experiments were performed with and without removal of the non-encapsulated calcein. When calcein was removed, this was done by size exclusion chromatography as described in Section 4.10. As detergent to destabilize the membrane of the nanocon-

[25] Cm stands for coumarin.

tainers Triton X-100 for liposomes and o-POE (octyl-polyoxyethylene) were tested. A solution of $CoCl_2$ (100 mM) was used as quencher.

For the experiments without removal of non-encapsulated calcein the steps were as follows: measurement of the fluorescence (F_{tot}) of the sample of NCs (2 ml), addition of Co^{2+} (5 μl) and measurement of fluorescence as (F_{in}), addition of detergent, o-POE (10 μl) and measurement of the fluorescence (F_{totq}).

For the experiments with removal of non-encapsulated calcein the procedure was: chromatographic separation on a Sepharose 4B column (1x30 cm) eluted with Mops, collection of the sample, measurement of the fluorescence (F_{tot}) of the sample of NCs (2 ml), addition of Co^{2+} (5 μl) and subsequent measurement of fluorescence as (F_{in}), addition of detergent, o-POE (10 μl) and subsequent measurement of the fluorescence (F_{totq}).

The trials inverting the last two steps of the sequence of measurements followed the sequence: chromatographic separation on a Sepharose 4B column (1x30 cm) eluted with Mops, collection of the sample, measurement of the fluorescence (F_{tot}) of the sample of NCs (2 ml), addition of detergent, o-POE (10 μl) and subsequent measurement of the fluorescence (F_{totq}), addition of Co^{2+} (5 μl) and subsequent measurement of fluorescence as (F_{in}).

4.13. Light Scattering

4.13.1. Theoretical description

Electromagnetic radiation can interact with matter in two different ways, absorption or scattering. In the case of absorption, the molecules gain energy, which can later be released in different forms. In the case of scattering, an incident beam of electromagnetic radiation interacts with the molecule in such a way that its direction is changed. When the energy of the wave does not change upon interaction with the molecule, the scattering is said to be elastic. When there is an absorption component, then the beam loses energy while interacts with the molecule, and the scattering is in this case inelastic.[244, 245]

In this section the word particle will be used to describe an entity scattering light, where that might be a coiled polymer, a self-assembled structure, or a particle itself. In static light scattering (SLS), the excess intensity of the solution containing the particles is compared to the scattered intensity of the pure solvent. The cause of scattering is the change in polarizability (α) of the molecules, which in turns accounts for changes in refractive index. The excess scattering intensity is proportional to the refractive index increment. Time-averaged measurements, that

is, static quantities, are performed for SLS. SLS provides information about weight average molecular weights, radii of gyrations, virial coefficients, and confomations.[246]

Particles in solution are in constant random movement due to thermal collisions (Brownian motion). When irradiated this results in the broadening of the spectrum lines, giving rise to a Doppler shift in the frequency of the lines. Due to their slow dynamics the broadening of the spectrum is quite small for polymers and small particles, therefore, experimentally the intensity-time correlation function is measured instead. The movement of the particles in solution results in fluctuations in the scattered intensity, which is measured in the case of quasielastic or dynamic light scattering (DLS)[26]. DLS renders information about the dynamics of a system, such as translational diffusion coefficient (D_{app}) from which the hydrodynamic radius (R_H) can be obtained using the Stokes-Einstein relation.

Static and dynamic light scattering differ mainly in the way the scattered photons are collected by the detector. If this is averaged over a certain time, then SLS is carried out. If the photon counting is correlated instead of averaged then DLS is being performed. Correlated in this context means that although the process is intrinsically random in a large scale of time, at a shorter time interval certain correlation exists, that is, there is a relationship of the movement between the particles. If the intensity of the photons arriving at the detector is correlated then an intensity-time correlation $G(\tau)$ is obtained.[245]

$$G(t) = \lim_{T\to\infty} \frac{1}{2T} \int_{-T}^{T} I(t)I(t+\tau)dt \qquad g_2(t) = \frac{\langle I(0)I(t)\rangle}{\langle I(0)\rangle^2}$$

$g_2(t)$ is the normalized intensity-time correlation function with I the intensity. The intensity-time correlation function decays from $< I(t)^2 >$ at $t = 0$ to $< I(t) >^2$ with $t \to \infty$.

The electric field correlation function $g_1(t)$ is given by:[244]

$$g_1(\tau) = \frac{\langle E_s^*(t)E_s(t+\tau)\rangle}{\langle I\rangle}$$

The electric field correlation function is difficult to measure, since $\langle I\rangle = \langle |E| \rangle^2$ the intensity-time correlation is related to the correlation function of the electric field. This relationship is expressed by the Siegert relation:[244]

$g_2(t) = A + B\langle g_1(t)\rangle^2$ for a Gaussian distribution $g_2(t) = |g_1(t)|^2$

[26] Also known as photon correlation spectroscopy.

Where A is the base line of $g_2(t)$ and B the initial value of the base line of the normalized correlation function.

The scattering vector $\mathbf{q}$ is an important parameter in DLS and can be expressed as:

$$\mathbf{q} = (4\pi/\lambda)\sin(\theta/2)$$

With λ being the wavelength of the incident light and θ the angle of observation or scattering angle.

Different procedures can be used to evaluate correlation functions. The most used ones are: the exponential decay, the cumulant analysis, the stretched-exponential, and the CONTIN. For monodisperse small particles, the correlation function decreases as a single exponential of the form:[244]

$$g_1(t) = A + B \cdot \exp(-\mathbf{q}^2 Dt) = A + B \cdot \exp(-\Gamma t)$$

For which the decay constant Γ is related to the translational diffusion coefficient D as $\Gamma = D\mathbf{q}^2$, and A and B are constants.

For polydisperse small particles, the decay can be shown to be the sum of the decay functions for each individual group of particles. In this case, the electric field correlation function $g_1(t)$ which is a function of the delay time t, is related to the distribution function $G(\Gamma)$ of the characteristic relaxation times (Γ) by,

$$g_1(t) = \int_0^\infty G(\Gamma) e^{-\Gamma t} d\Gamma$$

Usually, one way to solve multi exponential decay functions is to approximate the result by fitting a cumulant to the logarithm of the correlation function, this approach does not require prior knowledge of the form of $G(\Gamma)$. The cumulant expansion (Koppel) can be written as:[244]

$$\ln[g_1(t)] = -\Gamma_{avg} t + \mu_2 t^2/2 - \mu_3 t^3/6 + \ldots$$

Where μ_2 is the second cumulant and Γ_{avg} is the first cumulant or the average line width defined by:

$$\Gamma_{avg} = \int_0^\infty \Gamma G(\Gamma) d\Gamma$$

Γ_{avg} is related to the diffusion coefficient D and the scattering vector $\mathbf{q}$ by $\Gamma_{avg} = D\mathbf{q}^2$. The polydispersity of the solutions can be characterized by the variance, given by the normalized second cumulant, or polydispersity index (PD) defined as:[244]

$$\mathrm{PD} = \mu_2 / \Gamma_{avg}^2$$

Solutions and suspensions having relatively narrow distributions typically have values of $\mathrm{PD} = 0.02 - 0.08$

The coefficients of the cumulant expansion are related to the average diffusion coefficient, the polydispersity, and asymmetry or skewness.

Another broadly used method for polydisperse systems is the stretched-exponential analysis, also known as Williams-Watts,[247, 248] which describes $g_1(t)$ as:

$$g_1(t) = a_1 \cdot e^{\left(\frac{-t}{b_1}\right)^{\beta_1}} + a_2 \cdot e^{\left(\frac{-t}{b_2}\right)^{\beta_2}} + \ldots$$

With a_i the baseline, and $0 < \beta \leq 1$ a parameter describing the polydispersity of the system. The parameter b_i can be used to calculate then the relaxation time Γ as $\Gamma = 1/b$ and with it, then the apparent diffusion coefficient (D_{app}) as follows:

$$D_{app} = \frac{1}{b \cdot \mathbf{q}^2} = \frac{\Gamma}{\mathbf{q}^2}$$

CONTIN analysis is a mathematical approach for solving the autocorrelation function; its main feature is that it provides a distribution curve.[249, 250]

The diffusion coefficient depends on concentration in the following manner:

$$D_{app} = D_0(1 + kC)$$

Therefore, to obtain the diffusion coefficient at infinite dilution D_0, an extrapolation to zero concentration must be performed. The hydrodynamic radius (R_H) can be obtained from the diffusion coefficient at infinite dilution by the Stokes-Einstein equation[27]:

$$R_h = k_B T / 6\pi\eta D_0 \qquad \text{Equation 1}$$

Where k_B, T, and η are the Boltzmann constant, the absolute temperature, and the solvent viscosity, respectively.

4.13.2. Experimental part

Dynamic light scattering (DLS) experiments were performed at 20 °C (293 °K) using an ALV-Langen Goniometer equipped with a frequency doubled NdYAg-Laser (λ=532 nm orλ=633 nm). An ALV-5000/E Multiple Tau Digital Correlator calculates the photon intensity-time autocorrelation function $g_2(t)$. The apparatus allows the measurement at scattering angles between 30° and 150°.

[27] Valid for hard, non-interacting spheres.

Prior to measurements, the sample solutions were filtered with 0.45 μm and 0.22 μm Millipore filters (Millex Durapore-PVDF, Millipore), and placed in 10 mm diameter cylindrical quartz cells. Cells were then mounted in a thermostated optical matching bath (toluene bath).

The vesicle samples were prepared according to one of the methods of vesicle preparation. A series of concentration range (a minimum of 5) was then prepared from the original solution of vesicles. Typically, polymer concentrations ranged from 10 mg/ml to 1 mg/ml. Data analysis were done with the software ALV-5000/E/EPP and ALV-60X0 for Windows NT. Aquisition was performed until the correlation function did not change anymore, which was usually around 3 min. The analysis of the data consisted on an initial fit of the correlation function with either a simple (cumulant), regularized (CONTIN) or nonlinear fit (exponential or stretched-exponential), according to the best residual profile obtained and the expected decay process. Then the diffusion coefficient was plotted as a function of square scattering vector for every concentration and by extrapolation to zero angle the diffusion coefficient at zero angle (D_{app}) was obtained. The obtained $D_{app}(0°)$ were then plotted as a function of the concentration and by extrapolation to zero concentration the D_0 was obtained. By means of the Stokes-Einstein relation $R_H(0°)$ at infinite dilution was calculated.

For the investigation of the vesicles prepared by the direct dispersion method and Biobeads method, the following samples were studied by DLS: **Step 1)** 100 mg of polymer (S131) was dissolved in 10 ml of PBS under constant stirring overnight. After filtration (3 times with 0,45 μm (Millex Durapore-PVDF, Millipore)) a 3 ml aliquot was taken and measured by DLS. **Step 2)** To the remaining 7 ml 350 μl Triton X-100 1% were added (to achieve a 0.05% final concentration). After stirring for 6 h a 3 ml aliquot was taken and measured by DLS. **Step 3)** To the remaining 4 ml 100 mg Biobeads were added and the sample was stirred for 5 h. After removal of the Biobeads a 3 ml aliquot was taken and measured by DLS. **Step 4)** The remaining 1 ml was cleaned chromatographically to observe if chromatography affects the size of the aggregates. The eluted peak corresponding to the vesicles was analyzed by DLS.

4.14. Transmission and scanning electron microscopy

4.14.1. Theoretical description

The beam in an electron microscope consists of and electron beam generated by thermionic emission from a metal filament. The beam it is accelerated through a potential and focused with electromagnetic lenses. With an accelerating voltage of 100 kV, a 3.7×10^{-3} nm electron wavelength is obtained, thus allowing in principle atomic resolution. Nevertheless, the experimental achievable resolution is of 0.1 nm, and this, depending on the sample and instrument. In order to prevent scattering and absorption of the electrons by molecules in air, the system of an EM works under vacuum. From the many different interactions of the incident

electrons with the sample, different techniques arise. When the electrons pass through the sample, one talks about transmission electron microscopy (TEM). When a beam of electrons is scanned over a sample and low energy secondary scanning electron microscopy, because usually the beam is scanned over the sample in a raster mode. The electrons are scattered by the atomic potentials of the atoms in the sample, therefore, when the sample is not electron dense, the use of high contrast dye agents is needed (from Petty monolayers p 106).

4.14.2. Experimental part

TEM

Colodion (carbon-parlodion) coated copper grids (200-400 mesh/in, Electron Microscopy Science) were irradiated under vacuum in a glow discharge chamber (12 s). A drop (5 μl) of the polymeric vesicles dispersion was deposited onto the grid (adsorption time=30 s), and then blotted with filter paper. After 3 cycles of washing with water (one drop) and blotting, the samples were negatively stained with uranyl acetate ($UO_2(OAc)_2$, 1-2 %), incubation time 20 s., this last step was repeated once. The prepared grids were blotted and subsequently stored at room temperature until examination on the TEM. Morphological examination of the vesicles was performed using either a Hitachi H7000 or Philips EM 4000 operating at 100 kV.

The samples used for TEM were in most cases previously chromatographically purified to remove non-encapsulated materials. If that was not the case, then a previous dilution was necessary, otherwise the samples appeared quite dense. After treatment with ligand labeled NCs, cells were placed on coverslips and washed twice with PBS. Subsequently they were fixed in 4% paraformaldehyde and preserved in water in order to avoid salt residue crystallization on fixing. The coverslips were dried in a vacuum chamber prior to examination.

SEM

The cells were incubated at 4°C or 37°C with NCs. Subsequently they were fixated with 1% glutaraldehyde, were dehydrated (with increasing concentrations of ethanol), critical point dried (CPD), and finally platinum-sputtered.

4.15. FCS experiments

4.15.1. Technique description

Confocal Fluorescence correlation spectroscopy (FCS) is a well-established method to study fluorescent molecules in situ. FCS can provide information about different parameters, such as concentrations, molecular mobility, dynamics and transport properties like diffusion of fluorescently labeled molecules.[251, 252]

FCS is based on the detection and analysis of the spontaneous fluctuations in the fluorescence intensity emission of small molecules confined in a small sampling volume.[251]

In solution molecules diffuse due to Brownian motion and if they also emit, the emitted light is influenced by this diffusion process giving rise to spontaneous fluctuations of the fluorescent signal. [253] The detection volume, or confocal volume, is given by a double cone with a waist less than 1 μm in diameter obtained by a well-focused exciting laser beam. Selection of the fluorescence emitted only from this excitation region with an aligned pinhole in the image plane allows for highly resolved spatial focusing.[254, 255] The emitted photons are counted as they arrive to the detector diodes and an autocorrelation function is analyzed by a correlator. From the time analysis of the signal fluctuations the autocorrelation function $G(\tau)$ is obtained, from which the diffusion time (τ_D) and the average number of diffusing molecules can be calculated.[256, 257] The autocorrelation function has the form:

$$G(\tau) = \langle I(t) \cdot I(t+\tau) \rangle$$

With I the intensity emitted or fluorescence signal. After normalization with the squared mean intensity $\langle I \rangle^2$ the correlation function[28] takes the form:[253, 258]

$$G(\tau) = 1 + \left(\frac{1}{N}\right)\left(\frac{1}{1+\frac{4D\tau}{\omega^2}}\right)\left(\frac{1}{1+\frac{4D\tau}{z^2}}\right)^{1/2} \quad \text{or} \quad G(\tau) = 1 + \left(\frac{1}{N}\right)\left(\frac{1}{1+\frac{\tau}{\tau_D}}\right)\left(\frac{1}{1+\left(\frac{\omega}{z}\right)^2\frac{\tau}{\tau_D}}\right)^{1/2}$$

N is the number of independent fluorophores in the volume element defined as:

$$V = \pi^{3/2} \cdot \omega^2 \cdot z$$

With ω and z being the radius and length of the detection volume.[256, 258]

In most cases G(τ) can be approximated by an exponential decay function. For free diffusing molecules, the characteristic decay time (τ_D) obtained from G(τ) can be interpreted as the average time that the molecules spend in the detection volume. This average τ_D allows the calculation of mobility parameters such as diffusion constants since:

$$\tau_D = \omega^2 / 4D$$

Where D is the translational diffusion coefficient, from which the hydrodynamic radius (R_h) can be obtained via the Stokes-Einstein relationship:[259]

$$D = kT / 6\pi\eta R_h$$

[28] The autocorrelation function holds when the particle size is smaller than the volume element.[256] A. Pramanik, P. Thyberg, R. Rigler, *Chemistry and Physics of Lipids* **2000**, *104*, 35.

The zero time correlation $G(0)$ corresponds to the amplitude of the normalized correlation function. $G(0)$ is inversely proportional to the average number of particles in the measuring volume $G(0) = 1/\langle N \rangle$, for a dilute homogeneous dye solution.[254] Therefore, $G(0)$ allows the determination of the concentration in a local environment.

For a free dye in solution a typical diffusion time is of the order of 20-40 μs. If a fluorescent dye is covalently attached to a larger molecule, its fluorescent fluctuations will be influenced by the mobility of the large molecule by codiffusion and a higher overall diffusion time will be observed.[255] In particular, codiffusion can take place in vesicular systems carrying fluorescent molecules in their cavities, where the diffusion of the enclosing vesicle determines the diffusion of the dye. This results in an advantage of FCS over colocalization experiments, since co-diffusion is a more specific proof for the interaction between two dyes than colocalization.

The last is particularly true when using two instead of one fluorescent species. Two-dye systems, also called dual color detection is the most optimal way to prove ligand-receptor interactions.[252] The signals due to fluctuations of the fluorescence intensity of each species are compared through a crosscorrelation function. Crosscorrelation means that both fluorescent dyes are correlated in their motion, which is an indication of their spatial relationship.

4.15.2. Experimental part

FCS was performed with confocal illumination in an CSLM Confocor2 Zeiss (Jena, Germany) which was used in an epi-illumination setup. Dichroic filters and bandpass filters were used to select the proper excitation and emission wavelengths. The autocorrelation of the detector output signals were calculated by a two-channel digital correlator.

Five FCS measurements of 30 s were recorded on a chosen location for the pinhole, and averaged and fitted for determination of the diffusion time (τ) from which the translational diffusion coefficient D_τ could be calculated.

For the experiments to investigate sulforhodamine encapsulation in vesicles (polymer used JW05), different preparation methods and different concentrations of sulforhodamine were used. For calibration purposes (pinhole, and beam intensity) free non-encapsulated sulforhodamine was used. Free sulforhodamine B (10 nM) was used to calibrate the instrument and excited at 543 nm with an Argon laser. The pinhole diameter was 90 μm.

sample name	polymer %	Method	Sulforhodamine conc. (mM)	Chromat. Peak
DD-21	1	Dir Diss	4	1.1
DD-22	1	Dir Diss	4	1.2
DD-23	1	Dir Diss	20	1.1
DD-24	1	Dir Diss	20	1.2
EM 2p-25	2	Standard	4	2.1
EM 2p-26	2	Standard	4	2.2
EM 2p-27	1	Standard	20	2.1
EM 2p-28	1	Standard	20	2.2
EM 2p-29	2	Standard	20	2.1
EM 2p-30	2	Standard	20	2.2

Table 4.15.2.1: Data for the experiments with sulforhodamine encapsulation in polymer vesicles.

For the experiments to investigate the encapsulation of enzymes, Alexa-488-Avidin loaded vesicles were prepared by the standard injection/extrusion method and the direct dispersion method (see Section 4.8). The dye was excited with the 488 nm (5% transmission) line of an Argon laser (50% of 30 mV). The pinhole diameter was 70 μm. To calibrate the pinhole an analogue of Alexa488-Avidin of low molecular weight was used, in this case it was Alexa-488C5 maleimide (λ_{abs}=493 nm, ε_C=72000, λ_{em}=516 nm). For determining the diffusion time of Alexa-488-Avidin, a solution of 0.015 mg/ml was used. Vesicles were prepared by two different methods in the presence of a solution containing Alexa-488-Avidin (0.15 mg/ml) in PBS buffer and were chromatographically purified to remove non-encapsulated protein. For control purposes empty vesicles were also measured by FCS.

4.16. Density determinations

4.16.1. Theoretical description

Different experiments can be performed within the analytical ultracentrifugation technique, rendering different parameters. The experiments can be classified in equilibrium measurements and dynamical measurements. The equilibrium experiments comprise, sedimentation equilibrium and density gradient sedimentation equilibrium. Sedimentation velocity represents a dynamical measurement. Different parameters are obtainable through these experiments, for instance, sedimentation velocity gives the sedimentation coefficient s, whereas sedimentation equilibrium yields the z average molecular weight ($\overline{M}_z$) if the density is known, finally, density gradient measurements give the density υ of the macromolecules.[260]

Sedimentation equilibrium allows not only the determination of average molecular weight ($\overline{M}_z$) but also the quantification of the size distributions in polydisperse samples. One interesting feature of the analytical ultracentrifugation analysis in comparison with other techniques is that it does not require calibration, as in GPC, or assumptions regarding shape, as in

LS. Moreover, the method is also suitable for any molecule whose absorbance or refractive index differs from the solvent. The only inconvenience of the technique is the long times required for experimental analysis and the high cost of the equipment. Nevertheless, sedimentation analysis is still a valuable technique to study the change in molecular weight of associating macromolecules, such as dimers and trimers, rendering the molecular weight of the complex as it exists in solution.

Sedimentation equilibrium allows also the study of small molecules binding to macromolecules, the self-association of macromolecules, and heterogeneous macromolecular interactions. These studies can reveal the size of the individual molecules taking part on the complex formation, size of the complex, etc. It is also a very sensitive technique for the analysis of weak associations. Sedimentation velocity experiments provide sedimentation and diffusion coefficients, which in turn are related to the size and shape of the macromolecules. Sedimentation velocity is also suited for the study of ligand binding experiments; in these cases it is of advantage to use ligand and receptors with different absorbance characteristics.

In the centrifugation cell, the forces acting on the sample are three: the centrifugal force F_S, the buoyant force F_b, and the frictional force F_f.[260]

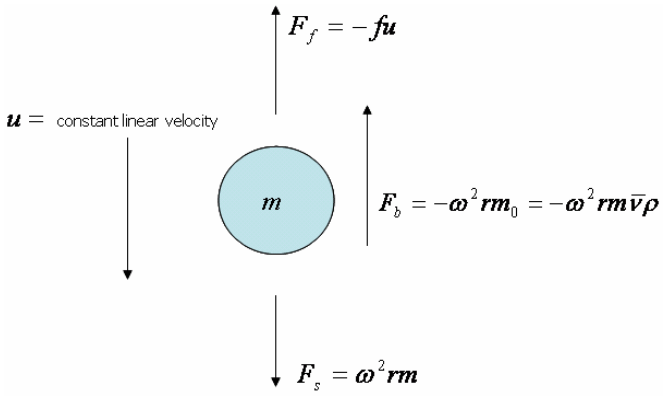

Figure 4.16.1: Schematic representation of the forces acting on a particle in a gravitational field.

$$F_s = \omega^2 rm \qquad F_b = -\omega^2 rm_0 = -\omega^2 rm\bar{v}\rho \qquad F_f = -fu$$

with ω the angular velocity, r the distance of the particle to the rotation axis, m the mass of the particle, $\bar{v}$ partial specific volume of the solute, ρ the density of the solvent, f frictional coefficient, and u constant linear velocity.

In equilibrium the forces are balanced, therefore,

$$F_s + F_b + F_f = 0$$

which after replacement of the above equations and rearranging gives:[260]

$$\frac{M(1-\bar{\nu}\rho)}{Nf} = \frac{u}{\omega^2 r} = s$$

with s the sedimentation coefficient, in other words, the velocity of the particle per unit gravitational acceleration.

$(1-\bar{\nu}\rho)$ = buoyant density term

The buoyant density is a measure of the tendency of a substance to float in some other substance, which is usually measured by density-gradient ultracentrifugation.

The density-gradient sedimentation equilibrium renders the particle's density, by using a self-forming gradient, the particles migrate to the position of equal density.

When the densities of the solute and solvent are equal, $(1-\bar{\nu}\rho)=0$, there is no tendency to move in either direction. This feature can be used to determine the density of macromolecules in density gradient sedimentation. During density gradient sedimentation measurements, the macromolecule eventually will form a layer where the solvent density is equal to their own, that is, the buoyant density.[260] However, a disadvantage of this procedure is that these types of static gradients require very long centrifugation times.

Due to the experiments performed with polymeric vesicles it is of interest to describe a few more details about the dynamic experiments of sedimentation velocity.

Sedimentation velocity

The sedimentation coefficient depends highly on the density of the solvent and the solution viscosity; therefore, by convention sedimentation coefficients are expressed in terms of a standard solvent, usually water at 20 °C.[260]

$$s_{20,w} = s_{obs}\left(\frac{\eta_{T,w}}{\eta_{20,w}}\right)\left(\frac{\eta_s}{\eta_w}\right)\left(\frac{1-\bar{\nu}\rho_{20,w}}{1-\bar{\nu}\rho_{T,s}}\right) \qquad \eta = \text{viscosity}$$

Sedimentation coefficients are concentration dependent, decreasing with increasing concentration. Therefore, it is customary to extrapolate to zero concentration to obtain the limiting (ideal) sedimentation coefficient.

$$s = \frac{s^0}{(1+k_s c)}$$

With c the concentration, k_s the concentration dependence coefficient, and s^0 the limiting ideal sedimentation coefficient extrapolated to zero concentration

4.16.2. Experimental part

A technique based on sedimentation velocity experiments has been described to determine the partial specific volume of lipid vesicles.[261] The technique makes use of D_2O/H_2O mixtures of different density. It was found that at the zero value of the viscosity corrected sedi-

mentation coefficient (ηs^0) the vesicles do not float or sediment, therefore, the density of the D_2O/H_2O mixtures at that point can be taken as the density of the vesicles. The partial specific volume of the solute, in this case the vesicles, is not other than the reciprocal of this density.

By using a rapid dynamical density gradient (RDDG) and special double sector centrifuge cells, this technique was adapted for lipid vesicles and complexes of lipidic vesicles with proteins.[178] We used a special synthetic boundary double sector bottom capillary cell (SBDS-BC) in which one sector is filled with the dense solution (D_2O) and the other is half-filled with the less dense solution containing the particles. During centrifugation the denser solvent is layered under the solution containing the solute, mixing thus with the less dense solvent and rendering a density gradient. The solute particles can then band in this gradient.

In order to determine the sedimentation coefficient at zero concentration s^0, the sedimentation coefficients of the vesicles are first measured at different vesicle concentrations in mixtures of D_2O/H_2O. Subsequently, the sedimentation coefficient extrapolated to zero concentration for each D_2O/H_2O mixture is multiplied by the relative viscosity of its corresponding D_2O/H_2O mixture. The obtained ηs^0 values, also termed viscosity-corrected sedimentation coefficient, are then plotted versus the density of the corresponding D_2O/H_2O mixture. The density corresponding to $\eta s^0 = 0$, obtained by interpolation of the least squares line intersecting the abscisa, is then the density of the solvent at which the solute neither flotates nor sediments, and therefore, it is also taken as the density of the solutes.

Absorbance at different wavelengths was used as detection of the concentration changes in the ultracentrifugation cell (Optima XL-A).

4.17. Selective cell targeting with biotinylated Nanocontainers

Cell cultures

COS-7 cells (ATCC Nr. CRL-1651) were cultured as already described, [262] one day prior to transfection cells were seeded at about 40% confluence onto ethanol-washed cover slips into 12-well Falcon plates. On the day of transfection, cell density was assessed, being in the range of $5x10^4$ cells/cm^2. Lipid-mediated transfection was performed with FuGENE™ (Roche Molecular Biochemicals) as described earlier.[262] Cells were transfected either with a plasmid carrying the open reading frame for EGFP (negative control) or with a plasmid containing the complete open reading frame of human SRA-1 fused in frame to the C-terminal end of EGFP. All subsequent experiments were carried out between 24 h and 48 h after transfection.

THP-1 monocyte line[263] was cultured according to manufacturer's instructions. Differentiation to functional macrophages with SRA-1 expression was achieved by adding 200 nM phorbolester.[263] Human vascular smooth muscle cells (VSMC) from pulmonary arteries were a

kind gift from M. Tamm and were cultured as described elsewhere. Human umbilical vein endothelial cells (HUVEC, ATCC) were cultured according to the manufacturer's instructions.

C. Saw and P. Broz kindly prepared the cell cultures.

Ligand functionalized NCs

Mixtures of pure, non-modified triblock copolymer and biotinylated polymer with a ratio 9:1 w/w were used to prepare the biotinylated NCs. For control experiments non-modified triblock-copolymer was used to prepare NCs (control NC). Sulforhodamine with an initial concentration ranging from 10 mM to 80 mM was encapsulated in the NCs.

To obtain ligand-functionalized NCs, biotinylated NCs were incubated with an excess streptavidin. Unbound streptavidin was removed by SEC (Sepharose 4B) with PBS as eluant. Subsequently these NCs were incubated with biotinylated polyG (poly-G, 23 nucleotides per strand) in a 1 to 1 ratio of biotin sites to polyG, to produce active targeting drug delivery systems. Due to the high binding affinity between biotin and streptavidin no further purification was necessary. To optimize the system, the following combinations of reactants were used to prepare streptavidin functionalized NCs.

Sample	Substance	Mw	Biotin %	C (mg/ml)	mmol in 1 ml	Aliquot (µl)	total mmol	Biotin/avidin ratio
A	NCs-biot	7000	10	10	1.43E-04	**400**	5.71E-05	9.92
	Avidin	66000		2	3.03E-05	190	5.76E-06	

Sample	Substance	Mw	Biotin %	C (mg/ml)	mmol in 1 ml	Aliquot (µl)	total mmol	Biotin/avidin ratio
B	NCs-biot	7000	10	10	1.43E-04	**400**	5.71E-05	0.99
	Avidin	66000		20	3.03E-04	190	5.76E-05	

Sample	Substance	Mw	Biotin %	C (mg/ml)	mmol in 1 ml	Aliquot (µl)	total mmol	Biotin/avidin ratio
C	NCs-biot	7000	10	1	1.43E-05	**400**	5.71E-06	0.99
	Avidin	66000		2	3.03E-05	190	5.76E-06	

Sample	Substance	Mw	Biotin %	C (mg/ml)	mmol in 1 ml	Aliquot (µl)	total mmol	Biotin/avidin ratio
D	NCs-biot	7000	10	3.33	4.76E-05	**450**	2.14E-05	1.57
	Avidin	66000		2	3.03E-05	450	1.36E-05	

Sample	Substance	Mw	Biotin %	C (mg/ml)	mmol in 1 ml	Aliquot (µl)	total mmol	Biotin/avidin ratio
F	NCs-biot	7000	10	3.33	4.76E-05	**450**	2.14E-05	3.14
	Avidin	66000		1	1.52E-05	450	6.82E-06	

Table 4.17.1: Calculations for the amounts of biotin and avidin used for the optimization of the preparation of avidin functionalized NCs.

Sample	Substance	Mw	Biotin %	C (mg/ml)	mmol in 1 ml	Aliquot (µl)	total mmol	Biotin/avidin ratio
G	NCs-biot	7000	10	3.33	4.76E-05	**450**	2.14E-05	1.57
	Avidin	66000		2	3.03E-05	450	1.36E-05	

Sample	Substance	Mw	Biotin %	C (mg/ml)	mmol in 1 ml	Aliquot (µl)	total mmol	Biotin/avidin ratio
H	NCs-biot	7000	5	3.33	2.38E-05	**450**	1.07E-05	1.57
	Avidin	66000		2	3.03E-05	225	6.82E-06	

Sample	Substance	Mw	Biotin %	C (mg/ml)	mmol in 1 ml	Aliquot (µl)	total mmol	Biotin/avidin ratio
I	NCs-biot	7000	1	3.33	4.76E-06	**450**	2.14E-06	1.57
	Avidin	66000		2	3.03E-05	45	1.36E-06	

Table 4.17.2: Calculations for the optimization of the initial percentage of biotin in NCs.

Cells were treated with NCs with a final concentration of 50 µg/ml. The standard incubation time was 2 h at 37°C.

Fluorescence microscopy experiments

The following microscopes were used: Zeiss Axiophot (Carl Zeiss, AG) and Nikon fluoromicroscope (Paul Bucher AG), both equipped with a Hamamatsu video imaging system

Cells incubated with NCs were fixed in 4% paraformaldehyde for 30 min at room temperature. Fixed cells were washed twice in PBS and then mounted in Mowiol containing 1% n-propyl gallate. Cells were examined using a Nikon Diaphot 300 microscope (Nikon AG, Küsnacht, Switzerland), equipped with a SenSys Video imaging system.

Analysis was performed with normalized pictures (Green and red channel for COS-7) with the ImageJ (Version 1.28u, NIH) computer program. After defining a region of interest (ROI) around a individual cell, the mean green fluorescence intensity wast measured, then the mean red fluorescence intensity in the same ROI was measured. The untreated control cells without receptor were used as reference values for the calculations.

Preliminary investigations using transfected COS-7 cells

For these test, targeting NC, and control NC, i.e., biotinylated NCs loaded with sulforhodamine B incubated with streptavidin and polyG, and non-biotinylated NCs with sulforhodamine B incubated with streptavidin, respectively. The last step of the functionalization of the NC, that is the incubation with polyG, in the case of biotinylated NC, was done just immediately before treating the cells. After 2 h of incubation at 37°C the coverslips were washed twice with PBS, then the cells were fixed in 4% paraformaldehyde for 10 min at room temperature. Fixed cells were washed twice in PBS and then mounted in Mowiol containing 1% n-propyl-gallate (Sigma).

Quantification by bispectral fluorescence microscopy

Transgenic COS-7 cells with or without the target scavenger receptor A1 were exposed to NCs with or without the ligand polyG. For each individual cell, the emitted light intensity was

measured by fluorescence microscopy in two spectral bands, i.e., the fluorescence intensity in the red channel (indicating NCs), and the fluorescence intensity in the green channel (indicating receptor/cell presence) was measured. The mean and standard deviations were calculated for the data corresponding to the negative control consisting of untreated cells.

The same type of experiments were repeated with THP-1 cells incubated with polyG functionalized NCs. The following controls were performed, NCs without biotin incubated with THP-1 cells and untreated cells.

Uptake kinetic experiments were performed with the same setting and different incubation times ranging from 30 to 270 min.

Mixed cell culture experiments

Cell cultures of THP-1, VSMC, and HUVEC were prepared alone or in mixtures. Fixation was achieved with 4% paraformaldehyde, followed by placement in Mowiol containing 1% n-propyl gallate. VSMC and HUVEC show faint green autofluorescence, while THP-1 showed a strong blue autofluorescence signal allowing thus localization and distinction of the different cell types. Digital fluorescence microscopy using the ImageJ software package (version 1.28u, NIH) was used for quantification. All cells in each multiple views were localized in the blue band, and NC uptake for each cell was then quantified by fluorescence intensity in the red band (590 nm).

Cytotoxicity tests

An apoptosis test was carried out with THP1 cells using camptothecin as apoptosis agent (positive control). Cell populations (10'000) were incubated with four different reagents: a) 100 μl buffer (untreated cells), b) 100 μl NC control (non-biotinylated), c) 100 μl ligand labeled NC (NC-b-s-bpolyG), and d) 10 μl camptothecin (conc). Apoptosis counts were performed after 4 and 24 h.

Cytotoxicity was assessed by [3H]adenine-release.[264] Cells labeled with [3H]adenine (1 μCi/ml) were incubated with NCs for 4 and 24 h, and [3H]adenine release was determined using an automated scintillation counter. A positive control consisting of cells treated with 10% ethanol was used. The negative control consisted of untreated cells.

4.18. Gold encapsulation

4.18.1. Pre-formed gold Nanoparticles encapsulation

Method 1 – Hydrophobic gold

To 15 ml of a solution of chloroauric acid in bidistilled water (0.0335 M, 0.5025 mmoles) (see Pic. 4.18.1, a) 10.20 ml of a solution of tetraoctyl ammonium bromide (TOAB) in toluene (0.0999 M, 1.02 mmoles) were added with stirring. Two layers formed, the organic upper layer was dark red orange and the lower aqueous layer a clear or slightly orange (see Pic. 4.18.1, b). This mixture was shaken until disappearance of the orange color of the aqueous phase. Subse-

quently 3.13 ml of a solution of lauryl mercaptan in toluene (0.0418 M, 0.131 mmoles) were added, followed by addition of 12.5 ml of an aqueous of sodium borohydride (0.4013 M, 5.02 mmoles) to the slowly stirring reaction mixture. An instant color change followed the addition of sodium borohydride, changing first to dark bordeaux[29] and then to a dark brown-black (see Pic. 4.18.1, c). The reaction was left stirring during 12 h open to the atmosphere. Subsequently it was left to decantate and both layers were separated. The organic phase was concentrated to about 5 ml in a rotary evaporator, 350 ml of ethanol were added and the solution was left at -60 °C for 2 h to precipitate, and then at 4 °C overnight. The dark brown precipitate was centrifuged, the supernatant was removed, and the precipitate was dried in a vacuum line.

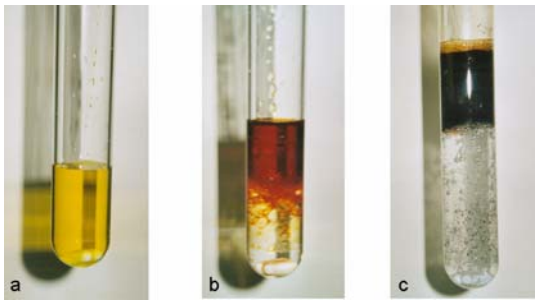

Pic. 4.18.1: Hydrophobic gold nanoparticle formation according to Leff et al.[197]

The hydrophobic-coated gold nanoparticles so obtained were suspended in ethanol in order to proceed for their encapsulation in polymer vesicles according to the standard method of vesicle preparation. The non-encapsulated gold nanoparticles were removed chromatographically by means of a column (1x14 cm Sepharose 4B) and the fractions collected were examined by TEM (see Section 4.14.2).

Method 2 – Hydrophilic gold

Preparation of the gold nanoparticles in toluene, in the presence of tetraoctyl ammonium bromide as stabilizer[265] was described above. Briefly, 30 ml of a solution of tetrachloroauric acid (30 mM) in bi-distilled water (see Pic. 4.18.2, a) were placed in a flask. A solution of tetraoctyl ammonium bromide (TOAB) in toluene (80 ml, 50 mM) was added to the aqueous solution of gold salt. The metal ions exchanged with the bromide in the organic phase, which was detected by a change of color from a yellow aqueous phase and a clear organic one into an orange organic upper phase and a slightly transparent aqueous one. Then the sample was transferred to a separating funnel and the aqueous phase was discarded. To the stirring organic phase (see Pic. 4.18.2, b) an aqueous solution of sodium borohydride (25 ml, 0.4 M) was added dropwise (see Pic. 4.18.2, c). Following 3 h of stirring, the sample was left to decantate (see

[29] The particular color of the colloidal gold suspension is due to the excitation of the surface plasmon vibrations.

Pic. 4.18.2, d), the aqueous phase was discarded, and the organic phase was washed several times to remove any inorganic products. This organic solution contained the pre-formed gold nanoparticles stabilized by TOAB.

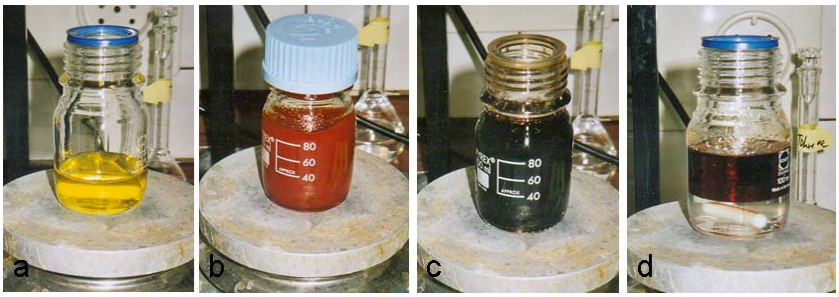

Pic. 4.18.2: Hydrophobic Au nanoparticle formation according to Gittings [199] and Brust.[265]

The preparation of the water-soluble gold nanoparticles involves one more step of thiol capping and exchange to an aqueous phase[199]. For this 65 mg of 11-mercaptoandecanoic acid were dissolved in 500 µl toluene (to achieve approx. a final 30-fold molar excess of thiol to nanoparticles) were added to a 3 ml aliquot of the already prepared particles in toluene at 70 °C. The resulting 11-mercaptoandecanoic acid (MUA) coated nanoparticles were insoluble in toluene. The particles were left to sediment overnight and then were washed with isopropanol to render them hydrophilic and remove the remaining toluene. Then the particles were suspended in the PBS buffer used for preparing the polymer vesicles.

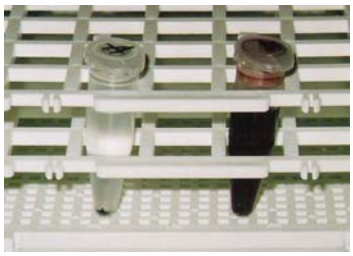

Pic. 4.18.3: Hydrophilic gold nanoparticle formation according to Gittings et al.[199]

With the resulting hydrophilic modified Au particles, polymer vesicles were prepared with two different polymers according to the standard injection/extrusion method and direct dispersion method already described (see Section 4.8.1 and 4.8.2 respectively). Non-encapsulated gold particles were removed by chromatographic separations using a Sepharose 4Bcolumn (1x14 cm) (see Section 4.10). The fractions collected by chromatography were analyzed by TEM (see Section 4.14).

4.18.2. In situ gold formation in vesicles

Method 1

In a first approach, we reproduced a method used to produce gold particles in liposomes.[196, 200] A bright yellow solution of $HAuCl_4$ (3.18 mM) in sodium citrate (10.2 mM), potassium carbonate (2.5 mM), and sodium chloride (55 mM) was used to prepare vesicles with two different polymers and two different preparation methods. The samples were prepared using this solution by the usual procedures (standard and direct dispersion methods, for details see Section 4.8) and were left stirring. In contrary to that expected according to the protocol used for liposomes,[196] in the case of polymeric vesicles it was not necessary to heat at 37 °C to promote particle formation. After 90 min all samples had reacted. The samples made by the direct dispersion method were of a deep purple/bordeaux color, typical of gold nanoparticles, whereas the samples made by the standard ethanol method presented a more translucid grayish color, typical of larger particles in suspension. A control solution containing only the salts of $HAuCl_4$ in the same buffer used to prepare the vesicle's samples was found to have reacted giving a precipitate of gold (formation of a gold mirror on the walls of the vial).

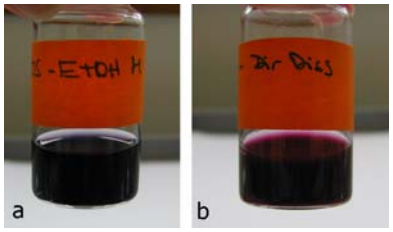

Pic. 4.18.4: Aspect of the vesicle's preparation with AU in situ method 1, a) standard method, b) direct dispersion method.

Subsequently, all samples were filtered with extrusion filters (Millex, Millipore) and non-encapsulated gold was separated by column chromatography on a Sephacryl column (10 cm) (see Section 4.10). A new column was needed for each sample since the non-encapsulated gold seemed to adsorb irreversibly to the gel. In order to prevent excessive dilution due to longitudinal dilution effects, the separations were carried out under applied pressure. The samples were then observed by TEM and some typical structures are depicted in Section 3.4.2.2.

For the modification of the AUM in situ 1, vesicles were prepared in an aqueous solution of $HAuCl_4$ (12.72 mM) either by the standard or direct dispersion method. The polymer concentration was 10 mg/ml and the final volume of each sample was 2 ml. All samples were stirred overnight, and no reduction of gold was observed during this time. To an aliquot of 1 ml of the vesicle dispersion, 1 ml of a solution of citric acid (120 mM) and potassium carbonate (30 mM) was added, and the samples were left stirring for 3 h. After this time a reddish-brownish suspension was obtained with the direct dispersion method, while a red to pinkish semitranslucid suspension was observed with the standard (ethanol) method. The samples were filtered and

subsequently the non-encapsulated gold was separated from the vesicles by size exclusion chromatography (Sephacryl S 300-HR, 1x9 cm). The samples were then observed by TEM.

Method 2

A slight modification of the preparation used before[200] was used.[203] A chloroauric solution of low pH (3) was used to avoid premature nucleation of gold particles.

To prepare polymer vesicles, 25 ml of a solution of $HAuCl_4$ (12.72 mM) were mixed with 25 ml of a solution containing citric acid (120 mM) and potassium carbonate (30 mM). The pH of the yellowish solution was 2.7. The normal protocols for preparation of standard vesicles and direct dispersion vesicles were then followed (see Section 4.8) using this solution as buffer medium, and two different polymers. Subsequently, all samples were left stirring overnight.

The solution containing the salt of chloroauric acid and the citric acid at pH 3, reacted in 3 h rendering a gold mirror on the walls of the vial, while the samples containing polymer took longer to react. After overnight stirring, all samples had either a pinkish (standard ethanol method) or a purple (direct dispersion) without the need of raising the pH. The samples were filtered with extrusion filters (Millex, Millipore) and the non-encapsulated gold was removed by chromatography with a Sephacryl column (1x10 cm). Pic. 4.18.5 shows the samples before and after the elapsed reaction time, and their chromatographic separation Pic. 4.18.6.

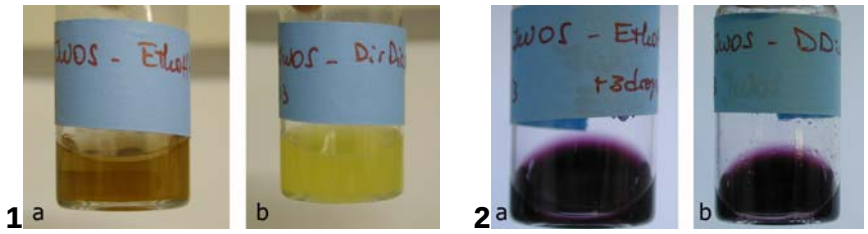

Pic. 4.18.5: Aspect of the vesicle preparations with the AU method 2 on the moment of preparation, 1a) standard method, 1b) direct dispersion method and after preparation, a) standard method, b) direct dispersion method..

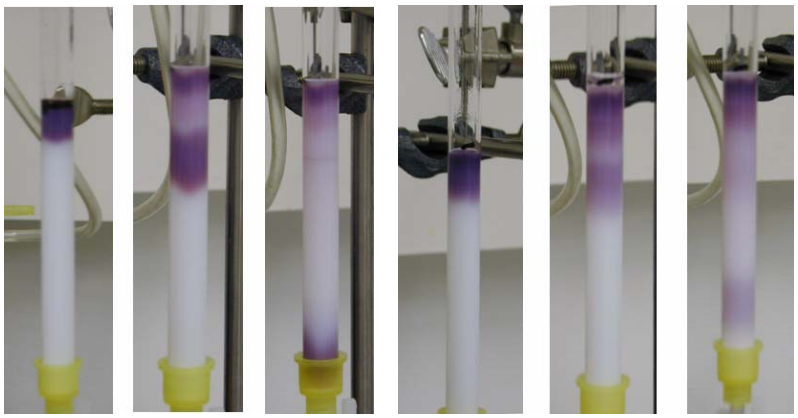

Pic. 4.18.6: Stages of the chromatographic separation of a sample of vesicles prepared with the AU in situ method 2 and standard ethanol method. It can be clearly seen the separation of the vesicles from the non-encapsulated gold particles. Left JW05, right S131.

Method 3

The AUM in situ 3 comprised the use of a solution of $NaAuCl_4$ and subsequent UV irradiation[205] step to promote the Au reduction. A 0.4 mM $NaAuCl_4$ solution was encapsulated in vesicles prepared different methods. In contrary to what was expected the vesicle samples reacted prior to UV irradiation, on stirring overnight. These samples were not further analyzed.

To promote the in situ formation of gold nanoparticles and to prevent precipitation prior to UV irradiation, vesicles were prepared from a 0.5 mM solution $HAuCl_4$. Again two polymers and two preparation methods were used. The samples were subsequently irradiated with a UV lamp for 5 h. Two procedures were tested, that is, in a first approach the vesicles were irradiated in the presence of free chloroauric acid as already described. A second approach was to remove the free chloroauric acid present in the sample before irradiation, but this failed since the gold precipitated reacted as soon as it came in contact with the chromatographic gel.

4.19. Quartz Crystal Microbalance

4.19.1. Theoretical description

Originally, the quartz crystal microbalance (QCM) was used to measure the mass uptake on a sensor surface, i.e., as a very precise balance.[266] A new developed technique for measuring in the presence of liquids allows not only the determination of the adsorbed mass onto a quartz crystal but also the dissipation of energy, therefore, its name, quartz crystal microbalance with dissipation (QCM-D).[266] An interesting feature of the QCM-D is that senses the water adsorbed or coupled to the adsorbed layer.[223] Applications of the QCM-D include real-time studies of surface adhesion and adsorption, molecular interactions, and functionalized surfaces.

The heart of the QCM-D is an AT-cut quartz crystal[30] sandwiched between two thin layers of gold, which act as sensing electrodes [31] (see Figure 4.19.1). Due to its piezoelectric properties, the quartz crystal can be then brought to oscillation,[266] i.e, exited to its resonant frequency, by applying an AC voltage across the electrodes.

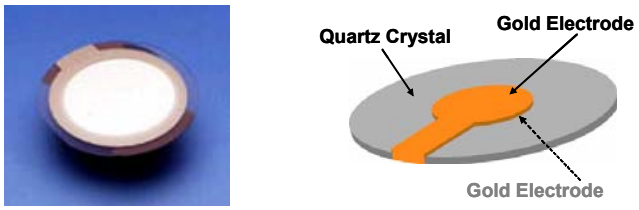

Figure 4.19.1: Sensor crystal, actual picture, and schematic representation. www.q-sense.com

[30] An AT-cut crystal is a crystal which oscillation mode is on the shear mode only, that is, the oscillation is parallel to the sensor's surface plane[221] E. Reimhult, F. Hoeoek, B. Kasemo, *Langmuir* **2003**, *19*, 1681.
[31] The sensor crystal has a diameter of 14 mm and the volume above the sensor is 50 μl.

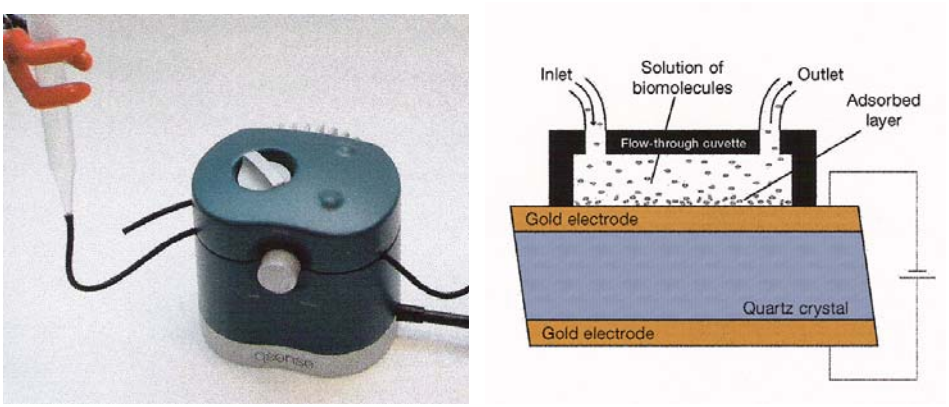

Figure 4.19.2: Left, QCM-D chamber, showing the introduction of a sample, right, schematic representation of the measuring chamber, the crystal covered with gold layers is not on scale. www.q-sense.com

Nowadays, the measurement relies on the detection of the decay of the frequency of the crystal, which gives not only information on the changes in frequency due to an adsorbed layer but also to the dissipation of energy caused when a dissipative (viscoelastic) material is adsorbed.[266] Moreover, the new detection allows for the simultaneous recording of the resonant frequency and its overtones, since the crystal is first exited and then the AC feed is disconnected, then the decay of the frequency of the freely oscillating crystal is recorded.[266]

The resonant frequency of an oscillating crystal is related to the total mass,[221] i.e., the mass of the crystal plus the mass of the adsorbed layer, which in turn accounts for any water coupled to the adsorbed layer.[266] The quartz crystal can be treated as a harmonic oscillator with a resonant frequency in vacuum, f_0, given by:[267]

$$f_0 = \frac{l_0}{2h_0}\sqrt{\frac{\mu_0}{\rho_0}}$$

With f_0 a function of the thickness h_0 of the quartz plate, its density ρ_0, and its elastic shear modulus μ_0.[267]

Two situations can be differentiated:[267] the adsorption of a thin rigid film and the adsorption of a viscoelastic film. In the former case, the frequency f decreases proportionally to the increase of the mass of the layer. Any mass added to the system Δm, is related to a frequency shift Δf according to the Sauerbrey relation:[266, 268]

$$\Delta m = -\frac{C \cdot \Delta f}{n}$$

Where n is the overtone number and C is a constant equal to 17.7 ng Hz^{-1} for a 5 MHz quartz crystal.[212] Moreover, when these conditions are met, the effective thickness d_{eff} of the film can be estimated by knowing the effective density (ρ_{eff}) of the adsorbed film:

$$d_{eff} = \frac{\Delta m}{\rho_{eff}}$$

When the layer adhered on the crystal does not obey the Sauerbrey relation due to its non-rigidity,[267] the terms related to energy loss due to viscosity and elasticity must be taken into account. Adhesion of a soft or dissipative material to the quartz crystal dampens the crystal's oscillation. The dissipation D of the crystal's oscillation is a measure of the lost energy by friction or viscosity. D is therefore, also a measure of the film's softness or visco-elasticity and can be described according to:[266]

$$D = \frac{1}{Q} = \frac{E_{dissipated}}{2\pi E_{stored}}$$

Where $E_{dissipated}$ is the total lost or dissipated energy during one oscillation cycle and E_{stored} is the total energy stored in the oscillator; Q is the absolute Q factor. [266] The dissipated energy can be also estimated from the dissipation factor D which is inversely proportional to the decay time constant:[267]

$$D = \frac{1}{\pi f \tau}$$

The dissipation of the crystal is measured by recording the frequency of a freely oscillating crystal at its resonant frequency. The decay curve has the form of a exponential damped sinusoidal,[266] as the sum of the sinusoidal frequency plus the exponential decay due to damping; the frequency and the dissipation terms can be extracted by fitting this curve.

In summary, by measuring both the frequency shift, which offers information about the adsorbed mass, and the dissipation energy, which gives information about the rigidity of the adsorbed layer, with the QCM-D a detailed characterization of films can be performed.

4.19.2. Experimental part

The instrument was a Q-Sense D300 (QCM Sense AB). To promote adsorption of polycations, the sensor's gold surface was modified by deposition of a 12 nm layer of niobium oxide. The buffer (PBS) was filtered (0.45 μm; Millipore) before addition to the sample reservoir.

All experiments were done in an axial flow chamber under batch conditions (exchange mode). The measuring chamber was temperature-stabilized with an accuracy of ± 0.05 °C. Before each experiment the crystal was rinsed with Milli-Q water, dried with N_2, and treated during 30 min in an UV/ozone chamber (UV clean Boekel Model 135500), and subsequently assembled in the chamber. The UV/ozone treatment oxidizes the surface evenly and removes organic contaminants, which are oxidized to H_2O and CO_2.[221] After each experiment the crystals were rinsed with water and placed vertically in a SDS (2%) solution for at least 40 min

before reuse. The measuring chamber was cleaned by passing a solution of detergent (Cobas Integra, Roche) for at least 1 h, rinsed with Milli-Q water, and dried with N_2.

The fundamental frequency (5 MHz) and its overtones (15, 25, and 35 MHz corresponding to the overtones, 3, 5, and 7 respectively) were measured for the crystal first on air (sampling frequency 0.5 Hz) and then in the presence of a layer of buffer (sampling frequency 2 Hz).

Poly(L-lysine)-g-poly(ethylene glycol)/poly(ethylene glycol)-biotin (PLL-g-PEG-b) (Prof. Dr. M. Textor, ETH Zürich) was used to create a biotinylated surface. A solution of the PLL-g-PEG-b containing 30% of biotin (0.5 mg/ml) in PBS and a streptavidin solution (0.02 mg/ml) in PBS were used for the immobilization of biotinylated vesicles. BSA (0.01 mg/ml) in PBS buffer was used for determination of unspecific protein adsorption. Vesicles were produced according to the standard preparation method in PBS buffer, with the following biotin percentages, 0, 10, 15, and 50 by mixing unmodified (JW05) and biotinylated polymer (JW05 ModA).

The measurement itself proceeded as follows. The external reservoir was filled with approximately 3 ml of the buffer liquid. Then the temperature reservoir (T-loop, Figure 4.19.3) was filled by allowing to flow approximately 1,5 ml of liquid through it (loop out). After waiting for 3 min for temperature stabilization, the side valve (control valve, Figure 4.19.3) was opened to allow 0,4 to 0,5 ml of liquid to flow though the crystal cell (lower outlet) and the measurement was conducted. This procedure was repeated for both the introduction of sample or for rinsing of the surface with buffer, with the corresponding sample in the external reservoir.

On the graphs, for clarity purposes, only the third or the fifth harmonic is shown (n=3 or 5). To be able to compare with the fundamental frequency and other overtones, the frequency was divided by 3 or 5 respectively.

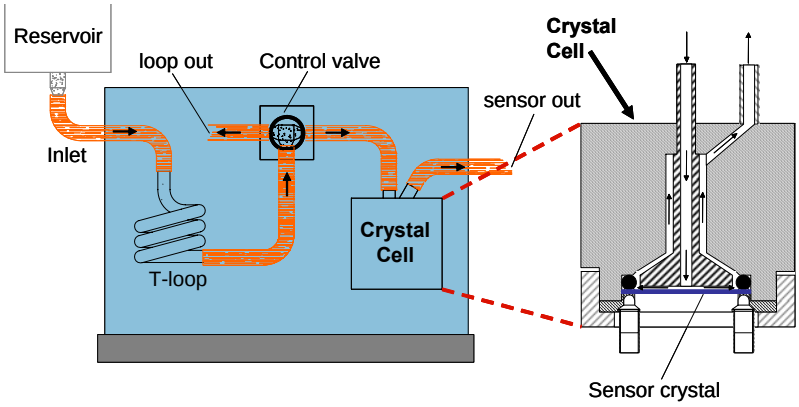

Figure 4.19.3: Schematic representation of the inner part of the measuring chamber, and the crystal cell in detail. www.q-sense.com

5. Appendix I

ABA triblock-copolymers containing hydrophobic middle blocks other than PDMS

5.1. Introduction, motivation and goals

As mentioned in the general introduction, block-copolymers can self-assemble into different morphologies depending on several variables, such as constitution of the blocks, block-length ratio, length of the polymer, temperature, solvent, etc.[34, 44] It is of interest to find other block-copolymers able to form vesicular structures, since diversity in the constituting blocks can offer a broader range of applications and a better or more specific performance. Therefore, the synthesis of ABA type triblock-copolymers with different blocks was investigated.

To narrow the infinite possibilities of such an approach, PMOXA was kept as the hydrophilic block. The reason for this is that there are not many hydrophilic blocks with better characteristics than PMOXA, and some with similar characteristics were already studied by other groups (e.g. Pluronics[32]).[33, 53, 269] Another reason for keeping the PMOXA as a constant parameter is that there are not many systems able to polymerize via cationic ring opening polymerization (see advantages of living polymerization systems in Section 3.1.1). Therefore, we tried to replace the PDMS middle-block by other hydrophobic blocks. Again, to keep the possibilities in a reasonable window, the synthesis was kept as similar as possible to the one for PMOXA-PDMS-PMOXA, since this synthetic pathway has not yet been tried with other middle blocks.

Two different middle blocks were chosen as candidates to replace PDMS, poly(propylene oxide) (PPO) and poly(tetrahydrofuran) (PTHF). PPO was chosen due to its characteristic temperature dependant solubility[269, 270] and low glass transition temperature (Tg= -78°C).[271] PTHF was chosen because its backbone is quite flexible (Tg= -86°C) and shows higher hydrophobicity than PPO. The use of hydrophobic middle blocks, with low glass transition temperatures (T_g) could provide systems that are in an "equilibrium" state in contrary to frozen structures.[54] Therefore, the importance of choosing polymers with low T_g.

In this appendix the synthesis of PMOXA-PPO-PMOXA and PMOXA-PTHF-PMOXA block-copolymers will be discussed. The formation of vesicular structures, the types of aggregates, size, and temperature dependence of these polymers was also investigated.

[32] Pluronics is a trade mark, it consists of ABA triblock-copolymers with the structure PEO-PPO-PEO.

5.2. Results and Discussion

5.2.1. Polymer synthesis: PMOXA-PPO-PMOXA and PMOXA-PTHF-PMOXA

Initially, the approach for the synthesis of PMOXA-PPO-PMOXA and PMOXA-PTHF-PMOXA was to use a similar synthetic pathway as for the already discussed PMOXA-PDMS-PMOXA[61] (see Section 3.1), that is, by activation of the telechelic starting block with triflates as depicted in the following scheme.

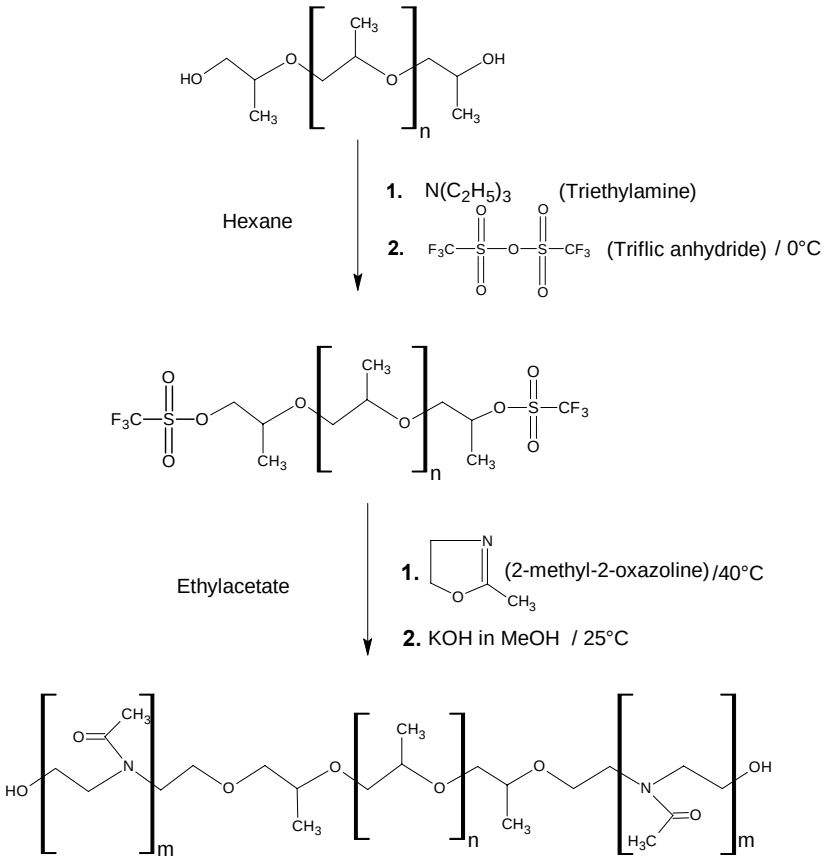

Scheme 5.2.1.1: Synthesis of PMOXA-PPO-PMOXA with TfSA activation.

Contrary to what reported by Kobayashi et al.[116] no copolymerization took place in the case of THF activated with triflates. Since this methodology was not always successful, another synthetic approach was adapted from the synthesis of PMOXA-PEO-PMOXA[272] and PMOXA-PPO-PMOXA.[273]

In this synthetic pathway, the alcohol end-groups of telechelic PPO and PTHF were activated via esterification with p-toluenesulfonic acid chloride (tosyl chloride). The sterically hindered base 2,6-lutidine acted both as solvent and base, to neutralize the protons produced in the activation reaction.[273] In a second step, the ring opening polymerization of 2-methyl-2-

oxazoline took place, with chloroform as solvent and a temperature of 50 °C, to ensure solubility of both chains throughout the reaction.

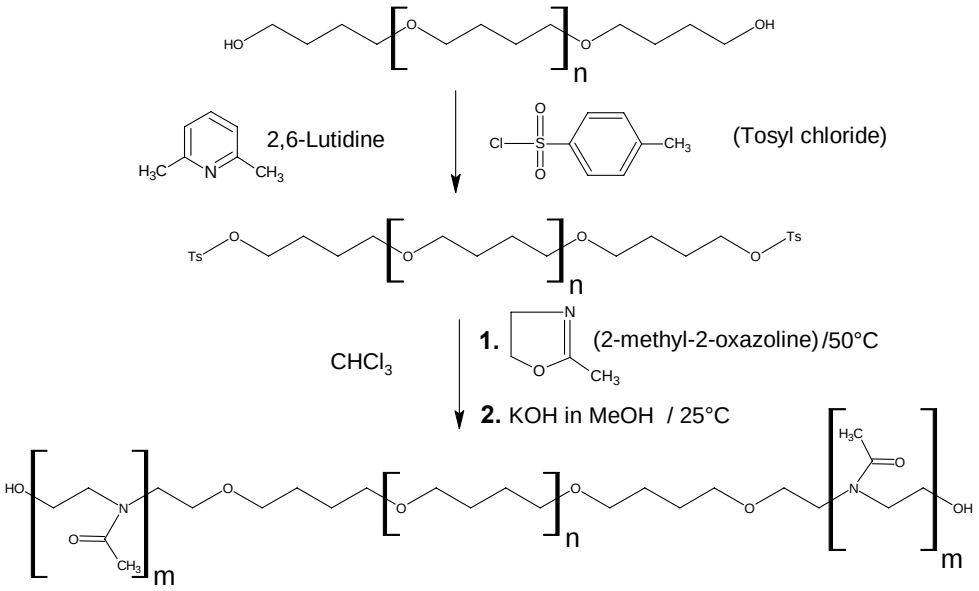

Scheme 5.2.1.2.: Synthesis of PMOXA-PTHF-PMOXA according to the new approach.

This approach proved successful for the synthesis of polymers with PTHF middle-blocks, but not for PPO. The esterification did not take place with PPO, as seen in ^{1}H-NMR. The main problem in the case of PTHF was the purification of the activated telechelic middle-block, since the crystallization, as suggested in the literature,[272, 273] did not work. Therefore, a purification step involving the extraction with diethylether and H_2SO_4 1 N was used. This purification step was complicated due to the formation of foams, which can be attributed to the slightly amphiphilic behavior of the activated middle-block. Moreover, the amounts of H_2SO_4 needed for the purification were too high.

In the case of the activation with TfSA the purification of the activated middle-blocks also posed difficulties. During the filtration over a cooled frit-glass there was always quite a loss of product that did not pass through the filter. Apparently, the highly viscous polymer blocked the pores of the filter quite fast. The use of TfSA as activator gave better results with PPO as middle-block, whereas for PTHF the activated middle-block was obtained only in one case. In the following tables, the results of both reaction pathways are summarized.

	Initial B block			Activation	Polymerization		Purification					
	Mw	n	mass	B-TfS mass	mass B-TfSA		total Mw	PMOXA	m	B block	Tot.mass	Yield
PPO	2700 g/mol	46	10 g	1.67 g	1.67 g		2870 g/mol	6 w%	1	94 w%	0.25 g	2.4%
PPO	3500 g/mol	60	10 g	8.12 g	8.12 g	(1)	6900 g/mol	49 w%	20	51 w%	0.9 g	49%
						(2)	4350 g/mol	20 w%	5	80 w%	4.1 g	
PTHF	2000 g/mol	28	5 g	1.50 g	1.50 g		22230 g/mol	91 w%	239	9 w%	0.15 g	0.3%

Table 5.2.1.1: Results for the synthesis of PMOXA-PTHF-PMOXA and PMOXA-PPO-PMOXA with triflate anhydride activation.

	Initial B block			Activation	Polymerization		Purification					
	Mw	n	mass	B-Ts mass	mass B-Ts		total Mw	PMOXA	m	B block	Tot.mass	Yield
PTHF	1000 g/mol	14	6 g	6.9 g	2.9 g	(1)	1680 g/mol	40 w%	4	60 w%	1 g	28%
					3.1 g	(2)	2870 g/mol	65 w%	11	35 w%	4.2 g	67%
PTHF	2900 g/mol	40	5 g	4.70 g	4.70 g		3630 g/mol	20 w%	4	80 w%	0.53 g	8%

Table 5.2.1.2.: Results for the synthesis of PMOXA-PTHF-PMOXA with tosylate activation.

Due to the limited capacity of the ultrafiltration cells, in many cases the raw block-copolymer had to be separated in two aliquots for purification. Interestingly, in some cases the obtained PMOXA chain length was different for the two separation batches. Although the reason is still not clear, one can imagine that if the polymerization rendered a broad molecular weight distribution, then during the solubilization a certain separation could take place. Another explanation would be the occurrence of depolymerization reactions.

5.2.2. Dynamic Light Scattering

As already discussed in Section 4.13, Dynamic light scattering allows the investigation of aggregates in solution. In order to investigate the formation of aggregates with the obtained block-copolymers, these were examined with DLS. For this, the standard method for production of vesicles was followed (see Section 4.8.1). The hydrodynamic radius R_H and the β parameter, which is an indicator of the polydispersity of the aggregates, are represented in Table 5.2.2.1.

$(A)_m$-$(B)_n$-$(A)_m$ Polymer		A-Block			B-Block			R_{Happ}	Polydisp
Code	Mn (g/mol)	Mn (g/mol)	w%	n	Mn (g/mol)	w%	n	(nm)	β
PMOXA-PPO-PMOXA	2870	85	6	1	2700	94	46	117	0.978
PMOXA-PPO-PMOXA (1)	6900	1700	49	20	3500	51	60	144	0.765
PMOXA-PPO-PMOXA (2)	4350	425	20	5	3500	80	60	134	0.952
PMOXA-PTHF-PMOXA (1)	1680	340	40	4	1000	60	14	109	0.956
PMOXA-PTHF-PMOXA (2)	2870	935	65	11	1000	35	14	95	0.943
PMOXA-PTHF-PMOXA	22230	10115	91	119	2000	9	28	112	0.965
PMOXA-PTHF-PMOXA	3630	365	20	4	2900	80	40	122	0.97

Table 5.2.2.1: DLS results of R_H (hydrodynamic radius) and β (polydispersity parameter) for PMOXA-PPO-PMOXA and PMOXA-PTHF-PMOXA block-copolymers.

In all cases the hydrodynamic radius was in the range of 90 to 150 nm, which are expected values for structures obtained by filtration through filters with pores of 200 nm diameter. Structures with larger diameters could not pass the pores, and are, therefore, excluded. The size distribution, given by the β parameter, indicates a rather low polydispersity. To confirm that these aggregates are indeed vesicular structures, more studies should be performed, for instance static light scattering, cryo-TEM, or freeze-fracture.

5.2.3. Temperature dependent swelling of the vesicles

In the case of block-copolymers containing PPO middle-blocks, it was also of interest to investigate the dependence of the vesicle size in relation to temperature changes. It is well known that the solubility of PPO in water changes in the range of 10-30 °C, and it was supposed that this could have an influence on the size of the aggregates. The trend in both the solubilities of PEO and PPO in water is a decrease in solubility with increasing temperature.[270]

With DLS measurements at 90° at different temperatures, the hydrodynamic radius of the aggregates was determined. The results are displayed in Graph 5.2.3.1.

As expected, the changes observed are dependant on heating and cooling of the samples. Another factor playing a role is the rate of heating and cooling, since in all polymeric systems kinetics are a dominant factor and sometimes the limiting one.

Unfortunately, it was not possible to obtain information on the concentration of the aggregates. Since both factors; concentration and size of the aggregates influence the scattered light, it was not possible to draw more precise conclusions about the temperature dependence of these aggregates. It is also worth mentioning that due to condensation of atmospheric vapors temperatures lower than 10 °C could not be used, moreover, due to evaporation of the toluene bath the highest temperature achievable with DLS could not surpass 30 °C.

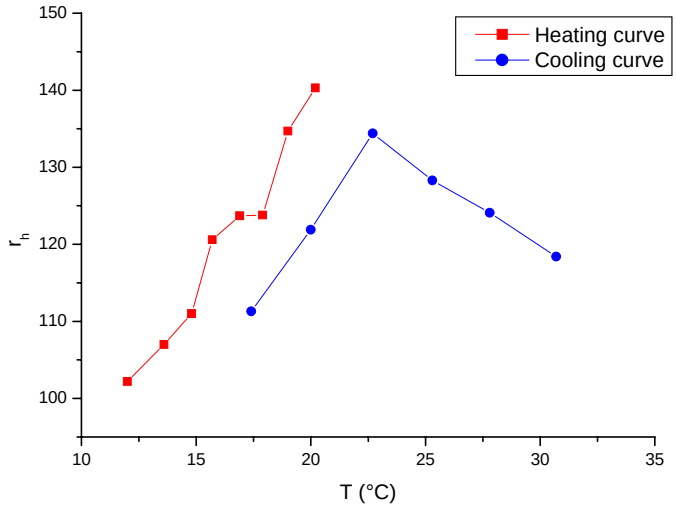

Graph 5.2.3.1: Temperature dependence of the vesicle size of PMOXA-PPO(3500)-PMOXA studied by DLS.

5.2.4. TEM studies

A complimentary technique to study the morphology characteristics of block-copolymers aggregates is TEM. For better comparison, the solutions used for DLS studies were investigated with TEM. It is important to notice that the type of polymer as well as impurities present in the

sample might influence the formation of vesicles or other aggregates. With PMOXA-PTHF-PMOXA M_n=22230 g/mol no vesicles could be observed, which can be attributed to the highly hydrophilic character (91 w% of PMOXA) of the polymer due to its long PMOXA side chains.

In contrast, PMOXA-$PPO_{(2700)}$-PMOXA formed small aggregates with a diameter of about 20 nm as well as rod-like aggregates. Whereas with PMOXA-$PPO_{(3500)}$-PMOXA polydisperse spheres with diameters between 25 and 100 nm were observed. This can be attributed to the coexistence of micelles and vesicles.[44] This last polymer was obtained with two different weight percentages of the hydrophilic block:one with 50 w% of the hydrophilic block, and the other with only 20 w% of the hydrophilic block. According to general considerations on the association and morphology of both lipids and block-copolymers it is expected that polymers with hydrophilic contents between 20-40 w% would tend to form vesicular structures.[31] Larger contents of hydrophilic blocks render the final copolymer too soluble, whereas lower contents usually show micellar aggregation behavior.

All block-copolymers containing PTHF as middle-block showed big aggregates in the range of 100 to 300 nm and spheres with a diameter of ca. 50 nm. It is not clear whether the irregular aggregates are a result of impurities or due to the characteristics of the middle block.

Table 5.2.4.1 shows the summarized results of the TEM investigation for the different polymers investigated.

$(A)_m$-$(B)_n$-$(A)_m$ Polymer		A-Block			B-Block			Radius TEM (nm)	Picture code
Code	Mn (g/mol)	Mn (g/mol)	w%	n	Mn (g/mol)	w%	n		
PMOXA-PPO-PMOXA	2870	85	6	1	2700	94	46	12-20	PPO a
PMOXA-PPO-PMOXA (1)	6900	1700	49	20	3500	51	60	30-90	PPO b
PMOXA-PPO-PMOXA (2)	4350	425	20	5	3500	80	60	25-115	PPO c
PMOXA-PTHF-PMOXA (1)	1680	340	40	4	1000	60	14	70-200	PTHF a
PMOXA-PTHF-PMOXA (2)	2870	935	65	11	1000	35	14	25-100	PTHF b
PMOXA-PTHF-PMOXA	22230	10115	91	119	2000	9	28	-	-
PMOXA-PTHF-PMOXA	3630	365	20	4	2900	80	40	20-400	PTHF c

Table 5.2.4.1: TEM observations for PMOXA-PPO-PMOXA and PMOXA-PTHF-PMOXA

The following pictures illustrate the aggregates found, for code information see Table 5.2.4.1

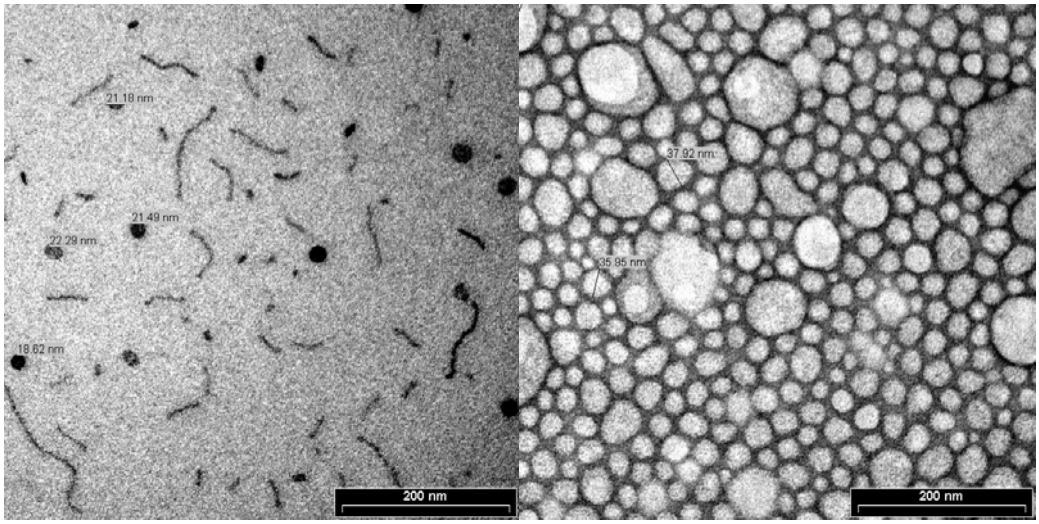

PPO a

PPO b

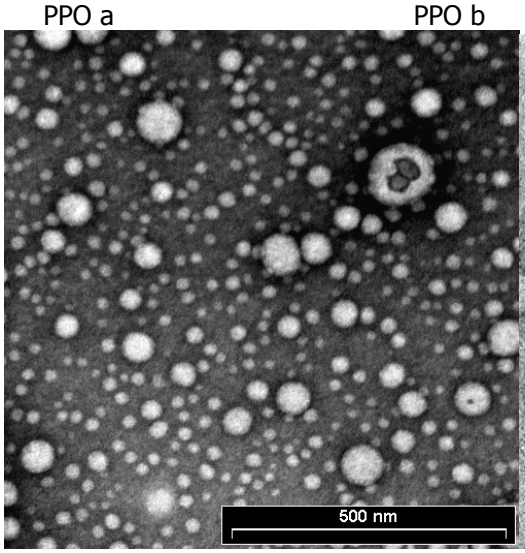

PPO c

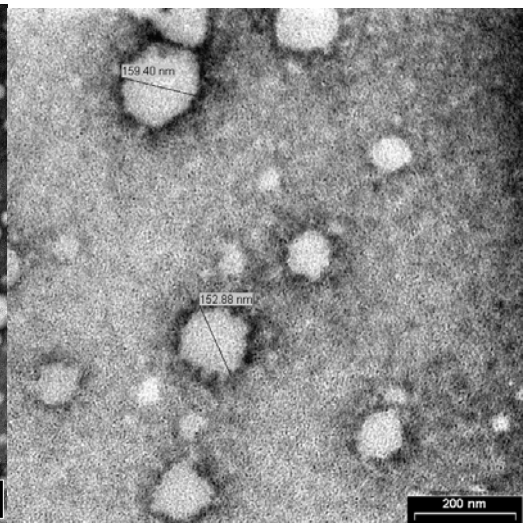

PTHF a

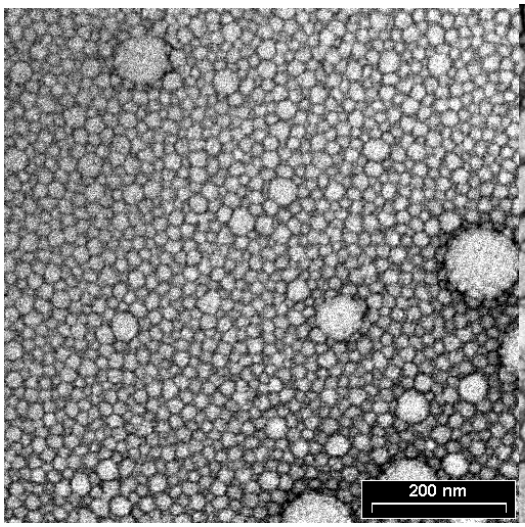

PTHF b

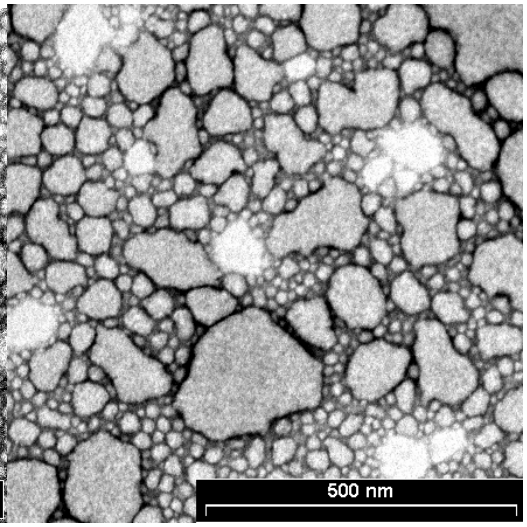

PTHF c

Pict. 5.2.4.1: TEM pictures of the polymers obtained, for code information see Table 5.2.4.1

Interestingly, the diameters observed with TEM, differ significantly from the radius obtained by DLS. It this still unclear what is the cause of this discrepancy, which was already determined with other systems and other operators. Some plausible causes of the smaller sizes obtained by TEM might be: **1)** the grids might promote the adsorption of smaller aggregates preferentially, **2)** the washing of the sample previous to staining might remove bigger aggregates, and **3)** drying on the grid might promote shrinking of the structures.

5.2.5. Langmuir-Films

The surface-active property of the block-copolymers was investigated as Langmuir-films. The spread monolayers for each polymer were compressed to obtain the corresponding surface pressure area isotherms. When possible, the collapse pressure Π_c and the limiting area A_0 for the solid phase were also determined.

When the solubility of the polymer is quite high the equilibrium between the floating monolayer and the solubilized polymer in the subphase can cause systematic errors in the determination of the surface-active properties.[154] Since the measurement of isotherms is highly dependent on temperature, they should be performed at constant temperature. Here, the measurements were done at room temperature, but without thermostatization.

Moreover, Langmuir troughs are mainly designed to be used with lipids, and since polymer molecules are large compared to lipid molecules, usually the available area to spread is quite small for polymers. This can be overcome by measuring the Π versus area isotherms with different amounts of spread aliquots. To get the complete curve the individual curves are superimposed. Small mismatching on the expansion of the isotherms can be accounted to solubility losses, as already discussed on the previous paragraph, which usually gives histeresis curves.

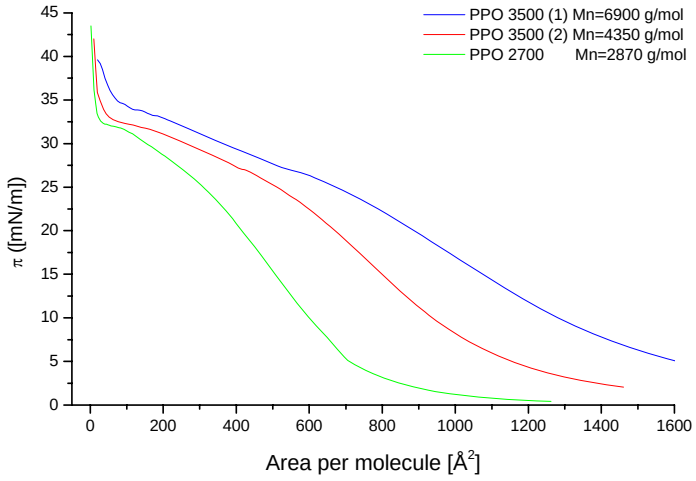

Graph 5.2.5.1: Surface pressure area per molecule isotherms of PMOXA-PPO-PMOXA polymers of different M_n

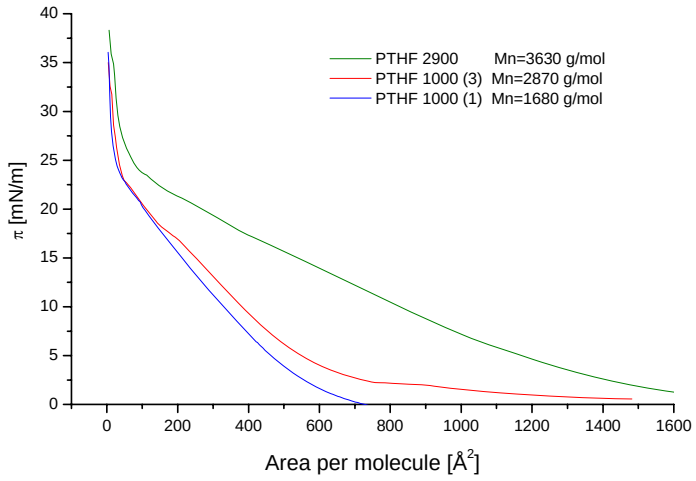

Graph 5.2.5.2: Surface pressure area per molecule isotherms of PMOXA-PTHF-PMOXA Polymers of different M_n

Interestingly, no collapse pressure was observed for either block-copolymers containing PPO or PTHF middle-blocks (Graph 5.2.5.1, Graph 5.2.5.2, and Graph 5.2.5.3). Most probably this is due to partial solubility of the block-copolymers in the subphase.

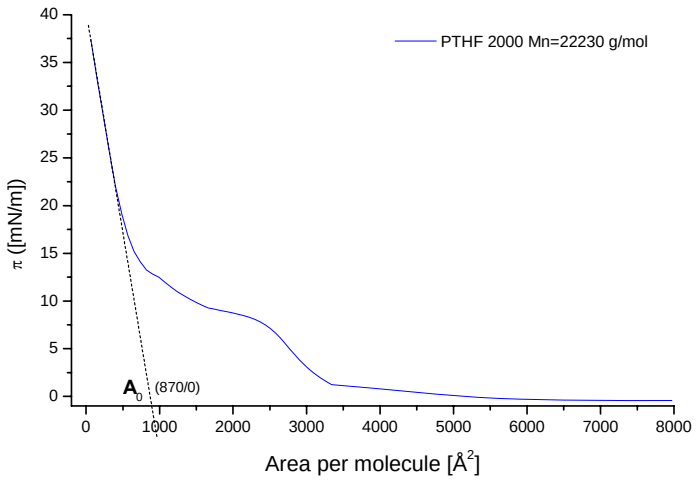

Graph 5.2.5.3: Isotherms of PMOXA-PTHF-PMOXA polymer, M_n = 22230 g/mol

The limiting area A_0, obtained by extrapolation of the slope of the isotherm curve in the condensed phase region, gives an indication of the area per molecule in a compressed condensed state. The results for the obtained A_0 for the polymers studied are summarized in the Table 5.2.1.1, along with the data of the polymers for better comparison.

$(A)_m$-$(B)_n$-$(A)_m$ Polymer		A-Block			B-Block			A_0 (Å^2)
Code	Mn (g/mol)	Mn (g/mol)	w %	n	Mn (g/mol)	w %	n	
PMOXA-PPO-PMOXA	2870	85	6	1	2700	94	46	58
PMOXA-PPO-PMOXA (1)	6900	1700	49	20	3500	51	60	365
PMOXA-PPO-PMOXA (2)	4350	425	20	5	3500	80	60	89
PMOXA-PTHF-PMOXA (1)	1680	340	40	4	1000	60	14	42
PMOXA-PTHF-PMOXA (2)	2870	935	65	11	1000	35	14	90
PMOXA-PTHF-PMOXA	22230	10115	91	119	2000	9	28	872
PMOXA-PTHF-PMOXA	3630	365	20	4	2900	80	40	114

Table 5.2.5.1: A_0 values for PMOXA-PPO-PMOXA and PMOXA-PTHF-PMOXA block-copolymers.

It is expected that monolayer-forming symmetric amphiphilic triblock-copolymers would undergo conformational changes upon compression of the film. For instance, in the gas-like and liquid-expanded regions, molecules are expected to be in a loose or coiled conformation (pan-cake and mushroom conformations), whereas in the condensed states molecules would adopt more compact structures,[154, 158] such an inverted stretched U turn (see Figure 4.7.6).

As already observed for PMOXA-PDMS-PMOXA block-copolymers, inspection of Table 5.2.5.1 indicates a relationship between the molecular weight of the hydrophilic block and the limiting area A_0. When plotting both variables as double logarithms, see Graph 5.2.5.4, a trend is evidenced. Linear regression fitting of the data renders a slope of approximately 0.6. The same scaling behavior was found for PMOXA-PDMS-PMOXA block-copolymers (see Section 3.1.3.4). In opposition to the expected behavior, with more stretched conformations in the condensed region for the hydrophilic block, the trend observed indicates coiled type conformations.

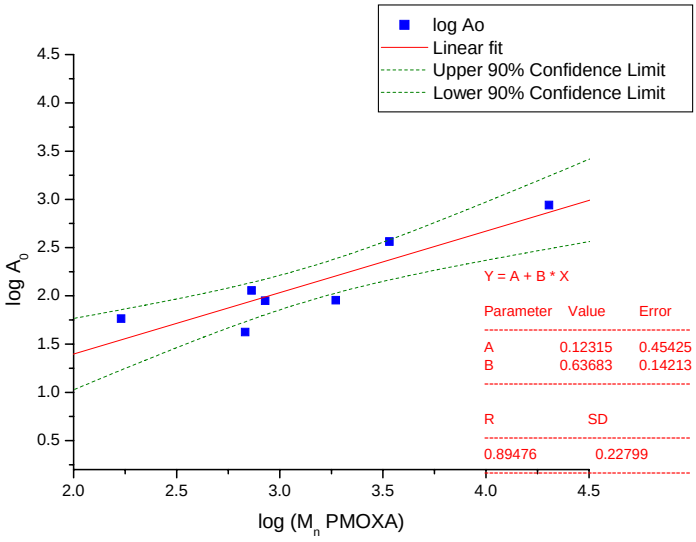

Graph 5.2.5.4: Double logarithm plot of M_n of PMOXA blocks versus A_0, for PMOXA-PPO-PMOXA and PMOXA-PTHF-PMOXA triblock-copolymers.

5.3. Conclusions

The synthesis of the triblock-copolymers PMOXA-PPO-PMOXA and PMOXA-PTHF-PMOXA was conducted obtaining moderate to low yields. With PPO activation with TfSA was more successful, whereas in the case of PTHF the activation with TsCl worked better.

Similar PMOXA-PPO-PMOXA polymers were investigated by Miyamoto et al.[273] These polymers had PMOXA contents higher than 75%, and therefore lie far beyond the expected 20-40 w% hydrophilic content necessary for the formation of vesicular structures.[31] The synthesis and surface activity of PMOXA-PTHF-PMOXA were already described by Kobayashi et al.[116] The results obtained here confirm the observations presented by these groups.

With the exception of one, all polymers gave aggregates or vesicular structures in aqueous solutions, which were investigated with TEM and DLS. To conclude about the real nature of the structures other studies should be performed such as SLS or cryo-TEM for instance. An unsolved problem is given by the discrepancy between the values obtained for the radius and diameter respectively by DLS and TEM.

Langmuir studies of the different block-copolymers rendered their characteristic surface pressure-area isotherms. The limiting area A_0 for the polymers studied showed a trend which is independent of the hydrophobic block and dependent of the hydrophilic one, indicating the existence of coiled conformations for the latter in the condensed phase.

Experimental part Appendix I

5.3.1. Materials

Poly(propylene oxide)[33] (CAS #: 25322-69-4) and poly(tetrahydrofuran)[34] (CAS #: 25190-06-1) were purchased from Aldrich, 2-methyl-2-oxazoline (CAS #: 1120-64-5), 2,6-lutidine (CAS #: 108-48-5) and all solvents were purchased from Fluka. All reactants and solvents were of the highest purity available. When not otherwise described the materials were used as purchased. Water was bi-distilled in an all-glass apparatus.

Scheme 5.3.1.1: Molecular formula of the polymers used as pre-polymers in this Appendix.

5.3.2. Polymer synthesis

5.3.2.1. Synthesis of PMOXA-PPO-PMOXA triblock-copolymers

PPO with TfSA-Activation

The synthesis of PMOXA-PPO-PMOXA with PPO of molecular weight 2700 is described as an example. The synthesis of the other PPO containing polymers followed the same procedure, for the amounts used refer to Table 5.3.2.1.1.

A total of 10.0 g of PPO (3.70 mM, M_n=2700 g/mol) was solubilized in 100 ml freshly distilled hexane and stirred during 18 h under reflux (Soxhlet). After cooling to room temperature, 1.19 ml (8.5 mM) of freshly distilled TEA was added and the reaction mixture was cooled to 0 °C. Subsequently, a mixture of 10 ml of hexane (fresh dist.) and 1.28 ml TfSA (7.8 mM) was added dropwise during 20 min and the reaction was left stirring at 0 °C for 1 h. The solvent and TEA were extracted by high vacuum, while the remaining highly viscous product was redissolved in cold hexane. This solution was filtered through a frit glass at 0 °C. Subsequently, the solvent was removed by high vacuum. A total of 1.67 g of brownish product was obtained, which was used as that for the next step of the polymerization.

The activated PPO (1.67 g (0.56 mM)) was dissolved in 100 ml freshly distilled ethyl acetate, and to this solution 1.7 g (19.97 mM) of fresh distilled 2-methyl-2-oxazoline were added. The reaction mixture was stirred for 64 h at 50 °C. After cooling to room temperature 2.24 ml of KOH (0.5 M in methanol) were added and the mixture stirred another 18 h. The sol-

[33] Poly(propylene oxide) is also known as poly(propylene glycol).
[34] Poly(tetrahydrofuran) is also known as poly(oxytetramethylene).

vent was eliminated with a rotavap, and the raw product was purified by ultrafiltration (water/ethanol 2:1, 3000 Da membrane, 3 bar). The purified product was dried by lyophilization.

		PMOXA-PPO-PMOXA	PMOXA-PPO-PMOXA (1)	PMOXA-PPO-PMOXA (2)
Activation	Mn B block	2700 g/mol	3500 g/mol	
	Initial mass B block	10 g	10 g	
	Initial moles B block	3.7 mmoles	2.86 mmoles	
	Solvent (Hexan)	100 ml	100 ml	
	TEA moles	8.5 mmoles	6.57 mmoles	
	TEA volume	1.19 ml	0.92 ml	
	TfSA moles	7.8 mmoles	6.06 mmoles	
	TfSA volume	1.28 ml	1.0 ml	
	Reaction time	80 min	80 min	
	Hexan redisolution	100 ml	100 ml	
	Activated B block (B-TfS) mass	1.67 g	8.12 g	
	Activated B block (B-TfS) moles	0.56 mmoles	2.17 mmoles	
	Yield activation step %	15%	75%	
Polymerization	Activated B block (B-TfS) mass	1.67 g	6.12 g	
	Activated B block (B-TfS) moles	0.56 mmoles	1.63 mmoles	
	Solvent (Ethylacetate)	100 ml	100 ml	
	Monomer moles	19.97 mmoles	71.67 mmoles	
	Monomer mass	1.7 g	6.1 g	
	Reaction time	64 h	64 h	
	Reaction temperature	50 °C	50 °C	
Termination	KOH in Methanol (0.5 M)	2.24 ml	8.6 ml	
	Reaction time	18 h	18 h	
Purification	Yield		Fraction 1 0.9 g	Fraction 2 4.1 g
Yield	Yield polymerization	0.25 g	5 g	
	Yield polymerization (percentual)	16%	66%	
	Total yield (activ. & polym.)	2%	49%	

Table 5.3.2.1.1: Reaction conditions for polymers with PPO middle block synthesized with TfSA.

	^{1}H-NMR ($CDCl_3$, 400MHz, δ in ppm)
PMOXA-PPO(2700)-PMOXA	1.0-1.2 (s, 138 H, C-CH_3), 2.0-2.2 (m, 6 H, $CH_3CON<$), 3.2-3.8 (m, 154 H, CHCH2O, O-CH2-CH2-N and >NCH2-CH2-N<)
PMOXA-PPO(3500)-PMOXA (1)	1.0-1.2 (s, 180 H, C-CH_3), 2.0-2.2 (m, 120 H, $CH_3CON<$), 3.2-3.8 (m, 348 H, CHCH2O, O-CH2-CH2-N and >NCH2-CH2-N<)
PMOXA-PPO(3500)-PMOXA (2)	1.0-1.2 (s, 180 H, C-CH_3), 2.0-2.2 (m, 30 H, $CH_3CON<$), 3.2-3.8 (m, 228 H, CHCH2O, O-CH2-CH2-N and >NCH2-CH2-N<)

Table 5.3.2.1.2: ^{1}H-NMR data of polymers with PPO middle block synthesized with TfSA activation.

	IR (KBr, [cm^{-1}])
PMOXA-PPO(2700)-PMOXA	3473 (O-H, st, broad), 2972 and 2885 (C-H, st), 1640 (C=O, st), 1109 (C-O-C, st, as)
PMOXA-PPO(3500)-PMOXA (1)	3475 (O-H, st, broad), 2970 and 2890 (C-H, st), 1645 (C=O, st), 1108 (C-O-C, st, as)
PMOXA-PPO(3500)-PMOXA (2)	3472 (O-H, st, broad), 2974 and 2866 (C-H, st), 1638 (C=O, st), 1110 (C-O-C, st, as)

Table 5.3.2.1.3.: IR data of polymers synthesized with TfSA activation and PPO middle block.

5.3.2.2. Synthesis of PMOXA-PTHF-PMOXA triblock-copolymers

PTHF 1000 with Ts-Cl Activation

The synthesis of PMOXA-PTHF-PMOXA with PTHF of molecular weight 1000 is described as an example. The synthesis of the other PTHF containing polymers, except for THF M_n=2000 g/mol followed the same procedure, for the amounts used refer to Table 5.3.2.2.1.

A total of 5.09 g of PTHF (5.09 mM, M_n=1000 g/mol) was dissolved in benzene and lyophilized to eliminate water. Once dried, the PTHF was dissolved in 30 ml of freshly distilled 2,6-lutidine and cooled to 0 °C. To this solution, 2.91 g p-toluenesulfonic acid chloride (15.30 mM) were added dropwise and this mixture was stirred during 4 h at 0 °C. This mixture was kept refrigerated at 4 °C for 5 days. An extraction with 6x100 ml 1 N H_2SO_4 and 150 ml diethylether was used as a purification step for the activated PTHF. The ether phase was filtered, dried over $MgSO_4$ and the solvent removed by rotavap. This yielded 6.93 g of a light yellow pasty intermediate. The intermediate was investigated by ^{1}H-NMR to assess the activation step. The spectrum of the tosylated intermediate showed two characteristic doublets at 7.7 ppm and 7.25 pm due to aromatic protons and a singlet at 2.5 ppm, due to the methyl protons of the tosyl group.[152] Moreover, the IR of the tosylated intermediate showed the disappearance of the band at 3430 cm^{-1} due to OH group and the appearance of bands at 750 cm^{-1} and 810 cm^{-1} ascribed to the tosyl aromatic groups and at 1170 cm^{-1} assigned to the sulphonate ester group.

For the polymerization, a total of 2.9 g of activated PTHF (2.51 mM) was dissolved in 20 ml of chloroform and stirred at 60 °C. To this solution, 1.69 ml (19.8 mM) of fresh distilled 2-methyl-2-oxazoline was added. The reaction mixture was stirred during 64 h at 50 °C. Once at room temperature, 10.20 ml of KOH (0.5 M in methanol) were added and the mixture was stirred for 6 h. The chloroform was removed by rotavap and the raw material was dissolved in 100 ml of a mixture of ethanol/H_2O 1:1. To remove the insoluble portion, the solubilized raw material was centrifuged 15 min at 3000 rpm and decanted. The soluble portion was purified by ultrafiltration (water/ethanol 3:1, 1000 Da membrane, 3 bar). The purified product was dried by lyophilization.

In the case of PTHF of molecular weight 1000 Da, the activated intermediate was separated in two portions, each of them was polymerized with 2-methyl-2-oxazoline with different initial ratio of initiator to monomer, in order to obtain different polymerization degrees of poly(methyloxazoline).

		PMOXA-PTHF-PMOXA(1)			PMOXA-PTHF-PMOXA
		(1)	(2)	(3)	
Activation	Mn B block	1000 g/mol			2900 g/mol
	Initial mass B block	5.09 g			5.02 g
	Initial moles B block	5.09 mmoles			1.73 mmoles
	Solvent (2,6-lutidine)	30 ml			30 ml
	TsCl moles	15.30 mmoles			5.19 mmoles
	TsCl mass	2.91 g			0.99 ml
	Reaction time	4 h			4 h
	Activated B block (B-Ts) mass	6.93 g			4.07 g
	Activated B block (B-Ts) moles	6.01mmoles			1.34 mmoles
	Yield activation step %	100%			77%
Polymerization	Activated B block (B-Ts) mass	2.9 g	3.1 g		4.07 g
	Activated B block (B-Ts) moles	2.51 mmoles	2.69 mmoles		1.34 mmoles
	Solvent (chloroform)	20 ml	20 ml		50 ml
	Monomer moles	19.8 mmoles	44.7 mmoles		45.7 mmoles
	Monomer volume	1.69 ml	3.8 ml		3.89 ml
	Reaction time	64 h	64 h		48 h
	Reaction temperature	50 °C	50 °C		50 °C
Termination	KOH in Methanol (0.5 M)	10.20 ml	10.20 ml		5.5 ml
	Reaction time	6 h	6 h		6 h
Purification	Yield		Fraction 1	Fraction 2	
			2.3 g	2.9 g	
Yield	Yield polymerization	1.0 g	5.2 g		0.53 g
	Yield polymerization (percentual)	28%	67%		11%
	Total yield (activ. & polym.)	28%	67%		8%

Table 5.3.2.2.1: Reaction conditions for PTHF middle block activated with tosyl chloride.

PTHF 2000 with TfSA Activation

The activation PTHF polymers with triflic anhydride (TfSA) was also examined, this was only successful in one case as it is described below.

A total of 5.0 g of PTHF (2.50 mM, M_n=2000 g/mol) was dissolved in 150 ml of hexane (fresh dist.) and for 18 h dried over reflux in a Soxhlet apparatus. At room temperature 0.801 ml (5.80 mM) of TEA (fresh dist.) were added. The reaction was then brought to 0 °C, and 0.866 ml of TfSA (5.30 mM) dissolved in 10 ml hexane (fresh dist.) were added dropwise over 45 min, and left reacting for another 60 min at 0 °C with constant stirring. After this the solvent and any unreacted TEA were eliminated by high vacuum. The remaining whitish product was dissolved in 100 ml hexane (fresh dist.) and subsequently filtered at 0 °C over a frit glass. The filtered solution was evaporated with high vacuum, obtaining 1.50 g of activated PTHF, which was used as such for the next step of the polymerization.

For the polymerization, 1.50 g (0.70 mM) of the intermediate were dissolved in 100 ml of freshly distilled ethyl acetate. To this solution 1.39 ml (16.3 mol) of freshly distilled monomer (2-methyl-2-oxazoline) was added and the reaction mixture was stirred for 64 h at 50 °C. Once at room temperature, 2.8 ml (1.40 mM) of KOH (0.5 M in methanol) was added and during 8 h stirred. The ethyl acetate was removed by rotavap and the remaining raw polymer was purified by ultrafiltration (water/ethanol 2:1, 3000 Da membrane, 3 bar). A white powder was obtained by lyophilization.

The ^{1}H-NMR and IR data of the polymers obtained with PTHF as middle block is presented in the tables below (Table 5.3.2.2.2 and Table 5.3.2.2.3).

	^{1}H-NMR ($CDCl_3$, 400MHz, δ in ppm)
PMOXA-PTHF(1000)-PMOXA (1)	1.5-1.8 (m, 56 H, C-CH_2-CH_2-C), 2.0-2.2 (m, 24 H, CH_3CON<), 3.2-3.6 (m, 96 H, >NCH_2-CH_2-N<, CH_2-O and O-CH_2-CH_2-N)
PMOXA-PTHF(1000)-PMOXA (2)	1.5-1.8 (m, 56 H, C-CH_2-CH_2-C), 2.0-2.2 (m, 66 H, CH_3CON<), 3.2-3.6 (m, 152 H, >NCH_2-CH_2-N< and CH_2-O and O-CH_2-CH_2-N)
PMOXA-PTHF(1000)-PMOXA (3)	1.5-1.8 (m, 56 H, C-CH_2-CH_2-C), 2.0-2.2 (m, 66 H, CH_3CON<), 3.2-3.6 (m, 152 H, >NCH_2-CH_2-N< and CH_2-O and O-CH_2-CH_2-N)
PMOXA-PTHF(2000)-PMOXA	1.5-1.8 (m, 112 H, C-CH_2-CH_2-C), 2.0-2.2 (m, 1428 H, CH_3CON<), 3.2-3.6 (m, 2024 H, >NCH_2-CH_2-N<, CH_2-O and O-CH_2-CH_2-N)
PMOXA-PTHF(2900)-PMOXA	1.5-1.8 (m, 160 H, C-CH_2-CH_2-C), 2.0-2.2 (m, 24 H, CH_3CON<), 3.2-3.6 (m, 200 H, >NCH_2-CH_2-N< and CH_2-O and O-CH_2-CH_2-N)

Table 5.3.2.2.2: ^{1}H-NMR data for the polymers with PTHF as middle block.

	IR (KBr, [cm^{-1}])
PMOXA-PTHF(1000)-PMOXA (1)	3480 (O-H, st, broad), 2946 and 2867 (C-H, st), 1642 (C=O, st), 1477, 1422,1246 and 1111 (C-O-C, st)
PMOXA-PTHF(1000)-PMOXA (2)	3454 (O-H, st, broad), 2942 and 2855 (C-H, st), 1630 (C=O, st), 1483, 1429,1244 and 1112 (C-O-C, st)
PMOXA-PTHF(1000)-PMOXA (3)	3487 (O-H, st, broad), 2946 and 2855 (C-H, st), 1632 (C=O, st), 1490, 1425,1258 and 1113 (C-O-C, st)
PMOXA-PTHF(2000)-PMOXA	no spectrum aquired
PMOXA-PTHF(2900)-PMOXA (1)	3440 (O-H, st, broad), 2942 and 2862 (C-H, st), 1631 (C=O, st), 1491, 1424, 1250 and 1117 (C-O-C, st)

Table 5.3.2.2.3: IR data for polymers with PTHF middle block synthesized with TfSA activation.

5.3.3. Dynamic Light Scattering

All vesicle dispersions were obtained as described for the standard solvent injection-extrusion method (Section 4.9.1). All samples were filtered with a 200 nm filters (Millex Durapore-PVDF, Millipore) and placed in cleaned cylindrical quartz cuvettes. The measurements were performed at 298 K, when not otherwise described, and at 90° degrees during 300 s. The analysis of the data was carried out with the program Win-ALV according to the Williams-Watts-method (see Section 4.13.1).

5.3.4. TEM studies

The same vesicle preparations as for DLS were used. Copper grids containing a layer of Collodion were glow-discharged previous to use. Subsequently, the vesicle suspension was deposited on the grid and left 10 s to adsorb, followed by negative staining with a 2% Uranyl acetate solution during 20 s.

5.3.5. Langmuir Films

After careful cleaning with chloroform the Langmuir trough was filled with bi-distilled water, previously filtered through filters of 450 nm pore diameter. The surface was cleaned by closing the movable barriers and by subsequently removing with a water pump all surface active material that could create a surface pressure between the two barriers.[274]

Once a stable subphase was proved the spreading of the desired sample was conducted. In short, solutions of the different block-copolymers in chloroform were prepared with concentrations of 1mg/ml. These were spread with the aid of a Hamilton microsyringe over the sub-phase. Different aliquots were spread, in order to obtain a total spread volume of 10, 20, 40, 80, 100, 100 200, 400, 600 and 800 μl. After an evaporation time of 15 min, the monolayes were compressed. For each aliquot addition a compression and expansion cycle was performed while measuring the isotherm. For the compression and expansion a constant barrier speed of 100 cm^2/min was used. For more details about Langmuir films see Section 4.7.

6. Appendix II

Nanotraps for substance recovery

6.1. Introduction, motivation and goals

In this section another application for the nanocontainers described in the main body of this thesis is presented. Their ability to encapsulate substrates has made polymeric nanocontainers an attracting system for shielding substances from unfavorable environmental conditions. Here, the possibility to use polymeric vesicles as trapping devices was investigated. In contrast to the previously described encapsulation of substances,[59] in this new approach, the encapsulation occurs after preparation of the nanocontainers. One interesting application would be in the area of substance recovery, i.e. to concentrate and recuperate a given molecule from a complex mixture. This could be of use for instance in water treatment plants. The nanotraps would act as vehicles by which a certain molecule could be separated from a mixture and easily recovered from it. The straightforward advantages for such recovery procedures are easier purification steps and the possibility to only retrieve one substance from a complex matrix.

As previously demonstrated,[8, 59, 275] combining artificial polymer nanostructures with a variety of biological systems broadens their applications spectrum. The low permeability of the polymer membrane can be overcome by insertion of channel proteins in the capsule's shell.[276] Therefore, hybrid materials with enhanced properties could be obtained by combining the high stability rendered by polymeric membranes and the high specificity of channel proteins.

The insertion of channel proteins thus provides a means to connect the interior of nanocontainers with the external bulk solution.[277] Usually, Nature has solved transport problems across membranes in a very elegant manner, via different approaches, from quite simple passive diffusion, to more advanced active transport involving a more complex machinery. For instance, porins render size-selective exclusion, allowing thus the passage of solutes below their cut-off across a membrane. Within this family, however, some members also display specific transport of solutes, such as LamB.[275, 278, 279] The more selective the transport, the better the sorting of molecules according to the selecting criteria can take place. This can be of interest in the removal of a specific substance from a mixture.

In Appendix I, the tailoring of the underlying polymers constituting the vesicles was investigated by changing the middle block of the constituting unimers, as one way to optimize their performance and characteristics. In this Appendix, we have used a genetically modified membrane protein of the family of the outer membrane proteins, so-called porins. The wild-

type FhuA, which in nature is involved in the iron uptake in cells, is an specific channel protein.[280-282]

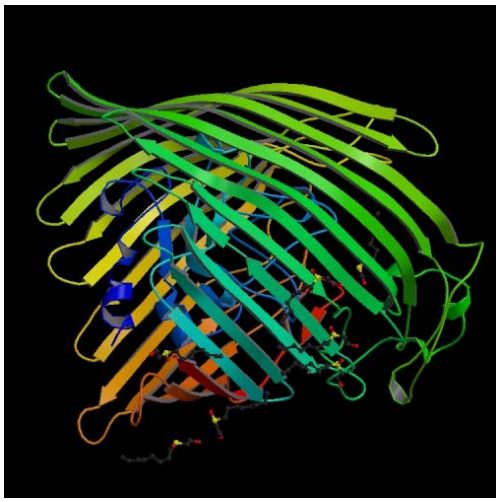

Pic. 6.1.1: Ribbon structure of the FhuA channel wild type (Protein code: 1B3), taken from http://www.rcsb.org/pdb/

This wild type can be converted into a non-specific channel by deleting the "cork" in the β-barrel channel, giving thus a mutant called FhuAΔ5-160.[280, 281] The genetically engineered resulting pore protein is non-specific and allows passive diffusion of substrates.[283, 284] Compared to other porins, deleting the loop in the channel of the FhuA yields a much larger pore, thus leading to a higher cut-off for the permeability of solutes.

As an example of this application, here we present the post-encapsulation of a fluorescent dye. By means of a pre-encapsulated polyelectrolyte and the incorporation of a pore-forming membrane-protein in the shell of the nanocontainers, molecules of the opposite charge sign of the polyelectrolyte which are small enough to pass through the channel protein can be entrapped in the nanocontainers (Figure 6.1.1).

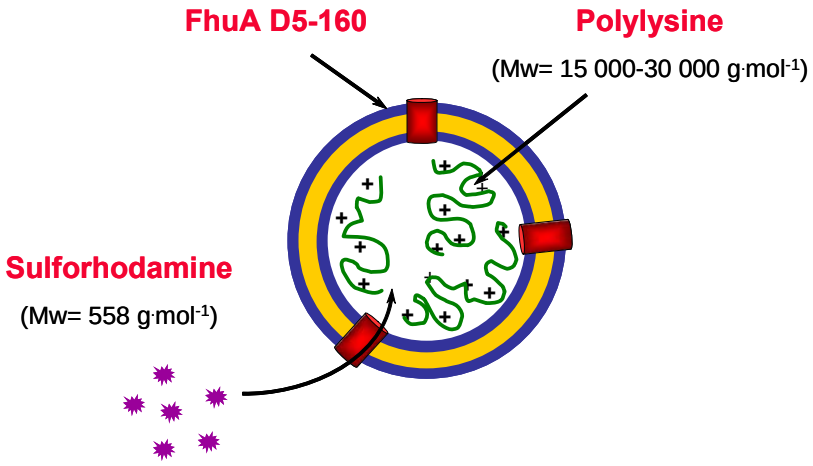

Figure 6.1.1: Schematic representation of the concept of entrapment within a nanocontainer.

6.2. Results and Discussions

Both the standard injection method and the direct dissolution/Biobeads method[163] (see Sections 6.4.4, 4.9.1 and 4.9.2) were applied to reconstitute FhuAΔ5-160 in triblock-copolymer vesicles. The incorporation of FhuA in the artificial polymer membrane was investigated using two different techniques. By means of a Wilhemy plate, as described in the following section, measuring the increase of surface pressure as the protein inserts in the polymer monolayer, incorporation of the channel protein can be demonstrated. In a second approach, by means of an enzymatic test the functionality of the protein inserted in the membrane was assessed[35].

6.2.1. Protein insertion in polymer Langmuir films

Protein-lipid interactions can be investigated with monolayer techniques. A change in the surface pressure resulting from the injection of a protein into the monolayer is indicative of an interaction between the monolayer and the protein. Typically, if a protein in solution can penetrate into the monolayer at the air-water interface, the molecules in the monolayer would be laterally compressed and the surface pressure would therefore increase.[237]

It is known that under appropriate conditions all proteins will interact with phospholipid monolayers.[285] However, condensed phospholipid monolayers usually do not mix homogeneously with proteins giving rise to poor insertion or islands. Most often homogeneous mixed-films are found when the phospholipid forms an expanded film at the air water interface. However, to be useful as a model of behaviour in a natural membrane, the monolayer must be compared to the bilayer at a surface pressure at which it most closely resembles the bilayer state.[285]

Because of the above mentioned considerations, and because amphiphilic block-copolymers behave analogously to their low molecular weight counterparts, insertion of the channel protein FhuAΔ5-160 in the amphiphilic polymeric membrane was investigated by Langmuir isotherms. To monitor the insertion of channel proteins, it is necessary to work at relative high surface pressures (~30 mN/m), i.e. with more condensed monolayers where the system can resemble the situation present in vesicular membranes.[286-288] Therefore, for insertion experiments a surface pressure of approximately 25 mN/m was chosen.

Initially, the isotherm for the block-copolymer monolayer was recorded. Then, the polymer monolayer was compressed to a final surface pressure of 25 mN/m. At this surface pressure, the protein was injected in the subphase and the increase in surface pressure was recorded versus time. A considerable increase of surface pressure was detected (data not shown). Since the protein stock solution contained detergent to stabilize it, a control with this

[35] Results not shown, see Alexandra Graff's PhD thesis (University of Basel, 2004).

detergent was done in order to account for the influence it might have on the surface pressure. For this the experiment was repeated injecting only octyl-POE in the subphase. The addition of octyl-POE did not increase the surface pressure, and therefore, the increase observed for the protein aliquot can be ascribed to interaction between the protein and the polymer layer, which probably results from insertion of the protein in the polymer membrane.

Conventional troughs with rectangular geometry are usually not the most adequate for membrane insertion experiments. Due to the large volume of the subphase, high amount of protein are needed to produce insertion in this type of trough. Therefore, in order to reduce the sample consumption for each measurement, a trough with different dimensions and geometry was used as suggested by Han et al.[237] The trough consisted on a cylindrical piece with a side orifice to allow protein injection in the subphase without disruption of the monolayer[237] (see also Section 4.7 and Figure 4.7.8).

For the FhuA insertion experiments with the cylindrical trough, an aliquot of the polymer was spread in order to obtain a final surface pressure of about 25 nm/m, and the surface pressure was recorded until stability was achieved. Then, an aliquot of the protein was injected into the subphase, and almost an instantaneous increase in surface pressure was observed, followed by a continuous but slow increase in surface pressure (Graph 6.2.1.1, blue curve).

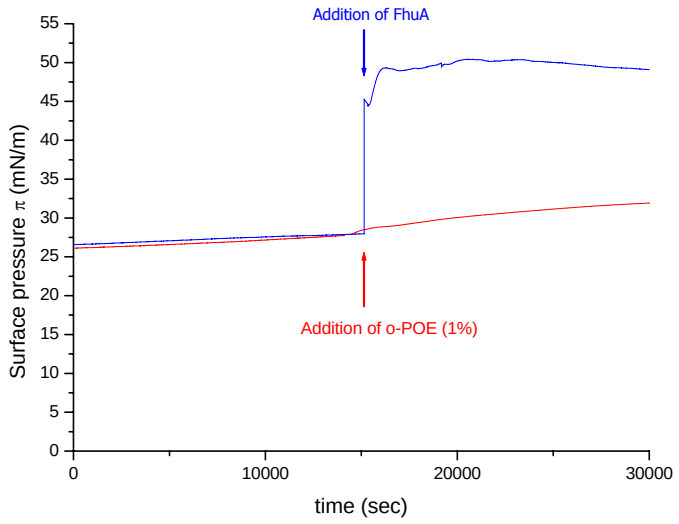

Graph 6.2.1.1: Surface pressure versus time diagrams for the insertion experiments with FhuAΔ5-160 (blue) and the control with o-POE (1%) (red). Arrows indicate the time when the addition of the substance took place.

A control consisting of a 1% octyl-POE solution was injected in the subphase of an already spread monolayer of polymer (Graph 6.2.1.1, red curve). In this case only a small in-

crease of surface pressure was observed. With this it can be concluded that FhuAΔ5-160 inserts successfully in the polymer membrane.

Interestingly, in the case of the monolayer obtained by spreading the polymer, the initial surface pressure was as expected (approximately 25 mN/m), from the calculations for the amount spread and the size of the trough. However, the surface pressure kept increasing very slowly until reaching a value of 33 mN/m. This was observed repeatedly, and can be ascribed to the characteristic slow dynamics of the polymers[46] forming the monolayer. This is usually not observed while measuring isotherms as the initial pressure is much lower in those cases, and the polymer monolayer is initially in a "gaseous" state. Moreover, while measuring isotherms, the polymer can undergo conformational changes due to the closing of the barrier, whereas in a trough with no barriers the polymer is left to achieve its equilibrium conformation, therefore, taking longer times. Another explanation for the increase of surface pressure on long experiments is due to evaporation of the subphase.

6.2.2. Entrapment of a dye molecule into pre-formed nanocontainers

In order to post-entrap a fluorescent dye into polymer nanocontainers, polymer vesicles containing encapsulated polyelectrolyte (poly(lysine)) and incorporated channel proteins (FhuAΔ5-160) were prepared. Two methods of vesicle preparation (see Section 6.4.4) were used in order to compare the efficiency of membrane proteins insertion into the polymer membrane, and compare entrapment capacities. Additionally, the following controls were performed (see Graph 6.2.2.1); vesicles with FhuA but no polyelectrolyte, vesicles without FhuA and with polyelectrolyte, and vesicles devoid of both channel protein and polyelectrolyte. In all cases, removal of non-encapsulated polylysine and non-inserted protein was achieved by SEC on a Sepharose 4B column, even controls prepared without encapsulated polyelectrolyte were also cleaned in this way to obtain the same final dilution for proper comparison.

All samples were then incubated with a sulforhodamine solution. If sulforhodamine (Mr=558.66 g/mol) is present in the bulk of the solution, it can freely diffuse through the pores of the membrane proteins, to enter in contact with the pre-encapsulated polyelectrolyte within the vesicles (see Figure 6.1.1). Since sulforhodamine is negatively charged, it can form a complex with the pre-encapsulated poly(lysine), and therefore would remain in the interior of the nanotraps. If no polyelectrolyte is present in the system, sulforhodamine is able to diffuse in and out of the nanocontainers, giving no net entrapment.

For the "direct dispersion/detergent and Biobeads" preparation method two procedures for the removal of non-entrapped dye were tested, namely chromatography and ultracentrifugation through filter membranes (Centricon Amicon YM, 30000 cut off, Millipore) in order to

compare purification efficiency. For the solvent-extrusion method only ultracentrifugation was used to remove non-entrapped sulforhodamine. In order to assess the entrapment of the fluorescence dye, the fluorescence spetra of the samples were recorded. The results are depicted in Graph 6.2.2.1 and Graph 6.2.2.2.

From the fluorescence results presented in Graph 6.2.2.1, it is clear that entrapment of sulforhodamine occurs only in the case of proteo-vesicles (blue curve), that is, nanocontainers with channel proteins in their membranes. This is corroborated by the controls performed. The small fluorescence observed in the case of the control consisting of nanocontainers with pore proteins but no polyelectrolyte (orange curve) can be explained by diffusion of the dye into the nanocontainers due to concentration gradients. Once the external sulforhodamine is removed, after a certain time the dye would diffuse to the bulk of the solution, a situation that is not encountered in the presence of encapsulated polyelectrolyte. Here, the fluorescence spectra were obtained shortly after removal of non-entrapped dye. Another explanation for the residual fluorescence in the control can be attributed to adsorbed fluorescent dye onto the surface of the nanocontainers. This is not surprising since most fluorescent dyes also show amphiphilicity.

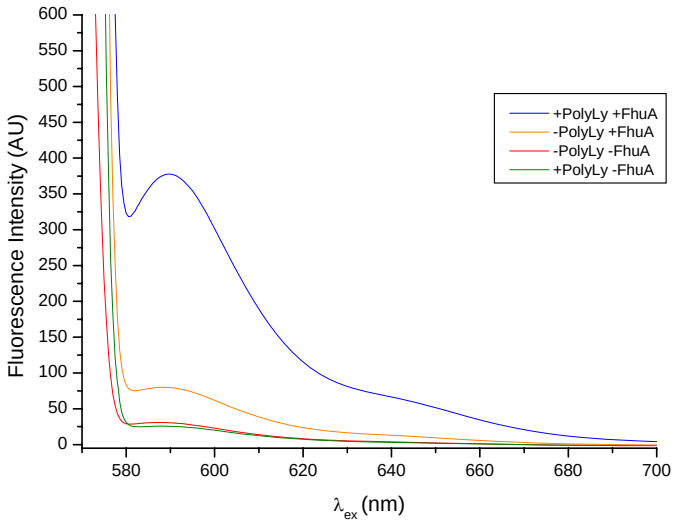

Graph 6.2.2.1: Fluorescence spectra of sulforhodamine post-encapsulation in NCs prepared by direct dispersion (see Section 4.8). Removal of non-entrapped sulforhodamine was achieved by ultracentrifugation (see Section 6.4.6). Results for entrapment vesicles containing poly(lysine) and FhuAΔ5-160 are shown in blue. The controls correspond to: vesicles with FhuA but no polylysine (orange), vesicles without FhuA and with polylysine (green), and vesicles devoid of both channel protein and polyelectrolyte (red).

Graph 6.2.2.2 presents the fluorescent spectra of vesicles with encapsulated polyelectrolyte and incorporated channel proteins obtained by different preparation methods and different dye removal procedures. Contrary to what expected from the sizes of the constituting vesicles in each method, the standard method gave higher fluorescence intensities than the direct

dispersion method, which can be interpreted as higher entrapment of the dye. This can be ascribed to a higher number of channel proteins inserted resulting in a more facilitated diffusion, due to more pores present in the system. Nevertheless, this supposition has to be proved for instance by quantifying the amount of protein in the resulting proteo-vesicles. This would require disruption of the vesicles to free the membrane proteins, resulting in a complicated experiment due to the high stability of the polymer vesicles upon detergent disruption.

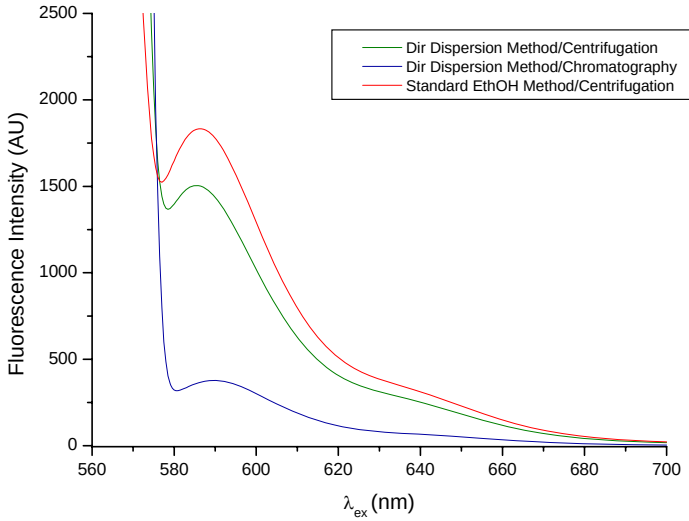

Graph 6.2.2.2: Fluorescence spectra of sulforhodamine post-encapsulation in NCs containing poly(lysine) and channel proteins (FhuAΔ5-160). Comparison of different NC preparation methods and purification of non-entrapped sulforhodamine: direct dispersion/Biobeads method with removal of non-entrapped sulforhodamine by ultracentrifugation (in green), direct dispersion/Biobeads method with removal of non-entrapped sulforhodamine by chromatography (in blue), and standard proteo-vesicle method with removal of non-entrapped sulforhodamine by ultracentrifugation (in red).

Comparison of vesicles with all parameters equal except for the procedure to remove non-entrapped dye (Graph 6.2.2.2, curves green and blue), shows the expected behavior. Chromatography purified nanocontainers show about a one-third emission than the ones purified by ultracentrifugation. This is not surprising considering the fact that with the column's length used, usually a one-third dilution of the sample is obtained.

6.3. Conclusions

Injection of FhuAΔ5-160 under an ABA triblock-copolymer monolayer gave rise to an increase in surface pressure which can be taken as indication of possible insertion in the artificial block-copolymer membrane. Since this type of proteins tend to show surface activity the surface pressure of the monolayer was kept higher than 25 mN/m to avoid unspecific effects.[289]

Insertion of the protein in the artificial polymer membrane was assessed by entrapment of a small solute diffusing through the pores of the channel protein. Furthermore, the system used demonstrates the feasibility of post-encapsulation of molecules into the block-copolymer nanocontainers. This is of interest in applications such as recovery from complex mixtures.

The introduction of channel proteins in artificial membranes allows the preparation of systems with a high degree of tunability. On one hand one can tune for example the properties of the underlying polymer blocks by choosing other chemical structures in order to obtain higher stability or responsiveness. On the other hand, the membrane proteins can also be tuned by molecular engineering, giving thus channels with desired characteristics, such as larger and non-specific pores, resistance to higher temperature or extreme conditions, or simple render specific recognition by introducing tags. This flexibility would allow a larger number of applications with the right combination of block-copolymer and pore forming protein.

Compared to membrane proteins with lower size exclusion, incorporation of FhuAΔ5-160 into block-copolymer membranes opens broader applications. In vivo, FhuA is known for its ability to transport phage DNA.[282] Therefore, the larger engineered channels could be used for DNA entrapment into the NCs. For example, during DNA sequence amplification a process called polymerase chain reaction (PCR), oligonucleotide sequences, so-called primers, are required to initiate the amplification process. The size exclusion limit of FhuAΔ5-160 would allow the discrimination of DNA sequences from the oligonucleotide primers. Only DNA-segments below a critical upper-size limit, determined by the cut-off of the channel protein used, would be able to pass across the pores and thus can be entrapped into such NCs. To retain the DNA segments or oligonucleotides inside the vesicles, one could use the simple principle described in this Appendix. The negatively charged oligonucleotide could be complexed in a similar manner as sulforhodamine, by the formation of electrostatic complexes with poly(lysine).

6.4. Experimental part Appendix II

6.4.1. Materials

For these studies the ABA triblock-copolymer used was S131 (M_n=8660 Da; $PDMS_m$=72, $PMOXA_n$=18), for more details about synthesis and characterization see Section 3.1. The expressing strain of genetically modified FhuAΔ5-160 (M_r=78000 Da) was a gift from U. Schwaneberg, Bremen, and was kindly expressed and purified by Dr. A. Graff. Poly(L-lysine) (M_w 15000 to 30000 Da) was purchased from Sigma. Extrusion filters (Millex Durapore-PVDF, pores 0.45 μm, 0.22 μm), and ultracentrifugation devices (Centricon Amicon YM cut-off 30000 Da) were from Millipore. Biobeads SM2 were from BioRad and were cleaned two times with methanol and then washed several times with water prior to use[224]. Sepharose 4B was from Sigma-Aldrich.

6.4.2. FhuAΔ5-160 expression and purification

The expression and purification steps were performed according to the procedure described for FhuA wild type.[290] The purification steps were followed and checked using a 10% SDS Page. The protein concentration was estimated as 0.6 mg/ml and stored in 1% octyl-POE (Alexis Company). This was further concentrated to obtain a 2.4 mg/ml solution with Centricon tubes (Centricon Amicon YM, Millipore, cut-off 30000 Da).

6.4.3. Protein insertion in polymer monolayers

The Π-A isotherms and Π(t) adsorption/insertion kinetics were recorded with a computer-interfaced film balance (Langmuir Film Balance equipped with a Wilhelmy balance, KSV).

Rectangular trough experiments

A 20 μl aliquot of polymer (S131, 2.2 mg/ml) in Cl_3CH was spread onto a PBS buffer subphase. Isotherm cycles were registered at a barrier speed of 15 mm/min. Then the barriers were compressed to a final surface pressure of 25 mN/m and 100 μl of protein (0.6 mg/ml) was injected into the subphase. A control experiment was performed with 100 μl of detergent (1% o-POE in PBS) injected into the subphase under a polymer monolayer at 25 mN/m.

Cylindrical trough experiments

A homemade circular Teflon trough of 6 cm diameter (total surface area 2826 mm^2) with a special orifice for subsequent protein addition was used (see Figure 4.7.8).

The trough was thoroughly cleaned with a tissue soaked in chloroform, the same procedure was followed with ethanol, and then the trough was left drying a few minutes. Subsequently, the through was filled with filtered buffer (Millex Durapore-PVDF 0.45 μm, Millipore).

The subphase was left to equilibrate, while the surface pressure was recorded. The surface of the trough was cleaned by aspiration until a stable surface pressure was obtained.

A 10 μl aliquot of polymer (S131, 1.033 mg/ml in Cl_3CH) was spread on a cleaned subphase (PBS) in the cylindrical trough. This volume of polymer was calculated in order to obtain a final surface pressure of about 25 mN/m (corresponding to a molecular area of 400 $Å^2$/molec), for the insertion of the protein. After 20 min allowance for the evaporation of the solvent the surface pressure was recorded versus time until a constant value was observed. Once a stable surface pressure was achieved (approx. 7 h) 50 μl of the channel protein (0.6 mg/ml FhuAΔ5-160 in 1% o-POE in PBS) was injected into the subphase through the lateral orifice of the trough. To account for the contribution of the detergent present in the FhuA sample, a 50 μl aliquot of o-POE (1%) was injected in the same fashion under a monolayer of polymer and the surface pressure was recorded.

6.4.4. Vesicle preparation

To encapsulate a polyelectrolyte, a 0.5 mg/ml poly(lysine) solution was used to prepare polymer vesicles by either the standard method (injection-extrusion) or the new preparation method (direct dispersion), for a detailed description see Sections 4.8 and 4.9. For these experiments the buffer of choice was Tris/HCl (10 mM). Control experiments in which just buffer solution was encapsulated in the void volume of the vesicles were also performed.

FhuAΔ5-160 reconstitution into vesicles obtained by standard method (solvent injection-extrusion method or ethanol method): The reconstitution of FhuA was performed following a slight change of the procedure described in Section 4.9.1. Here, the protein (20 μl of 2.4 mg/ml stock solution or 100 μl of a 0.6 mg/l stock solution) was not dissolved directly in the polymer-ethanol mixture but injected simultaneously with the polymer-ethanol solution into the buffer.

FhuAΔ5-160 reconstitution into vesicles obtained by direct dispersion method (direct dispersion/detergent and Biobeads method): The detailed procedure is already described in Section 4.9.2, the amount of protein used was either 20 μl of 2.4 mg/ml stock solution or 100 μl of a 0.6 mg/l stock solution.

6.4.5. Preparative Chromatography

Removal of non-encapsulated polylysine and non-inserted protein was achieved by SEC separation on a Sepharose 4B column (1x30 cm). For details see Section 4.10.

6.4.6. Entrapment of sulforhodamine, elimination with centrifugation

To 2 ml of a previously cleaned sample of vesicles, a 5 μl aliquot of sulforhodamine (8 mM) solution in Tris/HCl (10 mM) was added and the mixture was left to incubate under

stirring overnight. Removal of non-entrapped sulforhodamine was performed by centrifugation on tubes (Centricon Amicon YM, Millipore) of 30000 molecular weight cut-off. A series of centrifugation cycles (1800 rpm) of 20 min to 1 h were performed until all samples had been washed with an equal volume of buffer (9 ml of Tris/HCl). In order to obtain the same final concentration, all samples were taken to a final volume of 2 ml with buffer.

6.4.7. Entrapment of sulforhodamine, elimination with chromatography

A 1 ml aliquot of vesicle dispersion (direct dispersion/detergent and Biobeads method) was incubated with 10 μl of sulforhodamine (8 mM) solution in buffer with stirring for 24 h. Subsequently, sulforhodamine was removed chromatographically with a Sepharose 4B column (1x28 cm).

6.4.8. Steady state fluorescent measurements

The fluorescence spectra of the samples was recorded in a Jasco FP 773 instrument, with a λ_{ex} = 565 nm (10 nm bandpass) and λ_{em} = 570-700 nm (10 nm bandpass).

7. Summary

Self-assembling amphiphilic ABA triblock-copolymers, forming vesicular structures in aqueous solutions were the core material used in this thesis. The interest in amphiphilic block-copolymers resides basically in their improved characteristics in comparison to low molecular weight amphiphiles, such as higher mechanical stability. Moreover, the polymer brush coating of liposome-polymer hybrids (Stealth liposomes) is known to be effective on reducing uptake by reticuloendothelial system (RES). This led to the idea of avoiding the use of lipids at all in these structures and work with self-assembling polymers. This has been done in our group through the use of an ABA amphiphilic triblock-copolymer, consisting of poly(2-methyl-2-oxazoline)-b-poly(dimethylsiloxane)-b-poly(2-methyl-2-oxazoline) (PMOXA-PDMS-PMOXA), which surface contains a hydrophilic polymer with similar characteristics to poly(ethylene glycol). These two advantages of amphiphilic polymer vesicles, i.e. higher stability and the ability to avoid reticuloendothelial uptake led to two main research interests which were addressed in this work: the use of nanocarriers based on synthetic self-assembling polymers as active targeting drug delivery systems and the immobilization of vesicles on surfaces.

Both research topics shared the need to attach the polymer vesicles via docking sites. To address this a series of ABA triblock-copolymers were synthesized and functionalized to promote their interaction either with other molecules or with surfaces. The synthesis of the polymers was carried out via cationic ring opening polymerization of 2-methyl-2-oxazoline departing from a telechelic poly(dimethylsiloxane). Langmuir films proved the surface activity of the amphiphilic polymers obtained. From the functionalization point of view, biotinylated block-copolymers proved to be the most versatile modification, through the use of the wide spread biotin-streptavidin specific interaction. Vesicles were prepared by already stablished methods (solvent injection extrusion method) and new developed ones (direct dissolution), and were characterized by transmission electron microscopy (TEM), dynamic light scattering (DLS), and fluorescence correlation spectroscopy (FCS). Moreover, the density of the vesicles was determined by ultracentrifugation techniques.

To obtain active targeting drug-delivery systems, ligands were introduced onto the nanocontainer surface via coupling with streptavidin to the biotin moieties present on the nanocontainers surface. In vitro studies were performed to investigate the interactions of these ligand-functionalized nanocontainers with cells, in which uptake was followed via fluorescence microscopy. The selectivity of the interaction was also investigated with mixed cell cultures. Only ligand-functionalized nanocontainers were able of specific and selective targeting of receptor expressing cells. Absence of ligand resulted in no uptake by cells expressing targeting receptors, supporting thus the stealth characteristics of the polymer brushc constituting the nanocon-

tainer wall. Therefore, specific type of receptor targeting can be concluded for ligand-functionalized nanocontainers. Moreover, no cytotoxicity was observed for these artificial vesicles in preliminary studies.

In order to follow the pathway of the nanocontainers into the cells, gold nanoparticle encapsulation was tested. Neither pre-formed nor in situ formation of gold nanoparticles rendered gold encapsulation in polymer vesicles. Another approach was the use of a fluorescently labeled block-copolymer, for which the hydroxyl end groups of the triblock-copolymer were coupled covalently with a fluorescent molecule. However, for detection purposes encapsulation of fluorescent dyes was sufficient and proved more flexible in terms of concentration range and choice of dye.

To render surface-immobilized polymer vesicles, biotinylated polymers were used. Their adsorption onto a streptavidin decorated surface was studied with a quartz crystal microbalance with dissipation (QCM-D). The results were not conclusive since an unexpected adsorption was observed for vesicles without biotin moieties. This adsorption could be ascribed to unspecific polymer-protein interactions.

Other hydrophobic blocks with low T_g, such as poly(propylene oxide) and poly(tetrahydrofuran) were investigated as replacements for poly(dimethylsiloxane) in poly(2-methyl-2-oxazoline)-b-poly(dimethylsiloxane)-b-poly(2-methyl-2-oxazoline) block-copolymers. Their surface activity was studied with Langmuir films, which rendered typical isotherms. Their aggregation was assessed by transmission electron microscopy (TEM) and dynamic light scattering (DLS), mainly finding spherical aggregates that can be ascribed as vesicular structures.

Finally, these nanocontainers were studied as vehicles to entrap small solutes. By insertion of membrane proteins, the permeability characteristics of the nanocontainers can be improved. Langmuir film techniques showed protein-polymer interaction, which can be interpreted as insertion in the polymer membrane. Insertion was further confirmed by entrapment of small solutes in the cavity of the nanocontainers by forming a complex with an already encapsulated counterion. This post-encapsulation approach results interesting as a recovery system, in which a substance could be easily removed from a complex matrix system, allowing the concentration of the species of interest.

8. Outlook

Regarding the synthesis of the polymers here described, one possibility to explore would be the hydrolysis of the poly(2-methyl-2-oxazoline) in order to obtain poly(ethyleneimine) side chains[291, 292]. Poly(ethyleneimine) is well-known for its pH dependence, which would render stimuli responsive vesicles with direct applications in the field of controlled-release drug delivery systems. Moreover, such block-polyelectrolytes could find other applications in combination with techniques such as layer-by-layer deposition or in templating systems for inorganic materials.

Poly(2-ethyl-2-oxazoline) in acidic aqueous phase has the capability to undergo hydrogen bonding with a carboxyl H-donor functionality[152], e.g. PMAA or PAA. Complexation of PMOXA containing copolymers could be investigated in a similar manner, and be used in LbL type of deposition. Moreover, this pH sensitive hydrogen bonding with PMAA could be used to precipitate the methyloxazoline copolymers as an efficient way to recover the vesicles from solution. After forming a pellet this aggregates could then be redispersed at higher pH.[293]

Another possibility would be to prepare ABA triblock-copolymers with degradable middle blocks, such as PLA (poly(lactic acid)), PGA (poly(glycolic acid)), or PCL (poly(caprolactone)). The preparation of ABA type block-copolymers with tailored hydrophilic to hydrophobic ratios to promote aggregation into vesicular structures with degradable capability would result interesting for delivery purposes.

In the context of end-group functionalization of polymers, the use of thiol groups may be interesting from the point of view of producing cross-linked vesicles that can be reversibly brought to their non-crosslink state, therefore, easing the release of the encapsulated substances. Functionalization of vesicle-forming molecules, either with a disulfide group or with two thiol groups would render vesicular systems which can be switched on by oxidation, which is, polymerized, and subsequently, depolymerized or switched off by reduction. This reversible cross-linking process can be of use to promote controlled release of encapsulated substances.

In this thesis, it has been demonstrated that polymer-based drug-delivery vehicles allow the site-specific delivery of drugs by the incorporation of ligands to their surfaces. Nevertheless, issues related to the release of the drugs must be addressed in order to make these systems applicable.

The difficulties found in the delivering of substances from the highly stable compartment of the polymer vesicles can be taken as an advantage, for instance, to introduce in the body substances that should not get in contact with the cells or tissue due to their potential toxicity. One clear application in this area would be the use of nanocontainers as vehicles for introduction of magnetic particles in the body for magnetic resonance imaging. By encapsulation of contrast agents in the void volume of the nanocontainers, combined with the high speci-

ficity of targeting demonstrated in this thesis, there is hope for the practical application of these systems.

One idea for producing triggering release systems is to use block-copolymers with photo-cleavable bonds between the different blocks. Irradiation would result in the cleavage of the bonds, destabilizing the assembly and releasing the encapsulated material. This could be used for instance in combination with immobilization onto surfaces, providing systems that would release its contents upon external stimulus.

Moreover, one can further envision a system integrating both approaches, the surface immobilization of vesicular structures onto a biomaterial, and the use of such vesicles as drug delivery systems to release in situ drugs that might help during the healing process after implantation.

References

[1] E. Nakache, N. Poulain, F. Candau, A.-M. Orecchioni, J. M. Irache, *Handbook of Nanostructured Materials and Nanotechnology* **2000**, *5*, 577.

[2] F. Caruso, D. Trau, H. Moehwald, R. Renneberg, *Langmuir* **2000**, *16*, 1485.

[3] F. Caruso, W. Yang, D. Trau, R. Renneberg, *Langmuir* **2000**, *16*, 8932.

[4] H. Moehwald, H. Lichtenfeld, S. Moya, A. Voight, G. B. Sukhorukov, S. Leporatti, L. Daehne, I. Radtchenko, A. A. Antipov, C. Gao, E. Donath, *Surfactant Science Series* **2003**, *109*, 91.

[5] H. Mohwald, H. Lichtenfeld, S. Moya, A. Voigt, H. Baumler, G. Sukhorukov, F. Caruso, E. Donath, *Macromolecular Symposia* **1999**, *145*, 75.

[6] H. Moehwald, G. B. Sukhorukov, C. J. Gao, A. Fery, *Abstracts of Papers, 227th ACS National Meeting, Anaheim, CA, United States, March 28-April 1, 2004* **2004**, COLL.

[7] A. Voigt, N. Buske, G. B. Sukhorukov, A. A. Antipov, S. Leporatti, H. Lichtenfeld, H. Baumler, E. Donath, H. Mohwald, *Journal of Magnetism and Magnetic Materials* **2001**, *225*, 59.

[8] C. Nardin, S. Thoeni, J. Widmer, M. Winterhalter, W. Meier, *Chemical Communications* **2000**, 1433.

[9] Z. Dai, L. Daehne, E. Donath, H. Moehwald, *Journal of Physical Chemistry B* **2002**, *106*, 11501.

[10] A. Pohorille, D. Deamer, *Trends in Biotechnology* **2002**, *20*, 123.

[11] P. Walde, R. Wick, M. Fresta, A. Mangone, P. L. Luisi, *Journal of the American Chemical Society* **1994**, *116*, 11649.

[12] O. P. Tiourina, I. Radtchenko, G. B. Sukhorukov, H. Moehwald, *Journal of Membrane Biology* **2002**, *190*, 9.

[13] D. A. Hammer, D. E. Discher, *Annual Review of Materials Research* **2001**, *31*, 387.

[14] I. Hamley, *Introduction to Soft Matter: Polymers, Colloids, Amphiphiles and Liquid Crystals, Vol. 44*, **2000**.

[15] D. D. Lasic, *Liposomes: From Physics to Applications*, **1993**.

[16] C. Tanford, *Science* **1978**, *200*, 1012.

[17] R. Koebnik, K. P. Locher, P. Van Gelder, *Molecular Microbiology* **2000**, *37*, 239.

[18] F. Hucho, C. Weise, *Angewandte Chemie, International Edition* **2001**, *40*, 3100.

[19] M. Rosoff, Editor, *Vesicles. [In: Surfactant Sci. Ser., 1996; 62]*, **1996**.

[20] A. Ben-Naim, *Biophysical Chemistry* **2003**, *105*, 183.

[21] C. Tanford, *Journal of Molecular Biology* **1972**, *67*, 59.

[22] C. Tanford, *Proceedings of the International School of Physics Enrico Fermi* **1985**, *90*, 547.

[23] W. Blokzijl, J. B. F. N. Engberts, *Angewandte Chemie* **1993**, *105*, 1610.

[24] G. Odian, *Principles of Polymerization. 2nd Ed*, **1981**.

[25] G. R. Newkome, Z. Yao, G. R. Baker, V. K. Gupta, *Journal of Organic Chemistry* **1985**, *50*, 2003.

[26] D. A. Tomalia, H. Baker, J. Dewald, M. Hall, G. Kallos, S. Martin, J. Roeck, J. Ryder, P. Smith, *Polymer Journal (Tokyo, Japan)* **1985**, *17*, 117.

[27] R. W. Lenz, *Organic Chemistry of Synthetic High Polymers*, **1967**.

[28] J. E. McGrath, *Journal of Chemical Education* **1981**, *58*, 914.

[29] P. Alexandridis, *Current Opinion in Colloid & Interface Science* **1996**, *1*, 490.

[30] J. J. L. M. Cornelissen, M. Fischer, N. A. J. M. Sommerdijk, R. J. M. Nolte, *Science* **1998**, *280*, 1427.

[31] B. M. Discher, D. A. Hammer, F. S. Bates, D. E. Discher, *Current Opinion in Colloid & Interface Science* **2000**, *5*, 125.

[32] D. A. Hajduk, M. B. Kossuth, M. A. Hillmyer, F. S. Bates, *Journal of Physical Chemistry B* **1998**, *102*, 4269.

[33] A. V. Kabanov, V. Y. Alakhov, *Critical Reviews in Therapeutic Drug Carrier Systems* **2002**, *19*, 1.

[34] S. Burke, H. Shen, A. Eisenberg, *Macromolecular Symposia* **2001**, *175*, 273.

[35] D. E. Discher, A. Eisenberg, *Science* **2002**, *297*, 967.

[36] H. Shen, A. Eisenberg, *Angewandte Chemie, International Edition* **2000**, *39*, 3310.

[37] K. Yu, A. Eisenberg, *Macromolecules* **1998**, *31*, 3509.

[38] P. L. Soo, A. Eisenberg, *Journal of Polymer Science, Part B: Polymer Physics* **2004**, *42*, 923.

[39] R. Borsali, E. Minatti, J.-L. Putaux, M. Schappacher, A. Deffieux, P. Viville, R. Lazzaroni, T. Narayanan, *Langmuir* **2003**, *19*, 6.

[40] M. Breulmann, S. Forster, M. Antonietti, *Macromolecular Chemistry and Physics* **2000**, *201*, 204.

[41] J. Ding, G. Liu, *Journal of Physical Chemistry B* **1998**, *102*, 6107.

[42] M. Antonietti, S. Foerster, *Advanced Materials* **2003**, *15*, 1323.

[43] L. Zhang, A. Eisenberg, *Science* **1995**, *268*, 1728.

[44] B. M. Discher, Y.-Y. Won, D. S. Ege, J. C. M. Lee, F. S. Bates, D. E. Discher, D. A. Hammer, *Science* **1999**, *284*, 1143.

[45] O. Rheingans, N. Hugenberg, J. R. Harris, K. Fischer, M. Maskos, *Macromolecules* **2000**, *33*, 4780.

[46] S. Foerster, M. Antonietti, *Advanced Materials* **1998**, *10*, 195.

[47] A. Choucair, A. Eisenberg, *European Physical Journal E: Soft Matter* **2003**, *10*, 37.

[48] K. Yu, A. Eisenberg, *Macromolecules* **1996**, *29*, 6359.

[49] K. Yu, L. Zhang, A. Eisenberg, *Langmuir* **1996**, *12*, 5980.

[50] L. Zhang, A. Eisenberg, *Journal of the American Chemical Society* **1996**, *118*, 3168.

[51] Y. Yu, L. Zhang, A. Eisenberg, *Macromolecules* **1998**, *31*, 1144.

[52] N. P. Balsara, M. Tirrell, T. P. Lodge, *Macromolecules* **1991**, *24*, 1975.

[53] K. Schillen, K. Bryskhe, Y. S. Mel'nikova, *Macromolecules* **1999**, *32*, 6885.

[54] H. Kukula, H. Schlaad, M. Antonietti, S. Foerster, *Journal of the American Chemical Society* **2002**, *124*, 1658.

[55] F. Checot, S. Lecommandoux, Y. Gnanou, H.-A. Klok, *Angewandte Chemie, International Edition* **2002**, *41*, 1339.

[56] F. Checot, S. Lecommandoux, Y. Gnanou, H.-A. Klok, *Polymer Preprints* **2002**, *43*, 453.

[57] F. Checot, S. Lecommandoux, H. A. Klok, Y. Gnanou, *European Physical Journal E: Soft Matter* **2003**, *10*, 25.

[58] F. Ahmed, D. E. Discher, *Journal of Controlled Release* **2004**, *96*, 37.

[59] C. Nardin, J. Widmer, M. Winterhalter, W. Meier, *European Physical Journal E: Soft Matter* **2001**, *4*, 403.

[60] S. M. Benito, M. Sauer, W. Meier, *Encyclopedia of Nanoscience and Nanotechnology* **2004**, *6*, 301.

[61] C. Nardin, T. Hirt, J. Leukel, W. Meier, *Langmuir* **2000**, *16*, 1035.

[62] C. Nardin, M. Winterhalter, W. Meier, *Langmuir* **2000**, *16*, 7708.

[63] M. Sauer, D. Streich, W. Meier, *Advanced Materials* **2001**, *13*, 1649.

[64] M. Sauer, W. Meier, *Australian Journal of Chemistry* **2001**, *54*, 149.

[65] D. W. Yesair, *Phospholipids: Biochem., Pharm., Anal. Consid., [Proc. Int. Colloq. Lecithin], 5th* **1990**, 83.

[66] J. C. Ha, S. Y. Kim, Y. M. Lee, *Journal of Controlled Release* **1999**, *62*, 381.

[67] M. C. Woodle, D. D. Lasic, *Biochimica et Biophysica Acta* **1992**, *1113*, 171.

[68] K. Hristova, D. Needham, *Stealth Liposomes* **1995**, 35.

[69] T. M. Allen, C. Hansen, F. Martin, C. Redemann, A. Yau-Young, *Biochimica et Biophysica Acta* **1991**, *1066*, 29.

[70] G. Blume, G. Cevc, *Biochimica et Biophysica Acta* **1990**, *1029*, 91.

[71] A. Chonn, P. R. Cullis, *Current Opinion in Biotechnology* **1995**, *6*, 698.

[72] Y. Barenholz, *Current Opinion in Colloid & Interface Science* **2001**, *6*, 66.

[73] T. M. Allen, *Advanced Drug Delivery Reviews* **1994**, *13*, 285.

[74] P. Walde, S. Ichikawa, *Biomolecular Engineering* **2001**, *18*, 143.

[75] M. B. Yatvin, I. M. Tegmo-Larsson, W. H. Dennis, *Methods in Enzymology* **1987**, *149*, 77.

[76] J. N. Weinstein, *Pure and Applied Chemistry* **1981**, *53*, 2241.

[77] N. M. Wassef, G. R. Matyas, C. R. Alving, *Biochemical and Biophysical Research Communications* **1991**, *176*, 866.

[78] K. D. Lee, A. B. Kantor, S. Nir, J. C. Owicki, *Biophysical Journal* **1993**, *64*, 905.

[79] B. Rivnay, E. A. Bayer, M. Wilchek, *Methods in Enzymology* **1987**, *149*, 119.

[80] L. Huang, J. Connor, C. Y. Wang, *Methods in Enzymology* **1987**, *149*, 88.

[81] A. K. Patri, I. J. Majoros, J. R. Baker, *Current Opinion in Chemical Biology* **2002**, *6*, 466.

[82] R. Langer, *Science* **1990**, *249*, 1527.

[83] L. Brannon-Peppas, *International Journal of Pharmaceutics* **1995**, *116*, 1.

[84] J. Kreuter, *Journal of Controlled Release* **1991**, *16*, 169.

[85] G. S. Kwon, K. Kataoka, *Advanced Drug Delivery Reviews* **1995**, *16*, 295.

[86] G. S. Kwon, T. Okano, *Pharmaceutical Research* **1999**, *16*, 597.

[87] K. Kataoka, A. Harada, Y. Nagasaki, *Advanced drug delivery reviews* **2001**, *47*, 113.

[88] C. Allen, D. Maysinger, A. Eisenberg, *Colloids and Surfaces, B: Biointerfaces* **1999**, *16*, 3.

[89] V. P. Torchilin, *Journal of Controlled Release* **2001**, *73*, 137.

[90] I. M. Roitt, *Essential Immunology. 3rd Ed*, **1977**.

[91] A. S. Hoffman, P. S. Stayton, V. Bulmus, G. Chen, J. Chen, C. Cheung, A. Chilkoti, Z. Ding, L. Dong, R. Fong, C. A. Lackey, C. J. Long, M. Miura, J. E. Morris, N. Murthy, Y. Nabeshima, T. G. Park, O. W. Press, T. Shimoboji, S. Shoemaker, H. J. Yang, N. Monji, R. C. Nowinski, C. A. Cole, J. H. Priest, J. Milton Harris, K. Nakamae, T. Nishino, T. Miyata, *Journal of Biomedical Materials Research* **2000**, *52*, 577.

[92] S. Cammas, K. Suzuki, C. Sone, Y. Sakurai, K. Kataoka, T. Okano, *Journal of Controlled Release* **1997**, *48*, 157.

[93] C. Gao, S. Leporatti, S. Moya, E. Donath, H. Mohwald, *Chemistry--A European Journal* **2003**, *9*, 915.

[94] G. B. Sukhorukov, A. A. Antipov, A. Voigt, E. Donath, H. Mohwald, *Macromolecular Rapid Communications* **2001**, *22*, 44.

[95] X. Qiu, S. Leporatti, E. Donath, H. Moehwald, *Langmuir* **2001**, *17*, 5375.

[96] A. A. Antipov, G. B. Sukhorukov, H. Moehwald, *Langmuir* **2003**, *19*, 2444.

[97] A. Breitenbach, Y. X. Li, T. Kissel, *Journal of Controlled Release* **2000**, *64*, 167.

[98] L. D. Leserman, J. N. Weinstein, *Liposomes Immunobiol., Proc. Natl. Symp.* **1980**, 241.

[99] L. D. Leserman, J. Barbet, F. Kourilsky, J. N. Weinstein, *Nature* **1980**, *288*, 602.

[100] T. D. Heath, R. T. Fraley, D. Papahadjopoulos, *Science* **1980**, *210*, 539.

[101] D. Papahadjopoulos, R. Fraley, T. Heath, *Liposomes Immunobiol., Proc. Natl. Symp.* **1980**, 151.

[102] M. A. Cooper, A. Hansson, S. Lofas, D. H. Williams, *Analytical Biochemistry* **2000**, *277*, 196.

[103] W. Knoll, M. Liley, D. Piscevic, J. Spinke, M. J. Tarlov, *Advances in biophysics* **1997**, *34*, 231.

[104] G. Decher, *Science* **1997**, *277*, 1232.

[105] G. B. Sukhorukov, E. Donath, H. Lichtenfeld, E. Knippel, M. Knippel, A. Budde, H. Mohwald, *Colloids and Surfaces, A: Physicochemical and Engineering Aspects* **1998**, *137*, 253.

[106] H. Mohwald, H. Lichtenfeld, S. Moya, A. Voigt, G. Sukhorukov, S. Leporatti, L. Dahne, A. Antipov, C. Y. Gao, E. Donath, *Studies in Surface Science and Catalysis* **2001**, *132*, 485.

[107] A. Ulman, *Chemical Reviews* **1996**, *96*, 1533.

[108] C. Picart, P. Lavalle, P. Hubert, F. J. G. Cuisinier, G. Decher, P. Schaaf, J. C. Voegel, *Langmuir* **2001**, *17*, 7414.

[109] G. L. Kenausis, J. Voeroes, D. L. Elbert, N. Huang, R. Hofer, L. Ruiz-Taylor, M. Textor, J. A. Hubbell, N. D. Spencer, *Journal of Physical Chemistry B* **2000**, *104*, 3298.

[110] N.-P. Huang, R. Michel, J. Voros, M. Textor, R. Hofer, A. Rossi, D. L. Elbert, J. A. Hubbell, N. D. Spencer, *Langmuir* **2001**, *17*, 489.

[111] N.-P. Huang, J. Voeroes, S. M. De Paul, M. Textor, N. D. Spencer, *Langmuir* **2002**, *18*, 220.

[112] P. Persigehl, R. Jordan, O. Nuyken, *Macromolecules* **2000**, *33*, 6977.

[113] S. Kobayashi, T. Igarashi, Y. Moriuchi, T. Saegusa, *Macromolecules* **1986**, *19*, 535.

[114] S. Kobayashi, S. Iijima, T. Igarashi, T. Saegusa, *Macromolecules* **1987**, *20*, 1729.

[115] S. Kobayashi, *Prog. Polym. Sci.* **1990**, *15*, 751.

[116] S. Kobayashi, H. Uyama, E. Ihara, T. Saegusa, *Macromolecules* **1990**, *23*, 1586.

[117] S. Kobayashi, H. Uyama, Y. Narita, J. Ishiyama, *Macromolecules* **1992**, *25*, 3232.

[118] O. Nuyken, S. Pask, *Encycl. Polym. Sci. Eng.* **1989**, *16*, 494.

[119] T. Saegusa, H. Ikeda, *Macromolecules* **1973**, *6*, 805.

[120] S. L. N. Seung, R. N. Young, *J. Polym. Sci., Polym. Lett. Ed.* **1979**, *17*, 233.

[121] S. L. N. Seung, R. N. Young, *J. Polym. Sci., Polym. Lett. Ed.* **1980**, *18*, 89.

[122] P. J. Flory, *Principles of Polymer Chemistry*, **1953**.

[123] I. Yilgor, W. P. Steckle, Jr., E. Yilgor, R. G. Freelin, J. S. Riffle, *J. Polym. Sci., Part A: Polym. Chem.* **1989**, *27*, 3673.

[124] I. Yilgor, R. S. Ward, J. S. Riffle, *Polymer Preprints* **1987**, *28*, 369.

[125] J. Prinos, C. Panayiotou, *Polymer* **1995**, *36*, 1223.

[126] I. Yilgor, J. E. McGrath, *Advances in Polymer Science* **1988**, *86*, 1.

[127] N. P. Desai, J. A. Hubbell, *Biomaterials* **1991**, *12*, 144.

[128] M. C. Woodle, C. M. Engbers, S. Zalipsky, *Bioconjugate Chemistry* **1994**, *5*, 493.

[129] T. Oyama, J. Ozaki, Y. Chujo, *Polymer Bulletin* **1998**, *40*, 503.

[130] V. P. Torchilin, V. S. Trubetskoy, *Advanced Drug Delivery Reviews* **1995**, *16*, 141.

[131] S. Kobayashi, E. Masuda, S. Shoda, Y. Shimano, *Macromolecules* **1989**, *22*, 2878.

[132] W. Uhlig, *Polymers for Advanced Technologies* **1997**, *8*, 731.

[133] I. L. Baraznenok, V. G. Nenajdenko, E. S. Balenkova, *Tetrahedron* **2000**, *56*, 3077.

[134] V. G. Nenajdenko, P. V. Vertelezkij, A. B. Koldobskij, I. V. Alabugin, E. S. Balenkova, *Journal of Organic Chemistry* **1997**, *62*, 2483.

[135] W. P. Steckle, Jr., E. Yilgor, J. S. Riffle, M. Spinu, I. Yilgor, R. S. Ward, *Polymer Preprints* **1987**, *28*, 254.

[136] J. S. Riffle, G. Sinai-Zingde, J. M. DeSimone, A. M. Hellstern, D. H. Chen, I. Yilgor, *Polymer Preprints* **1988**, *29*, 93.

[137] J. Y. Chang, P. J. Park, M. J. Han, *Macromolecules* **2000**, *33*, 321.

[138] R. Jordan, K. Graf, H. Riegler, K. K. Unger, *Chem. Commun.* **1996**, 1025.

[139] S. Kobayashi, H. Uyama, H. Shirasaka, *Makromol. Chem., Rapid Commun.* **1990**, *11*, 11.

[140] O. Nuyken, G. Maier, A. Gross, H. Fischer, *Macromol. Chem. Phys.* **1996**, *197*, 83.

[141] R. Jordan, A. Ulman, *J. Am. Chem. Soc.* **1998**, *120*, 243.

[142] S. Kobayashi, H. Uyama, N. Higuchi, T. Saegusa, *Macromolecules* **1990**, *23*, 54.

[143] A. Gross, G. Maier, O. Nuyken, *Macromol. Chem. Phys.* **1996**, *197*, 2811.

[144] W. Meier, *Langmuir* **2000**, *16*, 1457.

[145] W. Steglich, G. Hoefle, *Angewandte Chemie, International Edition in English* **1969**, *8*, 981.

[146] R. Savic, L. Luo, A. Eisenberg, D. Maysinger, *Science* **2003**, *300*, 615.

[147] R. P. Staiger, E. B. Miller, *Journal of Organic Chemistry* **1959**, *24*, 1214.

[148] R. Weberskirch, O. Nuyken, *Journal of Macromolecular Science, Pure and Applied Chemistry* **1999**, *A36*, 843.

[149] T. Saegusa, Y. Chujo, *Makromol. Chem., Macromol. Symp.* **1991**, *51*, 1.

[150] E. J. Goethals, M. Van de Velde, A. Munir, *Cationic Polym. Relat. Processes, Proc. Int. Symp., 6th* **1984**, 387.

[151] J. M. Rodriguez-Parada, M. Kaku, D. Y. Sogah, *Macromolecules* **1994**, *27*, 1571.

[152] C. Kim, S. C. Lee, J. H. Shin, J.-S. Yoon, I. C. Kwon, S. Y. Jeong, *Macromolecules* **2000**, *33*, 7448.

[153] J. Schiewe, S. Goebel, M. Schwarz, R. Neubert, *Journal of Pharmaceutical and Biomedical Analysis* **1996**, *14*, 435.

[154] M. G. Munoz, F. Monroy, F. Ortega, R. G. Rubio, D. Langevin, *Langmuir* **2000**, *16*, 1083.

[155] D. Vollhardt, *Advances in Colloid and Interface Science* **1999**, *79*, 19.

[156] T. R. Baekmark, T. Wiesenthal, P. Kuhn, T. M. Bayerl, O. Nuyken, R. Merkel, *Langmuir* **1997**, *13*, 5521.

[157] T. R. Baekmark, T. Wiesenthal, P. Kuhn, A. Albersdoerfer, O. Nuyken, R. Merkel, *Langmuir* **1999**, *15*, 3616.

[158] M. G. Munoz, F. Monroy, F. Ortega, R. G. Rubio, D. Langevin, *Langmuir* **2000**, *16*, 1094.

[159] R. Blankenburg, P. Meller, H. Ringsdorf, C. Salesse, *Biochemistry* **1989**, *28*, 8214.

[160] S. Foerster, N. Hermsdorf, W. Leube, H. Schnablegger, M. Regenbrecht, S. Akari, P. Lindner, C. Boettcher, *Journal of Physical Chemistry B* **1999**, *103*, 6657.

[161] M. E. Yildiz, D. H. Adamson, R. K. Prud'homme, *Polymeric Materials Science and Engineering* **2004**, *90*, 572.

[162] T. Oberholzer, E. Meyer, I. Amato, A. Lustig, P.-A. Monnard, *Biochimica et Biophysica Acta* **1999**, *1416*, 57.

[163] J.-L. Rigaud, B. Pitard, D. Levy, *Biochimica et Biophysica Acta* **1995**, *1231*, 223.

[164] J. L. Rigaud, D. Levy, G. Mosser, O. Lambert, *European Biophysics Journal* **1998**, *27*, 305.

[165] G.-e. Yu, A. Eisenberg, *Macromolecules* **1998**, *31*, 5546.

[166] S. E. Burke, A. Eisenberg, *Polymer* **2001**, *42*, 9111.

[167] P. Beck, D. Scherer, J. Kreuter, *Journal of Microencapsulation* **1990**, *7*, 491.

[168] L. Luo, A. Eisenberg, *Journal of the American Chemical Society* **2001**, *123*, 1012.

[169] H. Shen, A. Eisenberg, *Macromolecules* **2000**, *33*, 2561.

[170] F. M. Menger, J. S. Keiper, *Current Opinion in Chemical Biology* **1998**, *2*, 726.

[171] F. M. Menger, M. I. Angelova, *Accounts of Chemical Research* **1998**, *31*, 789.

[172] F. M. Menger, J. S. Keiper, *Advanced Materials* **1998**, *10*, 888.

[173] M. Angelova, D. Dimitrov, *Faraday Discussions of the Chemical Society* **1986**, *81*, 303.

[174] N. Oku, D. A. Kendall, R. C. MacDonald, *Biochimica et Biophysica Acta* **1982**, *691*, 332.

[175] S. Massou, R. Albigot, M. Prats, *Biochemical Education* **2000**, *28*, 171.

[176] H. Sawahara, S. Goto, N. Kinoshita, *Chemical & Pharmaceutical Bulletin* **1991**, *39*, 227.

[177] J. H. Fuhrhop, J. Koning, *Membranes and Molecular Assemblies: The Synkinetic Approach*, **1998**.

[178] A. Lustig, A. Engel, M. Zulauf, *Biochimica et Biophysica Acta* **1991**, *1115*, 89.

[179] N. M. Green, *Advances in protein chemistry* **1975**, *29*, 85.

[180] J. N. Israelachvili, *Intermolecular and Surface Forces: With Applications to Colloidal and Biological Systems*, **1985**.

[181] M. Wilchek, E. A. Bayer, *Methods in Enzymology* **1990**, *184*, 5.

[182] M. B. Wilcheck, Edward A., *Avidin-biotin technology, Vol. 184*, Academic Press Inc., San Diego, California, **1990**.

[183] K. Takahashi, M. Takeya, N. Sakashita, *Medical Electron Microscopy* **2002**, *35*, 179.

[184] R. Kirsh, G. Poste, *Methods in Enzymology* **1987**, *149*, 147.

[185] M. Honda, H. Akiyama, Y. Yamada, H. Kondo, Y. Kawabe, M. Takeya, K. Takahashi, H. Suzuki, T. Doi, A. Sakamoto, S. Ookawara, M. Mato, P. J. Gough, D. R. Greaves, S. Gordon, T. Kodama, M. Matsushita, *Biochemical and Biophysical Research Communications* **1998**, *245*, 734.

[186] A. Matsumoto, M. Naito, H. Itakura, S. Ikemoto, H. Asaoka, I. Hayakawa, H. Kanamori, H. Aburatani, F. Takaku, et al., *Proceedings of the National Academy of Sciences of the United States of America* **1990**, *87*, 9133.

[187] M. P. J. De Winther, K. W. Van Dijk, L. M. Havekes, M. H. Hofker, *Arteriosclerosis, Thrombosis, and Vascular Biology* **2000**, *20*, 290.

[188] A. M. Pearson, A. Rich, M. Krieger, *Journal of Biological Chemistry* **1993**, *268*, 3546.

[189] Y. Yamada, T. Doi, T. Hamakubo, T. Kodama, *Cellular and Molecular Life Sciences* **1998**, *54*, 628.

[190] H. Loughrey, M. B. Bally, P. R. Cullis, *Biochimica et Biophysica Acta* **1987**, *901*, 157.

[191] H. C. Loughrey, K. F. Wong, L. S. Choi, P. R. Cullis, M. B. Bally, *Biochimica et Biophysica Acta* **1990**, *1028*, 73.

[192] S. Chiruvolu, S. Walker, J. Israelachvili, F. J. Schmitt, D. Leckband, J. A. Zasadzinski, *Science* **1994**, *264*, 1753.

[193] W. A. Dunn, A. L. Hubbard, N. N. Aronson, Jr., *Journal of Biological Chemistry* **1980**, *255*, 5971.

[194] K. Takahashi, M. Takeya, N. Sakashita, M. Yoshimatsu, K. Jinnouchi, *Atherosclerosis and Autoimmunity* **2001**, 29.

[195] H. Heider, E. S. Wintergerst, *FEBS Letters* **2001**, *505*, 185.

[196] R. M. Straubinger, K. Hong, D. S. Friend, D. Papahadjopoulos, *Cell* **1983**, *32*, 1069.

[197] D. V. Leff, P. C. Ohara, J. R. Heath, W. M. Gelbart, *Journal of Physical Chemistry* **1995**, *99*, 7036.

[198] M. Brust, M. Walker, D. Bethell, D. J. Schiffrin, R. Whyman, *Journal of the Chemical Society, Chemical Communications* **1994**, 801.

[199] D. I. Gittins, F. Caruso, *ChemPhysChem* **2002**, *3*, 110.

[200] K. Hong, D. S. Friend, C. G. Glabe, D. Papahadjopoulos, *Biochimica et Biophysica Acta* **1983**, *732*, 320.

[201] K. Gao, L. Huang, *Biochimica et Biophysica Acta* **1987**, *897*, 377.

[202] L. E. T. Stearne, R. M. Schiffelers, E. Smouter, I. Bakker-Woudenberg, I. C. Gyssens, *Biochimica Et Biophysica Acta-Biomembranes* **2002**, *1561*, 91.

[203] S. K. Huang, K. Hong, K. D. Lee, D. Papahadjopoulos, D. S. Friend, *Biochimica et Biophysica Acta* **1991**, *1069*, 117.

[204] Y. Zhou, C. Y. Wang, Y. R. Zhu, Z. Y. Chen, *Chemistry of Materials* **1999**, *11*, 2310.

[205] T. Sato, T. Ito, H. Iwabuchi, Y. Yonezawa, *Journal of Materials Chemistry* **1997**, *7*, 1837.

[206] K. Esumi, A. Suzuki, N. Aihara, K. Usui, K. Torigoe, *Langmuir* **1998**, *14*, 3157.

[207] K. Esumi, K. Matsuhisa, K. Torigoe, *Langmuir* **1995**, *11*, 3285.

[208] N. Toshima, Y. Shiraishi, T. Teranishi, M. Miyake, T. Tominaga, H. Watanabe, W. Brijoux, H. Bonnemann, G. Schmid, *Applied Organometallic Chemistry* **2001**, *15*, 178.

[209] R. Michel, I. Reviakine, D. Sutherland, C. Fokas, G. Csucs, G. Danuser, N. D. Spencer, M. Textor, *Langmuir* **2002**, *18*, 8580.

[210] C. Nardin, W. Meier, *Chimia* **2001**, *55*, 142.

[211] A. Rezania, R. Johnson, A. R. Lefkow, K. E. Healy, *Langmuir* **1999**, *15*, 6931.

[212] F. Hoeoek, A. Ray, B. Norden, B. Kasemo, *Langmuir* **2001**, *17*, 8305.

[213] A. Bernard, J. P. Renault, B. Michel, H. R. Bosshard, E. Delamarche, *Advanced Materials* **2000**, *12*, 1067.

[214] J. L. Wilbur, A. Kumar, E. Kim, G. M. Whitesides, *Advanced Materials* **1994**, *6*, 600.

[215] M. Mrksich, G. M. Whitesides, *Trends in Biotechnology* **1995**, *13*, 228.

[216] J. J. Hickman, S. K. Bhatia, J. N. Quong, P. Shoen, D. A. Stenger, C. J. Pike, C. W. Cotman, *Journal of Vacuum Science & Technology, A: Vacuum, Surfaces, and Films* **1994**, *12*, 607.

[217] K. S. Schanze, T. S. Bergstedt, B. T. Hauser, *Advanced Materials* **1996**, *8*, 531.

[218] S. A. Darst, M. Ahlers, P. H. Meller, E. W. Kubalek, R. Blankenburg, H. O. Ribi, H. Ringsdorf, R. D. Kornberg, *Biophysical Journal* **1991**, *59*, 387.

[219] S. Scheuring, D. J. Muller, P. Ringler, J. B. Heymann, A. Engel, *Journal of Microscopy* **1999**, *193*, 28.

[220] I. Hamley, *The Physics of Block Copolymers*, **1998**.

[221] E. Reimhult, F. Hoeoek, B. Kasemo, *Langmuir* **2003**, *19*, 1681.

[222] C. Larsson, M. Rodahl, F. Hoeoek, *Analytical Chemistry* **2003**, *75*, 5080.

[223] F. Hook, J. Voros, M. Rodahl, R. Kurrat, P. Boni, J. J. Ramsden, M. Textor, N. D. Spencer, P. Tengvall, J. Gold, B. Kasemo, *Colloids and Surfaces, B: Biointerfaces* **2002**, *24*, 155.

[224] P. W. Holloway, *Analytical Biochemistry* **1973**, *53*, 304.

[225] S. B. Zimmerman, N. F. Coleman, *Biopolymers* **1972**, *11*, 1943.

[226] T. C. Ward, *Journal of Chemical Education* **1981**, *58*, 867.

[227] V. Melzer, D. Vollhardt, G. Brezesinski, H. Moehwald, *Journal of Physical Chemistry B* **1998**, *102*, 591.

[228] E. Rogalska, R. Bilewicz, T. Brigaud, C. El Moujahid, G. Foulard, C. Portella, M. J. Stebe, *Chemistry and Physics of Lipids* **2000**, *105*, 71.

[229] M. C. Petty, *Langmuir-Blodgett films : an introduction*, Cambridge University Press., Cambridge ; New York, **1996**.

[230] www.ksvltd.fi, Helsinki, Finland.

[231] G. L. Gaines, Jr., *Insoluble Monolayers at Liquid-Gas Interfaces*, **1966**.

[232] G. Roberts, Editor, *Langmuir-Blodgett Films*, **1990**.

[233] D. J. Crisp, *Journal of Colloid Science* **1946**, *1*, 49.

[234] D. J. Crisp, *Journal of Colloid Science* **1946**, *1*, 161.

[235] M. Breton, *Journal of Macromolecular Science, Reviews in Macromolecular Chemistry* **1981**, *C21*, 61.

[236] Y. Ikada, H. Iwata, S. Nagaoka, F. Horii, M. Hatada, *Journal of Macromolecular Science, Physics* **1980**, *B17*, 191.

[237] X. H. Han, S. F. Sui, F. Y. Yang, *Thin Solid Films* **1996**, *284-285*, 789.

[238] D. W. Britt, G. Jogikalmath, V. Hlady, *Surfactant Science Series* **2003**, *110*, 415.

[239] A. Braithwaite, F. J. Smith, Editors, *Chromatographic Methods, 5th Edition*, **1996**.

[240] A. J. Pesce, C. G. Rosen, T. L. Pasby, *Fluorescence Spectroscopy. An Introduction for Biology and Medicine*, **1971**.

[241] M. G. Gore, Editor, *Spectrophotometry and Spectrofluorimetry: A Practical Approach, Second Edition*, **2000**.

[242] Q. Yu, A. Kandegedara, Y. Xu, D. B. Rorabacher, *Analytical Biochemistry* **1997**, *253*, 50.

[243] H. E. Mash, Y.-P. Chin, L. Sigg, R. Hari, H. Xue, *Analytical Chemistry* **2003**, *75*, 671.

[244] K. S. Schmitz, *An introduction to Dynamic Light Scattering by macromolecules*, Academic Press, Inc., San Diego, CA, USA, **1990**.

[245] R. Pecora, Editor, *Dynamic Light Scattering: Applications of Photon Correlation Spectroscopy*, **1985**.

[246] W. Burchard, *Static and dynamic light scattering from branched polymers and biopolymers, Vol. 48*, **1983**.

[247] G. Williams, D. C. Watts, *Transactions of the Faraday Society* **1970**, *66*, 80.

[248] G. Williams, D. C. Watts, S. B. Dev, A. M. North, *Transactions of the Faraday Society* **1971**, *67*, 1323.

[249] S. W. Provencher, *Computer Physics Communications* **1982**, 213.

[250] S. W. Provencher, *Computer Physics Communications* **1982**, 229.

[251] P. Dittrich, F. Malvezzi-Campeggi, M. Jahnz, P. Schwille, *Biological Chemistry* **2001**, *382*, 491.

[252] R. Rigler, *Journal of Biotechnology* **1995**, *41*, 177.

[253] Z. Foldes-Papp, U. Demel, G. P. Tilz, *Proceedings of the National Academy of Sciences of the United States of America* **2001**, *98*, 11509.

[254] S. Maiti, U. Haupts, W. W. Webb, *Proceedings of the National Academy of Sciences of the United States of America* **1997**, *94*, 11753.

[255] W. Wiegrabe, *American Laboratory* **2000**, *32*, 44.

[256] A. Pramanik, P. Thyberg, R. Rigler, *Chemistry and Physics of Lipids* **2000**, *104*, 35.

[257] J. Korlach, P. Schwille, W. W. Webb, G. W. Feigenson, *Proceedings of the National Academy of Sciences of the United States of America* **1999**, *96*, 8461.

[258] R. Rigler, Z. Foldes-Papp, F.-J. Meyer-Almes, C. Sammet, M. Volcker, A. Schnetz, *Journal of Biotechnology* **1998**, *63*, 97.

[259] K. Bacia, I. V. Majoul, P. Schwille, *Biophysical Journal* **2002**, *83*, 1184.

[260] G. Ralston, *Introduction to Analytical Ultracentrifugation*, Beckman Instr. Inc., Fullerton, CA, USA.

[261] C. Huang, J. P. Charlton, *Journal of biological chemistry* **1971**, *246*, 2555.

[262] H. Heider, S. B. Verca, S. Rusconi, R. Asmis, *BioTechniques* **2000**, *28*, 260.

[263] S. Tsuchiya, Y. Kobayashi, Y. Goto, H. Okumura, S. Nakae, T. Konno, K. Tada, *Cancer Research* **1982**, *42*, 1530.

[264] V. Shirhatti, G. Krishna, *Analytical Biochemistry* **1985**, *147*, 410.

[265] M. Brust, D. Bethell, D. J. Schiffrin, C. J. Kiely, *Advanced Materials* **1995**, *7*, 795.

[266] M. Rodahl, F. Hook, A. Krozer, P. Brzezinski, B. Kasemo, *Review of Scientific Instruments* **1995**, *66*, 3924.

[267] M. V. Voinova, M. Rodahl, M. Jonson, B. Kasemo, *Physica Scripta* **1999**, *59*, 391.

[268] G. Sauerbrey, *Zeitschrift fuer Physik* **1959**, *155*, 206.

[269] K. Mortensen, *Polymers for Advanced Technologies* **2001**, *12*, 2.

[270] M. Svensson, P. Alexandridis, P. Linse, *Macromolecules* **1999**, *32*, 637.

[271] S. Ishikawa, K. Ishizu, T. Fukutomi, *Polymer Bulletin* **1986**, *16*, 223.

[272] M. Miyamoto, Y. Sano, T. Saegusa, S. Kobayashi, *European Polymer Journal* **1983**, *19*, 955.

[273] M. Miyamoto, K. Aoi, H. Yamanaka, T. Saegusa, *Polymer Journal (Tokyo)* **1992**, *24*, 405.

[274] H. Burner, M. Winterhalter, R. Benz, *Journal of Colloid and Interface Science* **1994**, *168*, 183.

[275] A. Graff, M. Sauer, P. Van Gelder, W. Meier, *Proceedings of the National Academy of Sciences of the United States of America* **2002**, *99*, 5064.

[276] W. Meier, C. Nardin, M. Winterhalter, *Angewandte Chemie, International Edition* **2000**, *39*, 4599.

[277] W. Meier, *Chemical Society Reviews* **2000**, *29*, 295.

[278] R. Benz, K. Bauer, *European Journal of Biochemistry* **1988**, *176*, 1.

[279] P. Van Gelder, F. Dumas, J. P. Rosenbusch, M. Winterhalter, *European Journal of Biochemistry* **2000**, *267*, 79.

[280] V. Braun, M. Braun, *FEBS letters* **2002**, *529*, 78.

[281] V. Braun, M. Braun, *Current opinion in microbiology* **2002**, *5*, 194.

[282] M. Bonhivers, L. Plancon, A. Ghazi, P. Boulanger, M. Le Maire, O. Lambert, J. L. Rigaud, L. Letellier, *Biochimie* **1998**, *80*, 363.

[283] V. Braun, H. Killmann, R. Benz, *FEBS Letters* **1994**, *346*, 59.

[284] M. Braun, H. Killmann, V. Braun, *Molecular Microbiology* **1999**, *33*, 1037.

[285] M. N. Jones, D. Chapman, *Micelles, Monolayers, and Biomembranes*, **1995**.

[286] M. Winterhalter, H. Buerner, S. Marzinka, R. Benz, J. J. Kasianowicz, *Biophysical Journal* **1995**, *69*, 1372.

[287] A. Blume, *Biochimica et Biophysica Acta* **1979**, *557*, 32.

[288] A. Seelig, P. M. Macdonald, *Biochemistry* **1989**, *28*, 2490.

[289] A. L. J. Van Raalte, R. A. Demel, G. Verberkmoes, E. Breukink, R. C. A. Keller, B. De Kruijff, *European Journal of Biochemistry* **1996**, *235*, 207.

[290] K. P. Locher, B. Rees, R. Koebnik, A. Mitschler, L. Moulinier, J. P. Rosenbusch, D. Moras, *Cell* **1998**, *95*, 771.

[291] M. Miyamoto, Y. Sano, T. Saegusa, S. Kobayashi, *Eur. Polym. J.* **1983**, *19*, 955.

[292] D. A. Tomalia, D. M. Hedstrand, M. S. Ferritto, *Macromolecules* **1991**, *24*, 1435.

[293] S. C. Lee, Y. Chang, J.-S. Yoon, C. Kim, I. C. Kwon, Y.-H. Kim, S. Y. Jeong, *Macromolecules* **1999**, *32*, 1847.